# The Study of Iron Complexes and Iodine Oxides for C–H Bond Activation and Functionalization

Steven Edward Kalman
Hillsdale, NJ

B.S. Chemistry, Muhlenberg College, 2010

A Dissertation presented to the Graduate Faculty
of the University of Virginia in Candidacy for the Degree of
Doctor of Philosophy

Department of Chemistry

University of Virginia
April 2015

## ABSTRACT

KALMAN, STEVEN E. The Study of Iron Complexes and Iodine Oxides for C–H Bond Activation and Functionalization (Under the direction of Professor T. Brent Gunnoe).

The production of alkyl arenes from benzene and olefins comprises a major sector of the petrochemical industry. These compounds are typically synthesized by Friedel-Crafts or zeolite catalysis. As a result of the acid-based mechanism, these reactions result in polyalkylation, which requires an energy-intensive trans-alkylation step to obtain the desired monoalkylated product, do not provide a way to make anti-Markovnikov addition products, and offer poor control of regioselectivity on substituted arenes. We have been studying an alternative mechanism that involves transition metal-mediated olefin insertion and aromatic C–H activation that may improve upon the deficiencies mentioned for acid-mediated benzene alkylation. Transition metal complexes that catalyze olefin hydroarylation by metal-mediated olefin insertion and C–H activation are based on expensive noble metals (e.g., Ru, Ir, Pt). Our group has previously studied olefin hydroarylation using TpRu(L)(NCMe)Ph complexes (Tp = hydridotris(pyrazolyl)borate, L = neutral, two-electron donor). This Dissertation is focused on extending the catalytic activity observed for TpRu(L)(NCMe)Ph complexes to ruthenium's first row, Earth abundant counterpart, iron. However, examples of Fe complexes that can activate aromatic C–H bonds are rare.

The complex Cp*Fe(CO)(NCMe)Ph (Cp* = $\eta^5$-pentamethylcyclopentadienyl) was synthesized and characterized. It was found that this complex was able to activate the C–H bonds of benzene at 50 °C. Additionally, Cp*Fe(CO)(NCMe)Ph regioselectively activates the 2-position of furan, thiophene, and thiazole at, or below, room temperature. Cp*Fe(CO)(NCMe)Ph selectively activates the aromatic C–H bond of 2-methylfuran

over the methyl C–H bond, which provides evidence against an H atom abstraction mechanism. A combined experimental and computational mechanistic study was undertaken for the C–H activation reaction of Cp*Fe(CO)(NCMe)Ph and furan. From this study, the mechanism of furan C–H activation involves reversible NCMe dissociation from Cp*Fe(CO)(NCMe)Ph, reversible coordination of furan followed by rate-determining C–H activation by a σ-bond metathesis transition state, and subsequent NCMe coordination.

Applying Cp*Fe(CO)(NCMe)Ph to catalytic ethylene hydrophenylation resulted in the production of 1.2 turnovers of styrene and 0.6 turnovers of ethylbenzene. Studies indicate that β-hydride elimination from Cp*Fe(CO)($CH_2CH_2Ph$) to give an inactive Fe–hydride complex is likely competitive with benzene C–H activation. Attempts to catalyze ethylene hydroarylation using furan or thiophene were unsuccessful, which is attributed to prohibitively slow ethylene insertion into the Fe–aryl bond. Rather than catalyzing alkyne hydrophenylation, the reaction of Cp*Fe(CO)(NCMe)Ph and internal alkynes results in the formation of novel hydroxyindenyl and vinylidene ligands from intramolecular reactivity following alkyne insertion into the Fe–Ph bond of Cp*Fe(CO)(NCMe)Ph.

Under photolytic conditions, Cp*Fe[$P(OCH_2)_3CEt]_2$Ph activates the C–H bond at the 2-position of furan and thiophene and the 5-position of 2-methylfuran. While no catalysis was achieved with this complex under thermal or photolytic conditions, it was discovered that the reaction of Cp*Fe[$P(OCH_2)_3CEt]_2$(2-furyl) with excess 2-butyne affords a new ferrocenyl-type complex that forms via ring opening of the furyl ring. The synthesis of Fe complexes outside the Cp*Fe motif have also been investigated, including

Fe complexes based on phosphine-tethered cyclopentadienyl ligands and 2,6-bis(dihydrocarbylphosphinomethyl)pyridine ligands.

Additionally, the partial oxidation of light alkanes using periodate and chloride salts in trifluoroacetic acid has been studied. It was discovered that $KIO_4$ and KCl mediate the partial oxidation of methane to methyl trifluoroacetate and methyl chloride in 42% yield using low pressures of methane (860 kPa) at 200 °C in one hour. $KIO_4$ and KCl also functionalize ethane and propane in >20% yields. These results are relevant to the development of new technologies for the conversion of natural gas into liquid fuels.

## ACKNOWLEDGEMENTS

I learned pretty quickly that graduate school is not something that one does alone or is even capable of doing alone. I am indebted to so many people who have made this possible. First, I need to thank my advisor, Brent Gunnoe. Thank you for giving me the opportunity to work in your lab as an undergraduate and then, even after that, letting me return to your lab for graduate school. I imagine it's a rare experience to have an advisor who motivates his graduate students to succeed while being incredibly kind and supportive. I've learned so much, and I am extremely thankful for the experience I have had working for you. I also am grateful for my committee, Dr. Dean Harman, Dr. Cassandra Fraser (thanks for the espresso machine that sustained me through candidacy exam), Dr. Lin Pu, and Dr. Gary Koenig, for all your feedback over the past five years and for taking the time to read my dissertation. I need to especially thank Dean for being my mentor for the Tomorrow's Professor Today program and for helping me learn to be a better teacher.

I've been around the Gunnoe group for a long time (not all in grad school!), which has given me the occasion to work with and learn from so many talented chemists and great people. As an REU student at NC State, I was impressed by the great group of people in the lab, which was one of the major reasons I wanted to re-join the lab as a graduate student (even if it did mean I still had to work with iron). Nick was my graduate student mentor at NC State. I learned so much from him over those short couple of months. I need to thank all of the previous grad students and post-docs (from NC State and UVA): John, Colleen, Nick, Josh, Sam, Vijay, Joanna, Chong, Evan, Brad, Shaun, Samantha, JJ, Laurel, Brandon, Tamara, Jeremy, Mark, George, Ted, Zuming, Sarah,

Huimin, Yan, and Dominik. Thank you for all of your help and making working in the lab so enjoyable. I need to especially thank Samantha, who had to work in the lab with me for three years at Muhlenberg and four years at UVA. Thanks for your patience and for all the ways that you've helped me, even after you graduated by proofreading some of my dissertation! Also, thank you, Joanna, for being so helpful while you were in the group and even after you left.

To the current group members, Mike, Kathleen, Tristan, Ben, Junqi, John, Bridgette, Nichole, Shaojin, and Matt: You've all been so helpful and have made working in the lab a pleasure. For the grad students: Keep working hard and persevering, and keep everything in perspective. Thanks, Mike, for helping me to remember who and what is important. I've also mentored (I use that word loosely) two undergraduates, Anna and Dan, while being at UVA. Thank you both for your patience with me and for the things that you've taught me.

I also need to thank the faculty and staff in the Department of Chemistry for all of the ways they have assisted me during my time here. Thank you, Dr. Sabat, for working on all of those crystal structures and dealing with some really annoying crystals. Thank you, Dr. Ellena, for all of your help with the NMRs and being patient for when things stopped working or I didn't know how to do something. Also, thank you, Harman lab, for always being willing to help by lending chemicals or glassware. Thank you to my collaborators and their research groups: Dr. Dan Ess (Brigham Young University), Dr. Tom Cundari (University of North Texas), and Dr. John Groves (Princeton). I also want to thank my undergraduate research advisor, Dr. Joe Keane (Muhlenberg), for all that he has taught me and for all of the advice and help he has given me from college to now.

I am very grateful for all of the support that I've gotten outside of the lab. Thank you to my GCF friends and the wonderful people at Grace Community Church. You all have been so supportive with your prayers and love. Thanks, Jacob, for being a great friend and housemate. Thank you, Don and Charles and Donna, for caring for me, especially when I first moved down here. Thank you, Sean, for being such a constant friend ever since our days at the farm. Thank you to my Muhlenberg friends, especially my groomsmen, John, Paul, and Pat.

There is really no way that I can express the gratitude I have for my family. To all of my extended family and extended family-in-law: Thank you for your support and love. Thank you to my grandmothers, Grandma Sheila and Grandma Gladys. Grandpa Sidney Cherry, who passed away before I was born, and Grandpa Sidney Kalman, who passed away during my third year here: I miss you both.

I am incredibly blessed to have married into a wonderful family. Thank you, Mom (Angela) Weigle and Dad (Jack) Weigle and John and Faryn, for making me feel so welcomed in your family and for your love, prayers, and support over these past years.

I want to thank my brother, Joe, and my sister, Diane, for their love and for giving me a typical (yet, wonderful?) middle child experience as a kid. I love you both. I am so incredibly grateful for my loving parents, Fran and Jeff. They have given me more than I could have asked for and have supported me through so much over the years. I could not have done this without you. Thank you and I love you, Mom and Dad.

I really do not know how I could have possibly done this without the love and support of my beautiful, talented, caring, loving, funny, and intelligent wife, Caitlin. Thank you soooooooooo much for marrying me and being the absolute best wife and

friend I could have ever dreamed of having. I know that this wasn't easy, but the past (almost) two years have been the best because they were with you. Thank you for sticking by me, praying for me, and loving me. I love you!

Finally, I am forever grateful for God's grace and mercy and how He has sustained me through this whole process.

## TABLE OF CONTENTS

# LIST OF SCHEMES

## CHAPTER 1

**CHAPTER 2**

**CHAPTER 3**

**CHAPTER 4**

**CHAPTER 5**

**CHAPTER 6**



**CHAPTER 7**

# LIST OF FIGURES

## CHAPTER 1



## CHAPTER 2

**CHAPTER 3**

**CHAPTER 4**

**CHAPTER 5**

**CHAPTER 6**

**CHAPTER 7**

# LIST OF TABLES

## CHAPTER 1



## CHAPTER 3



## CHAPTER 5



## CHAPTER 6

# 1 Introduction

The synthesis of alkyl arenes is a large-scale process in the petroleum industry and is one whose demand continues to grow.[1] The importance of this process stems from the use of these simple arenes, from petroleum or natural gas, as precursors for a wide range of chemicals. These alkyl arenes are converted to a range of products, including plastics, elastomers, detergents, and pharmaceuticals (Scheme 1.1).[2-6] Among the chemicals derived from petroleum, benzene, toluene and xylene make up the foundation for many petrochemicals. The demand for benzene is particularly large. For instance, the world demand for benzene in 2004 was over 36 million tonnes. Predictions anticipate that the demand will increase by ~5% annually.[4] The majority of benzene (75%) is used to synthesize alkyl arenes, such as ethylbenzene.[1, 4] With the increased demand of plastics and elastomers, the worldwide consumption of ethylbenzene has continued to rise. For example, in 2004, the United States produces approximately 5 million tonnes of ethylbenzene. Nearly all of the ethylbenzene produced (99%) is converted to styrene, of which, ~65% is used to make polystyrene.[3, 4]

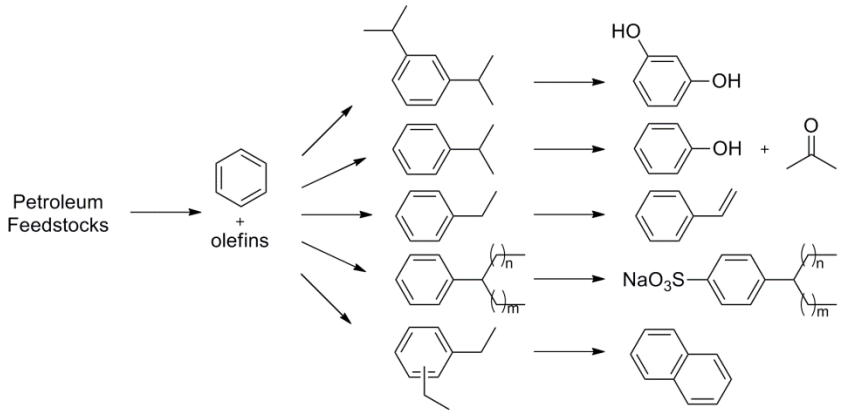


**Scheme 1.1.** Alkyl arenes, derived from benzene and olefins, and products from them.

With the desire to decrease the environmental impact of large-scale industrial processes in conjunction with the high demand for alkyl arenes, it is necessary to discover new industrially viable methods to replace the conventional methods (i.e., Friedel-Crafts alkylation, see below) used by the petrochemical industry. Transition metal catalysis may provide this opportunity. Furthermore, transition metal catalysts may be able to complement the selectivity of current methods and provide a foundation to synthesize new alkyl arenes that are not accessible by traditional means.[7]

## 1.1 Current Industrial Methods for the Synthesis of Alkyl Arenes

### 1.1.1 Friedel-Crafts Catalysis

The Friedel-Crafts (FC) reaction was discovered in the late 19$^{th}$ century by Charles Friedel and James Crafts and provides a means to synthesize alkyl arenes.[8-12] In one iteration of this reaction, an aromatic substrate such as benzene is functionalized by an alkyl halide in the presence of a Lewis acid, most commonly $AlCl_3$ (Scheme 1.2). The Lewis acid plays a critical role in the reaction since it makes the alkyl group sufficiently electrophilic to react with the π-electrons of the aromatic ring.

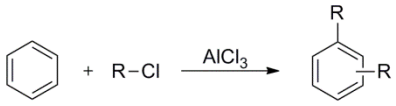


**Scheme 1.2.** Simplified Friedel-Crafts (FC) reaction.

While the initial discovery involved using alkyl halides as the electrophiles, it was later discovered that olefins could be used directly in conjunction with a combination of Lewis and Brønsted acids. The direct use of olefins is preferred in industry because the process is more straightforward. Olefins are readily available from the petroleum refining process, making them inexpensive to use.[9] One of the oldest industrial processes for the

synthesis of ethylbenzene was developed by Dow, which uses $AlCl_3$ as a catalyst with HCl as a co-catalyst to generate the essential ethyl carbocation from ethylene (Scheme 1.3).[9] The process runs under mild conditions (~100 °C and ~1 atm of ethylene). However, frequent regeneration of the $AlCl_3$ catalyst and the use of high $AlCl_3$ loading (~25%) is necessary in order to maintain high catalytic activity. Improvements based on FC catalysis have been made. For example, Monsanto developed a process that requires small amounts of $AlCl_3$ with very fast reaction times but uses elevated temperatures (160 - 180 °C).[9] Additionally, later HCl was replaced with HF since it is more volatile, which allows it to be more easily recycled.[9]

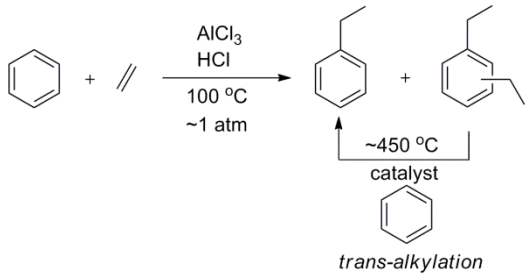


**Scheme 1.3.** Dow process for the synthesis of ethylbenzene.

From the 1930s to the mid-1960s, FC catalysis was the dominant method to produce alkyl arenes from arenes industrially.[9, 13] FC catalysis provided a way to make value added compounds from simple aromatic and olefinic substrates derived from petroleum by the net cleavage of a strong benzene C–H bond (BDE = ~110 kcal/mol) and formation of a new C–C bond. FC catalysis, however, has many drawbacks. Many of these drawbacks stem from the mechanism by which FC catalysis operates (i.e., electrophilic aromatic substitution) (Scheme 1.4).[7, 9, 11, 12] After initial protonation of the olefin by Brønsted acid, the π-electrons from benzene attack the newly formed carbocation to generate a Wheland intermediate in which the ring has been dearomatized.

Deprotonation of the Wheland intermediate by $[AlCl_4]^-$ rearomatizes the ring and forms ethylbenzene. Concomitantly, the acid catalysts (i.e., $AlCl_3$ and HCl) are regenerated.

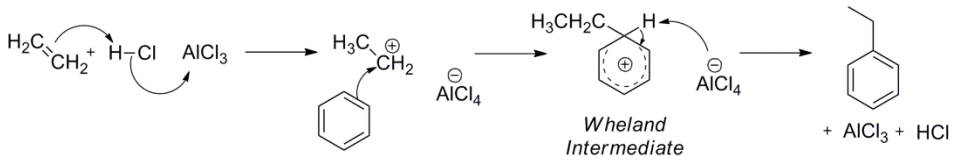


**Scheme 1.4.** Mechanism for Friedel-Crafts alkylation of benzene to produce ethylbenzene.

The ability of the benzene electrons to attack the carbocation is enhanced as the ring becomes more electron-rich. Thus, ethylbenzene will react 2 - 3 times more rapidly than benzene.[4] The result of this reactivity is that significant quantities of polyalkylated arenes form.[9] In order to increase the yield of the desired ethylbenzene, a second energy intensive trans-alkylation step is required (see Scheme 1.3) to convert di- and tri-alkylated benzenes into ethylbenzene. The success of this step is a result of the reversibility of the FC alkylation reaction. The trans-alkylation step involves the reaction of poly-alkylated benzenes with benzene over an acid catalyst to give the desired mono-alkylated product. In many cases, the poly-alkylated benzenes need to be separated from ethylbenzene by distillation, as the trans-alkylation reaction usually occurs in a separate reactor. The trans-alkylation reaction requires high temperatures, making this an energy intensive step.[2, 14] A related problem is that alkylation of electron-deficient arenes is not possible since the arene is not sufficiently electron-rich to react with the carbocation.[7, 12]

Additionally, the formation of the carbocation results in some limitations as well. For α-olefins, such as propylene, only the branched alkylbenzenes form (i.e., cumene forms over *n*-propylbenzene). This is the result of the rearrangement of a primary carbocation to a more stable secondary carbocation (Scheme 1.5), which is ~16 kcal/mol

more stable than the primary carbocation.[4] Thus, *n*-alkyl arenes cannot be made by FC catalysis using α-olefins. Long chain linear alkyl benzenes have had increased interest for their use in detergents. Industrially, linear alkyl benzenes are not truly linear. Rather, they get their name from being less branched than many other branched alkyl arenes. Truly linear alkylbenzenes cannot be made industrially, and thus, their utility has not been fully explored.[9, 13, 15] While FC acylation followed by a reduction can be used to generate linear alkyl arenes, this process is not industrially viable (Scheme 1.6).

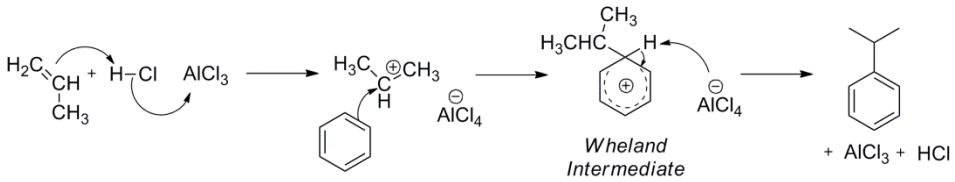


**Scheme 1.5.** Friedel-Crafts mechanism for alkylation of benzene with propylene.

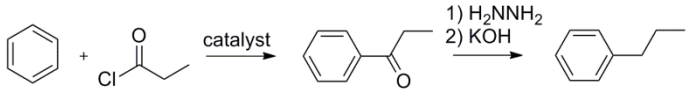


**Scheme 1.6.** FC acylation followed by Wolff-Kishner reduction to give linear *n*-propylbenzene.

Other drawbacks with FC catalysis are related to practical considerations. For instance, the isolation of the products is energy and time consuming due to the presence of acids in the reaction mixture. Thus, during isolation of the alkyl benzenes, it is necessary to neutralize the solution. This results in the problem of disposing large quantities of halogenated waste. Additionally, because the Brønsted acid catalysts are highly corrosive, they are dangerous to handle and require special reaction and storage vessels that will not corrode, which can be capital-intensive.[3, 9] HF, in particular, is highly corrosive and dangerous to handle.[13]

### 1.1.2 Zeolite Catalysis

Due to many of the drawbacks associated with traditional FC catalysis, including the large quantity of halogenated waste and the use of corrosive acids, alternative catalysts have been developed, namely heterogeneous catalysts based on zeolites. Prior to the development of zeolite catalysts, efforts were made to use acid-supported catalysts as a way to combat some of the problems with corrosion. However, it was found that the acids were released over time and the corrosion problems were not completely negated.[3, 9]

As a result, zeolites became the next step in the progression of catalysts for alkyl arene production.[1, 9, 13] Zeolites are porous crystalline aluminosilicates based on $SiO_4^{4-}$ and $AlO_4^{5-}$ tetrahedra. In natural zeolites, aluminum and silicon occupy all the tetrahedra and are linked by oxygen atoms. However, for synthetic zeolites these tetrahedra can be occupied by a range of atoms, including boron, gallium, germanium, iron, titanium, and others. Within the zeolite structure are cationic sites. By exchanging the cations within the zeolite structure, one has the ability to alter both the Brønsted acidity and Lewis acidity of the zeolite.[6, 16]

Additionally, zeolites have a variety of well-defined structures that result in a wide range of channel sizes and shapes. Zeolite pores typically have diameters between 0.25 and 1 nm. Zeolites also contain an inner volume with a high surface area that gives them the ability to absorb many reactants to mediate many reactions. Furthermore, zeolites are less environmentally hazardous (i.e., less corrosive, minimal problems with leaching, etc.), especially in comparison to tradition solid acid catalysts.[16]

One important property of zeolites that has contributed to their utility as catalysts for olefin hydroarylation is their shape selectivity.[4, 17] The shape selective catalyst can

differentiate between the reactants, products, or reaction intermediates according to their shape and size. There are three types of shape selectivity: 1) Reactant selectivity in which some of the molecules in a reactant mixture are excluded due to their shape and/or size; 2) product selectivity in which products formed that are too large for the pore size will not diffuse out of the zeolite; 3) restricted transition-state selectivity in which certain reactions are inhibited due to the shape/size of the transition state of that particular reaction. For ethylbenzene synthesis, transition state selectivity is primarily operative in improving yields of ethylbenzene, with product selectivity playing a secondary role (Scheme 1.7).[17] Despite these advantages, polyalkylation is still problematic, which necessitates a trans-alkylation step to improve yields of ethylbenzene.[1]

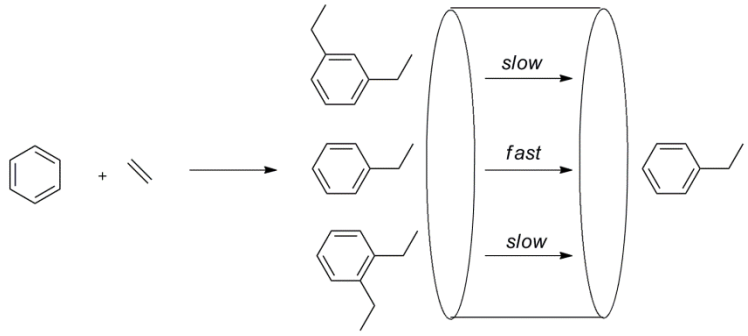


**Scheme 1.7.** Representation of product selectivity in ethylbenzene synthesis. Ethylbenzene diffuses out of pores more quickly than diethylbenzenes.

Because of the advantages discussed above, zeolites have become widely used in heterogeneous catalysis, including use in alkyl benzene production.[4, 13] In 1976, Mobil-Badger introduced the first industrial application of zeolite-catalyzed benzene alkylation. In this reaction setup, ethylbenzene was produced in the gas phase using a fix-bed reactor containing a zeolite based on ZSM-5.[4, 9] The ZSM-5 zeolites contain a three-dimensional ten-ring pore structure with high Si/Al ratio and are in the orthorhombic space group.

They are also hydrophobic and organophilic making them stable for catalysis in the presence of water.[16] The reaction requires high temperature (390 - 450 °C) and high pressure of ethylene (1.5 - 2 MPa). Besides the need for high pressures and temperatures, the catalyst had to be recycled every 40 - 60 days due to coke deposit in the zeolite pores. Despite this, the regeneration can be performed in situ by blowing air over the catalyst surface to allow for combustion of the coke. Due to the high frequency of recycling the catalyst, it was necessary to maintain two reactors to ensure high productivity. Later, due to the formation of polyalkylated benzenes, the addition of a trans-alkylation reactor further improved this technology. Two important improvements over traditional FC catalysis include the recyclability of the catalyst and that it is non-corrosive.[3, 4, 9]

Zeolite-catalyzed ethylbenzene production was further improved over the next few decades. In 1989, UOP/Lummus/Unocal developed a process using a zeolite Y catalyst, which has pore dimensions of approximately 0.74 nm x 0.74 nm,[4] that produced ethylbenzene in the liquid phase, allowing for lower energy consumption and increased catalyst longevity. This catalyst operates at lower temperatures (240 - 270 °C) than the Mobil-Badger catalyst. The change from the medium-pore ZSM-5 to the larger pore Zeolite Y was necessary due to problems with diffusion control.[3, 4, 9]

Other notable improvements in zeolite technology for ethylbenzene production include Lummus Global, Inc. and Chemical Research & Liscensing's CDTECH process in 1994. Here, a zeolite Y catalyst is used and includes the ability to withdraw ethylbenzene from the reaction by distillation with polyalkylbenzenes being sent to a separate trans-alkylation reactor. In 1995, Mobil/Raytheon used a MCM-22 catalyst in the liquid phase that allowed a catalyst lifetime of over 3 years before regeneration.[13] The

MCM-22 catalyst is more selective than zeolite Y or beta catalysts at comparable levels of activity. Trans-alkylation occurs in a separate reactor, initially in the vapor phase but more recently in the liquid phase. In 1996, Lummus/UOP introduced the EBOne process. In this technology alkylation occurs over zeolite beta-based catalyst EBZ-500 while trans-alkylation occurs over an EBZ-100 catalyst. These catalysts have excellent stability with relatively low costs of operation.[3, 4]

Zeolite catalysts have significantly improved benzene alkylation and their use has become wide-spread. However, in 2004 it has been estimated that >20% of ethylbenzene plants still use traditional FC catalysts with the remaining plants using zeolite-based catalysts.[1] Due to the large-scale production of ethylbenzene, it is expected that more improvement will be introduced in the future. It should be noted, however, that since zeolite catalysis operate by an acid-catalyzed reaction, several drawbacks remain, which include polyalkylation and the inability to make truly linear alkyl arenes when using α-olefins. Furthermore, the synthesis of styrene directly from benzene and ethylene is not possible by an acid-catalyzed mechanism.[7] These aspects, and the primary goals of catalyst development in the Gunnoe group, will be discussed below (see Section 1.3).

## 1.2 Transition Metal-Mediated C–C Coupling Reactions

While the petrochemical industry uses either traditional FC catalysis or zeolite catalysis for the production of alkylbenzenes, there have been significant advances in transition metal-catalyzed C–C bond forming reactions for the synthesis of alkyl aromatics that have proven to be very useful for synthetic organic chemistry with applications in fine chemicals.[18] While palladium has demonstrated the most utility for these reactions, other transition metals have applications including nickel, platinum, and copper.[19-24]

### 1.2.1 Types of C–C Cross-Coupling Reactions

There are several variations of cross-coupling reactions involving the formation of C–C bonds with aromatic substrates. Broadly, the reactions can take place by one of two general mechanisms.[18] The first, and most common, is a catalytic cycle involving a transmetallation step (Scheme 1.8, left). Examples of reactions that go by this mechanism include the Miyaura-Suzuki, Migita-Stille, and Songashira reactions.[18] In this mechanism, a low valent metal center oxidatively adds an Ar–X bond. A transmetallation step, typically involving an organometallic or organo-main group reagent, substitutes the M–X bond for a M–R bond. Finally, reductive elimination forms the new C–C bond and regenerates the active catalyst. A variation on this mechanism is shown on the right in Scheme 1.8, which, rather than a transmetallation step, the C–C bond forms via an insertion reaction. The Heck-Mizokori reaction goes by this catalytic cycle. The step that is common for both mechanisms is the oxidative addition of an organohalide or pseudohalide, such as triflate. (Ar–X for alkyl arene synthesis).[18]

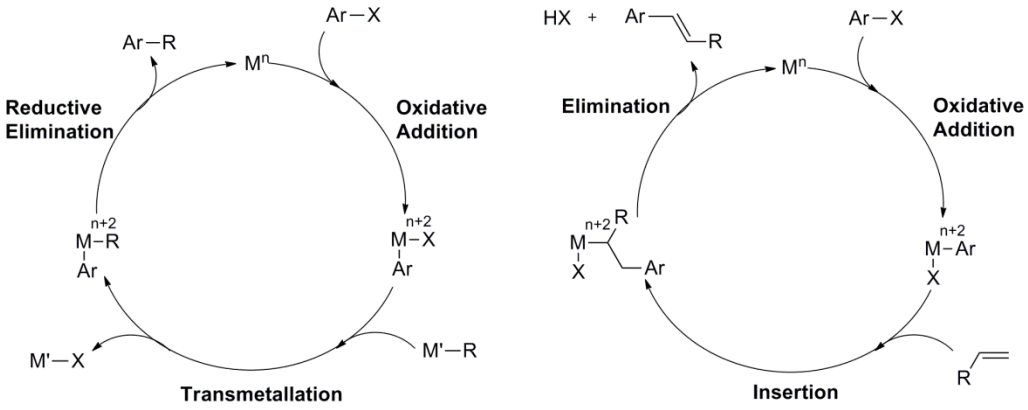


**Scheme 1.8.** C–C cross coupling catalytic cycle involving transmetallation (left) and insertion (right).

The first of these cross-coupling reactions was the Mizoroki-Heck reaction, which was discovered independently by the groups of Mizoroki and Heck in the early 1970s but was more fully developed by Heck in subsequent papers.[19, 25] A general Heck reaction is shown in Scheme 1.9. The reaction utilizes a Pd catalyst and couples an organohalide and an olefin to give a more substituted olefin. The palladium catalyst can be ligated by a variety of ligands;[18, 19] however, examples of ligand-free reactions are also known.[18, 19] As is the case for most Pd-catalyzed coupling reactions, the active catalyst is Pd(0), which can either be used directly or generated in situ from a Pd(II) source, with $Pd(OAc)_2$ being the most common. The Heck reaction has a large scope and is performed under relatively mild conditions. Many variations have been discovered, including intramolecular cyclization reactions and enantioselective reactions.[18, 20, 26]

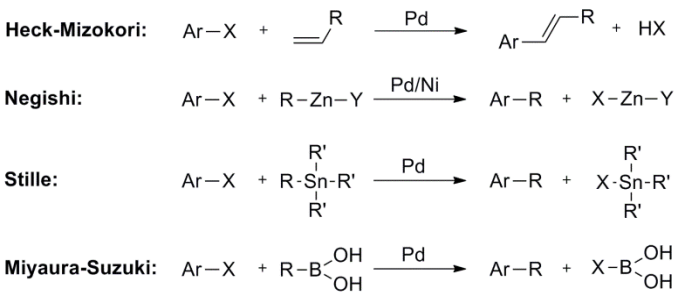


**Scheme 1.9.** General reactions schemes for four of the main C–C coupling reactions.

Shortly after the Heck reaction was discovered, Negishi reported a new cross coupling reaction that involved the formation of a new C–C bond by reaction of an organozinc reagent and an organohalide (Scheme 1.9).[26] The reaction works well with either a Pd catalyst or a Ni catalyst. Conveniently, the organozinc reagents can be prepared in situ, and there are a variety of organozinc reagents available. Additionally, the Negishi reactions generally exhibit good yield, selectivity, and tolerance of a variety

of functional groups. A related reaction is the Kumada coupling in which an organomagnesium compound is used in place of an organozinc reagent.[18]

Shortly thereafter, the Stille reaction was discovered.[19] The Stille reaction utilizes an organotin reagent as the coupling partner to the organohalide (Scheme 1.9). Palladium is the most common catalyst for this transformation, although examples of copper and nickel-catalyzed variations are known.[18] The reaction has excellent functional group compatibility, and the reactants and products are typically moisture and air stable. Related to the Stille reaction is the Hiyama reaction, which utilizes an organosilicon compound in place of the tin reagent, which helps combat issues relating to the toxicity of tin; however, at this point the Hiyama reaction is not nearly as versatile as the Stille reaction.[18, 19]

Another well-known C–C coupling reaction, and likely the most well-studied, is the Miyaura-Suzuki reaction, which is the coupling of an organohalide with an organoboron reagent (Scheme 1.9).[24] Palladium generally serves as the catalyst, although examples using other transition metals have been disclosed. Many boronic acids and esters are available commercially, and the boron by-product is easily removed from the reaction. There is good functional group tolerance and mild conditions can be used. In fact, variations are known in which water is used as the solvent.[18, 19, 24]

### 1.2.2 Drawbacks of C–C Coupling Reactions

In the previous section, some advantages of transition metal catalyzed C–C cross coupling reactions are highlighted. While these reaction are useful, which is evidenced by the 2010 Nobel Prize in Chemistry being awarded to Heck, Suzuki, and Negishi for their achievements,[27] commercial applications have been limited to fine and commodity

chemicals.[18] With the large demand of ethylbenzene and other alkylbenzenes, these coupling reactions are impractical for the petrochemical industry.

For all the reactions discussed, an organohalide is necessary. These reagents are often expensive, and stoichiometric halogenated waste is produced both during the preparation of Ar–X and as a result of their use as starting materials in coupling reactions. Furthermore, the use of a stoichiometric organometallic or organo-main group reagent increases the expense and requirements needed to handle waste, which is considerably toxic in some cases (e.g., tin). For both the organohalide and the organometallic/main group reagent, it is necessary to synthesize those compounds first before they can be used in forming a new C–C bond. Therefore, the reagents cannot be used directly from petroleum feedstocks.[7, 18, 28, 29]

## 1.3 Synthesis of Alkyl Arenes by Aromatic C–H Activation

Because of the drawbacks of traditional C–C cross coupling reactions and Friedel-Crafts/Zeolite catalysis, the synthesis of alkyl arenes by an alternative mechanism using a molecular transition metal catalyst is of interest. An idealized catalytic cycle is shown in Scheme 1.10. The reaction consists of two keys steps: 1) Olefin insertion into a metal–aryl bond and 2) aromatic C–H activation.[7, 29, 30] A more detailed discussion of each of these steps will be presented in Sections 1.3.1 and 1.3.2.

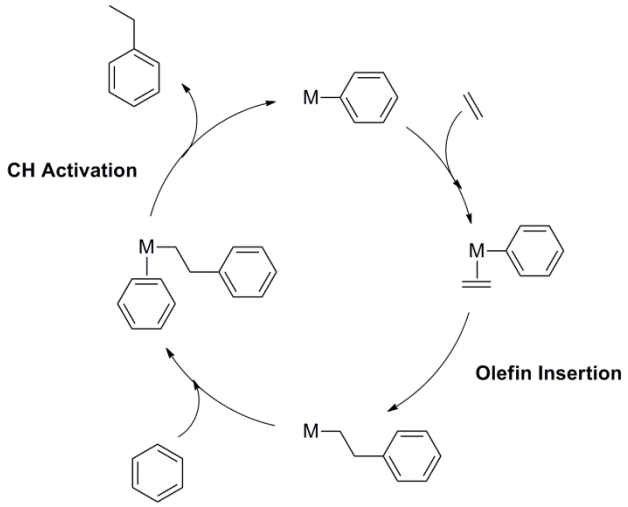


**Scheme 1.10.** Simplified catalytic cycle for olefin hydroarylation involving transition metal-mediated olefin insertion and C–H activation with benzene and ethylene as the substrates to give ethylbenzene.

By studying and developing catalysts based on a mechanism shown in Scheme 1.10, it is anticipated that there will be several advantages.[7, 30]

1) Avoid polyalkylation – In acid-based aromatic alkylations, ethylbenzene is a more activated substrate than benzene.[4] Thus, polyalkylation is common. A mechanism that involves C–H activation may afford selective single alkylation.
2) Control selectivity for α-olefins – A major drawback to current technologies is that the mechanism involves a carbocation, which will re-arrange to the more stable, internal carbocation.[4, 12] Since the proposed mechanism in Scheme 1.10 does not involve any carbocations, one may be able to control selectivity to favor linear alkyl arenes, which would complement current industrial processes.

3) Control 1,2-, 1,3-, and 1,4-selectivity – In cases where dialkylbenzenes are desirable, a mechanism like the one shown in Scheme 1.10 might allow for the controlled synthesis of the desired isomer. For example, in FC catalysis *ortho* and *para* substituted dialkylbenzenes are favored with the inability to control selectivity.[12]

4) Alkylation of electron-deficient arenes – Because the aromatic ring acts as a nucleophile in acid-catalyzed reactions, it is very challenging to alkylate electron-deficient arenes by this route. With a mechanism that involves olefin insertion and C–H activation, alkylations of electron-deficient arenes would be possible, which could be useful for the synthetic organic chemistry community.[9, 12]

5) Direct oxidative conversion of olefins and arenes to give vinyl arenes – As mentioned earlier, 99% of ethylbenzene is converted to styrene.[3, 4] Thus, it would be desirable to directly synthesize styrene from ethylene and benzene as well as synthesize other important vinyl arenes, such as *para*-methylstyrene.[9] This is not possible with FC or zeolite catalysis but is possible with transition metal catalysis involving C–H activation.

### 1.3.1 Transition Metal-Mediated C–H Activation

As mentioned above, C–H activation is a crucial step in the catalytic cycle shown in Scheme 1.10. As such, a discussion of some of the details and key examples of transition metal-mediated C–H activation is warranted. In this Dissertation, C–H activation will be defined as the cleavage of a C–H bond by coordination to a transition metal. In contrast, there are examples of C–H bond cleavage by single electron processes

in which the metal center does not directly interact with the C–H bond. A brief discussion of this will be addressed later (Section 1.5.2).

A simplified molecular orbital picture of the bonding interactions between a transition metal and a C–H bond is shown in Figure 1.1. The first bonding interaction is σ-donation from the C–H σ orbital to a vacant metal σ-symmetric orbital. The second interaction is π-back donation from a filled metal dπ orbital into the σ* orbital of the C–H bond. These interactions can reduce the bond order of the C–H bond and, thus, weaken or "activate" the bond.[31] A C–H bond coordinated to a transition metal is an example of a σ-complex, which is a key intermediate for C–H activation. σ-complexes are not limited to C–H bonds, having been observed for other covalent bonds.[32, 33] The σ-complex has been observed experimentally.[31, 34-36] Several studies using infrared spectroscopy as well as isotopic labeling/kinetic isotope effects have been reported that provide evidence for such intermediates.[35, 36] Furthermore, in 1998, Ball provided key evidence by obtaining $^1$H NMR spectral data of a σ C–H complex.[37] In this study, the low temperature (–80 °C) irradiation of a cyclopentane solution of $CpRe(CO)_3$ allowed for the observation of a multiplet at –2.32 ppm, which has been assigned to the C–H bond of cyclopentane that is coordinated to the metal center (Scheme 1.11). Later, Ball and coworkers observed coordination of cyclohexane to the metal center, which showed preference for the axial C–H bond.[38] Goldberg and Brookhart observed a Rh-methane σ-complex using a (PNP)Rh(I) methyl complex (Scheme 1.12).[39] In this experiment, the Rh–Me bond was protonated at –110 °C and monitored by NMR spectroscopy. Combined experimental and computation studies suggested the σ-methane complex is best described as a $\kappa^2$-C,H σ-complex.

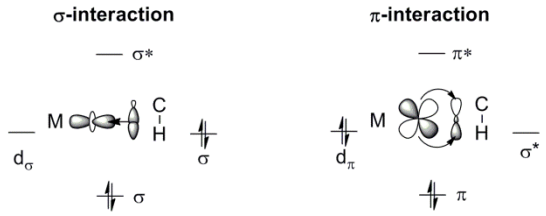


**Figure 1.1.** Simplified molecular orbital diagram for coordination of a C–H group to a metal.

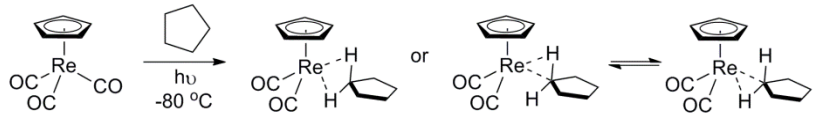


**Scheme 1.11.** Observation of C–H σ-complex by $^1$H NMR spectroscopy.

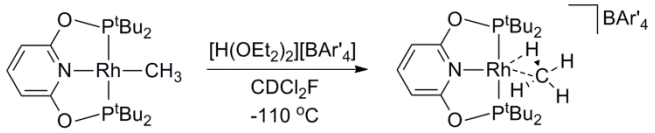


**Scheme 1.12.** Generation of Rh methane σ-complex at low temperature (Ar' = 3,5-bis(trifluoromethyl)phenyl).

The necessity of the C–H bond to coordinate to the metal center prior to activation is an important consideration because it requires a coordinatively unsaturated intermediate. As might be anticipated, the C–H bond is a weak ligand,[36, 40] which adds to the challenges of activating alkane C–H bonds. Aromatic C–H bonds tend to be more readily activated due to the availability of pre-coordination of the substrate through the π electrons and the strength of the incipient M–aryl bond.[31, 35]

The activation of C–H bonds by transition metals has been a significant area of research for the past 50 years, and significant developments and discoveries have been made.[7, 29, 31, 34, 35, 41-47] In order to discuss some of the important contributions in this arena, this survey will be guided by the four different types of C–H activation

mechanisms: 1) Oxidative addition (OA), 2) σ-bond metathesis (SBM), 3) electrophilic substitution, and 4) 1,2-addition of C–H bonds across M–X bonds (X = NR, OR, $NR_2$, etc).[42] The current discussion will be focused on other metals besides Fe, as this will be addressed separately at another point (Section 1.5.2). It is worth noting that oxidative addition and σ-bond metathesis are most relevant for olefin hydroarylation catalysts, and the detail of discussion for each of these mechanisms will reflect that.[7]

**1.3.1.1 C–H Activation by Oxidative Addition (OA)**

The oxidative addition of a C–H bond typically occurs with a low valent transition metal and involves the direct insertion of that metal into the C–H bond, which results in the +2 increase in oxidation state of the metal (Scheme 1.13).[42, 48] In some cases, C–H activation by oxidative addition can be promoted by chelation of a Lewis base attached to the substrate possessing the C–H bond.[28, 31, 35] This pre-coordination brings the C–H bond in close proximity to the metal and allows it to be more easily activated. An example of this phenomenon can be seen in the case of $(PPh_3)_3IrCl$.[35, 49] Upon heating, one of the C–H bonds from a phenyl group on $PPh_3$ oxidatively adds to give the correspond Ir(III)–H complex (Scheme 1.14). The concept of chelate-assisted C–H activation has been utilized for the functionalization of hydrocarbons since it provides a means to regioselectively functionalize hydrocarbons.[50, 51]

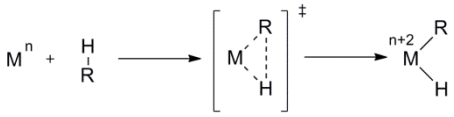


**Scheme 1.13.** Schematic representation of C–H activation by oxidative addition.

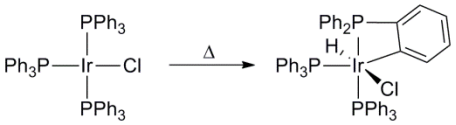


**Scheme 1.14.** Cyclometallation of $PPh_3$ on $(PPh_3)_3IrCl$ by C–H oxidative addition.

C–H bond oxidative addition is also known to proceed through a one-electron oxidation of the metal. For instance, Wayland reported an example of a Rh(II) porphyrin complex that activates methane under mild conditions to give a $Rh–CH_3$ and a Rh–H complex. (Scheme 1.15).[52] Mechanistic studies suggested a bimetallic, highly linear transition state on the basis of a highly negative $\Delta S^{\ddagger}$ (–37 cal $mol^{-1}$ $K^{-1}$) and a large primary kinetic isotope effect (8.6).

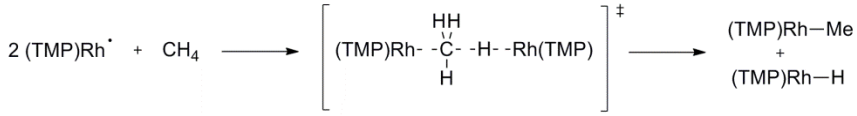


**Scheme 1.15.** Methane CH activation by Rh porphyrins (TMP = tetramesitylporphyrinato).

As mentioned earlier, intermolecular C–H activation is more challenging than chelate-assisted C–H activation. This is because the inability for the substrate to pre-coordinate to the metal center raises the $\Delta S$ for the reaction. With intermolecular C–H activation by oxidative addition, arenes are activated more readily than alkanes. Consequently, there are several examples of transition metal complexes oxidatively adding aromatic C–H bonds.[31, 35] One example, and often considered the first example, is the $(dmpe)_2Ru$ fragment (dmpe = 1,2-bis(dimethylphosphino)ethane).[53] The reactive Ru(0) complex is generated in situ by photolysis of the Ru(II) dihydride, which goes on to add a C–H bond of naphthalene (Scheme 1.16). Another key example was reported by

Green and co-workers in which photoelimination of dihydrogen from $Cp_2WH_2$ in the presence of benzene led to $Cp_2W(Ph)(H)$ (Scheme 1.16).[54]

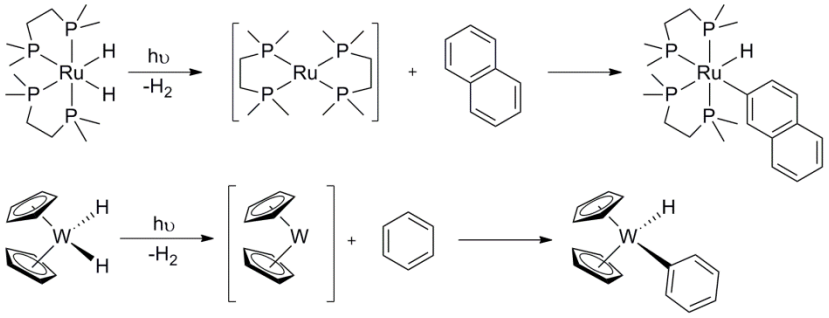


**Scheme 1.16.** Early examples of aromatic C–H activation by oxidative addition.

About 15 years after these early examples of aromatic C–H activation, Bergman and Graham independently discovered that Cp*Ir complexes could mediate the oxidative addition of alkane C–H bonds.[55, 56] For example, Bergman's $Cp^*Ir(PMe_3)H_2$ complex photolytically releases $H_2$ and oxidatively adds a C–H bond from cyclohexane. Graham's $Cp^*Ir(CO)_2$ photolytically extrudes CO to generate a coordinatively unsaturated metal fragment that can activate neopentane among other hydrocarbons (Scheme 1.17).

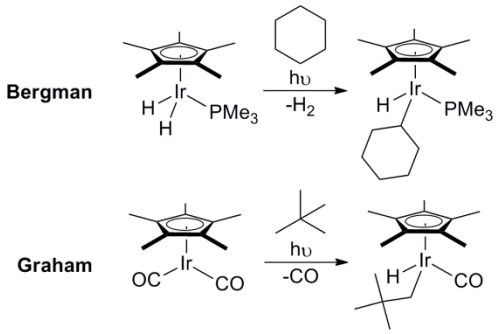


**Scheme 1.17.** Alkane C–H activation by Cp*Ir(I) complexes.

A key finding from Bergman's work, and later studied in detail by many other groups, is that the metal complex preferentially activates the stronger C–H bond.[55, 57] In other words, for *n*-alkanes the metal center breaks the primary C–H bond (BDE = ~98

kcal/mol) over the secondary C–H bond (BDE = ~95 kcal/mol). Selectivity, both thermodynamic and kinetic, is of critical importance for extending such C–H activation reactions to functionalization reactions. Briefly, the reason for this preference is, in part, based on thermodynamics.[57-59] The difference in bond energies between M–$C_{primary}$ and H–$C_{primary}$ is greater than the difference in bond energies between M–$C_{secondary}$ and H–$C_{secondary}$ (Scheme 1.18). Thus, the formation of the stronger M–C bond provides a thermodynamic driving force. A similar rationale based on thermodynamics can be used for the preference for metal centers to oxidatively add aromatic C–H bonds over alkane C–H bonds.[57] Also at play here is the ability for aromatic molecules to coordinate to the metal center through the π electrons, which provides a kinetic advantage for aromatic C–H bond activation.

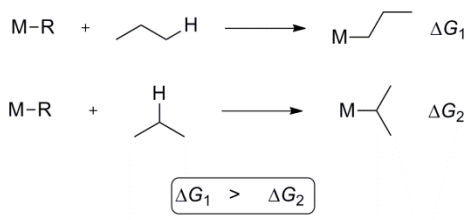


**Scheme 1.18.** Thermodynamic preference for C–H activation of primary C–H bonds over secondary C–H bonds.

Jones and co-workers utilized the Tp´Rh(C≡NR) (Tp´ = tris(3,5-dimethylpyrazolyl)borate) metal fragment to study the thermodynamics of various C–H bonds relative to the M–C of the respective products from oxidative addition (Scheme 1.19).[60] By a series of competition experiments with different hydrocarbons, the ratios of products could be used to determine the relative activation barriers for the oxidative addition of each hydrocarbon. Furthermore, in $C_6H_6$ all the alkane products converted to Tp´Rh(C≡NR)(Ph)(H), which allowed for the determination of the activation barrier for

the R–H reductive elimination. This study demonstrated that the change in M–C bond strength is ~1.2 times greater than the change in C–H bond strengths, which rationalized the observed selectivity where the activation of the stronger C–H bond is thermodynamically and kinetically preferred.

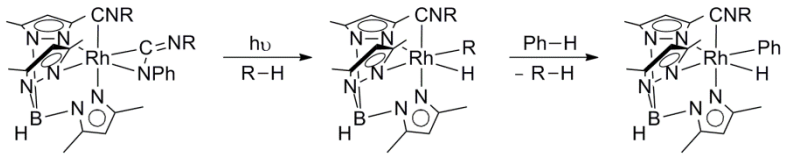


**Scheme 1.19.** Reaction scheme for the determination of relative M–C bond strengths using Tp'Rh(C≡NR) fragment.

Thus far, the complexes described that undergo C–H oxidative addition have been metals in low oxidation states. While many of the seminal examples have followed this pattern, it is relevant to point out that there are instances where the starting complex and product are at the same oxidation state by undergoing an oxidative addition/reductive elimination sequence. Furthermore, in some cases, oxidative addition occurs at higher oxidation states. As an example, Bergman reported that the cation $[Cp^*Ir(PMe_3)(L)Me]^+$ (L = $CH_2Cl_2$ or $N_2$) activates hydrocarbon C–H bonds with very high selectivity to give the corresponding $[Cp^*Ir(PMe_3)(L)(R)]^+$ complexes under very mild conditions, at temperatures as low as –10 °C.[61, 62] Experimental and computational mechanistic studies have demonstrated that reaction likely proceeds by initial $CH_2Cl_2$/RH ligand exchange followed by oxidative addition of the substrate C–H bond. Finally, reductive elimination releases $CH_4$ (Scheme 1.20).[63, 64]

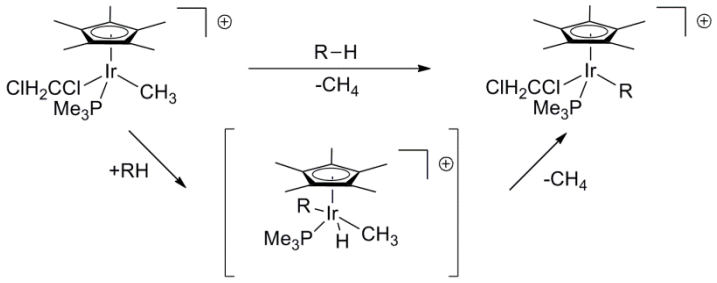


**Scheme 1.20.** C–H activation at Ir(III) goes by oxidative addition/reductive elimination.

### 1.3.1.2 C–H Activation by σ-Bond Metathesis (and Oxidative Hydrogen Migration)

Many significant contributions to C–H activation have been reported using low valent metal complexes that promote oxidative addition of the C–H bond. The ability for the metal center to π-back bond into the C–H σ* is often important for breaking C–H bonds by this mechanism.[35] However, in the early 1980s, Watson reported the C–H activation of hydrocarbons using $Cp^*_2LuMe$ (Scheme 1.21).[65] Lu(III) is a $d^0$ complex, and thus does not have available d-electrons to donate to the C–H bond. In cases where the metal has a low d-electron count, σ-bond metathesis (SBM) is often the mechanism invoked for C–H bond activation.[35, 42] Scheme 1.22 shows the mechanism for SBM with its 4-center, 4-electron transition state. In SBM, coordination to the metal center makes the C–H bond more acidic, which is then deprotonated by the nucleophilic M–R.

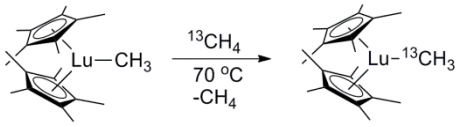


**Scheme 1.21.** C–H activation of methane by a $d^0$ lutetium complex.

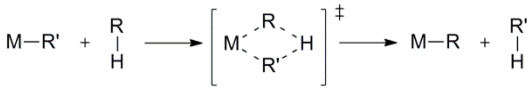


**Scheme 1.22.** Mechanism of C–H activation by σ-bond metathesis (SBM).

Many early transition metal and lanthanide complexes have been reported to activate C–H bonds by a SBM mechanism since Watson's initial publication. For instance, shortly after Watson's landmark publication, Bercaw and co-workers demonstrated C–H activation by a scandium complex (Scheme 1.23).[66] Additionally, this report demonstrated a catalytic H/D exchange between hydrogen and hydrocarbons by a proposed SBM C–H activation mechanism. From these studies, the authors were able to conclude that there is an increase in reactivity of C–H bonds with increasing s-character of the reacting bonds. Put another way, C–H activation is more facile for sp > $sp^2$ > $sp^3$ C–H bonds. Considering the 4-centered, 4-electron transition state (Scheme 1.22), the transition state would be expected to be more stabilized with the more non-directional (i.e., more s-character) the reacting orbitals are, allowing for better overlap. This observation is, indeed, consistent with the reactivity trends demonstrated for some oxidative addition reactions.[57, 60]

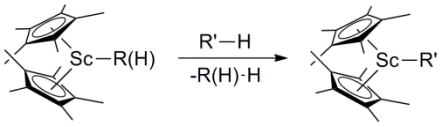


**Scheme 1.23.** C–H activation by a Sc(III) complex.

An important extension of Sc-mediated C–H activation was the report of catalytic methane functionalization by Sadow and Tilley.[67, 68] Scandium is able to catalyze both the dehydrosilylation of methane and the hydromethylation of olefins. Due to the

similarities between hydromethylation of olefins and olefin hydroarylation, discussion will be limited to this catalytic example.[68] The complex studied was $Cp^*_2ScCH_2CMe_3$, which stoichiometrically activates alkane C–H bonds including $CH_4$. An important observation was that C–H activation of $CH_4$ was more facile than other hydrocarbons, including $C_6H_6$ because this is opposite the trend observed for other C–H activation reactions. Rigorous kinetic analysis suggested two competitive pathways for methane activation. The first is the traditional direct metalation via a SBM mechanism. Another mechanism is also operative that involves catalysis by a Sc–H complex that is generated in situ, which has been confirmed by the rate enhancement with addition of independently prepared Sc–H. In this mechanism, the Sc–H activates $CH_4$ to release $H_2$, which then hydrogenates the Sc– $CH_2CMe_3$ complex. The complex $Cp^*_2ScCH_2CMe_3$ catalyzes the addition of a methane C–H bond across the double bond of propylene (Scheme 1.24). The substrate scope is limited to propylene and methane and the activity of the catalyst is quite low, giving 4 TOs of isobutene overnight at 80 °C, with the slow step being olefin insertion.[68] Nonetheless, catalytic C–H functionalization reactions involving SBM are quite rare, making this a substantial advancement in C–H activation chemistry.

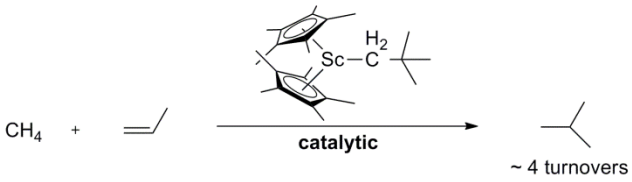


**Scheme 1.24.** Hydromethylation of propylene catalyzed by a Sc complex.

More recently, $d^6$ and $d^8$ transition metals have been suggested to activate C–H bonds by a mechanism resembling SBM. Due to the ability of the metal center to donate

d-electrons to the activated hydrogen, the transition state would be 4 centered, 6-electrons (Scheme 1.25). Thus, the transition state might be considered more oxidative (i.e., the metal center is donating electrons) in nature compared to a traditional SBM transition state. This property of the transition state has led to the name of oxidative hydrogen migration (OHM) for this type of mechanism.[69] In SBM there is minimal contact between the metal center and the transferred hydrogen, but that is not the case for OHM where a partial bond can be observed between the metal center and the hydrogen, somewhat akin to oxidative addition.[33, 69, 70] It is helpful to consider a continuum between oxidative addition and SBM in which OHM occupies the midpoint.[33, 69] As might be anticipated, this mechanism is operative in later metals with occupied d orbitals where there is some π-back bonding from the metal center to the C–H bond. In the case of OHM, the transition state takes a more kite-like structure due to more significant interaction with the transferred hydrogen.[71] The OHM mechanism was originally coined by Goddard and co-workers with another common name being σ-complex-assisted metathesis (σ-CAM). However, the name OHM will be used in this discussion.[33]

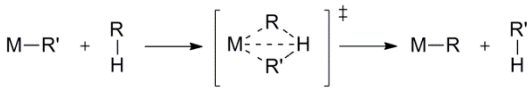


**Scheme 1.25.** Mechanism for C–H activation by oxidative hydrogen migration (OHM).

An important study that highlights the continuum mentioned above and helps provide some notion of an OHM mechanism was a computational study of methane activation by group 8 complexes of the Tp (Tp = hydridotris(pyrazolyl)borate) ligand by Eisenstein and co-workers.[72] In this report, the authors calculated that methane activation occurs by a SBM mechanism for Fe and oxidative addition/reductive elimination for Os.

However, it was noted that the mechanism for Ru is concerted as in SBM but still has features of oxidative addition. This continuum can be explained by the fact that the more electron rich the metal center (i.e., 3d<4d<5d), the greater propensity for the metal center to favor a higher oxidation state.[72]

This concept has been further expounded by Goddard and co-workers in their computational study of our group's TpRu(CO)(NCMe)Ph olefin hydroarylation catalyst and Periana's Ir(III) catalyst.[69, 73] In the calculated C–H activation transition states, there is a 1.61 Å Ru–H interaction and an Ir–H distance of 1.58 Å (Figure 1.2). The M–H interactions are on the order of a typical M–H bond, but the mechanism is concerted, which is distinct from oxidative addition.[69, 73] In the computational study, no stable Ru(IV) or Ir(V) intermediates could be isolated, ruling out oxidative addition. The bond between the metal centers and the transferred hydrogen is not consistent with SBM and is thus evidence for a distinct mechanism. Our group in collaboration with the Cundari group (U. North Texas) calculated a transition state for C–H activation by TpRu complexes consistent with OHM.[74]

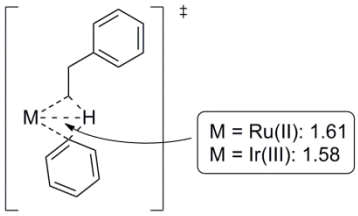


**Figure 1.2.** Calculated M–H bond lengths in OHM transition state for Ru and Ir hydroarylation catalysts. Bond lengths in Å. M = Tp(CO)Ru(II) or *cis*-$(acac)_2$Ir(III).

### 1.3.1.3 C–H Activation by 1,2-Addition Across M–X Bonds

Another mechanism for C–H activation is called 1,2-addition across M–X bonds (X = NR, O, $NR_2$, OR, etc.).[71] The mechanism for 1,2-addition across M–X bonds closely

resembles that of SBM in that it is a concerted mechanism involving four atoms. The major difference is the presence of a lone pair of electrons on the X ligand (Scheme 1.26). The lone pair has been implicated as having an effect during the transition state, making the transition state for 1,2-addition across M–X bonds a six electron transition state.[71, 75, 76] The first examples of C–H activation by 1,2-addition across M–X bonds were reported independently by the groups of Bergman and Wolczanski using Zr imidos.[77, 78] Horton and co-workers have reported an example of a vanadium imido complex, and Mindiola and co-workers have reported an example of a scandium complex for 1,2-addition across a Sc–NAr bond.[79, 80] More recently, late transition metals have been demonstrated to mediate C–H activation by 1,2-addition across M–X bonds. Later transition metals have the ability to be more redox flexible allowing the possibility to develop catalytic reactions.[71] The Gunnoe group reported H/D exchange of benzene across a Ru–heteroatom bonds, and Periana and coworkers reported C–H activation of benzene across an Ir(III)–OMe bond.[81-83]

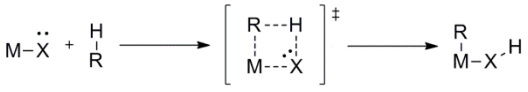

**Scheme 1.26.** Mechanism for C–H activation by 1,2-addition across M–X bonds (X = NR, O, $NR_2$, OR).

### 1.3.1.4 C–H Activation by Electrophilic Substitution

The final mechanism of C–H activation that will be discussed herein is known as electrophilic substitution. The mechanism for electrophilic substitution can be seen in Scheme 1.27. Through coordination of the C–H bond, the H atom becomes acidic and is deprotonated by non-coordinated base. Protonation of the X group completes the

transformation. In general, electrophilic late transition metals mediate this transformation, often in polar media.[31, 42]

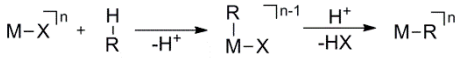

**Scheme 1.27.** Mechanism for C–H activation by electrophilic substitution.

An early example of electrophilic substitution is Shilov's Pt-catalyzed alkane functionalization in protic media (Scheme 1.28).[31, 35] Using Pt(II) salts, Shilov discovered that H/D exchange of alkanes occurs in DOAc. An important observation is a preference for the activation of stronger C–H bonds. For example, in branched alkanes, H/D exchange was slower for the more hindered position, suggesting a metal-mediated process. With the addition of a Pt(IV) oxidant and use of water as the solvent, catalytic conversion of RH to RCl and ROH was observed. The mechanism for this transformation involves initial electrophilic alkane activation by Pt(II), followed by oxidation of Pt(II)–R to Pt(IV)–R by the stoichiometric Pt(IV) oxidant. Nucleophilic attack of the R group by water or $Cl^-$ completes the functionalization (Scheme 1.29).

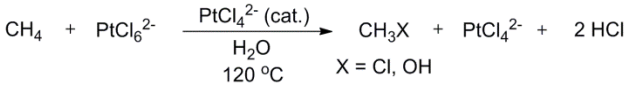

**Scheme 1.28.** Functionalization of methane via electrophilic activation (Shilov system).

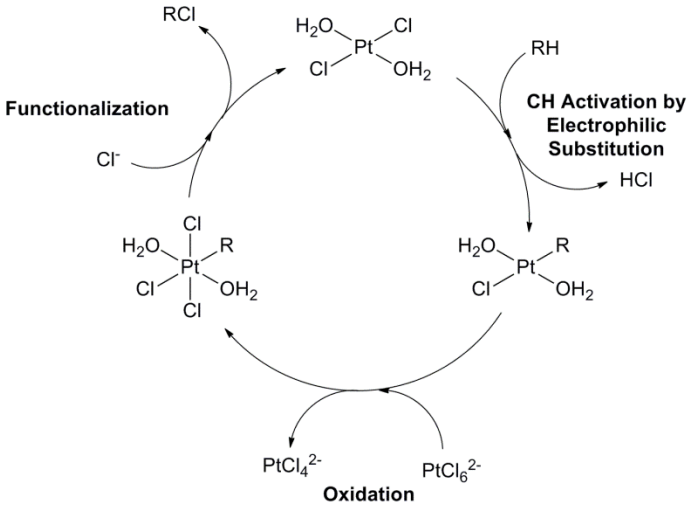


**Scheme 1.29.** Proposed catalytic cycle for alkane function by the Shilov system.

The mechanism of C–H activation in Shilov's Pt(II) system has been debated.[35, 84, 85] Using model compounds, some groups have suggested that C–H activation may go by oxidative addition. Others favor the single-step electrophilic activation. Computational studies performed by Siegbahn and Crabtree on C–H activation on Pt(II) indicate that oxidative addition is slightly lower in energy.[86]

An improvement to the Shilov system was made with the Periana/Catalytica system in which a bipyrimidine Pt(II) catalyst effected the functionalization of methane to methylbisuflate in oleum (Scheme 1.30).[87] Instead of an expensive Pt(IV) oxidant, $SO_3$ serves as the oxidant.[87] However, the production of <1 M of methyl bisulfate limits the industrial viability of this reaction since it requires the challenging separation of the methyl bisulfate from sulfuric acid.[88] A computational study demonstrated that this Pt complex activates C–H bonds by the electrophilic substitution mechanism.[89]

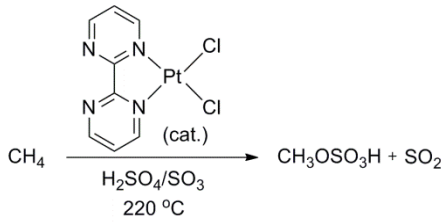


**Scheme 1.30.** Periana-Catalytica system for methane functionalization.

### 1.3.2 Insertion of Carbon–Carbon Multiple Bonds into Metal–Aryl Bonds

As mentioned earlier, catalytic olefin hydroarylation as shown in Scheme 1.10 requires the insertion of an olefin into a M–Ar (Ar = aryl) bond as the C–C bond forming step. Transition metals are capable of inserting a variety of unsaturated molecules into M–R (R = H, alkyl or aryl) bonds, including carbon monoxide, carbon dioxide, isonitriles, alkynes, olefins, and many more.[32, 48] Depending on the molecule, insertion can take place by 1,1-migratory insertion or 1,2-migratory insertion (Scheme 1.31). Since insertion results in a coordinatively unsaturated metal complex, insertion is often accompanied by the coordination of another ligand.[48]

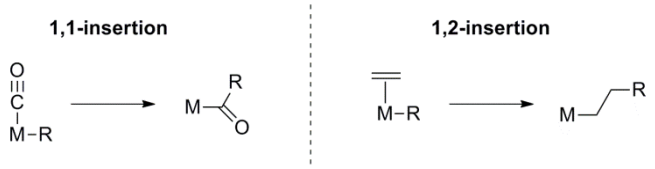


**Scheme 1.31.** The 1,1-insertion of CO and the 1,2-insertion of $C_2H_4$ into M–R bond.

One model for insertion is a nucleophilic attack of the hydrocarbyl ligand on the unsaturated substrate. The transition state for the insertion of an olefin into a M–R is shown in Figure 1.3. The olefin becomes polarized in the transition state such that the β carbon develops positive charge as its forms a new σ bond with the R group.[48] Thus, one might anticipate that olefin insertions should be facilitated by more electrophilic metal

centers (i.e., more electron-deficient) as well as polarized olefins since the partial charges that develop in the transition state would be better stabilized.

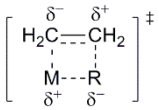

**Figure 1.3.** Olefin insertion transition state with partial charges.

Another way to examine the propensity of a metal center to mediate olefin insertion is to study the bonding interactions in an $\eta^2$-olefin complex that precedes olefin insertion (Figure 1.4).[32, 48] There are two bonding interactions in $\eta^2$-olefin complexes, olefin to metal σ bonding and metal to olefin π bonding. A qualitative molecular orbital diagram for the π system in an olefin provides reasoning for these bonding interactions. The overlap of parallel p orbitals for each C in the olefin gives a π bonding orbital and a π* antibonding orbital. When an olefin binds to a metal center in an $\eta^2$ fashion, a single face of the π orbital is oriented toward the metal center. If the metal has a vacant d orbital of σ symmetry, donation of electron density from the olefin π orbital to the vacant d orbital occurs. Additionally, the olefin π* orbital is π symmetric with filled d orbitals of the metal center. Thus, a filled metal d orbital will donate electron density into the olefin π* orbital. While both of these interactions contribute to the overall bonding in $\eta^2$ olefin complexes, for π-basic transition metal complexes, the π-back-bonding typically dominates. Since the dominant bonding interaction is expected to be dπ → π* back bonding from the metal center to the olefin in metals with filled dπ orbitals, a metal center that is more electron-rich or π-basic would be expected to have more significant overlap with the olefin π* orbital (Figure 1.4). This would result in a more stable M–$\eta^2$-olefin, which would provide a lower ground state prior to olefin insertion, making olefin

insertion less facile. This concept will be revisited during the discussion of previous olefin hydroarylation catalysts (Section 1.4).[30]

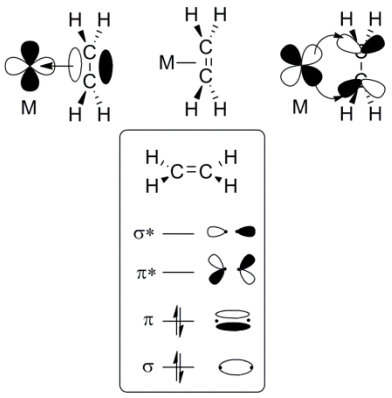


**Figure 1.4.** Transition metal dπ to π* back bonding and olefin σ donation to metal dσ orbital in $\eta^2$-olefin complex.

### 1.3.3 Catalytic Olefin Hydroarylation

In Scheme 1.10, a catalytic cycle for olefin hydroarylation by transition metal-mediated olefin insertion and aromatic C–H activation is shown.[7, 30] One of the greatest challenges for developing transition metal catalysts for this reaction is avoiding any one of the many side reactions that are anticipated to have similar energetic profiles to the steps of the catalytic cycle. For example, a catalytic cycle with four possible side reactions is shown in Scheme 1.32.

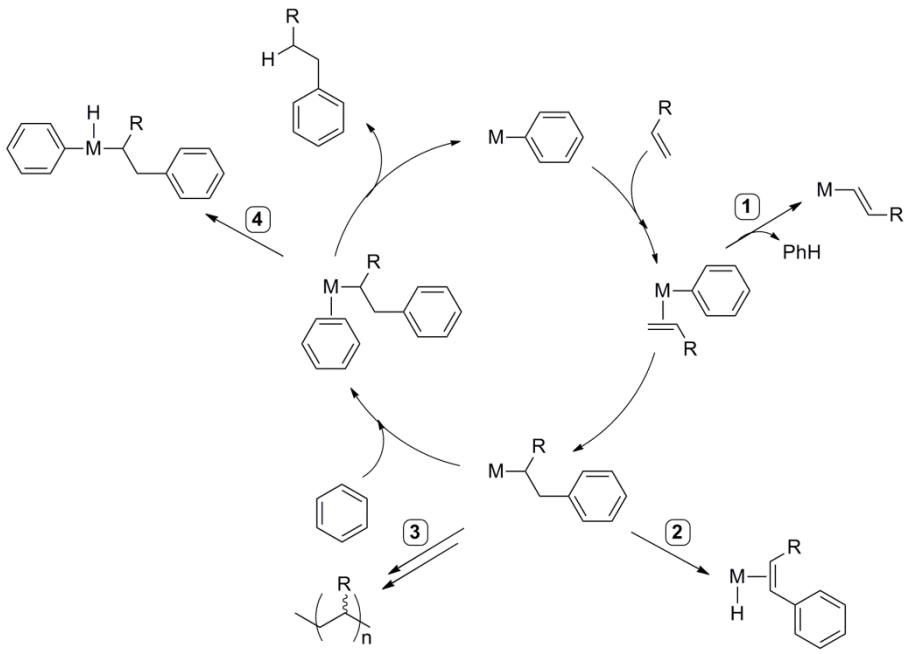


**Scheme 1.32.** Catalytic cycle for olefin hydroarylation with potential side reactions.

The potential side reactions include:[7, 30]

1) C–H activation of the olefin – An olefinic $sp^2$ C–H bond and an aromatic $sp^2$ C–H bond have similar bond dissociation energies (~110 kcal/mol). Thus, prior to olefin insertion, the metal can activate the olefin's C–H bond and remove the catalyst from the cycle.
2) Irreversible β-hydride elimination – After olefin insertion, the phenethyl intermediate can undergo β-hydride elimination. If this is reversible, then the catalyst can continue along the cycle. If it is irreversible, it results in a M–H species that may not be catalytically active or may be unstable. In some cases, formation of vinyl arene is desirable. Thus, a fundamental goal is to control β-hydride elimination sequences.[7, 90]
3) Polymerization/Oligomerization - If olefin insertion is too facile, multiple consecutive insertions may take place leading to polymers or oligomers.

4) Irreversible oxidative addition of C–H bond – Especially for low valent metals and second or third row metals, C–H activation may occur by an oxidative addition mechanism. If the metal is too reducing, the oxidative addition could place the catalyst in a thermodynamic sink.

Due to these competitive side reactions, the ability to develop catalysts for olefin hydroarylation is a substantial challenge. Successful catalysts must be active for C–H activation but kinetically favor the activation of aromatic $sp^2$ C–H bonds over olefin $sp^2$ C–H bonds. Furthermore, active catalysts must mediate olefin insertion with a rate within a narrow window since, if too slow, polymerization is possible and olefin $sp^2$ C–H activation becomes more competitive. Designing catalysts that can accomplish this balancing act is not trivial; however, the use of homogeneous transition metal complexes allows for the ability to tune the catalysts and study the impact of electronics and sterics on the overall catalytic cycle. Some of these details will be addressed in the following sections.

## 1.4 Previous Examples of Transition Metal Catalysts for Olefin Hydroarylation

In the following sections, key examples of catalytic olefin hydroarylation will be discussed. Because the emphasis of this project is to develop catalysts for unactivated arenes and olefins (e.g., benzene and ethylene), emphasis will be placed on the development and studies of transition metal catalysts for catalytic olefin hydroarylation of unactivated substrates. However, in order to provide historical context for these catalysts, some discussion will be focused on early catalysts for activated substrates.

### 1.4.1 Catalysts Involving Chelate-Assisted C–H Activation

As mentioned previously, chelation-assistance provides a means to control the regioselectivity and facilitate the activation of C–H bonds. An early example of using a

transition metal catalyst to add an arene C–H bonds across an olefin was reported by Jordan in 1989 where he used the cationic $[Cp_2Zr(Me)(THF)]^+$ as a pre-catalyst for the C–H addition of α-picoline across propylene in the presence of $H_2$ (Scheme 1.33).[91] Greater than 40 TOs of the functionalized product were obtained with catalysis ceasing only after starting materials were consumed. The reaction occurred at room temperature over the course of one day. The coupling reaction was highly selective with no other products observed, but the substrate scope was limited to propylene and α-picoline. Coordination of the pyridine through the nitrogen rationalizes the high selectivity for C–H functionalization at the *ortho* position.

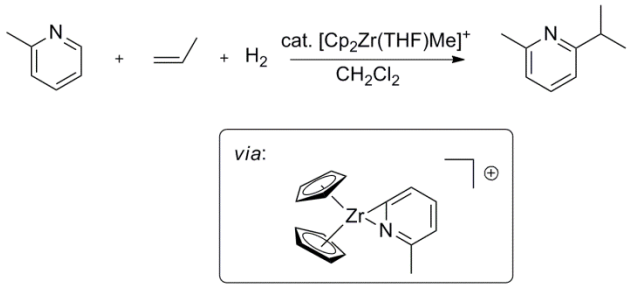


**Scheme 1.33.** Zr-catalyzed C–H addition of α-picoline to propylene.

A seminal work in the area of olefin hydroarylation came from Murai and co-workers in 1993.[92] In this report, the authors demonstrated the catalytic addition of aromatic C–H bonds of aromatic ketones to olefins by chelate-assisted C–H activation using the complex $RuH_2(CO)(PPh_3)_3$ (Scheme 1.34). The reaction is highly efficient, and it did not require the use of a gross excess of one of the starting materials (e.g., as a solvent), which was unprecedented at the time. Moreover, for the aromatic substrates studied, the reaction is 100% regioselective for the *ortho* position, suggesting the involvement of the carbonyl functionality to direct the C–H activation. Since this work,

several reports of chelate-assisted hydroarlyation of olefins and alkynes have been published, which highlights the broad interest of such reactions for organic synthesis.[28, 50, 51]

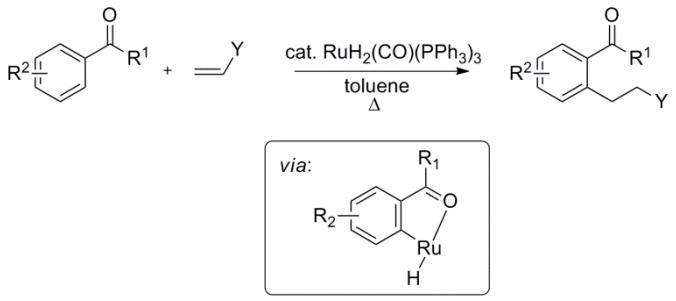


**Scheme 1.34.** Ru-catalyzed C–H addition of aromatic ketones to olefins (Y = $SiR_3$, alkyl; $R^1$ = alkyl chain or ring; $R^2$ = alkyl group or fused ring).

### 1.4.2 Intermolecular Hydroarylation using Heteroaromatic Substrates

Heteroaromatic molecules are important motifs in many natural products and compounds of biological and medicinal relevance. As such, the functionalization of heteroaromatics by C–H addition across C–C multiple bonds is an active area of interest.[93, 94] In the early 2000s, Bergman and Ellman published several papers demonstrating the addition of heteroaromatic C–H bonds across multiple C–C bonds.[95] In one variation, they demonstrated the first example of intermolecular hydroheteroarylation of an olefin using a Rh-phosphine catalyst (Scheme 1.35). One important observation from this study was that in cases where the olefin could isomerize to a more substituted olefin (e.g., α-olefins to internal olefins) they observed selectivity for the linear product. Subsequent studies demonstrated that the mechanism of the transformation involved the intermediacy of an *N*-heterocyclic carbene (NHC)-Rh complex. This system has very good substrate scope and could be used in the synthesis of biologically-active compounds.[95]

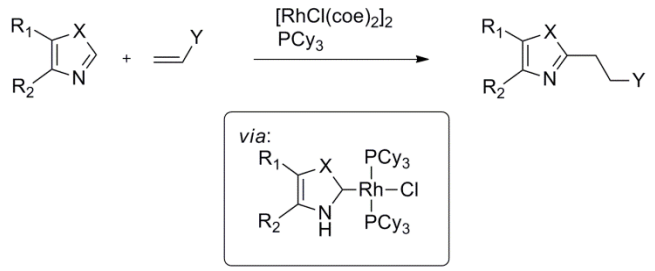


**Scheme 1.35.** Rh-catalyzed hydroarylation of *N*-heterocycles involving the intermediacy of an NHC-Rh complex.

Several years later, Hiyama and co-workers disclosed the Ni-catalyzed hydroheteroarylation of vinyl arenes (Scheme 1.36).[96] The Ni catalyst employed used an NHC ligand , and the mechanism is proposed to go through oxidative addition of the C–H bond to Ni(0) with olefin insertion and subsequent reductive elimination. Several different heterocycles are capable of being functionalized, including benzothiazoles, benzoimidazoles, and benzofurans.[96]

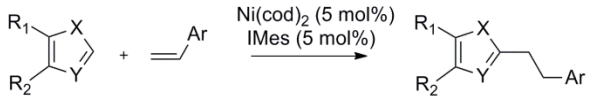


**Scheme 1.36.** Ni-catalyzed hydroarylation of vinyl arenes (IMes = 1,3-bis(2,4,6-trimethylphenyl)imidazol-2-ylidene).

Our group has also reported examples of hydroarylation using heteroaromatic substrates.[97] The complex TpRu(CO)(NCMe)Ph catalyzes ethylene hydroarylation of furan and thiophene (Scheme 1.37).[97] The C–H activation is regioselective at the α-position, giving either 17 TO of ethylfuran after 24 h or 3 TO of ethylthiophene after 12 h (no additional product was observed after this time). Contrary to ethylene hydrophenylation, the hydroarylation using these heteroaromatic substrates performed

better with increased ethylene pressures.[97] This observation is relevant to Chapter 3 of this Dissertation.

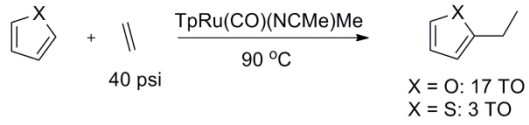


**Scheme 1.37.** Ethylene hydroarylation of furan and thiophene catalyzed by TpRu(CO)(NCMe)Me.

### 1.4.3 Hydroarylation of Olefins using Hydrocarbons: Platinum Catalysts

Most relevant to this Dissertation is the hydroarylation of olefins using unactivated substrates. The next several sections will highlight important contributions in this arena based on the identity of transition metal involved. There are two main mechanisms by which the Pt complexes operate: 1) FC catalysis by in situ generation of acid and 2) olefin hydroarylation by C–H activation.[7]

In 2004, Tilley and co-workers reported the hydrophenylation of several olefins, including norbornene, 2-butene, propylene, cyclopentene, and cyclohexene, using [2-(2-pyridyl)indole]Pt($C_2H_4$)Cl or [($C_2H_4$)PtCl(μ-Cl)]$_2$ in conjunction with $AgBF_4$ (Scheme 1.38).[98] Without the addition of a Ag(I) salt, no reaction is observed. The reaction proceeds at 80 °C and gives good yields of the alkyl arene product (>60%). For example, the reaction of benzene and propylene gave a 79% yield (~8 TOs) of cumene after 20 h with no *n*-propylbenzene observed. Performing hydroarylation of cyclohexene with toluene results in predominantly *ortho* and *para* substituted products. The reaction yield was 87% while the same reaction with benzene was just 65%. These observations strongly imply that a FC mechanism is operative.

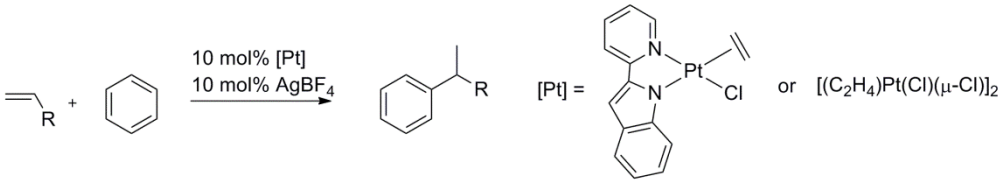


**Scheme 1.38.** Pt(II) and Ag(I)-mediated olefin hydrophenylation.

Tilley, Bergman, and co-workers studied the mechanism of Pt initiated olefin hydroarylation in more detail using $(COD)Pt(OTf)_2$ and $(^tbpy)Pt(OTf)_2$ (COD = 1,5-cyclooctadiene, $^t$bpy = 4,4'-di-*tert*butyl-2,2'-bipyridine) as the Pt complexes and benzene with norbornene or cyclohexene as the substrates.[99] One important observation was that the reaction of $(COD)Pt(OTf)_2$ and 2 equiv. of cyclohexene resulted in the olefin coupled product, which would provide a source of HOTf (Scheme 1.39). Experimentally, it was determined that reaction of the Pt complex with olefins did indeed generate HOTf in situ, which serves as the active catalyst in a FC-type reaction mechanism.


**Scheme 1.39.** Coupling of olefins to generate HOTf.

In 2008, Goldberg and co-workers reported the first example of Pt(II)-catalyzed intermolecular olefin hydroarylation reaction involving C–H activation.[100] They found that (dmpp)Pt complexes (dmpp = 3,5-dimethyl-2-(2-pyridyl)pyrrolide) catalyzes the addition of arene C–H bonds across unactivated olefins, such as ethylene and propylene (Scheme 1.40). For example, the reaction of benzene and ethylene at 100 °C in the presence of a catalytic amount of $(dmpp)Pt(SMe_2)Ph$ gave 36 TO of ethylbenzene.

Importantly, the hydrophenylation of propylene gave some of the linear product (B:L::85:15). Furthermore, the hydroarylation of ethylene using toluene produced predominantly *meta* and *para* substituted arenes. These data in conjunction with other mechanistic experiments provide evidence against a FC mechanism and are more consistent with the mechanism shown in Scheme 1.41, which involves insertion of the olefin into a Pt–Ph bond followed by cyclometallation via oxidative addition of the phenethyl ligand. Reductive C–H formation and subsequent benzene C–H activation releases the alkyl arene product and regenerates the active catalyst.[100]

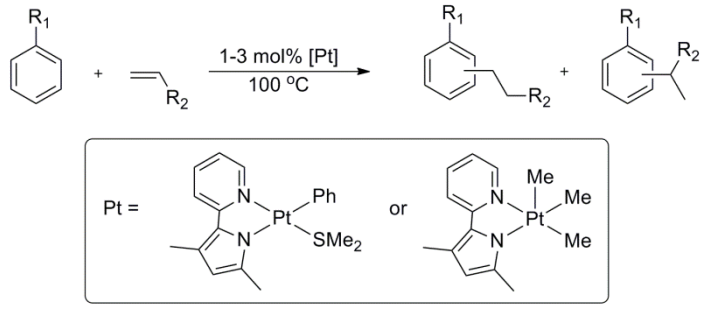


**Scheme 1.40.** Hydroarylation of unactivated olefins using (dmpp)Pt complexes.

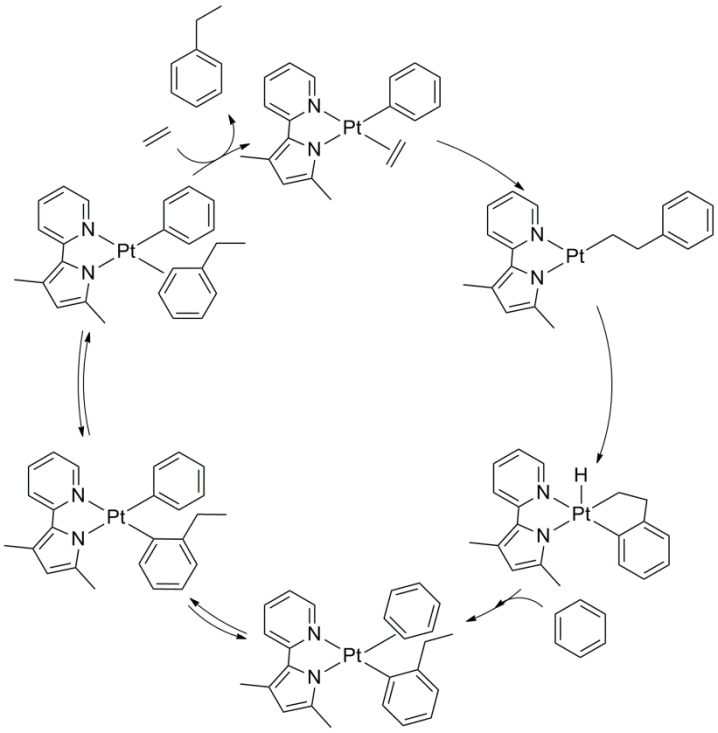


**Scheme 1.41.** Proposed catalytic cycle for ethylene hydrophenylation catalyzed by (dmpp)Pt.

More recently, Goldberg and co-workers published a follow-up paper examining the selectivity of hydroarylation of α-olefins in more detail.[101] By changing the substituents on the dmmp backbone, they could increase the relative amount of linear alkyl arene product (anti-Markovnikov) from the hydroarylation reaction (Scheme 1.42). For instance, removal of the methyl groups on the pyrrolide portion of the ligand (B, Scheme 1.42) gave 11 TON of product with a 52:48 branched to linear ratio, while using the original catalyst (A, Scheme 1.42) gave 18 TO with 84:13 branched to linear ratio for the hydrophenylation of propylene. By inserting a methyl group on the pyridyl portion of the ligand (C, Scheme 1.42), the activity decreased and the branched to linear ratio increased along with increased amounts of vinyl arene. Having a methyl group on the pyrrolide portion of the ligand (A) is expected to disfavor the Pt–propylene rotamer that

leads to the linear product. Another explanation is that the methyl group affects the relative insertion barriers between 1,2-insertion and 2,1-insertion. The reason for the increase in vinyl arene production using C could be related to the fact that the pyridyl portion is not *trans* to the phenyl group as in A and B. When β-hydride elimination occurs, the $\eta^2$-vinyl arene ligand may be more easily displaced due to the difference in *trans* effect as a result of the different isomers.[101]

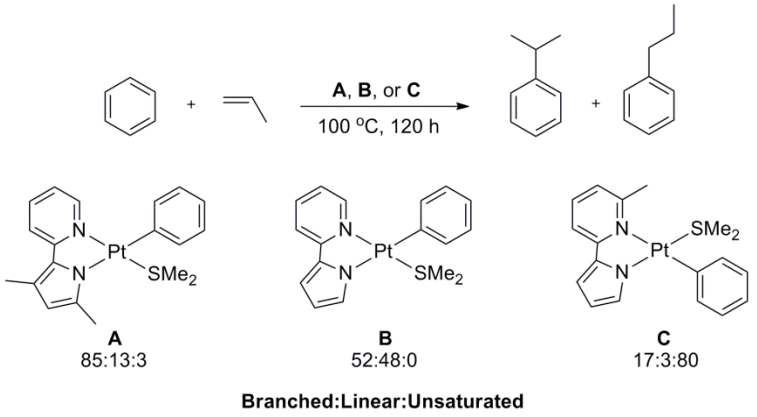


**Scheme 1.42.** Pt pre-catalysts evaluated for branched:linear selectivity for the hydrophenylation of propylene.

Our group has published a series of papers on cationic Pt(II) pre-catalysts for olefin hydroarylation.[90, 102-106] The first catalyst reported by our group was [($^t$bpy)Pt(Ph)(THF)][BAr'$_4$] ($^t$bpy = di-4,4'-(*tert*-butyl)-2,2'-bipyridine, Ar' = 3,5-bis(trifluoromethyl)phenyl).[102, 103] The hydrophenylation of ethylene at 100 °C using [($^t$bpy)Pt(Ph)(THF)][BAr'$_4$] (0.025 mol%) gave 53 TO of ethylbenzene (EtPh) and 11 TO of diethylbenzene ($Et_2C_6H_4$) in a 1:2.6:1.6 ratio of *ortho*:*meta*:*para* after 16 h. An increased amount of products are observed by increasing the temperature to 120 °C (108 TO EtPh and 17 TO $Et_2C_6H_4$). In one experiment, an 89% yield based on $C_2H_4$ was determined for this catalytic reaction. Catalysis is hindered by increased ethylene

pressure; however, by maintaining a low pressure of ethylene through the reaction, there is minimal catalyst decomposition up to 70 h at 100 °C. A detailed combined experimental and computational mechanistic investigation was performed that provided evidence for the catalytic cycle shown in Scheme 1.43, where $[(^{t}bpy)Pt(CH_2CH_2Ph)(C_2H_4)]^+$ could also lie off the catalytic cycle. It was determined that benzene C–H activation is the rate determining step of the catalytic cycle.[103] While it is hoped that olefin hydroarylation involving C–H activation would avoid the production of dialkylbenzenes, this was not the case using $[(^{t}bpy)Pt(Ph)(THF)][BAr'_4]$ as catalyst. Mechanistic studies suggest that the dialkylbenzenes result from competitive C–H activation of coordinated EtPh versus EtPh dissociation.[103]

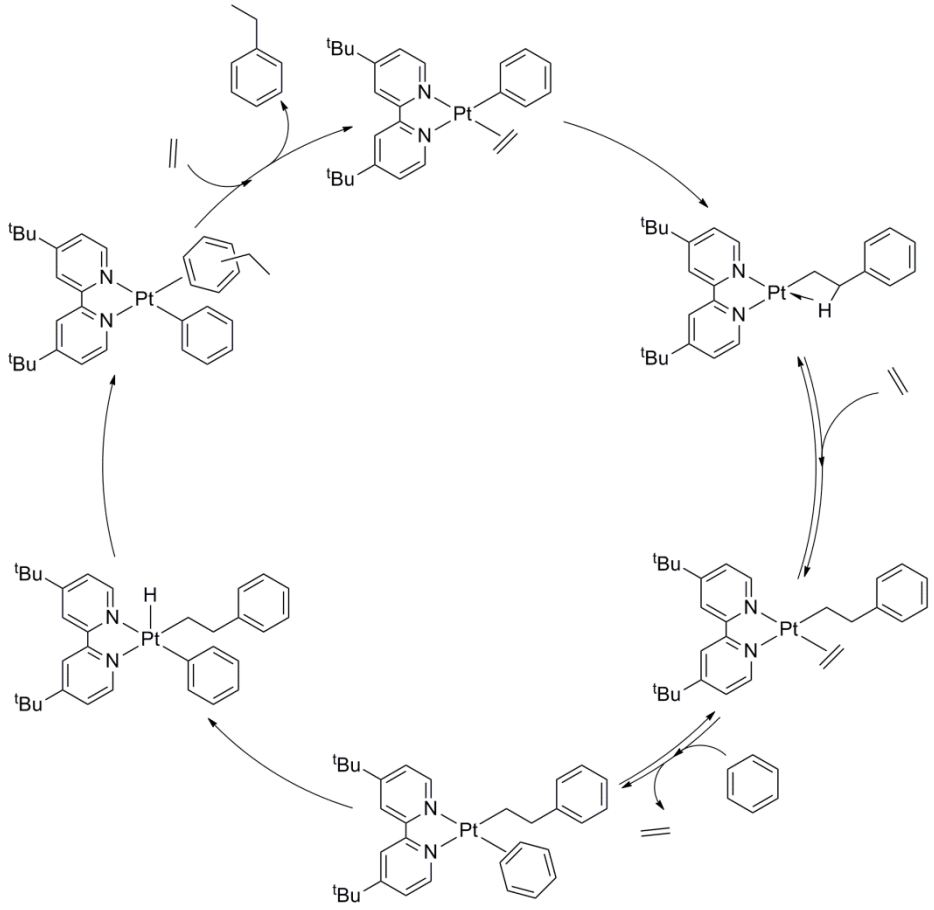

**Scheme 1.43.** Proposed catalytic cycle for ethylene hydrophenylation catalyzed by $[(^{t}bpy)PtPh]^{+}$ complexes. All species in catalytic cycle are cationic.

Further studies based on the (N~N)Pt(II) (N~N = bidentate nitrogen chelate) catalyst motif provided insight into how the electronic and steric profiles of the 2,2'-bipyridyl ligand affects selectivity and activity.[90, 104-106] This was accomplished by varying the substituents in the 4,4'-position of the bipyridyl ligand, increasing the chelate ring size of the ligand, and adding substituents to the the 6,6' position of the bipyridyl ligand. From these studies, some important trends became clear. For the series of catalysts $[(^{X}bpy)Pt(Ph)(THF)]^{+}$ ($^{X}bpy$ = 4,4'-di-X-2,2'-bipyridine) more electron-withdrawing substituents resulted in increased production of styrene relative to ethylbenzene.[90] For instance, when X = OMe, an EtPh:styrene ratio of 30:1 is observed,

while a 1:10 ratio is observed when X = $NO_2$. Second, by increasing the electron-donating ability of the bpy ligand, greater selectivity for anti-Markovnikov addition products are observed when using α-olefins.[106] For the hydrophenylation of propylene, a 2.9:1 branched to linear ratio is observed for the original $^t$bpy catalyst, while that increases (i.e., more Markovnikov product) to 4.6:1 when X = $NO_2$. Increasing the chelate ring size from the 5-membered ring in $^t$bpy to the 6-membered ring using dipyridylmethane (dpm) (Figure 1.5) as ligand increases catalytic longevity and activity. The dpm catalyst is ~3.5 times more active than the ($^t$bpy)Pt catalyst and gives a final turnover number of 469 at 100 °C after 110 h.[104] The source of this improved performance has been determined to be a result of an entropic advantage of the larger chelate ring.[104]

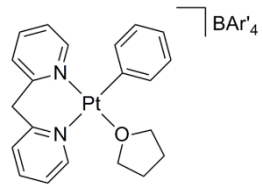


**Figure 1.5.** Structure of [(dpm)Pt(Ph)(THF)]BAr'$_4$ catalyst.

### 1.4.4 Hydroarylation of Olefins using Hydrocarbons: Iridium Catalysts

The first example of a well-defined transition metal catalyst for the hydrophenylation of benzene using a mechanism involving olefin insertion and C–H activation was reported by Matsumoto and Periana in 2000.[107] The initial report used the binuclear Ir(III) catalyst, [Ir($\mu$-acac-O,O,C$^3$)-(acac-O,O)(acac-C$^3$)]$_2$ (Scheme 1.44). The hydrophenylation of ethylene proceeded at 180 °C to give 455 TO of EtPh after 3 h. The hydrophenylation of propylene gave 13 TOs of alkyl arene. Importantly, the reaction was selective for the anti-Markovnikov addition product (~1.6:1).

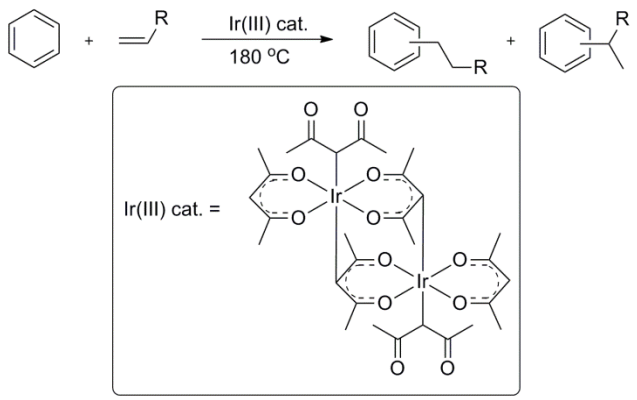


**Scheme 1.44.** Olefin hydrophenylation catalyzed by a binuclear Ir(III) complex.

Further work established that the active catalyst is monomeric [$(acac)_2$Ir(Ph)].[108, 109] Indeed, *trans*-[$(acac)_2$Ir(Ph)(L)] (L = $H_2O$, pyridine) complexes could be used directly as pre-catalysts for this reaction. Under catalytic conditions, the *trans*-acac isomer is in equilibrium with the *cis*-acac isomer, which is the active isomer since C–H activation and olefin insertion require a *cis* relationship of the phenyl ligand and the labile ligand (i.e., $H_2O$, pyridine). The *trans* isomer has been determined to be the kinetically preferred isomer, while the *cis* isomer is the thermodynamically preferred isomer. Interestingly, independent reactions involving either *trans*-[$(acac)_2$Ir(Ph)(L)] or *cis*-[$(acac)_2$Ir(Ph)(L)] demonstrated that the *trans* isomer is the more active pre-catalyst. Contrary to the Pt(II) and the Ru(II) systems (see Section 1.4.5), olefin insertion is the rate-determining step of olefin hydroarylation. Additionally, vinyl arenes are not observed as products in the reaction, which may be a result of reversible β-hydride elimination.

### 1.4.5 Hydroarylation of Olefins using Hydrocarbons: Ruthenium Catalysts

Most germane to this Dissertation is the work that our group has done using Ru(II) catalysts. The majority of the work has been based on the TpRu(L)(NCMe)Ph motif (Figure 1.6).[30, 110] This catalyst design is advantageous for several reasons. First,

the use of the anionic facially coordinating Tp ligand (Tp = hydridotris(pyrazolyl)borate) provides a rigid structure and keeps all other available coordination sites in a *cis* relationship, which avoids the need for isomerization of the catalyst to be active for C–H activation and olefin insertion during the catalytic cycle. Also, the labile NCMe ligand can be readily substituted by either an olefin or an aromatic substrate. Finally, the ancillary ligand L provides a means to control the electronic and steric environment of the Ru metal center. This ability is important for understanding how the electronics and the sterics of the complex affect catalysis and how one might design a better catalyst.

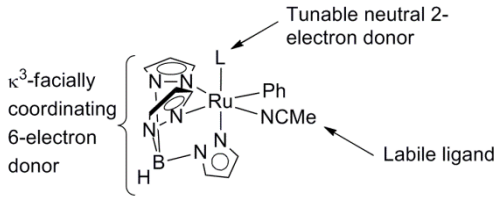


**Figure 1.6.** Ru(II) catalyst design for olefin hydroarylation.

The first catalyst that was discovered in our laboratory was TpRu(CO)(NCMe)Ph.[74, 111] A summary of some of the key results for the hydrophenylation of ethylene, propylene, and 1-hexene from the initial publication is shown in Table 1.1. The hydrophenylation of ethylene is selective for the formation of EtPh giving 77 TOs after 8 h at 90 °C using 25 psi of $C_2H_4$ with 0.1 mol% of catalyst. It should be noted that TpRu(CO)(NCMe)Ph has been proposed to decompose by a bimolecular pathway.[112] Thus, Dr. Evan Joslin discovered that if the catalyst loading is reduced from 0.1 mol% to 0.025 mol% and 15 psi of $C_2H_4$ is used (versus 25 psi), a maximum of 415 TON of ethylbenzene is observed after 40 h.[110] In the case of the two α-olefins studied, propylene and 1-hexene, selectivity for the linear alkylbenzene (~1.6:1) is observed. For 1-hexene, there is no evidence for isomerization to 2-hexene during

catalysis. These data collectively support a non-FC reaction pathway. Experimental and computational studies (Cundari group, U. North Texas) were initiated to determine the mechanism of this transformation, which is shown in Scheme 1.45.[74]

**Table 1.1.** Summary of results for hydrophenylation with TpRu(CO)(NCMe)Ph as catalyst. Conditions are 90 °C, 25 psi olefin, 0.1 mol% Ru, 4 h. [a]8 h. [b]50 equiv of olefin (based on Ru), 6 h.

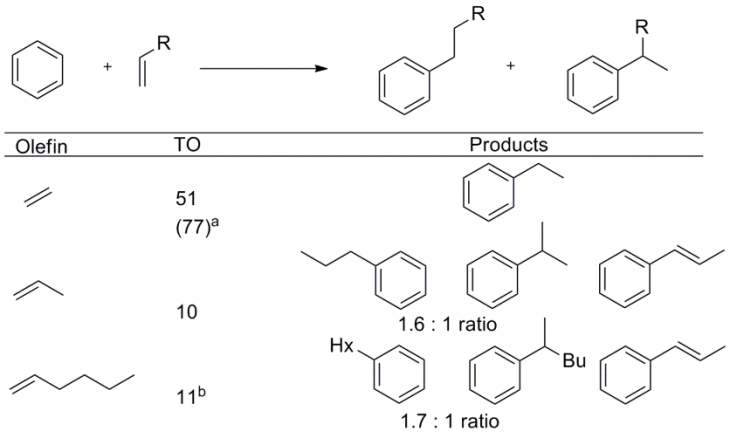

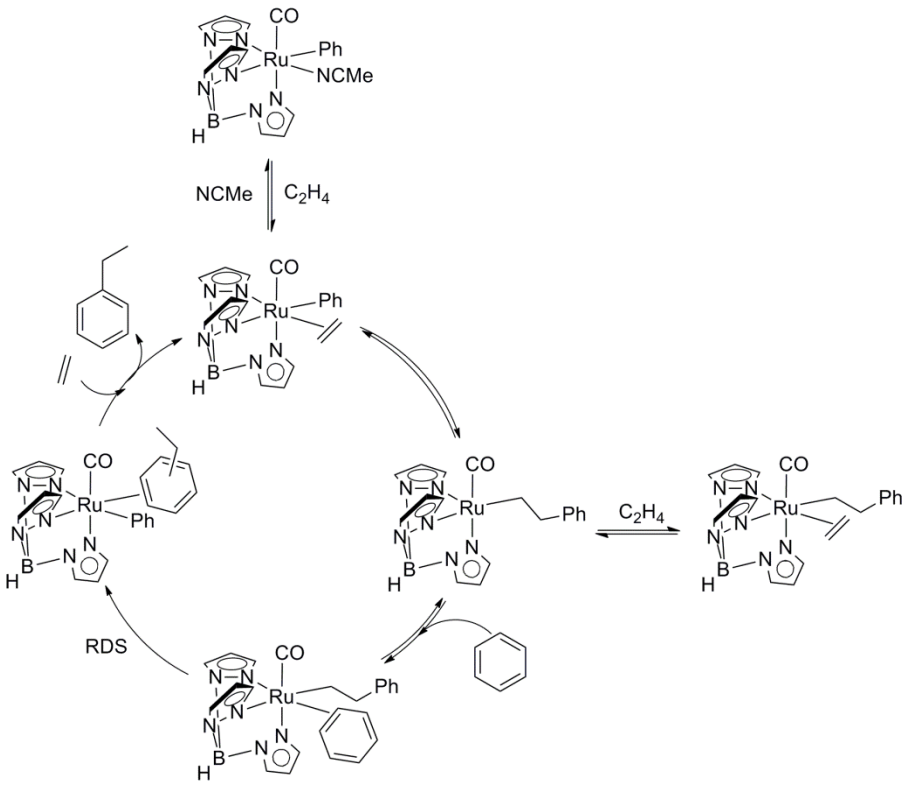


**Scheme 1.45.** Proposed catalytic cycle for ethylene hydrophenylation catalyzed by TpRu(CO)(NCMe)Ph.

Catalysis is initiated by NCMe dissociation and coordination of ethylene. Insertion of ethylene into the Ru–Ph bond yields the phenethyl intermediate TpRu(CO)($CH_2CH_2Ph$), which upon coordination of another equivalent of ethylene gives TpRu(CO)($CH_2CH_2Ph$)($C_2H_4$). This complex has been determined to be the catalyst resting state. Dissociation of ethylene followed by coordination of benzene and subsequent C–H activation gives the EtPh, which is displaced by another equivalent of ethylene to complete the catalytic cycle. Performing catalysis with a 1:1 molar ratio of $C_6H_6$:$C_6D_6$ reveals a kinetic isotope effect (KIE) of 2.1(1). The KIE for stoichiometric benzene C–H(D) activation is statistically identical (2.5(5)). This suggests that benzene C–H activation is the rate limiting step of the catalytic cycle. Computational studies

support this proposal and further describe the C–H mechanism as oxidative hydrogen migration (see Section 1.3.1.2).[74]

The use of well-defined homogeneous transition metal complexes provides an opportunity to study the impact of systematic variations to the electronic and sterics of a catalyst. The Gunnoe group has synthesized and evaluated the activity of a series of complexes of the type TpRu(L)(NCMe)Ph (L = $PMe_3$, P(*N*-pyrrolyl)$_3$, $P(OCH_3)_2Et$, $P(O)(OCH_2)_2CMe$) for aromatic C–H activation and ethylene hydrophenylation.[30, 110] Figure 1.7 shows a comparison of the steric and electronic properties of the various ligands studied.[110] The Ru(III/II) potentials have been used to quantify the electron richness of the metal center. A greater potential is needed to oxidize a more electron deficient complex from Ru(II) to Ru(III).

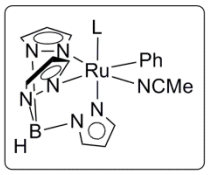


| Ligand | CO | | | | |
|---|---|---|---|---|---|
| $E_{1/2}$ (V) (vs NHE) | 1.03 | 0.82 | 0.69 | 0.54 | 0.29 |
| Cone Angle (°) | 95 | 145 | 108 | 101 | 118 |

**Figure 1.7.** Comparison of the electronic and steric properties of TpRu(L)(NCMe)Ph complexes.[110, 113, 114]

The mechanistic study of ethylene hydrophenylation using TpRu(CO)(NCMe)Ph suggested that benzene C–H activation is the rate-limiting step of the catalytic cycle.[74] A comparison of the rates of stoichiometric C–D activation of $C_6D_6$ may give insight into which catalysts will be the most active (Scheme 1.46).[30, 110] It was determined that the more electron-rich metal complex, TpRu($PMe_3$)(NCMe)Ph has the fastest rate of

stoichiometric benzene C–H activation, while TpRu(CO)(NCMe)Ph had the slowest rate of C–H activation.[115] Contrary to the prediction based on the kinetics of benzene C–H activation, TpRu($PMe_3$)(NCMe)Ph was a poor catalyst for ethylene hydrophenylation. This is a result of competitive olefin C–H activation, which results in the generation of TpRu($PMe_3$)($\eta^3$-$C_3H_4Me$) from $C_2H_4$ C–H activation, ethylene insertion and subsequent isomerization (Scheme 1.47).

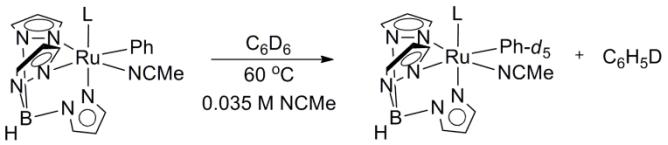


| L | $k_{obs}$ ($10^{-5}$ $s^{-1}$) |
|---|---|
| $PMe_3$ | 1.36 |
| $P(OCH_2)_3CEt$ | 1.20 |
| $P(O)(OCH_2)_2CMe$ | 0.72 |
| CO | 0.46 |

**Scheme 1.46.** Degenerate C–D activation of $C_6D_6$ by TpRu(L)(NCMe)Ph complexes.

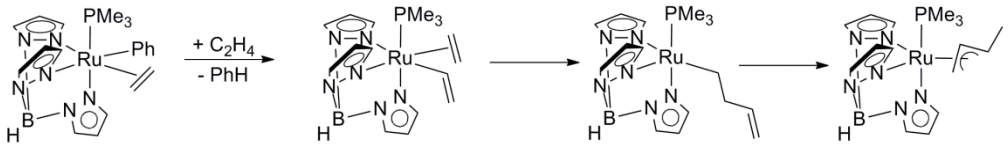


**Scheme 1.47.** Formation of TpRu($PMe_3$)($\eta^3$-$C_3H_4Me$) due to competitive ethylene C–H activation.

Increased sterics of the Ru catalyst may favor more anti-Markovnikov addition products when using α-olefins. However, catalytic efficiency is also heavily influenced by the steric profile of the catalyst. For example, TpRu[$P(pyr)_3$](NCMe)Ph was not an active catalyst for ethylene hydrophenylation due to the unfavorable thermodynamics of coordination of ethylene to the Ru center.[116] Thus, a proper balance of sterics and electronics must be obtained to give highly active catalysts. Using catalysts based on

$P(OCH_2)_3CEt$ and $P(O)(OCH_2)_2CMe$ did result in catalytic turnover, with the less electron donating $P(O)(OCH_2)_2CMe$ giving a maximum turnover of 90 (compared to 20 TO for the $P(OCH_2)_3CEt$ catalyst).[110, 117] It was determined that TpRu[$P(OCH_2)_3CEt$](NCMe)Ph and TpRu[$P(O)(OCH_2)_2CMe$](NCMe)Ph still result in catalyst deactivation through formation of TpRu(L)($\eta^3$-$C_3H_4Me$).

The comparison of catalysts revealed some important points.[110] Increasing the donor ability of the ancillary ligand does increase the rate of stoichiometric C–H activation, which has been determined to be the rate-limiting step of the catalytic cycle. However, what appears to be most important for catalysis is the rate of olefin insertion because olefin C–H activation becomes competitive when insertion is too slow. This is highlighted by the observation that the less electron-rich Ru complexes result in more turnovers by ethylbenzene. It has therefore been predicted that overall cationic Ru(II) catalysts may be more active catalysts since they are expected to be more electrophilic than the charge-neutral TpRu(L)(NCMe)Ph catalysts. By using tris(pyrazolyl)alkane ligands in place of the anionic Tp ligand, it is possible to determine the impact of an overall cationic catalyst on its activity in ethylene hydrophenylation.

Dr. Evan Joslin and Dr. Samantha Burgess prepared and evaluated the catalytic competency of [$HC(pz^5)_3$)Ru($P(OCH_2)_3CEt$)(NCMe)Ph][$BAr'_4$] ($HC(pz^5)_3$ = tris(5-methyl-pyrazolyl)-methane) (Scheme 1.48).[118] It was discovered that this catalyst is long-lived and highly active for ethylene hydrophenylation, giving a maximum of 565 TON (compared to 20 TON for TpRu($P(OCH_2)_3CEt$)(NCMe)Ph) at 90 °C after 131 h. This corresponds to a 95% yield based on $C_2H_4$ as the limiting reagent. While C–H activation is slower with [$HC(pz^5)_3$)Ru(CO)(NCMe)Ph][$BAr'_4$] ($k_{obs}$ ~ 5.7 x $10^{-7}$ $s^{-1}$) than

TpRu(P(OCH$_2$)$_3$CEt)(NCMe)Ph ($k_{obs}$ = 1.2 x $10^{-5}$ $s^{-1}$), the catalyst is stable at high temperatures (175 °C), giving ~350 TO after 16 h when some deactivation is observed. Mechanistic studies were performed and provided evidence that a similar mechanism was operative for the cationic catalyst as the charge-neutral catalysts. Catalyst deactivation proceeds via olefin C–H activation to give the $\eta^3$-allyl complex [HC(pz$^5$)$_3$)Ru(P(OCH$_2$)$_3$CEt) )($\eta^3$-C$_3$H$_4$Me)][BAr'$_4$]. It is anticipated that decreasing the electron donating ability further would increase catalytic activity.[118]

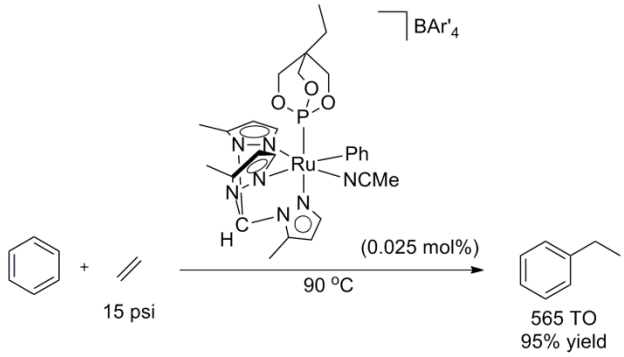


**Scheme 1.48.** Ethylene hydrophenylation by [HC(pz$^5$)$_3$)Ru(P(OCH$_2$)$_3$CEt)(NCMe)Ph][BAr'$_4$].

### 1.4.6 Summary of Transition Metal Olefin Hydroarylation Catalysts

The preceding sections have reviewed the advancements in transition metal mediated olefin hydroarylation. A summary of the best catalysts reported to date is in Table 1.2. The catalyst that gives the highest TON is [HC(pz$^5$)$_3$)Ru(P(OCH$_2$)$_3$CEt)(NCMe)Ph][BAr'$_4$] (TON = 565) at 90 °C.[118] What appears to be critical for the success of this catalyst is that it is has a relatively electrophilic Ru metal center. This combination appears to enable rapid olefin insertion to avoid competitive olefin C–H activation yet the Ru center can still mediate benzene C–H activation and disfavor multiple olefin insertions. The TpRu(CO)(NCMe)Ph catalyst also

gives high TON of 415 at 90 °C, but its overall stability is limited due to a bimolecular decomposition pathway.[110, 112] The Ir(III) catalyst [Ir($\mu$-acac-O,O,C$^3$)-(acac-O,O)(acac-C$^3$)]$_2$ is also a highly active catalyst, giving a TON of 455 at 180 °C.[107] This catalyst is also the fastest with a turnover frequency of 4.2 x $10^{-2}$ $s^{-1}$, although it is not as long-lived as the other catalysts reported. The most active Pt(II) catalyst is [(dpm)Pt(Ph)(THF)][BAr'$_4$], which produces 469 TO of ethylbenzene at 100 °C.[104]

**Table 1.2.** Comparison of the most active transition metal olefin hydroarylation catalysts.[104, 107, 110, 118] Cells marked with n/a denote no data available.

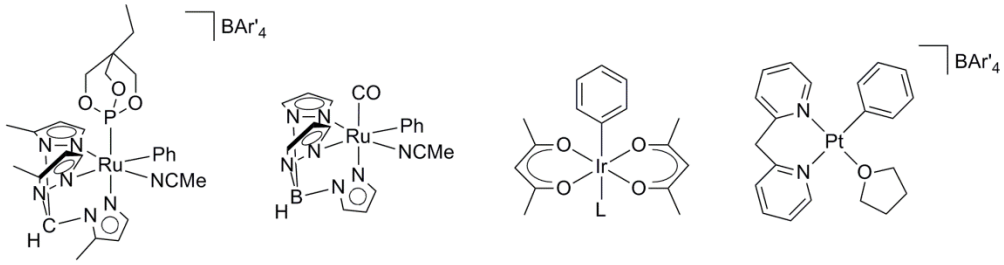


| Catalyst | TON | TOF ($10^{-2}$ $s^{-1}$) | L:B ($C_3H_7$) | EtPh: Styrene | EtPh: $Et_2C_6H_4$ |
|---|---|---|---|---|---|
| **A** | 565 | >2 | n/a | n/a | n/a |
| **B** | 415 | 0.67 | 1.6:1 | n/a | n/a |
| **C** | 455 | 4.2 | 1.5:1 | n/a | n/a |
| **D** | 469 | 1.8 | 1:4.4 | 200:1 | 5:1 |

The square planar Pt(II) catalysts have drawbacks in that they are not selective for linear alkylbenzenes when using α-olefins. This is likely a result of the square planar geometry, which does not allow for adequate steric control of the regioselectivity of the olefin insertion step. The Gunnoe group has demonstrated that this selectivity could be improved through modulation of the electronics and sterics of the catalyst,[104, 106] and

Goldberg and co-workers have shown that this selectivity could be improved by decreasing the steric hindrances in the square plane.[101] However, these changes are modest and still do not give selectivity for the desired linear product. The Pt(II) systems also result in significant quantities of the dialkylbenzenes, which is not observed in the Ru(II) and Ir(III) catalysts.[7, 30]

Additionally, the Pt(II) systems have the propensity to form styrene, which appears to result in catalyst decomposition. This, again, may be attributed to the square planar geometry of these complexes. Calculations have shown that the Ru(II) and Ir(III) catalysts do undergo β-hydride elimination from the M–$CH_2CH_2Ph$ intermediates, but that this is reversible.[69, 73, 74, 109] For the square planar complexes, the ability to associative displace coordinated styrene may provide a kinetic disadvantage, rendering styrene formation irreversible.[103] However, the [(dpm)Pt(Ph)(THF)][$BAr'_4$] catalyst is considerably more selective for ethylbenzene over styrene than the [($^t$bpy)Pt(Ph)(THF)][$BAr'_4$] catalyst, reaching selectivity of ~200:1 (EtPh:styrene).[104]

While efforts are currently underway in the Gunnoe group to develop Pt(II) systems that do not suffer from these drawbacks based on the square planar geometry, it appears that the octahedral coordination environment of Ir(III) and Ru(II) offers the best combination of selectivity and activity. Less work developing more selective catalysts for linear alkylbenzenes has been done with the Ir(III) systems in comparison to Ru(II). The challenge with the Ru(II) systems TpRu(L)(NCMe)Ph is that the catalysts are very sensitive to the size of the ancillary ligand (L). Other than TpRu(CO)(NCMe)Ph none of the other Ru(II) complexes have catalyzed propylene hydrophenylation, likely a result of the inability to coordinate propylene to the Ru center.

Further work on the $[HC(pz^5)_3)Ru(L)(NCMe)Ph][BAr'_4]$ catalyst design could lead to catalysts that are both highly active and highly selective for the hydrophenylation of α-olefins. Besides pursuing Ru(II) catalysts with this structural motif, using another metal center while keeping an octahedral coordination environment might also lead to catalysts with the desirable features of high stability, high activity, and high selectivity.

## 1.5 Iron as a Catalyst for Olefin Hydroarylation by C–H Activation and Olefin Insertion

### 1.5.1 Rationale for using Iron

Section 1.4.5 highlighted some of the advancements our group has made in the development of Ru(II) catalysts for olefin hydroarylation. One question that we wanted to study was whether it was feasible to make a catalyst with iron, ruthenium's first-row counterpart. And, if so, we wanted to understand how using a first-row transition metal would affect catalytic activity for analogous complexes.

A driving force to use Fe as a catalyst, besides the fundamental questions, is that Fe is an Earth-abundant metal.[119, 120] In fact, Fe is the second most abundant metal in the Earth's crust and is inexpensive. Table 1.3 shows the price per ounce of a few transition metals.[121] Iron costs about one cent per ounce making the development of catalytic processes based on Fe highly desirable. Additionally, iron compounds are relatively non-toxic. Indeed, the human body uses several iron based metalloproteins for transport or metabolism.[122]

**Table 1.3.** Market prices of various transition metals.[121]

| Metal | Price ($/oz) |
|---|---|
| iron | 0.01 |
| ruthenium | 57 |
| palladium | 799 |
| iridium | 551 |
| platinum | 1,225 |
| rhodium | 1,194 |

Over recent years, the development of Fe catalysts has surged.[119, 120, 123, 124] Some notable examples include Chirik's olefin hydrosilylation catalyst,[125] Chen and White's C–H oxidation catalysts,[126, 127] and Morris's asymmetric transfer hydrogenation catalyst (Figure 1.8).[128] What lacks from the literature are highly active catalysts for functionalization by Fe mediated C–H activation.

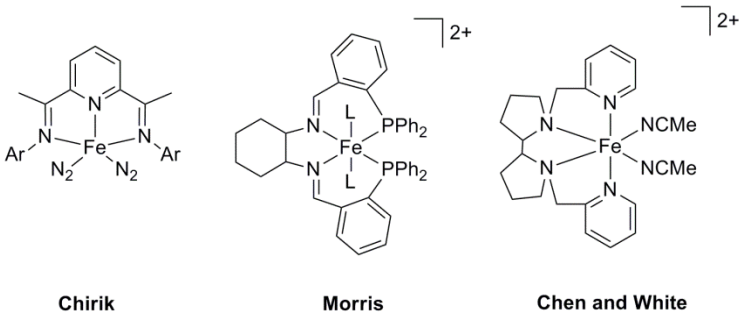


**Figure 1.8.** Some examples of Fe-based homogeneous catalysts.

### 1.5.2 Iron-mediated C–H Activation

Iron catalysts for C–H bond functionalization are rare. Here it is worth defining again how the term "C–H activation" is used in this Dissertation: the cleavage of a C–H bond by direct interaction (i.e., within the coordination sphere) with the metal center. There are many examples of Fe oxo catalysts that functionalize C–H bonds through single-electron pathways. A biological example is the P450 enzyme.[129] This enzyme contains an Fe center that oxidizes hydrocarbons by a series of single electron pathways. Many of these oxidation type catalysts involve Fe-oxo species that abstract a hydrogen as the initial step.[129] Additionally, there are catalytic reactions that involve Fe salts that likely are radical processes.[123, 124] These reactions that involve single-electron C–H bond cleavage are limited by the strength of C–H bond that can be functionalized and often exhibit poor selectivity.[129] We are interested in developing Fe catalysts that break C–H bonds by a two-electron process since we expect them to selectively activate aromatic C–H bonds (Scheme 1.49).

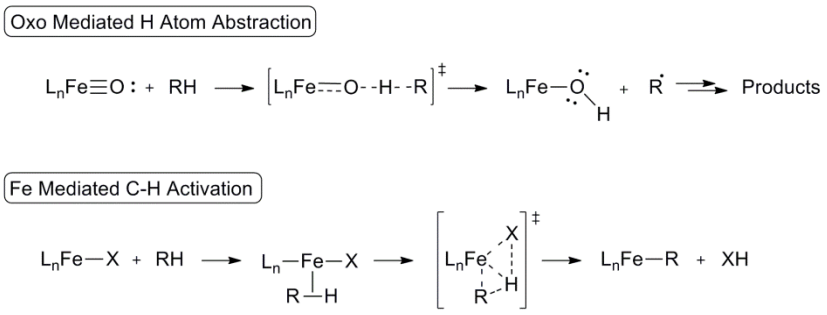


**Scheme 1.49.** Comparison of Fe-oxo mediated H atom abstraction and Fe-mediated C–H activation.

Examples of C–H activation by Fe complexes are rare but have been reported. In thelate 1970s, Tolman and Ittel reported the C–H activation chemistry of $(dmpe)_2Fe(Np)(H)$ (dmpe = bis-1,2-(dimethylphosphinoethane), Np = 2-naphthyl)

(Scheme 1.50).[130, 131] When this complex is treated with an aromatic substrate (ArH), the $(dmpe)_2Fe(Ar)(H)$ forms via reductive elimination of NpH and oxidative addition of ArH.

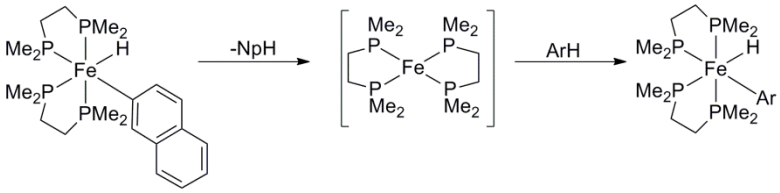


**Scheme 1.50.** C–H activation of arenes by $(dmpe)_2Fe(Np)(H)$.

About 10 years later, Field and Baker found that irradiation of $(dmpe)_2FeH_2$ generates the $(dmpe)_2Fe(0)$ fragment, which can cleave the C–H bonds of unactivated alkenes to give the corresponding vinyl hydride complexes (Scheme 1.51).[132] The researchers also discovered that in situ prepared $(depe)_2Fe(Me)(H)$ [(depe = 1,2-bis(diethylphosphinoethane) rapidly reductively eliminates methane upon warming to generate the reactive Fe(0) fragment (Scheme 1.52).[133]

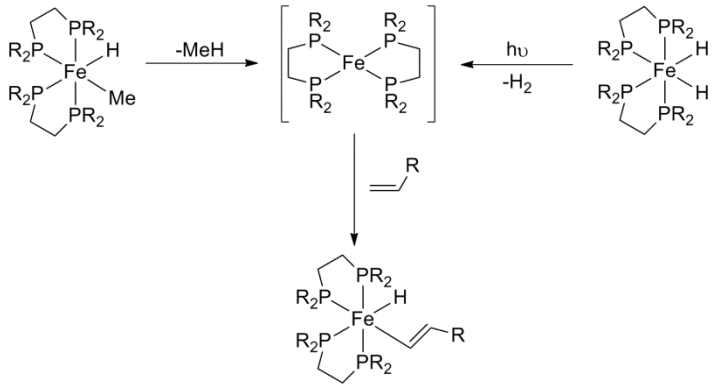


**Scheme 1.51.** C–H activation of olefins starting from bis-phosphine ligated Fe complexes.

Catalytic benzene C–H activation has been achieved by Jones and co-workers. Photolyzing a benzene solution of $Fe(PMe_3)_2(CNR)_3$ with C≡NR (R = Me, $^t$Bu, $CH_2CMe_3$, Ph, 1,6-xylyl) gives up to ~8 TO of the corresponding aldimine (Scheme

1.52).[134] The concentration of C≡NR must be kept low because photolysis is used to dissociate C≡NR.

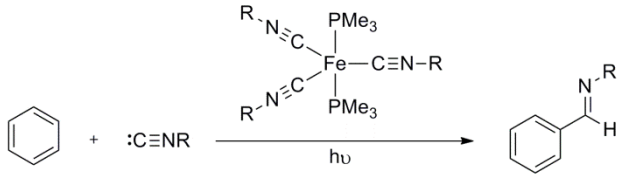


**Scheme 1.52.** Aldimine formation via benzene C–H activation by an Fe complex.

Hartwig and co-workers demonstrated that photolysis of Cp*Fe(CO)$_2$[BCat(Me)$_2$] (cat = $O_2C_6H_4$) in the presence of pentane produces sub-stoichiometric (20% based on Fe) amounts of 1-pentylboronate ester (Scheme 1.53).[135, 136] The C–H activation of pentane/pentane-$d_{12}$ gave a small primary KIE of $k_H/k_D$ = 1.9, suggesting C–H cleavage is rate-determining. Additional mechanistic investigations supported a non-radical reaction pathway.

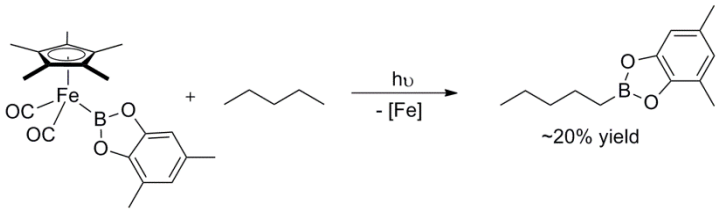


**Scheme 1.53.** Stoichiometric borylation of pentane by an Fe complex.

In 2008, Ohki and Tatsumi reported the C–H activation of heteroaromatics by Cp*Fe($\kappa^2$-(C,C)-L$^{iPr}$) (L$^{iPr}$ = $CH_2CH(CH_3)$(3-isopropyl-4,5-dimethylimidazol-2-ylidene-1-yl).[137] The complex regioselectively activates the 2-position of furan, thiophene, benzofuran and benzothiophene at room temperature (Scheme 1.54). The complex can also activate the 4-position of pyridine at elevated temperatures. In a subsequent paper, the researchers prepared the related Cp*Fe(L$^{Me}$)Me complex (L$^{Me}$ = 1,3,4,5-tetramethyl-

imidazol-2-ylidene), which also activates the C–H bonds of furan and thiophene.[138] This complex can also activate benzene C–H bonds, however in only 40% yield after 7 days at 80 °C. Cp*Fe($L^{Me}$)Me was applied to the catalytic borylation of furans and thiophenes using *tert*-butylethylene as a hydrogen acceptor (Scheme 1.55).

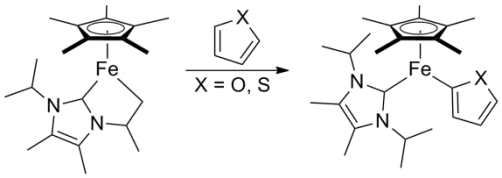


**Scheme 1.54.** Heteroaromatic C–H activation by an Fe NHC complex.

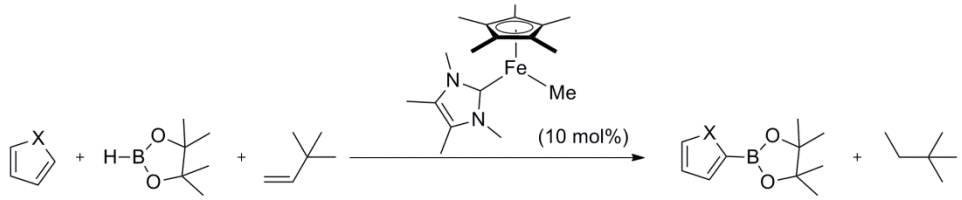


**Scheme 1.55.** C–H borylation catalyzed by a half-sandwich Fe complex.

## 1.6 Thesis Aims

Inspired by the success of our group's TpRu(L)(NCMe)Ph catalysts for olefin hydroarylation, this Dissertation is directed toward the development of an Fe catalyst for olefin hydroarylation. Studies were focused on developing Fe complexes that can perform the steps of the catalytic reaction and understanding these steps in more detail with the ultimate goal of developing an Fe catalyst. Chapter 2 demonstrates the evolution from our TpRu(CO)(NCMe)Ph catalyst to an Fe complex, Cp*Fe(CO)(NCMe)Ph, capable of aromatic C–H activation under very mild conditions. Having developed an Fe complex capable of aromatic C–H activation, Chapter 3 highlights attempts to catalyze the hydroarylation of olefins and alkynes. In Chapter 3, several stoichiometric C–C bond formation reactions involving the formation of hydroxyindenyl and vinylidene ligands are

described. Chapter 4 presents the synthesis and preliminary reactivity studies of $Cp^*Fe[P(OCH_2)_3CEt]_2Ph$, which is capable of mediating C–H bond activation reactions and insertion reactions under photolytic conditions. In Chapter 5, the synthesis of Fe complexes outside the Cp* ligand motif is presented. Chapter 6 highlights some results from another research project in our laboratory, namely selective alkane functionalization using periodate and chloride salts. Finally, Chapter 7 provides a summary of the work present herein along with some discussion of future directions toward developing an Fe catalyst for olefin hydroarylation.

## 1.7 References

(1) Perego, C.; Ingallina, P. *Green Chem.* **2004**, *6*, 274-279.

(2) Macquarrie, D. J. In *Catalytic Asymmetric Friedel-Crafts Alkylations*, Bandini, M.; Umani-Ronchi, A., Eds. Wiley-VCH: Weinheim, 2009.

(3) Gerzeliev, I. M.; Khadzhiev, S. N.; Sakharova, I. E. *Petrol. Chem.* **2011**, *51*, 39-48.

(4) Perego, C.; Ingallina, P. In *Advances in Nanoporous Materials*, Stefan, E., Ed. Elsevier: Oxford, 2009; Vol. 1, pp 97-149.

(5) Somorjai, G. A.; Rioux, R. M. *Catal. Today* **2005**, *100*, 201-215.

(6) Corma, A. *Chem. Rev.* **1997**, *97*, 2373-2419.

(7) Andreatta, J. R.; McKeown, B. A.; Gunnoe, T. B. *J. Organomet. Chem.* **2011**, *696*, 305-315.

(8) You, S. L.; Cai, Q.; Zeng, M. *Chem. Soc. Rev.* **2009**, *38*, 2190-2201.

(9) Olah, G.; Molnar, A., *Hydrocarbon Chemistry*. 2nd ed.; Wiley-Interscience: New York, 2003.

(10) Corma, A.; Garcia, H. *Chem. Rev.* **2003**, *103*, 4307-4365.

(11) Roberts, R. M.; Khalaf, A. A., *Friedel-Crafts Alkylation Chemistry: A Century of Discovery*. Marcel Dekker, Inc.: New York, 1984.

(12) Olah, G. A., *Friedel-Crafts Chemistry*. John Wiley & Sons: New York, 1973.

(13) Perego, C.; Ingallina, P. *Catal. Today* **2002**, *73*, 3-22.

(14) Jan, D.-Y. Y.; Barger, P. T. Processes on Industrial C-C Bond Formation. In *Zeolites in Industrial Separation and Catalysis*, Kulprathipanja, S., Ed. Wiley-VCH: Weinheim, 2000; pp 505-519.

(15) Kocal, J. A.; Vora, B. V.; Imai, T. *Appl. Catal., A* **2001**, *221*, 295-301.

(16) Broach, R. W. Zeolite Types and Structures. In *Zeolites in Industrial Separation and Catalysis*, Kulprathipanja, S., Ed. Wiley-VCH: Weinheim, 2010; pp 29-59.

(17) Degnan, T. F. *Journal of Catalysis* **2003**, *216*, 32-46.

(18) Corbet, J. P.; Mignani, G. *Chem. Rev.* **2006**, *106*, 2651-2710.

(19) *Metal-catalyzed Cross-coupling Reactions*. Wiley-VCH: Weinheim, 1998.

(20) Beletskaya, I. P.; Cheprakov, A. V. *Chem. Rev.* **2000**, *100*, 3009-3066.

(21) Fortman, G. C.; Nolan, S. P. *Chem. Soc. Rev.* **2011**, *40*, 5151-5169.

(22) Fu, G. C. *Acc. Chem. Res.* **2008**, *41*, 1555-1564.

(23) Negishi, E.; Anastasia, L. *Chem. Rev.* **2003**, *103*, 1979-2017.

(24) Suzuki, A. *Acc. Chem. Res.* **1982**, *15*, 178-184.

(25) Heck, R. F.; Nolley, J. P. *J. Org. Chem.* **1972**, *37*, 2320-&.

(26) Negishi, E.; King, A. O.; Okukado, N. *J. Org. Chem.* **1977**, *42*, 1821-1823.

(27) The Nobel Prize in Chemistry 2010. http://www.nobelprize.org/nobel_prizes/chemistry/laureates/2010/ (January 14, 2015),

(28) Kuhl, N.; Hopkinson, M. N.; Wencel-Delord, J.; Glorius, F. *Angew. Chem. Int. Ed.* **2012**, *51*, 10236-10254.

(29) Goj, L. A.; Gunnoe, T. B. *Curr. Org. Chem.* **2005**, *9*, 671-685.

(30) Foley, N. A.; Lee, J. P.; Ke, Z. F.; Gunnoe, T. B.; Cundari, T. R. *Acc. Chem. Res.* **2009**, *42*, 585-597.

(31) Shilov, A. E.; Shul'pin, G. B. *Chem. Rev.* **1997**, *97*, 2879-2932.

(32) Hartwig, J. F., *Organotransition Metal Chemistry: From Bonding to Catalysis*. University Science Books: Sausalito, 2009.

(33) Perutz, R. N.; Sabo-Etienne, S. *Angew. Chem. Int. Ed.* **2007**, *46*, 2578-2592.

(34) Crabtree, R. H. *J. Chem. Soc. Dalt. Trans.* **2001**, 2437-2450.

(35) Goldberg, K. I.; Goldman, A. S., *Activation and Functionalization of C-H Bonds*. American Chemical Society: Washington, DC, 2004; Vol. 885.

(36) Young, R. D. *Chem. Eur. J.* **2014**, *20*, 12704-12718.

(37) Geftakis, S.; Ball, G. E. *J. Am. Chem. Soc.* **1998**, *120*, 9953-9954.

(38) Lawes, D. J.; Darwish, T. A.; Clark, T.; Harper, J. B.; Ball, G. E. *Angew. Chem. Int. Ed.* **2006**, *45*, 4486-4490.

(39) Bernskoetter, W. H.; Schauer, C. K.; Goldberg, K. I.; Brookhart, M. *Science* **2009**, *326*, 553-556.

(40) Cowan, A. J.; George, M. W. *Coord. Chem. Rev.* **2008**, *252*, 2504-2511.

(41) Balcells, D.; Clot, E.; Eisenstein, O. *Chem. Rev.* **2010**, *110*, 749-823.

(42) Labinger, J. A.; Bercaw, J. E. *Nature* **2002**, *417*, 507-514.

(43) Ritleng, V.; Sirlin, C.; Pfeffer, M. *Chem. Rev.* **2002**, *102*, 1731-1769.

(44) Gunnoe, T. B. Physical Inorganic Chemistry: Reactions, Processes, and Applications. In *Physical Inorganic Chemistry: Reactions, Processes, and Applications*, Bakac, A., Ed. John Wiley & Sons: Hoboken, NJ, 2010; Vol. 2, pp 495-549.

(45) Bergman, R. G. *Nature* **2007**, *446*, 506-506.

(46) Godula, K.; Sames, D. *Science* **2006**, *312*, 67-72.

(47) Jia, C. G.; Kitamura, T.; Fujiwara, Y. *Acc. Chem. Res.* **2001**, *34*, 633-639.

(48) Crabtree, R. H., *The Organometallic Chemistry of the Transition Metals*. 5th ed.; John Wiley and Sons: New York, 2009.

(49) Bennett, M. A.; Milner, D. L. *Chem. Comm.* **1967**, *1967*, 581.

(50) Neufeldt, S. R.; Sanford, M. S. *Acc. Chem. Res.* **2012**, *45*, 936-946.

(51) Bruckl, T.; Baxter, R. D.; Ishihara, Y.; Baran, P. S. *Acc. Chem. Res.* **2012**, *45*, 826-839.

(52) Sherry, A. E.; Wayland, B. B. *J. Am. Chem. Soc.* **1990**, *112*, 1259-1261.

(53) Chatt, J.; Davidson, J. M. *J. Chem. Soc.* **1967**, *1967*, 843.

(54) Green, M. L. H.; Knowles, P. J. *J. Chem. Soc., Chem. Comm.* **1970**, 1677-&.

(55) Janowicz, A. H.; Bergman, R. G. *J. Am. Chem. Soc.* **1982**, *104*, 352-354.

(56) Hoyano, J. K.; Graham, W. A. G. *J. Am. Chem. Soc.* **1982**, *104*, 3723-3725.

(57) Jones, W. D. Advances in CH Activation. In *Comprehensive Organometallic Chemistry III*, Crabtree, R. H.; Mingos, M. P., Eds. Elsevier: Oxford, 2007; pp 699-723.

(58) Jones, W. D.; Feher, F. J. *Acc. Chem. Res.* **1989**, *22*, 91-100.

(59) Clot, E.; Megret, C.; Eisenstein, O.; Perutz, R. N. *J. Am. Chem. Soc.* **2006**, *128*, 8350-8357.

(60) Jones, W. D.; Hessell, E. T. *J. Am. Chem. Soc.* **1993**, *115*, 554-562.

(61) Burger, P.; Bergman, R. G. *J. Am. Chem. Soc.* **1993**, *115*, 10462-10463.

(62) Arndtsen, B. A.; Bergman, R. G. *Science* **1995**, *270*, 1970-1973.

(63) Strout, D. L.; Zaric, S.; Niu, S. Q.; Hall, M. B. *J. Am. Chem. Soc.* **1996**, *118*, 6068-6069.

(64) Niu, S. Q.; Hall, M. B. *J. Am. Chem. Soc.* **1998**, *120*, 6169-6170.

(65) Watson, P. L. *J. Am. Chem. Soc.* **1983**, *105*, 6491-6493.

(66) Thompson, M. E.; Baxter, S. M.; Bulls, A. R.; Burger, B. J.; Nolan, M. C.; Santarsiero, B. D.; Schaefer, W. P.; Bercaw, J. E. *J. Am. Chem. Soc.* **1987**, *109*, 203-219.

(67) Sadow, A. D.; Tilley, T. D. *Angew. Chem. Int. Ed.* **2003**, *42*, 803-805.

(68) Sadow, A. D.; Tilley, T. D. *J. Am. Chem. Soc.* **2003**, *125*, 7971-7977.

(69) Oxgaard, J.; Muller, R. P.; Goddard, W. A.; Periana, R. A. *J. Am. Chem. Soc.* **2004**, *126*, 352-363.

(70) Vastine, B. A.; Hall, M. B. *J. Am. Chem. Soc.* **2007**, *129*, 12068-12069.

(71) Webb, J. R.; Burgess, S. A.; Cundari, T. R.; Gunnoe, T. B. *Dalton Trans.* **2013**, *42*, 16646-16665.

(72) Lam, W. H.; Jia, G. C.; Lin, Z. Y.; Lau, C. P.; Eisenstein, O. *Chem. Eur. J.* **2003**, *9*, 2775-2782.

(73) Oxgaard, J.; Goddard, W. A. *J. Am. Chem. Soc.* **2004**, *126*, 442-443.

(74) Lail, M.; Bell, C. M.; Conner, D.; Cundari, T. R.; Gunnoe, T. B.; Petersen, J. L. *Organometallics* **2004**, *23*, 5007-5020.

(75) Ess, D. H.; Gunnoe, T. B.; Cundari, T. R.; Goddard, W. A.; Periana, R. A. *Organometallics* **2010**, *29*, 6801-6815.

(76) Cundari, T. R.; Grimes, T. V.; Gunnoe, T. B. *J. Am. Chem. Soc.* **2007**, *129*, 13172-13182.

(77) Cummins, C. C.; Baxter, S. M.; Wolczanski, P. T. *J. Am. Chem. Soc.* **1988**, *110*, 8731-8733.

(78) Walsh, P. J.; Hollander, F. J.; Bergman, R. G. *J. Am. Chem. Soc.* **1988**, *110*, 8729-8731.

(79) With, J. d.; Horton, A. D. *Angew. Chem. Int. Ed.* **1993**, *32*, 903-905.

(80) Wicker, B. F.; Fan, H. J.; Hickey, A. K.; Crestani, M. G.; Scott, J.; Pink, M.; Mindiola, D. J. *J. Am. Chem. Soc.* **2012**, *134*, 20081-20096.

(81) Feng, Y.; Lail, M.; Barakat, K. A.; Cundari, T. R.; Gunnoe, T. B.; Petersen, J. L. *J. Am. Chem. Soc.* **2005**, *127*, 14174-14175.

(82) Feng, Y. E.; Lail, M.; Foley, N. A.; Gunnoe, T. B.; Barakat, K. A.; Cundari, T. R.; Petersen, J. L. *J. Am. Chem. Soc.* **2006**, *128*, 7982-7994.

(83) Tenn, W. J.; Young, K. J. H.; Bhalla, G.; Oxgaard, J.; Goddard, W. A.; Periana, R. A. *J. Am. Chem. Soc.* **2005**, *127*, 14172-14173.

(84) Stahl, S. S.; Labinger, J. A.; Bercaw, J. E. *Angew. Chem. Int. Ed.* **1998**, *37*, 2181-2192.

(85) Lersch, M.; Tilset, M. *Chem. Rev.* **2005**, *105*, 2471-2526.

(86) Siegbahn, P. E. M.; Crabtree, R. H. *J. Am. Chem. Soc.* **1996**, *118*, 4442-4450.

(87) Periana, R. A.; Taube, D. J.; Gamble, S.; Taube, H.; Satoh, T.; Fujii, H. *Science* **1998**, *280*, 560-564.

(88) Periana, R. A.; Bhalla, G.; Tenn, W. J.; Young, K. J. H.; Liu, X. Y.; Mironov, O.; Jones, C. J.; Ziatdinov, V. R. *J. Mol. Catal. A: Chem.* **2004**, *220*, 7-25.

(89) Mironov, O. A.; Bischof, S. M.; Konnick, M. M.; Hashiguchi, B. G.; Ziatdinov, V. R.; Goddard, W. A.; Ahlquist, M.; Periana, R. A. *J. Am. Chem. Soc.* **2013**, *135*, 14644-14658.

(90) McKeown, B. A.; Gonzalez, H. E.; Friedfeld, M. R.; Brosnahan, A. M.; Gunnoe, T. B.; Cundari, T. R.; Sabat, M. *Organometallics* **2013**, *32*, 2857-2865.

(91) Jordan, R. F.; Taylor, D. F. *J. Am. Chem. Soc.* **1989**, *111*, 778-779.

(92) Murai, S.; Kakiuchi, F.; Sekine, S.; Tanaka, Y.; Kamatani, A.; Sonoda, M.; Chatani, N. *Nature* **1993**, *366*, 529-531.

(93) Wang, X. L.; Zhou, L. H.; Lu, W. J. *Curr. Org. Chem.* **2010**, *14*, 289-307.

(94) Cho, S. H.; Kim, J. Y.; Kwak, J.; Chang, S. *Chem. Soc. Rev.* **2011**, *40*, 5068-5083.

(95) Lewis, J. C.; Bergman, R. G.; Ellman, J. A. *Acc. Chem. Res.* **2008**, *41*, 1013-1025.

(96) Nakao, Y.; Kashihara, N.; Kanyiva, K. S.; Hiyama, T. *Angew. Chem. Int. Ed.* **2010**, *49*, 4451-4454.

(97) Pittard, K. A.; Lee, J. P.; Cundari, T. R.; Gunnoe, T. B.; Petersen, J. L. *Organometallics* **2004**, *23*, 5514-5523.

(98) Karshtedt, D.; Bell, A. T.; Tilley, T. D. *Organometallics* **2004**, *23*, 4169-4171.

(99) Bowring, M. A.; Bergman, R. G.; Tilley, T. D. *Organometallics* **2011**, *30*, 1295-1298.

(100) Luedtke, A. T.; Goldberg, K. I. *Angew. Chem. Int. Ed.* **2008**, *47*, 7694-7696.

(101) Clement, M. L.; Grice, K. A.; Luedtke, A. T.; Kaminsky, W.; Goldberg, K. I. *Chem. Eur. J.* **2014**, *20*, 17287-17291.

(102) McKeown, B. A.; Foley, N. A.; Lee, J. P.; Gunnoe, T. B. *Organometallics* **2008**, *27*, 4031-4033.

(103) McKeown, B. A.; Gonzalez, H. E.; Friedfeld, M. R.; Gunnoe, T. B.; Cundari, T. R.; Sabat, M. *J. Am. Chem. Soc.* **2011**, *133*, 19131-19152.

(104) McKeown, B. A.; Gonzalez, H. E.; Gunnoe, T. B.; Cundari, T. R.; Sabat, M. *ACS Catal.* **2013**, *3*, 1165-1171.

(105) McKeown, B. A.; Gonzalez, H. E.; Michaelos, T.; Gunnoe, T. B.; Cundari, T. R.; Crabtree, R. H.; Sabat, M. *Organometallics* **2013**, *32*, 3903-3913.

(106) McKeown, B. A.; Prince, B. M.; Ramiro, Z.; Gunnoe, T. B.; Cundari, T. R. *ACS Catal.* **2014**, *4*, 1607-1615.

(107) Matsumoto, T.; Taube, D. J.; Periana, R. A.; Taube, H.; Yoshida, H. *J. Am. Chem. Soc.* **2000**, *122*, 7414-7415.

(108) Periana, R. A.; Liu, X. Y.; Bhalla, G. *Chem. Comm.* **2002**, 3000-3001.

(109) Bhalla, G.; Bischof, S. M.; Ganesh, S. K.; Liu, X. Y.; Jones, C. J.; Borzenko, A.; Tenn, W. J.; Ess, D. H.; Hashiguchi, B. G.; Lokare, K. S.; Leung, C. H.; Oxgaard, J.; Goddard, W. A.; Periana, R. A. *Green Chem.* **2011**, *13*, 69-81.

(110) Joslin, E. E.; McMullin, C. L.; Gunnoe, T. B.; Cundari, T. R.; Sabat, M.; Myers, W. H. *Organometallics* **2012**, *31*, 6851-6860.

(111) Lail, M.; Arrowood, B. N.; Gunnoe, T. B. *J. Am. Chem. Soc.* **2003**, *125*, 7506-7507.

(112) Joslin, E. E. Synthesis and Characterization of Ru(II) Complexes as Potential Catalysts in Olefin Hydroarylation. University of Virginia, Charlottesville, VA, 2013.

(113) Tolman, C. A. *Chem. Rev.* **1977**, *77*, 313-348.

(114) Moloy, K. G.; Petersen, J. L. *J. Am. Chem. Soc.* **1995**, *117*, 7696-7710.

(115) Foley, N. A.; Lail, M.; Lee, J. P.; Gunnoe, T. B.; Cundari, T. R.; Petersen, J. L. *J. Am. Chem. Soc.* **2007**, *129*, 6765-6781.

(116) Foley, N. A.; Lail, M.; Gunnoe, T. B.; Cundari, T. R.; Boyle, P. D.; Petersen, J. L. *Organometallics* **2007**, *26*, 5507-5516.

(117) Foley, N. A.; Ke, Z. F.; Gunnoe, T. B.; Cundari, T. R.; Petersen, J. L. *Organometallics* **2008**, *27*, 3007-3017.

(118) Burgess, S. A.; Joslin, E. E.; Gunnoe, T. B.; Cundari, T. R.; Sabat, M.; Myers, W. H. *Chem. Sci.* **2014**, *5*, 4355-4366.

(119) Bullock, R. M., *Catalysis without Precious Metals*. Wiley-VCH Verlag & Co.: Weinheim, Germany, 2010.

(120) Enthaler, S.; Junge, K.; Beller, M. *Angew. Chem. Int. Ed.* **2008**, *47*, 3317-3321.

(121) MetalPrices.com. http://www.metalprices.com/ (March 7, 2015),

(122) Liu, J.; Chakraborty, S.; Hosseinzadeh, P.; Yu, Y.; Tian, S. L.; Petrik, I.; Bhagi, A.; Lu, Y. *Chem. Rev.* **2014**, *114*, 4366-4469.

(123) Jia, F.; Li, Z. *Org. Chem. Front.* **2014**, *1*, 194-214.

(124) Sun, C. L.; Li, B. J.; Shi, Z. J. *Chem. Rev.* **2011**, *111*, 1293-1314.

(125) Tondreau, A. M.; Atienza, C. C. H.; Weller, K. J.; Nye, S. A.; Lewis, K. M.; Delis, J. G. P.; Chirik, P. J. *Science* **2012**, *335*, 567-570.

(126) Chen, M. S.; White, M. C. *Science* **2010**, *327*, 566-571.

(127) Chen, M. S.; White, M. C. *Science* **2007**, *318*, 783-787.

(128) Zuo, W. W.; Lough, A. J.; Li, Y. F.; Morris, R. H. *Science* **2013**, *342*, 1080-1083.

(129) Gunay, A.; Theopold, K. H. *Chem. Rev.* **2010**, *110*, 1060-1081.

(130) Ittel, S. D.; Tolman, C. A.; English, A. D.; Jesson, J. P. *J. Am. Chem. Soc.* **1978**, *100*, 7577-7585.

(131) Tolman, C. A.; Ittel, S. D.; English, A. D.; Jesson, J. P. *J. Am. Chem. Soc.* **1979**, *101*, 1742-1751.

(132) Baker, M. V.; Field, L. D. *J. Am. Chem. Soc.* **1986**, *108*, 7433-7434.

(133) Baker, M. V.; Field, L. D. *J. Am. Chem. Soc.* **1986**, *108*, 7436-7438.

(134) Jones, W. D.; Foster, G. P.; Putinas, J. M. *J. Am. Chem. Soc.* **1987**, *109*, 5047-5048.

(135) Waltz, K. M.; Hartwig, J. F. *Science* **1997**, *277*, 211-213.

(136) Waltz, K. M.; Hartwig, J. F. *J. Am. Chem. Soc.* **2000**, *122*, 11358-11369.

(137) Ohki, Y.; Hatanaka, T.; Tatsumi, K. *J. Am. Chem. Soc.* **2008**, *130*, 17174-17186.

(138) Hatanaka, T.; Ohki, Y.; Tatsumi, K. *Chem. Asian J.* **2010**, *5*, 1657-1666.

# 2 The Development and Study of Aromatic C–H Activation by Fe(II) Complexes

## 2.1 Introduction

As discussed in Chapter 1, the activation of aromatic C–H bonds plays a central role in the proposed catalytic cycle for transition metal-catalyzed olefin hydroarylation. While the C–H activation of aromatic substrates has been widely reported for second and third row transition metals, the cleavage of C–H bonds by non-radical routes using first row metals is considerably less common.[1-3] One explanation for the reduced reactivity of first row transition metals toward C–H activation is that that the first row metals have weaker M–R bonds compared to second and third row transition metals.[4, 5] For benzene C–H activation, the thermodynamics of the reaction are, in part, determined by the bond strength of the M–Ph product (Scheme 2.1). If this M–C bond is weak, the reaction may be endothermic and not observed. Additionally, a weak incipient M–C bond during the C–H activation transition state would raise the activation barrier of C–H bond activation (Scheme 2.1). Furthermore, a weaker M–C bond dissociation energy (BDE) might lead to bond homolysis (Scheme 2.2). The generation of a carbon-based radical from bond homolysis could lead to H atom abstraction of weak C–H bonds. For designing catalysts for olefin hydroarylation, it is important that the bond cleavage is selective from strong aromatic C–H bonds (BDE > 110 kcal/mol). Finally, first row transition metals have reduced π-basicity compared to their second and third row counterparts. The reduced π-basicity of first row transition metals gives them a kinetic disadvantage since weaker π-back donation from a filled metal dπ orbital to the C–H σ* orbital could reduce the rate of C–H activation.[6, 7]

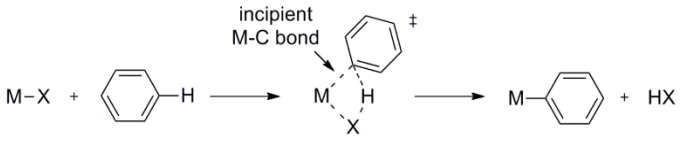


**Scheme 2.1.** Importance of M–C bond dissociation energy for benzene C–H activation.


**Scheme 2.2.** M–Ph bond homolysis could lead to reaction with weak C–H bonds.

Both in nature and in the laboratory, Fe has been shown to functionalize C–H bonds via a radical process.[8-14] For example, the enzyme P450 functionalizes hydrocarbons by a process that involves a radical-rebound mechanism from a high valent Fe-oxo complex. In a radical-rebound mechanism, a high valent Fe-oxo abstracts a hydrogen atom from a hydrocarbon resulting in an Fe–OH and a carbon-based radical, which then recombines or "rebounds" with the hydroxide to give ROH (Scheme 2.3).[8, 15] The major drawback from developing catalysts that operate by a radical mechanism is that, in general, they are unable to functionalize aromatic C–H bonds (typically, >110 kcal/mol) (Scheme 2.3).[8] The ability for an Fe-oxo to abstract an H atom requires that the resulting O–H bond is stronger than the C–H bond that is being broken.[8, 16] Thus, the development of Fe complexes that activate strong C–H bonds is an area of important study. However, Fe-mediated C–H activation, especially is catalytic reactions, has not been thoroughly developed.[17, 18]

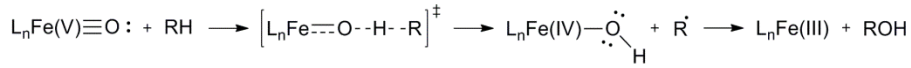


**Scheme 2.3.** C–H functionalization by Fe-oxo complexes by a radical-rebound mechanism.

As reviewed in Chapter 1, there have been a few examples of Fe complexes capable of aromatic C–H activation by a process that does not involve the generation of free radicals. Ittel and Tolman have reported C–H activation starting from $(dmpe)_2Fe(napthyl)(H)$ (dmpe = 1,2-bis(dimethylphosphino)ethane),[19, 20] while Field and Baker demonstrated the use of $(dmpe)_2FeH_2$ as a precursor for C–H oxidative addition reactions under photolytic conditions.[21] In both of these cases, reductive elimination generates a highly reactive $(dmpe)_2Fe(0)$ complex that readily inserts into C–H bonds. Field and Baker also reported C–H activation from a $(depe)_2Fe(0)$ (depe = 1,2-bis(diethylphosphino)ethane) intermediate that was generated by reductive elimination from $(depe)_2Fe(Me)(H)$.[22] Similarly, Jones and co-workers reported the use of $(PMe_3)_2(RN{\equiv}C)_3Fe$ complexes as catalysts for the addition of benzene C–H bonds across isonitriles to give aldimines.[17] Finally, during the course of this work, Ohki and Tatsumi demonstrated aromatic C–H activation using a half-sandwich Fe complex ligated by *N*-heterocyclic carbenes.[18, 23]

Because a foundation of this work was our laboratory's success with TpRu(L)(NCMe)Ph (Tp = hydridotris(pyrazolyl)borate, L = CO, $PMe_3$, P(*N*-pyrrolyl)$_3$, $P(OCH_2)_3CEt$, $P(O)(OCH_2)_2CMe$) catalysts for olefin hydroarylation, we initially sought to develop related TpFe(L)(NCMe)Ph complexes that were capable of activating strong aromatic C–H bonds.[24-28] We hoped that the reactivity observed for TpRu complexes could be translated to similar Fe complexes. In this chapter, the progression from TpFe complexes to the discovery of a half-sandwich Fe complex capable of aromatic C–H activation will be shown as well as a mechanistic study of this process using a combined experimental and computational approach. The study of aromatic C–H activation by

Cp*Fe(CO)(NCMe)Ph (**2.6**) has been previously published.[29] Dr. Alban Petit and Prof. Daniel Ess (BYU) performed the computational studies in collaboration with Prof. Thomas Cundari (U. North Texas), and Dr. Michal Sabat (UVa) solved the crystal structures.

## 2.2 Results and Discussion

### 2.2.1 Fe Complexes of the Hydridotris(pyrazolyl)borate Ligand (Tp)

Because of the success with olefin hydroarylation catalysts based on the TpRu(L)(NCMe)Ph motif, our initial investigations into developing Fe complexes capable of aromatic C–H activation started with a study of TpFe complexes (Figure 2.1).[24-28, 30-33] A survey of the literature demonstrates that examples of TpFe(R) complexes (R = hydrocarbyl ligand) are very rare.[34-38] In reports of attempted syntheses of TpFe complexes, it is clear that decomposition to $Tp_2Fe$ is prominent.[36, 38] To the best of our knowledge, there is only one example of a heterolyptic TpFe(L)(L')R (R = Me or Ph) complex, TpFe(CO)($PMe_3$)Me.[36] Thus, as a starting point, the synthesis of this complex was carried out according to Scheme 2.4. In our hands, TpFe(CO)($PMe_3$)Me (**2.1**) had poor stability and attempts at stoichiometric benzene C–H activation and ethylene hydrophenylation were futile. For example, heating a $C_6D_6$ solution up to 70 °C eventually led to broadening of the $^1$H NMR resonances, possibly indicating decomposition to a paramagnetic species. Additionally, a benzene solution of **2.1** was treated with ethylene (25 psi) and heated at 90 °C for 4 h. No ethylbenzene was observed. Increasing the temperature (120 °C) and pressure of ethylene (40 psi) still resulted in no ethylbenzene production by GC-FID. Removal of the volatiles and analysis by $^1$H NMR spectroscopy indicated decomposition to a paramagnetic species. The failure of this complex likely stems from the combination of poor stability and the strongly

coordinating ligand set. Thus, ligand exchange of $PMe_3$ or CO with $C_2H_4$ likely require high temperatures; however, at higher temperatures (>70 °C) a decomposition pathway is competitive. Additional efforts to remove one of the co-ligands (i.e., CO and $PMe_3$) were not successful.

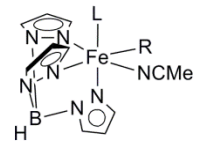


**Figure 2.1.** Target TpFe(L)(NCMe)R complexes.

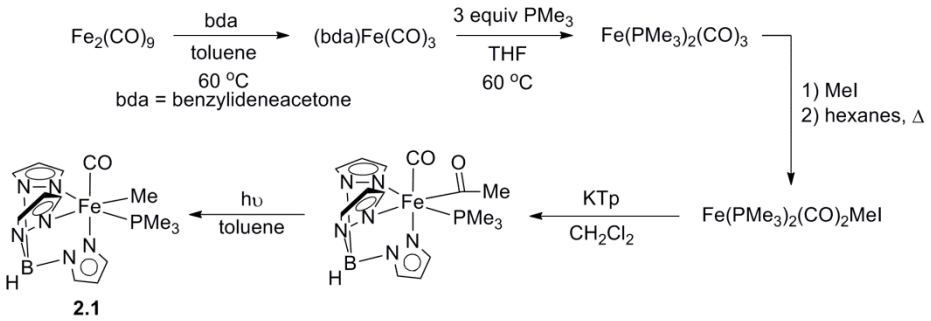


**Scheme 2.4** Synthesis of TpFe(CO)($PMe_3$)Me (**2.1**).

We explored an alternative synthetic route to access TpFe(L)(NCMe)Ph complexes, specifically the complex $TpFe(CO)_2Ph$ from which a CO ligand could either be removed oxidatively or photolytically. The known complex *cis*-$Fe(CO)_4I_2$ was treated with KTp in order to synthesize $TpFe(CO)_2I$ via a metathesis reaction (Scheme 2.5).[39] This reaction provided a product that had $^1H$ NMR data consistent with the desired product (Figure 2.2), as well as CO stretches at 2060 and 2017 $cm^{-1}$ ($CH_2Cl_2$) in the IR spectrum; however, the metathesis reaction was highly inconsistent, and in most cases decomposition to the pink $Tp_2Fe$ was observed.

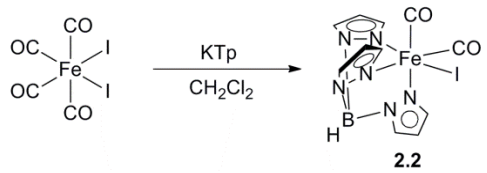


**Scheme 2.5.** Synthesis of $TpFe(CO)_2I$ (**2.2**).

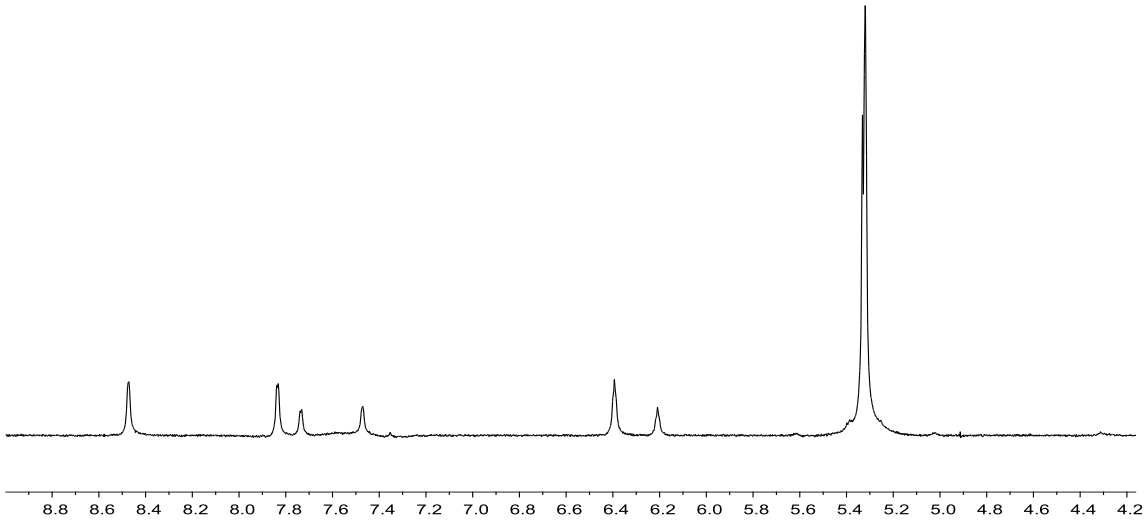


**Figure 2.2.** $^1H$ NMR spectrum of $TpFe(CO)_2I$ (**2.2**) in $CD_2Cl_2$ (upfield region omitted).

### 2.2.2 The Synthesis and Study of Fe Complexes of the Cyclopentadienyl Ligand (Cp)

Due to the instability and synthetic challenges associated with developing Fe complexes for C–H activation based on the Tp ligand, efforts shifted to the synthesis of CpFe complexes. Cyclopentadienyl ligands are known to be similar to Tp ligands. Both classes of ligands are six-electron donors (with similar electron donating abilities) and bind to the metal center in a pseudo-*fac* coordination mode.[40] In terms of developing catalysts for olefin hydroarylation, $CpFe(CO)_2Ar$ complexes have been shown to mediate

olefin insertion.[41] Additionally, the breadth of CpFeR complexes known in the literature demonstrates the relative high stability (versus TpFeR) of this class of compounds.[42] Thus, the synthesis of a complex of the type CpFe(CO)(L)Ph (L = labile ligand) was explored.

Just prior to the commencement of the present study, an efficient synthesis for $CpFe(CO)_2Ph$ (**2.3**) was reported, which involved the reaction of $CpFe(CO)_2I$ with CuOTf and $Bu_3SnPh$ in 1,4-dioxane (Scheme 2.6).[43] With $CpFe(CO)_2Ph$ in hand, we subjected the complex to catalytic hydrophenylation conditions (Scheme 2.7). Based on previous studies, we anticipated that at elevated temperatures, a CO ligand could dissociate and allow for ethylene coordination.[41] Initially, a benzene solution with 0.025 mol% of **2.3** (relative to benzene) was heated at 120 °C with 30 psi of $C_2H_4$, but no products were observed by GC/MS after 16 h. However, heating the reaction solution at 150 °C with 125 psi of $C_2H_4$ resulted in the production of ethylbenzene (~0.5 TO), styrene (~0.5 TO), and propiophenone in sub-stoichiometric amounts after ~4 h (Scheme 2.7). We also observed ferrocene by GC/MS, which could be a decomposition product of $CpFe(CO)_2Ph$ (**2.3**). The formation of propiophenone likely proceeds by stepwise insertion of CO and ethylene into the Fe–Ph bond followed by C–H activation or Fe–$CH_2$ bond homolysis and subsequent H atom abstraction (Scheme 2.8). Some attempts were made to catalytically make propiophenone by adding CO to the reaction. For instance, a benzene solution of **2.3** (0.025 mol%) was heated at 150 °C with 30 psi $C_2H_4$ and either 30 psi or 90 psi of CO. Analysis of the organic products by GC/MS revealed the production of ~0.4 TO of ethylbenzene with no evidence of propiophenone. Because CO dissociation is likely involved in the reaction, the presence of added CO may suppress

dissociation and limit reactivity. While $CpFe(CO)_2Ph$ (**2.3**) is an ineffective catalyst for ethylene hydrophenylation, these results highlight the potential for Fe-based catalysts since we have observed ethylbenzene formation. While we do not have mechanistic data, ethylbenzene formation may suggest that complex **2.3** mediates ethylene insertion and C–H activation.

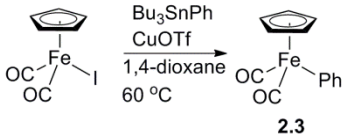


**Scheme 2.6.** Previously reported synthesis of $CpFe(CO)_2Ph$ (**2.3**).

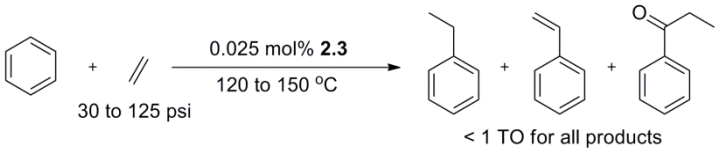


**Scheme 2.7.** Attempted catalytic ethylene hydrophenylation using $CpFe(CO)_2Ph$ (**2.3**).

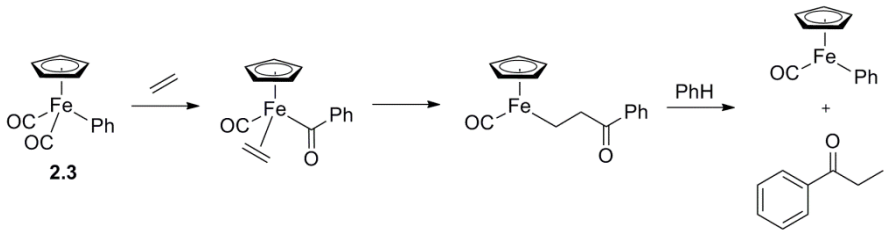


**Scheme 2.8.** Possible mechanism for the formation of propiophene from the reaction of $CpFe(CO)_2Ph$ (**2.3**), ethylene, and benzene.

Next, the synthesis of CpFe(CO)(L)Ph (L = labile ligand) was investigated. We considered two likely pathways from $CpFe(CO)_2Ph$ (**2.3**): 1) removal of CO using an oxidant to generate $CO_2$ and 2) photolytic dissociation of CO. In the first method, $CpFe(CO)_2Ph$ (**2.3**) was treated with either pyridine-*N*-oxide (PyO) or trimethylamine-*N*-oxide ($Me_3NO$) in a coordinating solvent (i.e., pyridine or NCMe). The CO stretches in

the IR spectrum of **2.3** appear at 2011 $cm^{-1}$ and 1953 $cm^{-1}$.[44] A CO stretching frequency above 2000 $cm^{-1}$ suggests that the CO ligand is relatively electrophilic and may be susceptible to oxidative removal. Additionally, some reactions with PyO were performed in non-coordinating solvents (e.g., chloroform, *ortho*-dichlorobenzene) since reduction of PyO leads to formation of pyridine, which could coordinate to the Fe center. Reactions with $Me_3NO$ and PyO eventually led to intractable mixtures of products.

An alternative synthetic route for CpFe(CO)(L)Ph (L = labile ligand) was pursued that involved the photolysis of $CpFe(CO)_2Ph$ in a coordinating solvent such as pyridine or NCMe. Photolytic dissociation of CO ligands from transition metal complexes is well known.[7] Excitation of an electron from a Fe–CO π-bonding orbital to an Fe–CO π* orbital by UV or visible light allows for dissociation under ambient temperatures, eventually leading to $CO_{(g)}$ being released from the reaction solution.

The photolytic reaction of $CpFe(CO)_2Ph$ in NCMe-$d_3$ led to the clean conversion of the starting material by $^1H$ NMR spectroscopy to a new product, likely CpFe(CO)(NCMe-$d_3$)Ph. The reaction never led to complete conversion of the starting material (75-80% conversion). It is possible that dissolved CO competes with NCMe for coordination to the Fe center, which may explain why the conversions are <100%. Thus, pyridine was used as a ligand, with the hope that it would coordinate to the Fe center more strongly. Photolysis of $CpFe(CO)_2Ph$ in pyridine-$d_5$ led to ~90% conversion to CpFe(CO)(py-$d_5$)Ph. Scaling up the reaction in protio-pyridine led to the isolation of CpFe(CO)(py)Ph (**2.4**) in ~62% yield (Scheme 2.9). The $^1H$ NMR spectrum of **2.4** is shown in Figure 2.3. There is some broadening, which may be attributed to small amounts of paramagnetic impurities. The product exhibits a single $\nu_{CO}$ of 1928 $cm^{-1}$ in

the IR spectrum, which is consistent with the proposed structure. Following our study with complex **2.4**, this complex was cleanly isolated as an alcohol dehydrogenation pre-catalyst.[45] In this report, complex **2.4** was synthesized by photolysis of $CpFe(CO)_2Ph$ (**2.3**) in toluene with excess pyridine at 5 °C.

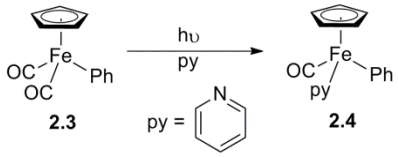


**Scheme 2.9**. Synthesis of CpFe(CO)(py)Ph (**2.4**).

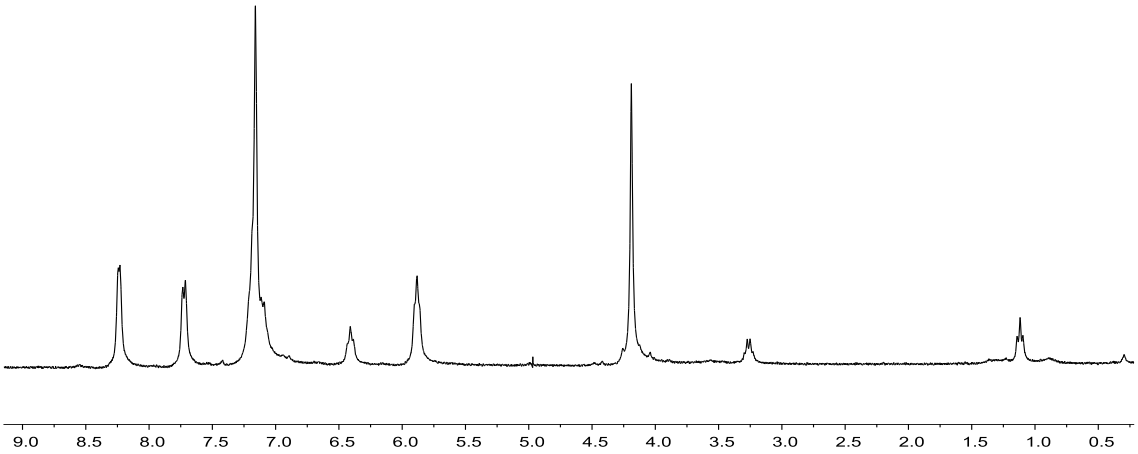


**Figure 2.3.** $^1$H NMR spectrum of CpFe(CO)(py)Ph (**2.4**) in $C_6D_6$.

The complex CpFe(CO)(py)Ph (**2.4**) was accessed for competency in the C–D activation of $C_6D_6$. Gentle heating (50 °C) in $C_6D_6$ led to the broadening of the resonances in the $^1$H NMR spectrum along with a new peak growing in ~6.5 ppm. The identity of this peak is unknown. Further heating led to no discernable Cp proton

resonances, indicating decomposition of the starting material. An NMR scale experiment was performed by dissolving CpFe(CO)(py)Ph in $C_6D_6$ and pressurizing the NMR tube with 50 psi of ethylene (Scheme 2.10). Upon heating the reaction (90 °C), styrene was observed, although quantification proved challenging due to the broad resonances. Considerable broadening of the proton resonances made any additional assignment challenging. These data demonstrate that decomposition of **2.4** competes with productive reactivity in ethylene hydrophenylation.

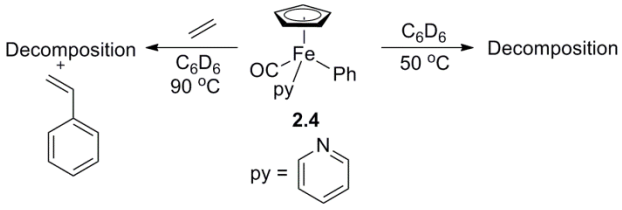


**Scheme 2.10.** Reaction of CpFe(CO)(py)Ph (**2.4**) with $C_6D_6$ and with $C_6D_6$ and $C_2H_4$.

The study of CpFe(CO)(py)Ph demonstrated the feasibility of synthesizing an Fe complex with a labile ligand that could potentially allow for reaction with aromatic C–H bonds and unsaturated substrates. The poor thermal stability and challenges with clean synthesis made this particular complex unsuitable for additional study. Consequently, investigation into related Fe complexes with improved stability was pursued.

### 2.2.3 Synthesis and Characterization of Cp*Fe(CO)(NCMe)Ph

Based on the previous work with TpFe and CpFe (See sections 2.2.1 and 2.2.2), the need to develop an Fe complex with greater thermal stability while maintaining a similar structural motif to the TpRu catalysts led us to pursue the synthesis of Cp*Fe (Cp* = pentamethylcyclopentadienyl) complexes. Like Cp and Tp, Cp* is pseudo-facially coordinating 6-electron donor. Studies have demonstrated that, in some cases, Cp* is more donating than Tp and Cp, which may facilitate C–H activation.[40] Additionally, a

potential reason for the poor stability of the CpFe(CO)(py)Ph complex is the propensity for the Cp ligand to ring slip,[7] which may allow access to other side reactivity. A ring slip is when the Cp ligand rearranges from the $\eta^5$-coordination mode to the $\eta^3$-coordination mode. This rearrangement typically occurs to accommodate additional electrons on the metal center. Ring slips have been implicated during associative substitution mechanisms for some transition metal complexes.[7] Cp* ligands are known to give more stable complexes than their Cp analogues.[7]

Thus, we targeted Cp*Fe(CO)(L)Ph (L = labile ligand) complexes to begin our investigation of C–H activation by Cp*Fe complexes. We followed a similar pathway to the CpFe complexes described above. As a starting point, the complex $Cp^*Fe(CO)_2I$ was synthesized according to published procedures.[46] Prior to beginning this study, the only known synthesis of $Cp^*Fe(CO)_2Ph$ (**2.5**) gave very low yields.[47] However, it was found that by modifying the conditions for the synthesis of $CpFe(CO)_2Ph$ (**2.3**), the desired complex could be obtained in good yield.[43] Thus, heating a mixture of $Cp^*Fe(CO)_2I$, $Bu_3SnPh$, and CuOTf in 1,4-dioxane led to the isolation of $Cp^*Fe(CO)_2Ph$ (**2.5**) in 67% yield following column chromatography (Scheme 2.11). The NMR spectral data match the proposed structure (Figure 2.4). Carbonyl stretching frequencies at 1994 $cm^{-1}$ and 1937 $cm^{-1}$ in the IR spectrum are consistent with a dicarbonyl species. Additionally, a single crystal suitable for an X-ray diffraction study was grown from a saturated pentane solution of complex **2.5** (Figure 2.5). The Fe–Ph bond distance measures 2.002(2) Å with the Fe–C bond lengths of the CO ligands at 1.756(1) Å. It should be noted that during the preparation and review process for our initial publication, an alternative synthesis for complex **2.5** was reported that gave comparable yields.[48] The authors of this report also

disclosed the structure of complex **2.5**. Their metrics are consistent with the data we reported.

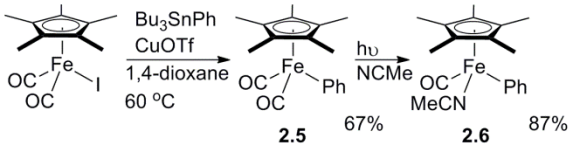


**Scheme 2.11.** Synthesis of Cp*Fe(CO)$_2$Ph (**2.5**) and Cp*Fe(CO)(NCMe)Ph (**2.6**).

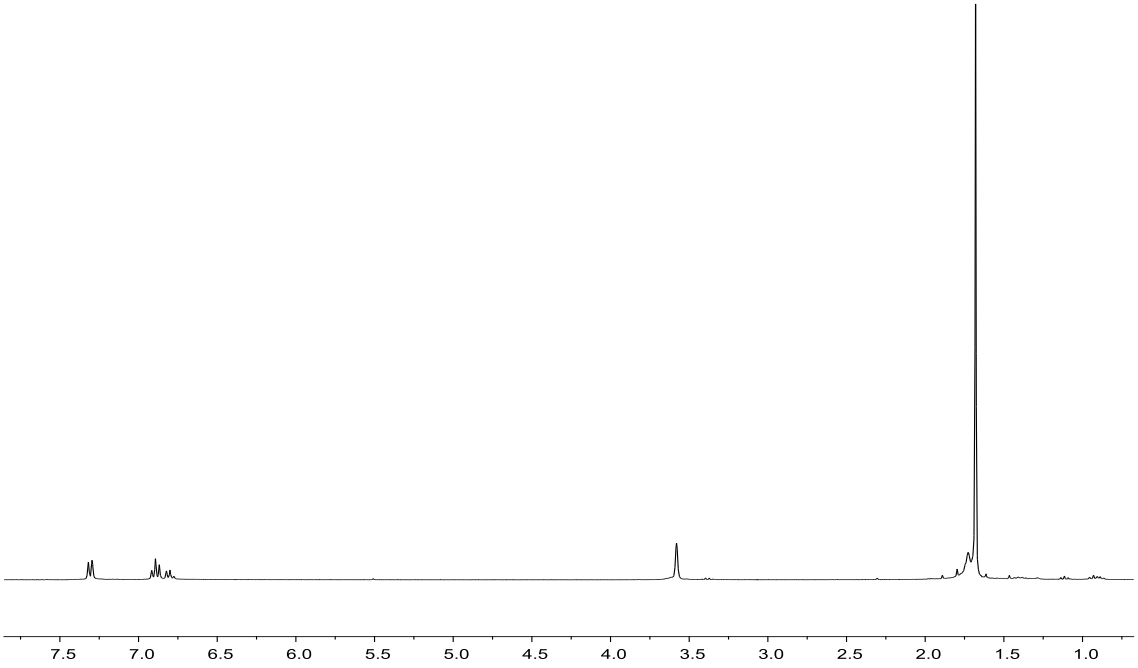


**Figure 2.4.** $^1$H NMR spectrum of Cp*Fe(CO)$_2$Ph (**2.5**) in THF-$d_8$.

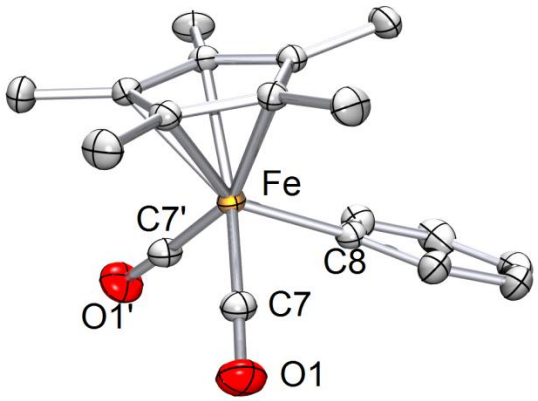


**Figure 2.5.** ORTEP drawing of Cp*Fe(CO)$_2$Ph (**2.5**) (50% probability ellipsoids; H atoms omitted). Selected bond lengths (Å): Fe–C7/C7′ 1.756(1), Fe–C8 2.002(2), C7–O1/C7′–O1′ 1.151(2). Selected bond angles (deg): C7–Fe–C7′ 95.87(8), C7/C7′–Fe–C2 91.30(5).

Dissolving Cp*Fe(CO)$_2$Ph (**2.5**) in NCMe and photolyzing at 0 °C for a total of 3 h resulted in the gradual change of the solution color from yellow to red-orange (Scheme 2.11). Importantly, the reaction vessel with degassed after the first two hours by freeze-pump-thaw cycles. Without the degassing process, the reaction does not go to completion and eventually leads to decomposition after prolonged photolysis. Furthermore, it is important to keep the reaction vessel chilled in an ice-water bath since photolysis in the absence of the ice bath led to decomposition. After work-up, the desired complex Cp*Fe(CO)(NCMe)Ph (**2.6**) was isolated in 87% yield as an red-orange solid. The complex is stable for at least a month in the solid-state if stored under inert atmosphere at –35 °C. The product is stable for hours in solution or the solid-state at room temperature if kept under an inert atmosphere.

Complex **2.6** is characterized by a singlet at 2.52 ppm in the $^1$H NMR spectrum for the coordinated NCMe along with the expected aryl and Cp* resonances (Figure 2.6). The CO stretching frequency shows up at 1903 cm$^{-1}$ in the infrared spectrum, which not only is evidence for a single CO ligand but highlights the electron richness of the Fe

center. For comparison, our previously reported TpRu(CO)(NCMe)Ph complex exhibits a CO stretch at 1935 $cm^{-1}$.[24] In addition, Cp*Fe(CO)(NCMe)Ph (**2.6**) was characterized by single crystal X-ray diffraction (Figure 2.7). The Fe–$C_{Ph}$ bond length is 1.990(1) Å, the Fe–$C_{CO}$ bond length is 1.741(1) Å, and the Fe–$N_{NCMe}$ bond length is 1.903(1) Å. The Fe–$C_{Ph}$ bond length in **2.6** is slightly reduced compared to that of complex **2.5** (2.002(2) Å).

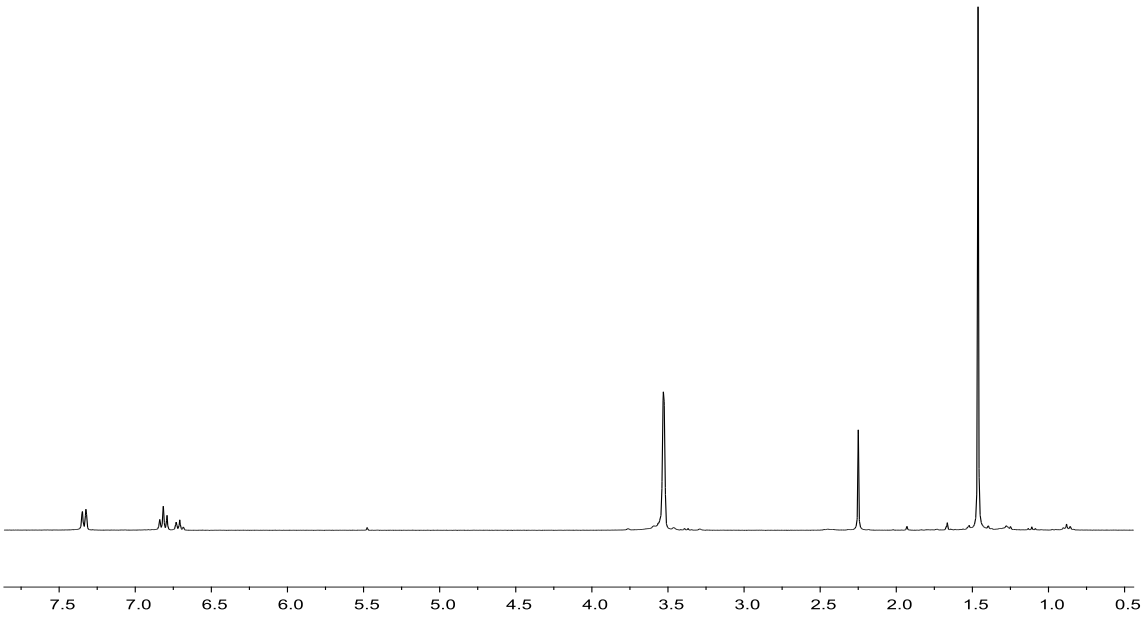


**Figure 2.6.** $^{1}$H NMR spectrum of Cp*Fe(CO)(NCMe)Ph (**2.6**) in dioxane-$d_8$.

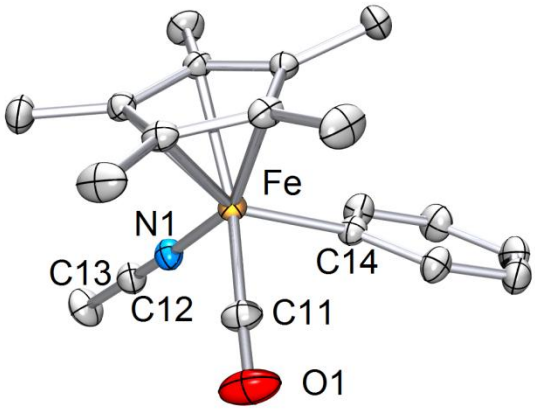


**Figure 2.7.** ORTEP drawing of Cp*Fe(CO)(NCMe)Ph (**2.6**) (50% probability ellipsoids; H atoms omitted for clarity). Selected bond lengths (Å): Fe–C14 1.990(1), Fe–C11

1.741(1), Fe–N1 1.903(1), C11–O1 1.154(2). Selected bond angles (deg): C11–Fe–N1 98.00(6), C11–Fe–C14 91.79(6), N1–Fe–C14 89.76(5).

### 2.3.4 C–H Activation of Benzene by Cp*Fe(CO)(NCMe)Ph (2.6)

Heating a $C_6D_6$ solution of Cp*Fe(CO)(NCMe)Ph (**2.6**) at 50 °C resulted in the gradual disappearance of the phenyl resonances with persistence of the coordinated NCMe and Cp* resonances (Figure 2.8). Cp*Fe(CO)(NCMe)(Ph-$d_5$) (**2.6-*d*$_5$**) forms in ~80% yield based on $^1$H NMR spectroscopy using hexamethyldisilane (HMDS) as an internal standard (Scheme 2.12). During the course of the reaction, a new Cp* peak begins to grow in, and with prolonged heating or heating at higher temperatures insoluble materials are observed in the NMR tube. The new Cp* peak is assigned to $Cp^*Fe(CO)_2Ph$ (**2.5**) and $Cp^*Fe(CO)_2$(Ph-$d_5$) (**2.5-*d*$_5$**), which has been further characterized by infrared spectroscopy ($\nu_{CO}$ = 1994 and 1937 cm$^{-1}$). Complexes **2.5** and **2.5-*d*$_5$** likely form from either a reaction in which two equivalents of complex **2.6** or **2.6-*d*$_5$** react to give $Cp^*Fe(CO)_2Ph$ and unidentified Fe product(s). Another possibility is that complexes **2.6** and **2.6-*d*$_5$** decompose to release free CO in solution, which can coordinate to Cp*Fe(CO)(NCMe)Ph (**2.6**). Either way, this is a relatively minor decomposition pathway giving ~10% of **2.5** and **2.5-*d*$_5$** with the remaining mass balance likely belonging to unidentified decomposition products. A kinetic analysis was performed for the C–D activation of $C_6D_6$. In this experiment, a 0.047 M $C_6D_6$ solution of **2.6** (pseudo-first order conditions) was heated in a temperature calibrated NMR probe at 49 °C while $^1$H NMR spectra were acquired. By monitoring the disappearance of the *ortho*-phenyl resonance of **2.6**, a first order decay plot was constructed (Figure 2.9), which gives a $k_{obs}$ is 4.6(5) x 10$^{-4}$ s$^{-1}$ at 49 °C.

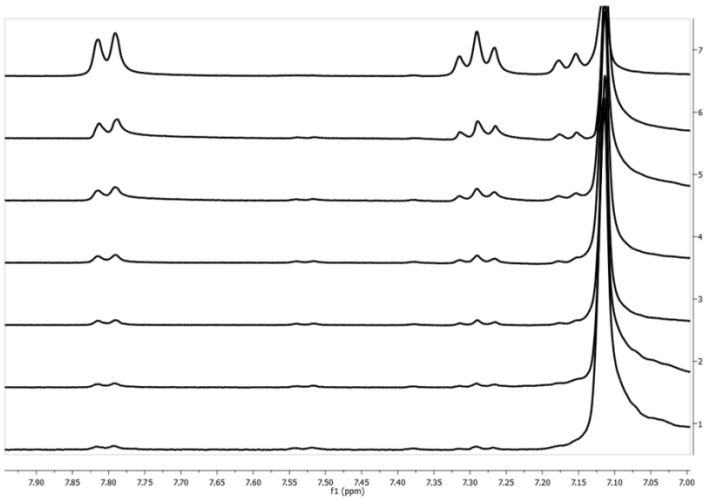


**Figure 2.8.** $^{1}$H NMR spectra (aryl region) from the reaction of Cp*Fe(CO)(NCMe)Ph (**2.6**) and $C_6D_6$.

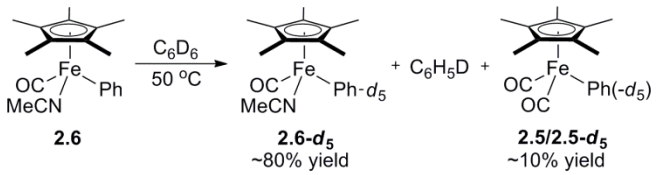


**Scheme 2.12.** C–D activation of benzene by Cp*Fe(CO)(NCMe)Ph (**2.6**).

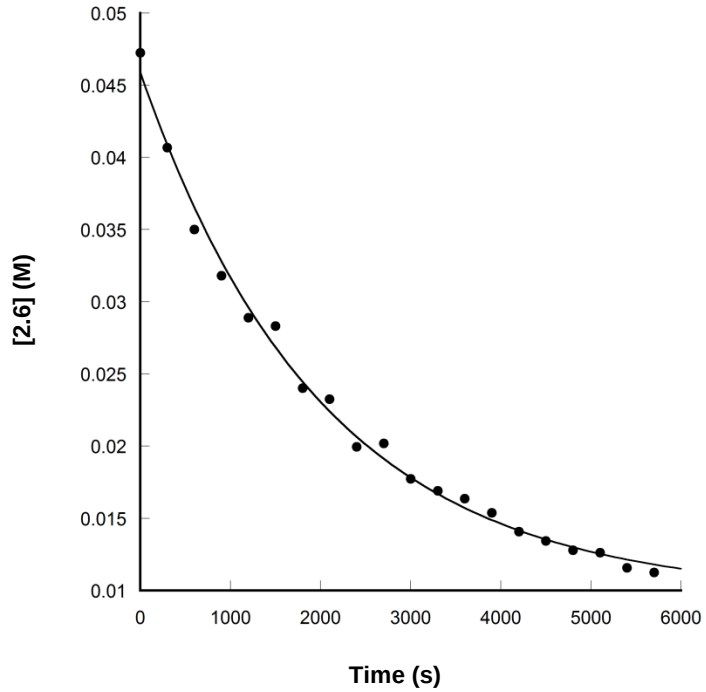


**Figure 2.9.** First-order decay plot for the reaction of Cp*Fe(CO)(NCMe)Ph (**2.6**) and $C_6D_6$ ([**2.6**] = 0.047 M, 49 °C).

The C–H activation of benzene from an Fe(II) complex is very rare, especially under mild conditions (<50 °C). The only other Fe(II) complex capable of benzene C–H activation is Cp*Fe($L^{Me}$)Me ($L^{Me}$ = 1,3,4,5-tetramethyl-imidazol-2-ylidene), which requires 7 days at 80 °C to obtain a 40% NMR yield of the phenyl complex.[18] In comparison, complex **2.6** requires just hours at milder temperatures and gives a higher yield than Cp*Fe($L^{Me}$)Me.

### 2.3.5 Computational Study of C–D(H) Activation of Benzene by Cp*Fe(CO)(NCMe)Ph (2.6)

To explore the mechanism of $C_6D_6$ C–D (modeled as C–H) bond activation by **2.6**, the group of Prof. Daniel Ess (BYU) utilized M06 density functional calculations with SMD solvent corrections to calculate possible intermediates and transition states.[49-51] Comparison of the M06 optimized structure of **2.6** (Figure 2.10) shows a good fit in the

bond lengths and angles compared to the X-ray structure shown in Figure 2.7. For example, computations predict an Fe–$C_{Ph}$ bond length of 1.98 Å, which is very close to the experimentally determined bond length of 1.990(1) Å. Starting from complex **2.6**, C–H activation begins with NCMe dissociation to create a vacant coordination site. The enthalpy ($\Delta H$) penalty for NCMe dissociation along the singlet energy surface is 27.1 kcal/mol. The resulting Cp*Fe(CO)(Ph) singlet complex (**2.7$^{s}$**) shows an unrestricted wave function with a spin contamination $<S^2>$ value of 0.23, which suggests open-shell character and a possible high-spin state of lower energy. Indeed, the triplet Cp*Fe(CO)(Ph) complex (**2.7$^{t}$**) is adiabatically 16.4 kcal/mol more stable than **2.7$^{s}$**. The structures **2.7$^{s}$** and **2.7$^{t}$** show that after loss of NCMe, the CO and Ph groups reorient slightly, but the only major bond length change is a decrease in the Fe–Ph bond length from 1.98 Å in **2.6** to 1.91 Å and 1.94 Å in **2.7$^{s}$** and **2.7$^{t}$**, respectively. The calculated structures **2.7$^{s}$** and **2.7$^{t}$** are similar.

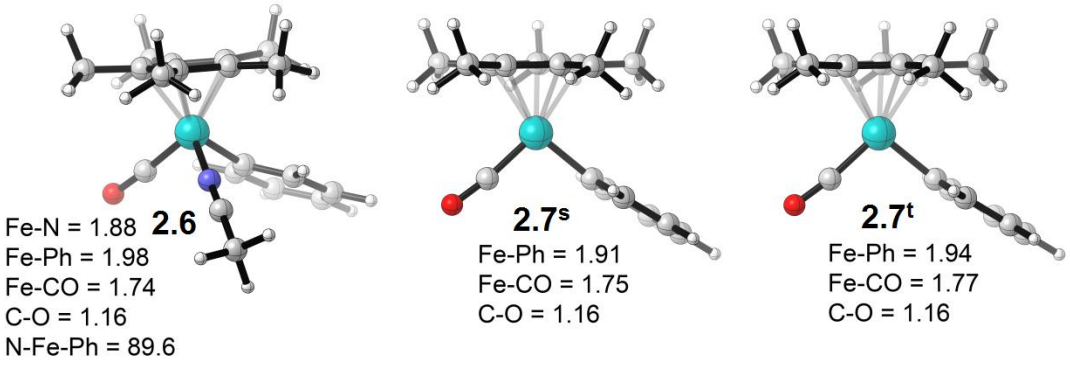


**Figure 2.10.** M06 ground-state structures. Bond lengths reported in Å and angles in degrees.

Consideration of spin states and their interconversion are important for first row transition metals.[52-54] Direct conversion of **2.7$^{s}$** to **2.7$^{t}$** can occur through a singlet-triplet intersystem crossing, called a minimum energy crossing point (MECP). The optimized

structure of **MECP-1** (Figure 2.11) connects **2.7**$^{s}$ to **2.7**$^{t}$ and has an energy and geometry nearly identical to **2.7**$^{t}$. Although it is possible that NCMe dissociates before singlet-triplet intersystem crossing, there is a lower energy pathway for conversion of complex **2.6** to **2.7**$^{t}$. This pathway involves singlet-triplet interconversion with partial NCMe dissociation (Fe−N = 2.18 Å) via **MECP-2** with a $\Delta H$ value of 9.0 kcal/mol relative to **2.6**. Optimization of the resulting triplet structure after **MECP-2** resulted in the triplet NCMe π-complex **2.8**$^{t}$ with $\Delta H$ = 4.6 kcal/mol. Structure **2.7**$^{t}$ is then accessed upon NCMe dissociation. These structures suggest that NCMe dissociation is facile through a dissociative mechanism. An interchange coordination mechanism that remains on the singlet energy surface is unlikely due to the reluctance of the Fe metal center to increase its ligand coordination number.

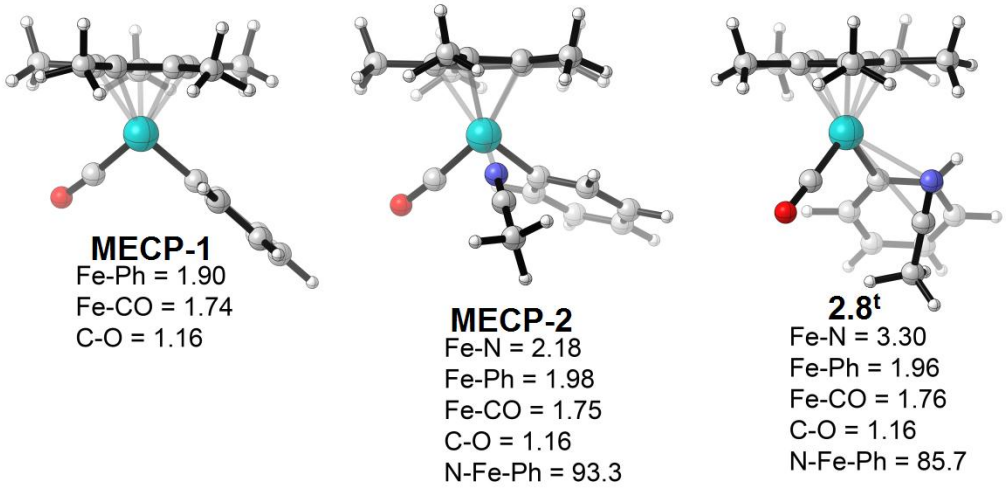


**Figure 2.11.** MECPs and triplet π-complex **2.8**$^{t}$. Bond lengths reported in Å and angles in degrees.

Scheme 2.13 outlines the lowest energy pathway calculated for benzene C–H activation by complex **2.6**. As discussed above, **2.7**$^{t}$ is generated via **MECP-2** followed by NCMe loss. Although **2.7**$^{t}$ is a viable intermediate, Fe–Ph group exchange from this

species on the triplet energy surface showed barriers too high to be reasonable, and it is therefore a dead-end intermediate. As a result, a second intersystem crossing step to return to the singlet energy surface is required during the C–H bond coordination/activation mechanistic stage. There are two possible pathways for this intersystem crossing. The first pathway involves conversion of **2.7$^{t}$** to **2.7$^{s}$** via **MECP-1** followed by benzene coordination on the singlet surface. The second pathway, which is lower in energy, involves intersystem crossing along with benzene coordination via **MECP-3** to give singlet **2.9$^{s}$** directly from **2.7$^{t}$**. The structure and energy of **MECP-3** is nearly identical to **2.9$^{s}$** (Figure 2.12). The enthalpy of triplet **2.9$^{t}$** is 24.0 kcal/mol and confirms that the singlet-triplet crossing point occurs just prior to structure **2.9$^{s}$**.

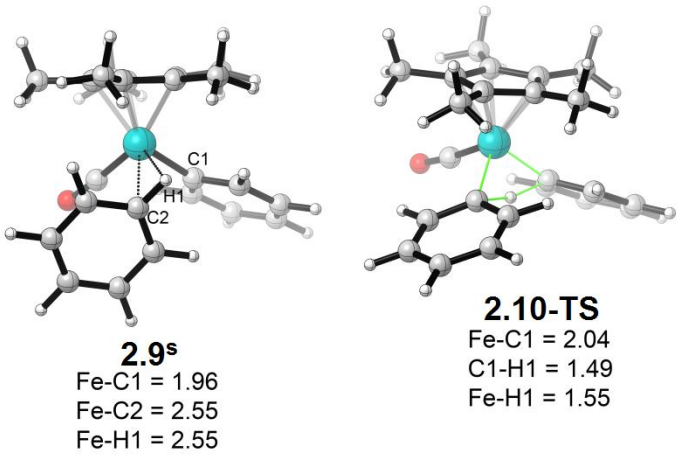


**Figure 2.12.** M06 structures for benzene coordination and C–H bond cleavage. Bond lengths reported in Å.

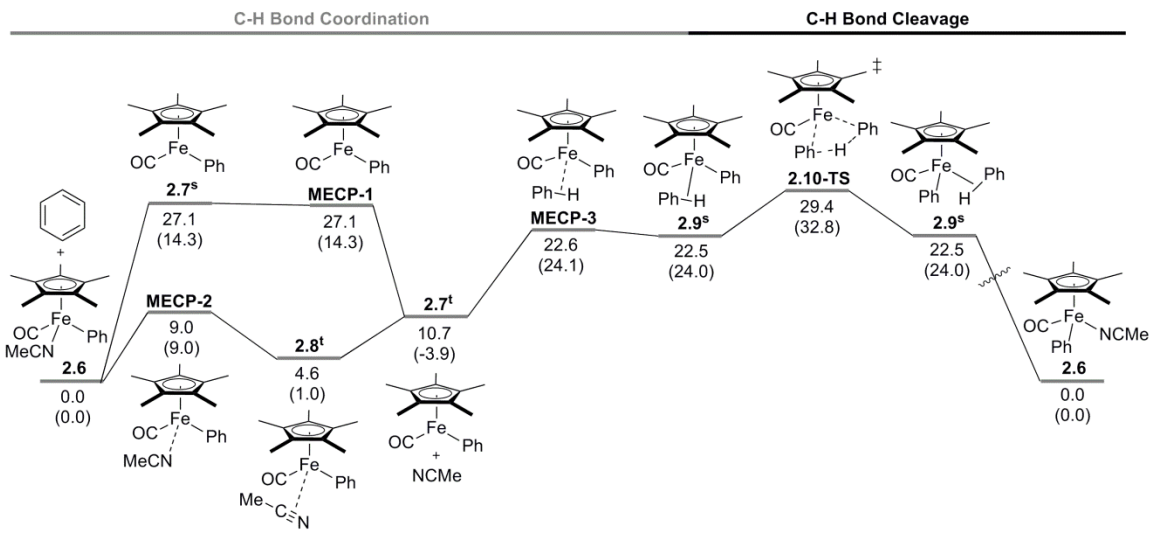


**Scheme 2.13.** M06/6-311++G(3df,3dp)[LANL2TZ(f)]//M06/6-31G(d,p)[LANL2DZ] calculated enthalpies (free energies at 298 K) for C–H activation of benzene by Cp*Fe(CO)(NCMe)Ph (**2.6**) in benzene solvent (kcal/mol). Free benzene and NCMe are included in the calculations when not coordinated to Fe (though not explicitly shown).

Structure **2.9$^{s}$** involves $\eta^2$-C,H-benzene coordination. Because of the orientation of the Fe–Ph group, no true $\eta^2$-C,C-benzene coordination complex could be located. For Ru(II) complexes, $\eta^2$-C,H-benzene coordination in preference to $\eta^2$-C,C-benzene coordination has been taken to imply steric congestion at the metal center.[26] From intermediate **2.9$^{s}$**, the lowest energy pathway for C–H bond cleavage occurs via a four-centered σ-bond metathesis type transition state **2.10-TS** (Figure 2.11) with a calculated $\Delta H^{\ddagger}$ of 29.4 kcal/mol. In this transition state structure, the Fe–Ph bond length is stretched to 2.04 Å, and the benzene C–H bond partial bond length is 1.49 Å. The transition state **2.10-TS** directly connects to another $\eta^2$-C,H-benzene coordination complex **2.9$^{s}$**. At this point NCMe can replace coordinated benzene from **2.9$^{s}$** to regenerate **2.6**. This last step is also susceptible to spin intersystem crossings, but they are not pictorially represented in Scheme 2.10.

Using computational modeling, we have ruled out several other C–H activation mechanisms for Fe–Ph group exchange (Scheme 2.14). The first involves the generation of a so-called "tuck-in" type complex directly from **2.6**. In this mechanistic pathway a methyl C–H bond of the Cp* group undergoes intramolecular σ-bond metathesis with the Fe–Ph group to give a cyclometalated Cp* group and $\eta^2$-CH-benzene coordination. The calculated $\Delta H^{\ddagger}$ for this process is 50.9 kcal/mol. The $\Delta G^{\ddagger}$ for forming the tuck-in complex after dissociation of NCMe is 54.6 kcal/mol. Consistent with the high energies from the calculations, we have observed no deuterium incorporation into the Cp* methyl resonances ($^1$H NMR spectroscopy) for the reaction of **2.6** and $C_6D_6$.

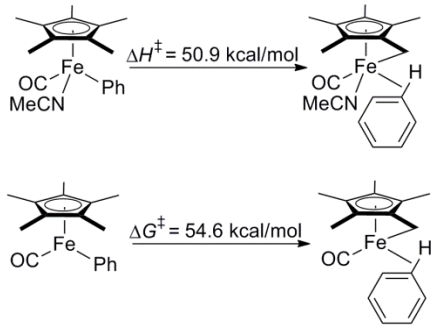


**Scheme 2.14.** Prohibitively high barriers for C–H activation via a tuck-in complex.

We have also considered an Fe(II) to Fe(IV) oxidative addition from **2.7$^{s}$** and **2.7$^{t}$** to give the seven-coordinate diphenyl hydride intermediate Cp*Fe(CO)(Ph)(Ph)(H) (Scheme 2.15). All optimizations starting with seven-coordinate Fe hydride structures reverted back to **2.9$^{s}$**. Lastly, our calculations suggest several hydrogen abstraction mechanisms from both **2.7$^{s}$** and **2.7$^{t}$** are unlikely pathways. For example, the $\Delta H$ to give Cp*Fe(CO)(Ph)(H) and $\bullet C_6H_5$ is 48.4 kcal/mol relative to **2.7$^{s}$**. Eisenstein and coworkers have found similar results from their theoretical study on methane C–H activation by $TpFe(PH_3)(R)$.[55]

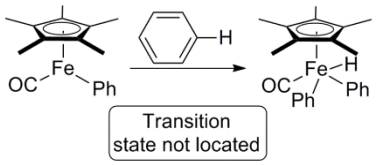


**Scheme 2.15.** Transition state not located for C–H activation by oxidative addition.

### 2.3.6 Reactions of Cp*Fe(CO)(NCMe)Ph (2.6) with Heteroaromatic Substrates

The ability of **2.6** to activate benzene prompted us to explore the possibility of the C–H activation of heteroaromatic substrates under similar mild conditions. The addition of excess furan to a THF or dioxane solution of complex **2.6** results in the rapid liberation of free $C_6H_6$ and the formation of a new Fe complex identified as Cp*Fe(CO)(NCMe)(2-furyl) (Figure 2.13). Attempts to isolate and purify the NCMe coordinated complex Cp*Fe(CO)(NCMe)(2-furyl) proved challenging. Therefore, following the reaction with furan, one equivalent of $PPh_3$ was added to isolate the C–H activated product as Cp*Fe(CO)($PPh_3$)(2-furyl) (**2.11**) in 96% isolated yield (Scheme 2.16). The $^1$H NMR spectrum of **2.11** shows the expected Cp* peak at 1.42 ppm with the three furyl peaks resonating at 7.62, 5.99, and 5.64 ppm (Figure 2.14). The single downfield furyl resonance (7.62 ppm) with the two further upfield peaks along with the splitting pattern of d, dd, and d, respectively, provide evidence for C–H activation at the 2 position of furan. The $PPh_3$ protons appear as a broad resonance at 7.35 ppm (see below for discussion of this peak shape). The coordinated $PPh_3$ resonates at 77.8 ppm in the $^{31}$P NMR spectrum, and the CO stretch is at 1913 $cm^{-1}$ in the infrared spectrum, confirming the persistence of a terminal CO ligand. The regioselectivity of the C–H activation was confirmed by an X-ray diffraction study of complex **2.11** (Figure 2.15). The Fe–$C_{furyl}$ bond distance is 1.960(1) Å, while the Fe–$C_{CO}$ bond measures 1.730(1) Å. The Fe–P bond in **2.11** is slightly shorter than the Fe–P bond in the cationic

$[Cp^*Fe(CO)_2(PPh_3)]PF_6$ (2.252(1) Å).[56] This could be a manifestation of greater π-back bonding in the more electron rich $Cp^*Fe(CO)(PPh_3)$(2-furyl) (**2.11**).

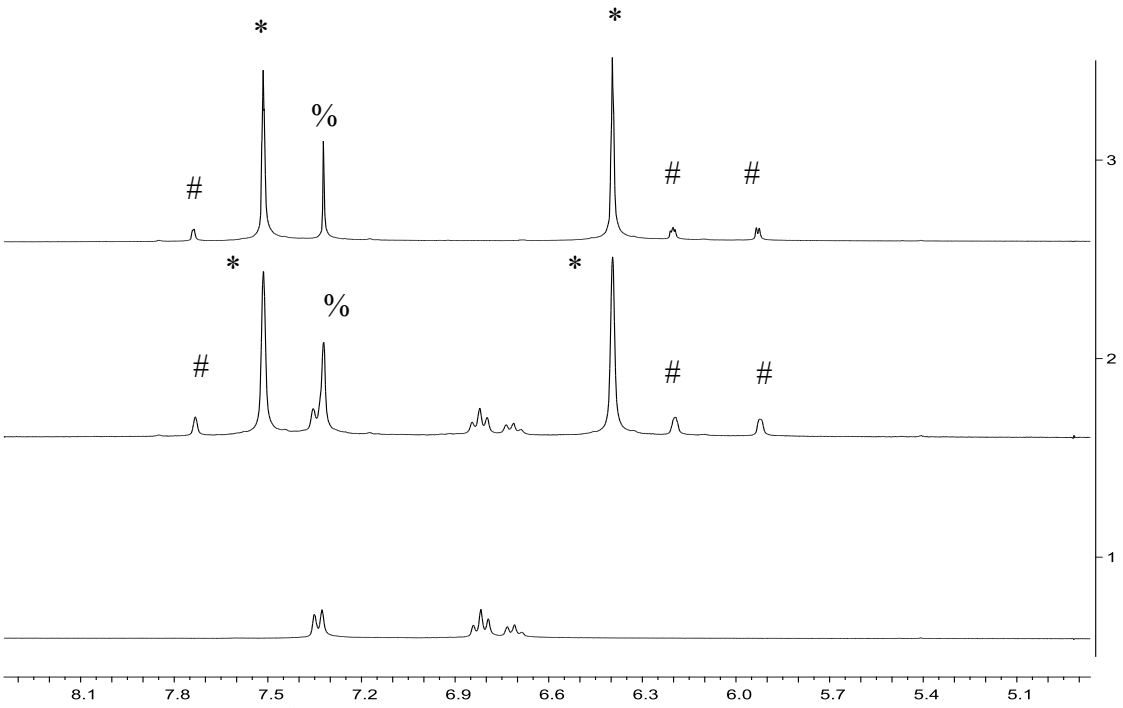


**Figure 2.13.** Stacked $^1H$ NMR spectra showing aryl region for complex **2.6** (1), after addition of 10 equiv furan (< 15 min) (2), and after 1 h of reaction in dioxane-$d_8$. Furan is marked with an asterisk (*), 2-furyl resonances are marked with pound symbol (#) and free $C_6H_6$ is marked with a percent sign (%).

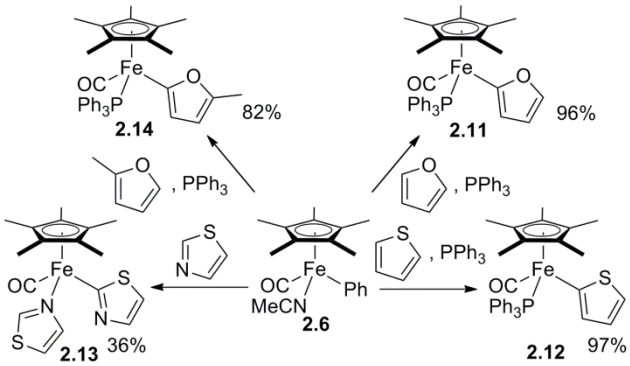


**Scheme 2.16.** C–H activation of heteroaromatic substrates by Cp*Fe*(CO)(NCMe)Ph (**2.6**).

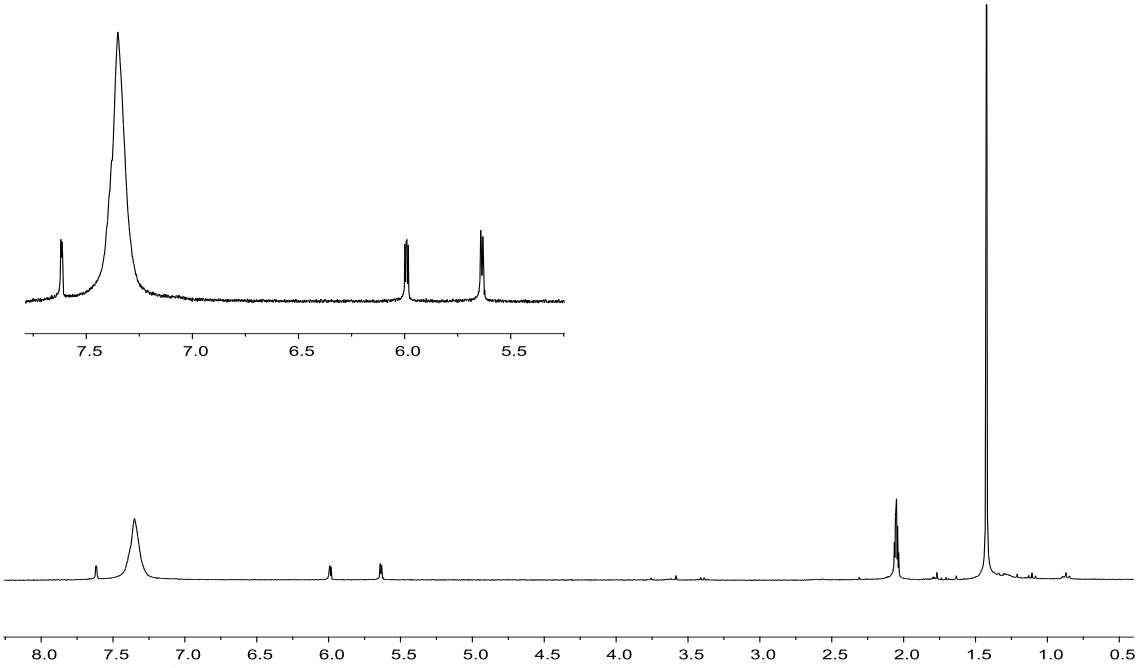


**Figure 2.14.** $^{1}$H NMR spectrum of Cp*Fe(CO)(PPh$_3$)(2-furyl) (**2.11**) in acetone-$d_6$.

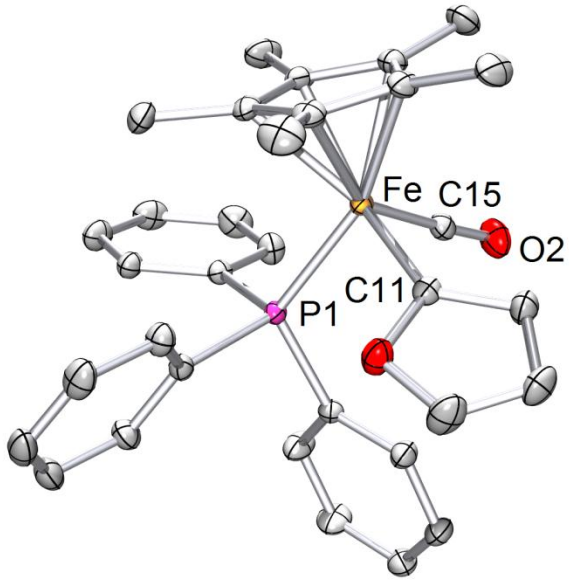


**Figure 2.15.** ORTEP drawing of Cp*Fe(CO)(PPh$_3$)(2-furyl) (**2.11**) (50% probability ellipsoids; H atoms omitted). Selected bond lengths (Å): Fe–P1 2.2142(3), Fe–C15 1.730(1), C15–O2 1.159(2), Fe–C11 1.960(1). Selected bond angles (deg): C11–Fe–C15 89.59(5), C15–Fe–P1 89.65(4)

Complex **2.6** also reacts with thiophene to activation the 2-position C–H bond. Thus, treating a THF solution of **2.6** with thiophene then $PPh_3$ afforded Cp*Fe(CO)($PPh_3$)(2-thienyl) (**2.12**) in 97% isolated yield (Scheme 2.16). The $^1$H NMR spectrum of complex **2.12** can be seen in Figure 2.16. In the $^1$H NMR spectrum, three thienyl peaks can be observed at 7.19 (d), 6.77 (dd), and 6.33 (br s) ppm with a broad multiplet around 7.39 ppm for the $PPh_3$ ligand. The $^{31}$P NMR spectrum shows a single resonance at 74.0 ppm. The carbonyl stretching frequency shows up at 1913 cm$^{-1}$, which is identical to that of complex **2.11**, suggesting similar electron donor abilities of the 2-furyl and 2-thienyl ligands.

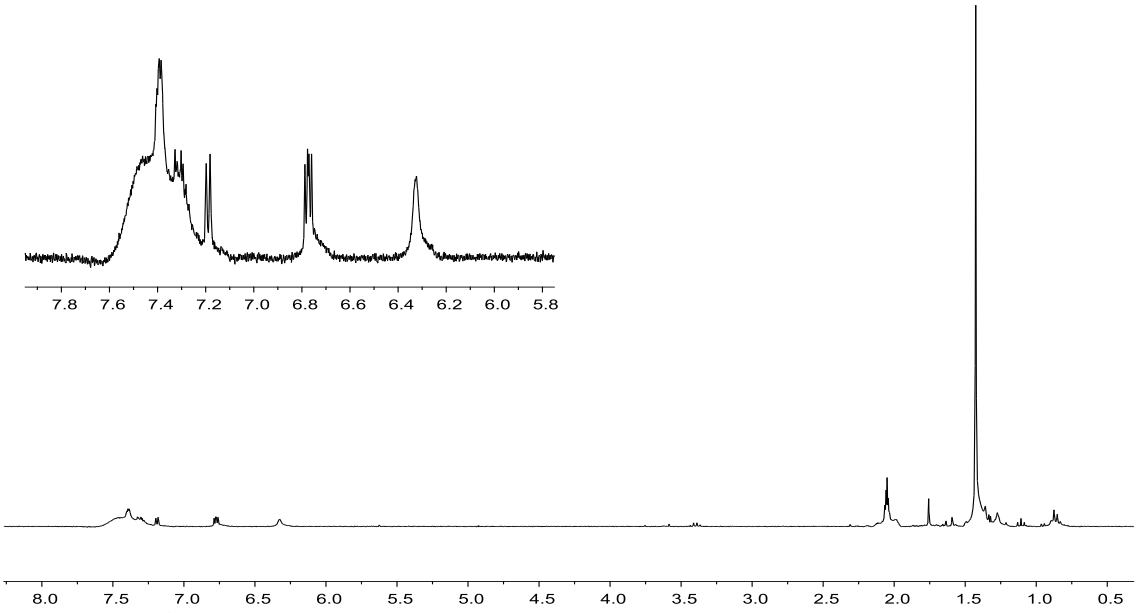


**Figure 2.16.** $^1$H NMR spectrum of Cp*Fe(CO)($PPh_3$)(2-thienyl) (**2.12**) in acetone-$d_6$.

As mentioned above, the $^1$H and $^{13}$C NMR spectra for complexes **2.11** and **2.12** exhibit broadened resonances for the $PPh_3$ ligand. A variable-temperature $^1$H NMR experiment was performed on **2.12**, and decoalescence of the Cp* resonance was observed (Figure 2.17), which indicates rapid exchange between two Cp*Fe complexes.

We first considered a fluctional process involving reversible cyclometalation of the $PPh_3$ ligand (Scheme 2.12). However, when free thiophene (0.5 equiv) was added to a THF-$d_8$ solution of **2.12**, no changes to the peak shape or chemical shifts for **2.12** in the $^1$H NMR spectrum were observed. Additionally, only one CO stretch is observed in the IR spectrum. Since the time scale for obtaining an IR spectrum is shorter than the time scale for obtaining a $^1$H NMR spectrum, the observation of one CO stretch provides evidence against two electronically different Cp*Fe species in equilibrium. These data, taken in account with only one resonance in the $^{31}$P NMR spectrum, implicate that the fluxionality observed is not due to reversible phosphine cyclometalation but possibly a result of hindered rotation of $PPh_3$ (Scheme 2.17). Thus, the two Cp* methyl peaks observed in Figure 2.17 likely correspond to the Cp* methyl peaks of two rotamers about the Fe–$PPh_3$ bond axis. At room temperature, one set of resonances are observed (including broad $PPh_3$ resonances) because the rotation about the Fe–$PPh_3$ is rapid on the NMR time scale. However, two sets of resonances are observed at low temperature because the rotation about the Fe–$PPh_3$ becomes slow on the NMR time scale.

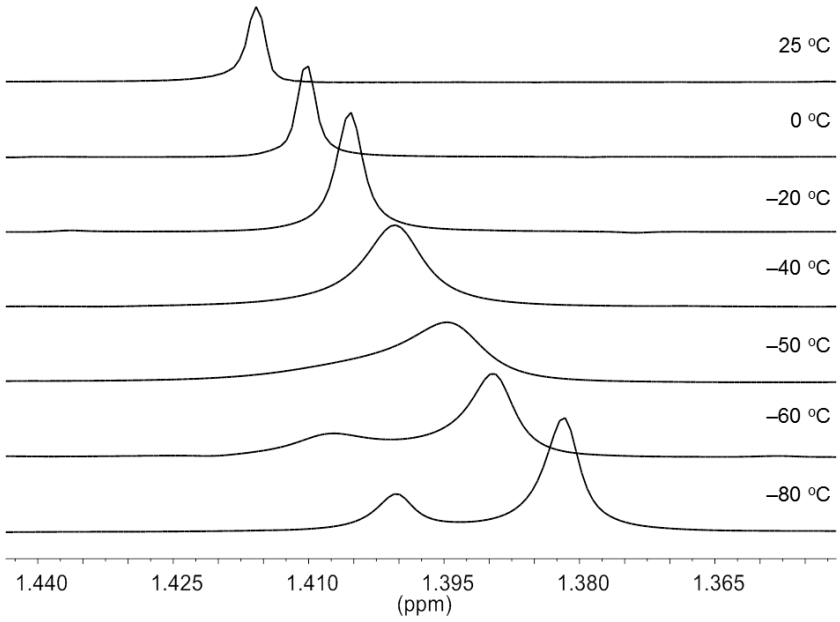


**Figure 2.17.** $^{1}$H NMR spectra (Cp* region) of Cp*Fe(CO)($PPh_3$)(2-thienyl) (**2.12**) at various temperatures.

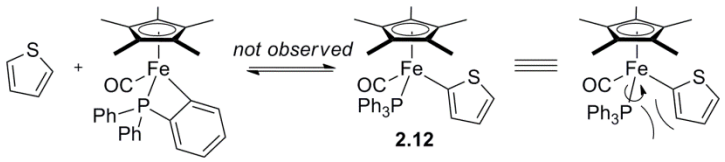


**Scheme 2.17.** Fluxionality observed for Cp*Fe(CO)($PPh_3$)(2-thienyl) (**2.12**).

The reaction of **2.6** with thiazole produces Cp*Fe(CO)(thiazole)(2-thiazolyl) (**2.13**) in 36% isolated yield (Scheme 2.16). The modest isolated yield is a result of the isolation procedure rather than low reaction yields. Complex **2.13** is characterized by five aryl peaks, two from the 2-thiazolyl ligand and three from a coordinated thiazole ligand (Figure 2.18) and a terminal carbonyl stretch at 1910 $cm^{-1}$ in the IR spectrum. Unfortunately, we were unable to obtain a single crystal suitable for an X-ray diffraction study. Thus, to determine the coordination isomer of the thiazole ligand, calculations were employed, which suggest the *N*-bound thiazole complex is more favorable than the

*S*-bound isomer by 13.5 kcal/mol (Scheme 2.18). The formation of **2.13** proceeds via an intermediate (observed by $^{1}$H NMR spectroscopy), which is likely Cp*Fe(CO)(thiazole)Ph (Scheme 2.19).

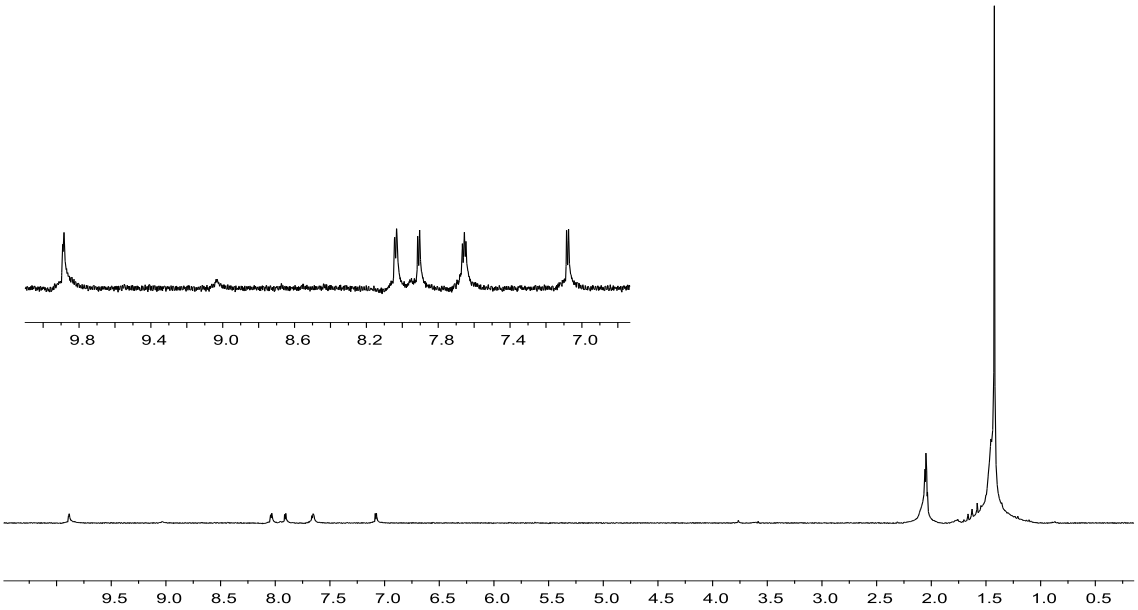


**Figure 2.18.** $^{1}$H NMR spectrum of Cp*Fe(CO)(thiazole)(2-thiazolyl) (**2.13**) in acetone-$d_6$.

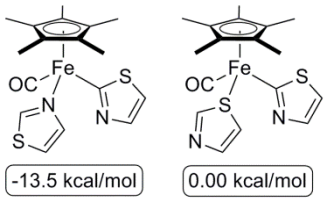


**Scheme 2.18.** Two possible coordination isomers for Cp*Fe(CO)(thiazole)(2-thiazolyl) (**2.13**). Relative ground state energies determined using MO6 DFT calculations.

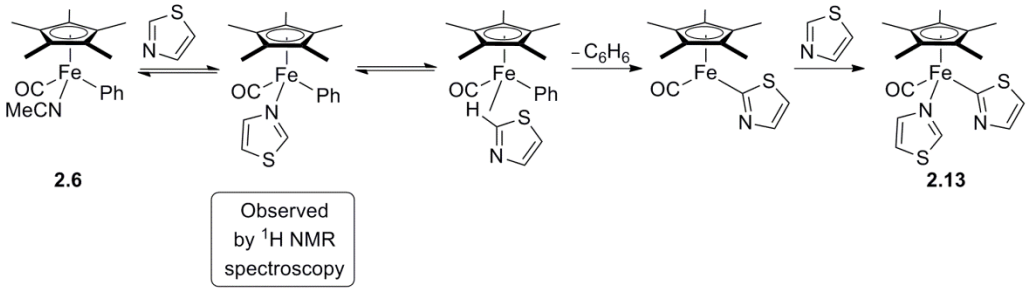


**Scheme 2.19.** Possible mechanism for the formation of Cp*Fe(CO)(thiazole)(2-thiazolyl) (**2.13**) from Cp*Fe(CO)(NCMe)Ph (**2.6**) and thiazole involving the intermediacy of Cp*Fe(CO)(thiazole)Ph.

We have proposed that aromatic C–H activation by Cp*Fe(CO)(NCMe)Ph (**2.6**) occurs by non-radical pathways. To test this hypothesis, we treated Cp*Fe(CO)(NCMe)Ph (**2.6**) with 2-methylfuran. The substrate 2-methylfuran was chosen because it contains weak C–H bonds (methyl C–H BDE ~86 kcal/mol) and strong aromatic C–H bonds (furyl C–H bond ~120 kcal/mol) (Figure 2.19).[57] If an H atom abstraction mechanism were operative, we would anticipate selectivity for the weaker methyl C–H bond. In contrast, C–H activation by a non-radical pathway (i.e., σ-bond metathesis) would most likely be selective for the aryl C–H bonds.[8] Consistent with our hypothesis, we observed selective activation of the 5-position on the furyl ring over the methyl position. The C–H activated product was isolated in 82% yield as Cp*Fe(CO)($PPh_3$)[2-(5-methylfuryl)] (**2.14**) (Scheme 2.11). The selectivity for the aryl position is demonstrated by a singlet at 2.12 ppm, which corresponds to the methyl group of the furyl ring and two overlapping signals at 5.52 ppm for the two furyl protons in the $^1$H NMR spectrum (Figure 2.20). The $^{31}$P NMR spectrum shows a singlet a 77.7 ppm, and the infrared spectrum shows a stretch at 1913 $cm^{-1}$ for the terminal CO ligand. Similar to complexes **2.11** and **2.12**, complex **2.14** also exhibits broadened $^1$H and $^{13}$C NMR resonances in the downfield region of the spectra, which may also be attributed to

slow rotation around the Fe–$PPh_3$ bond. This selectivity, in which Fe activates a stronger aromatic C–H bond in preference to a weaker $CH_3$ bond, suggests that C–H activation proceeds via a pathway that does not involve H atom abstraction to form furyl free radicals, consistent with the M06 density functional calculations (see above).

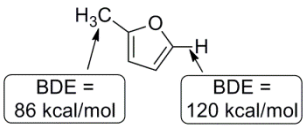


**Figure 2.19.** Bond dissociation energies (kcal/mol) for 2-methylfuran. Values were obtained from the same study for accurate comparision.[57]

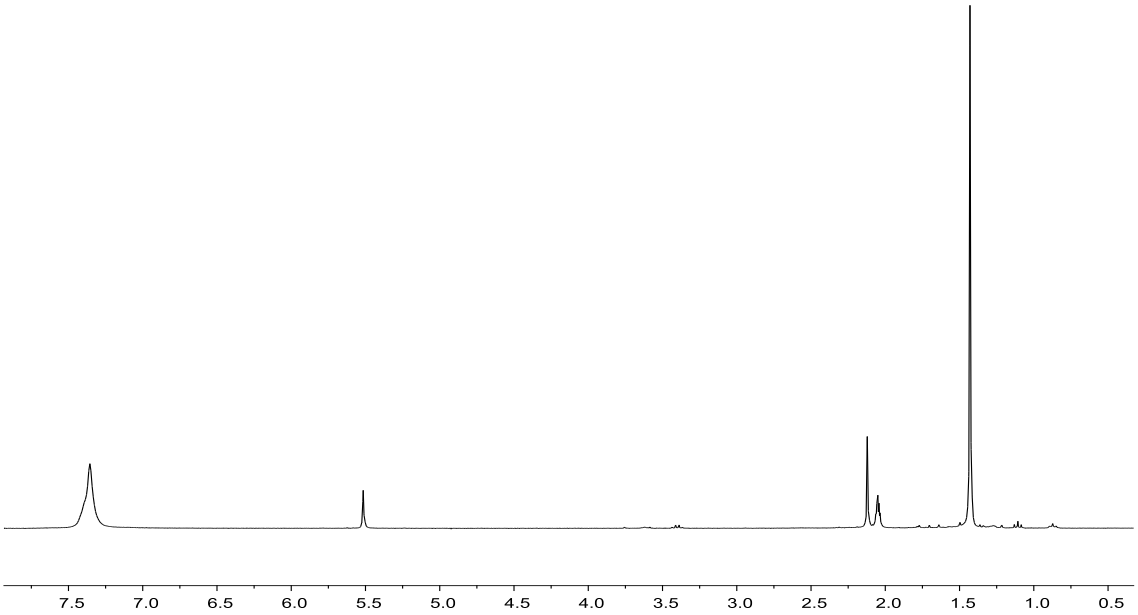


**Figure 2.20.** $^1$H NMR spectrum of Cp*Fe(CO)($PPh_3$)[2-(5-methylfuryl)] in acetone-$d_6$ (**2.14**).

### 2.3.7 Experimental Mechanistic Study of Furan C–H Activation

To experimentally probe these C–H activation reactions, we studied several kinetic features for the reaction of **2.6** with furan. Under pseudo-first order conditions ([**2.6**] = 0.055 M, [furan] = 0.55 M, 400 μL THF-$d_8$) in **2.6** at 3 °C, the reaction of **2.6** with furan gave a plot of [**2.6**] vs. time that shows a first-order exponential decay (Figure

2.21), which demonstrates the reaction is first order with respect to Fe complex. Varying the equivalents of furan relative to **2.6** revealed that the reaction rate has a first-order dependence on the concentration of furan at low concentrations with saturation kinetics at higher concentrations of furan (Figure 2.22). The rate of reaction has an inverse first order dependence on the concentration of free NCMe (Figure 2.23), which likely indicates that NCMe dissociation occurs before the rate determining step.

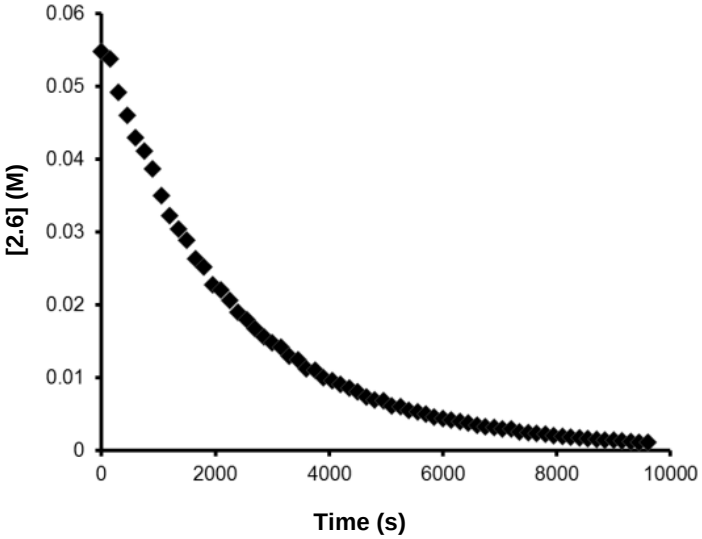


**Figure 2.21.** Sample first-order decay plot for the reaction of **2.6** and furan (10 equiv relative to **2.6**) at 3 °C ($R^2$ = 0.99) in THF-$d_8$.

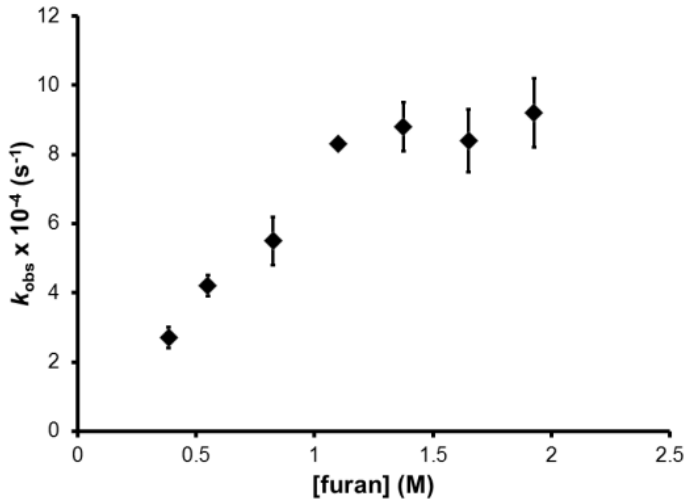


**Figure 2.22.** Plot of pseudo first-order rate constants ($k_{obs}$) versus [furan] for the reaction of **2.6** with excess furan at 3 °C ([**2.6**] = 0.055 M in THF-$d_8$). Data are the result of an average of at least three different kinetic experiments.

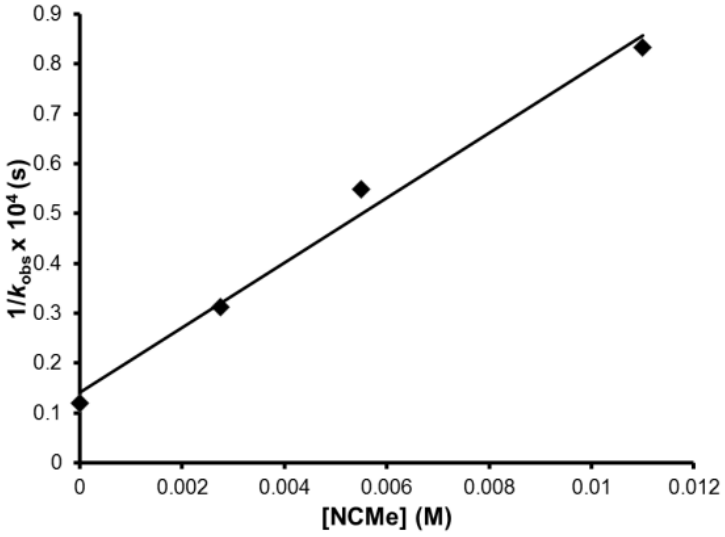


**Figure 2.23** Plot of $1/k_{obs}$ versus [NCMe] ($R^2$ = 0.99) for the reaction of **2.6** with excess furan at 3 °C ([**2.6**] = 0.055 M in THF-$d_8$). Data are the result of an average of at least three different kinetic experiments.

In order to determine the intermolecular kinetic isotope effect, we treated complex **2.6** with 10 equivalents of a 1:1 molar solution of furan and furan-$d_4$ and analyzed the

relative quantities of $C_6H_6$ and $C_6H_5D$ by GC/MS (Scheme 2.14), revealing a kinetic isotope effect of 5.0(4). Additionally, we have examined the kinetic isotope effect with a large excess of furan (50 equivalents), and $k_H/k_D$ = 4.8(1), which is statistically equivalent with that determined with 10 equivalents of furan. The ratio of $C_6H_6$:$C_6H_5D$ does not change over time. The relatively large primary kinetic isotope effect provides evidence that furan C–H bond activation proceeds before or during the rate limiting step.

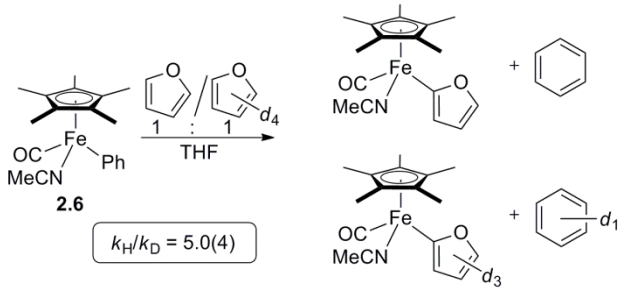


**Scheme 2.20.** Determination of the kinetic isotope effect for the reaction of complex **2.6** and furan ([**2.6**] = 0.030 M, room temperature, 1.5 mL THF, 10 equiv (relative to **2.6**) of a 1:1 molar ratio solution of furan and furan-$d_4$).

Kinetic data for the C–H activation of furan (10 equiv) were obtained between –12 °C and 13 °C. Using the Eyring equation, which is derived from transition state theory, the activation parameters from this reaction can be determined. The Eyring equation can be rearranged to take the form of y = mx + b (see Figure 2.24). Plotting $\ln(k_{obs}/T)$ (y) versus 1/T (x) gives a linear plot (Figure 2.24). From this line equation, activation parameters of $\Delta H^{\ddagger}$ = 23.5(4) kcal/mol and $\Delta S^{\ddagger}$ = 12(2) cal/mol·K are calculated. The $\Delta H^{\ddagger}$ value is determined from the slope (m = $-\Delta H^{\ddagger}/R$), and $\Delta S^{\ddagger}$ is extracted from the y-intercept (b = $\ln(k_B/h) + \Delta S^{\ddagger}/R$). It is important to note that since the Eyring plot data were not collected under saturation conditions, the value of $k_{obs}$ had to be corrected by dividing the experimentally determined $k_{obs}$ by [furan]. The rate equation

under pseudo-first order conditions is approximated as rate = $k$[**2.6**][furan]. Thus, the $k_{obs}$ that must be used in the Eyring plot is $k_{obs} = k/$[furan].

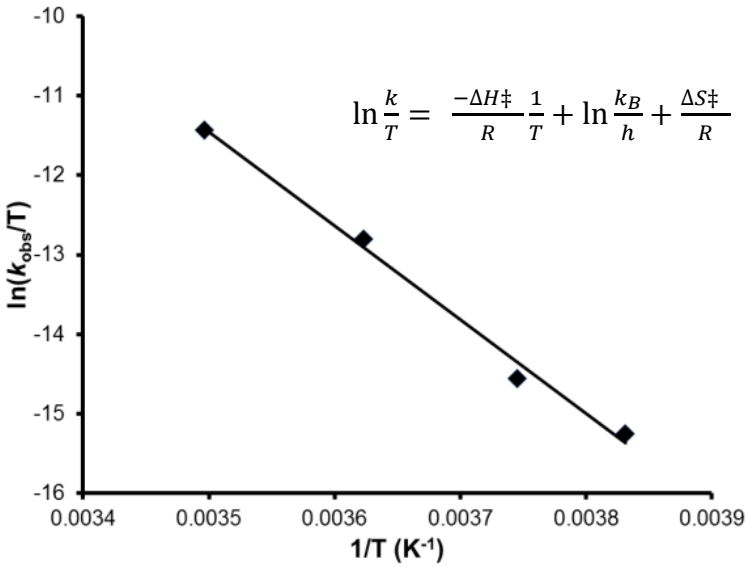


**Figure 2.24.** Eyring plot for furan C–H activation by Cp*Fe(CO)(NCMe)Ph (**2.6**) ($R^2$ = 0.99; –12 °C to 13 °C, [**2.6**] = 0.055 M in THF-$d_8$).

### 2.3.8 Computational Study of Furan C–H Activation

Prof. Daniel Ess (BYU) computed the enthalpy profile for reaction of **2.6** with furan in THF solvent (Scheme 2.21). We have found a nearly identical mechanism for benzene and furan C–H activation by **2.6**. The initial steps of NCMe dissociation and intersystem crossing are identical with the benzene mechanism shown in Scheme 3. The energies of **MECP-2**, **2.8$^t$**, and **2.7$^t$** in THF solvent are a few tenths of a kcal/mol lower than in benzene solvent. From **2.7$^t$**, furan coordinates via **MECP-4** (Figure 2.25, $\Delta H$ = 15.9 kcal/mol) to give singlet **2.15$^s$**, which involves the formation of a true $\eta^2$-C,C-complex Cp*Fe(CO)($\eta^2$-C,C-furan) with a $\Delta H$ of 13.0 kcal/mol.

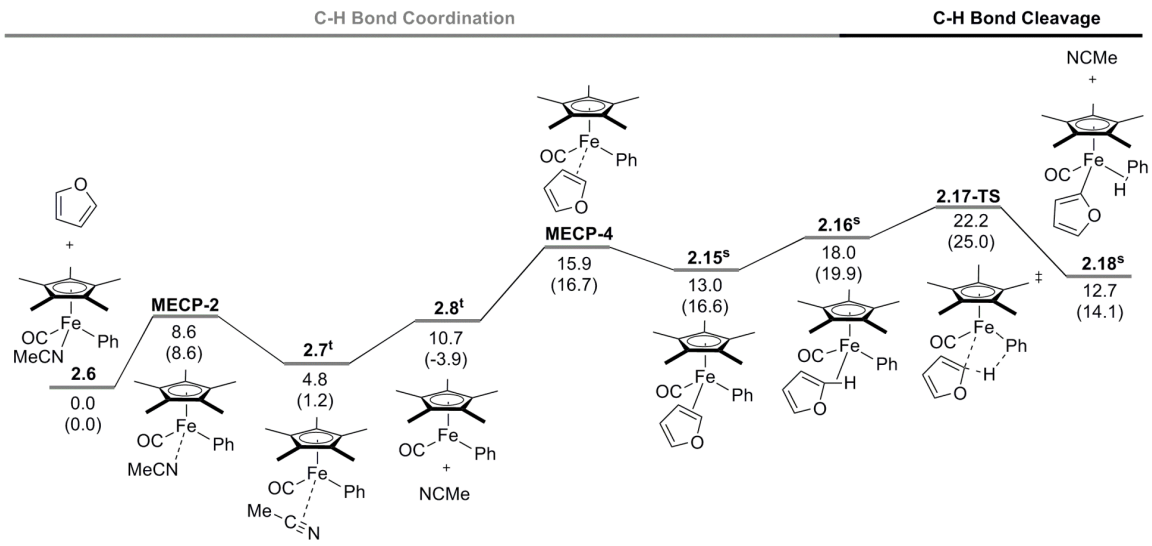


**Scheme 2.21.** Calculated enthalpies (free energies at 298 K) for C–H activation of furan by Cp*Fe(CO)(NCMe)Ph (**2.6**) in THF solvent (kcal/mol). Free furan and NCMe are included in the calculations when not coordinated to Fe (though not explicitly shown).

The $\eta^2$-C,C-complex **2.15$^s$** is less endergonic than the benzene complex **2.9$^s$** because it involves π-back bonding and σ-donation in contrast to mainly σ type interactions in **2.9$^s$**. For π-basic metals, furan is known to bind stronger than benzene in a dihapto-coordination mode.[58] The calculated $\Delta H^{\ddagger}$ for C–H bond cleavage of furan via the σ-bond metathesis transition state **2.17-TS** is 22.2 kcal/mol, which is in good agreement with the experimental value for $\Delta H^{\ddagger}$ of 23.5(4) kcal/mol. Despite the 8 kcal/mol computed stronger C–H bond strength of furan ($\Delta H$ = 118 kcal/mol) versus benzene ($\Delta H$ = 110 kcal/mol), the $\Delta H^{\ddagger}$ value for furan C–H activation is ~7 kcal/mol lower than the benzene $\Delta H^{\ddagger}$ value. The lower $\Delta H^{\ddagger}$ for C–H activation of furan than benzene could be a result of the more stable Cp*Fe(CO)(2-furyl)($\eta^2$-C,H-benzene) intermediate **2.18$^s$** ($\Delta H$ = 12.7 kcal/mol) compared with Cp*Fe(CO)(Ph)($\eta^2$-C,H-benzene) (**2.9$^s$**) ($\Delta H$ = 22.5 kcal/mol). The thermodynamic stability of **2.18$^s$** is manifested in **2.17-TS** as stability

gained from formation of a more stable Fe–furyl bond compared with the formation of a Fe–Ph bond in **2.10-TS**.[59]

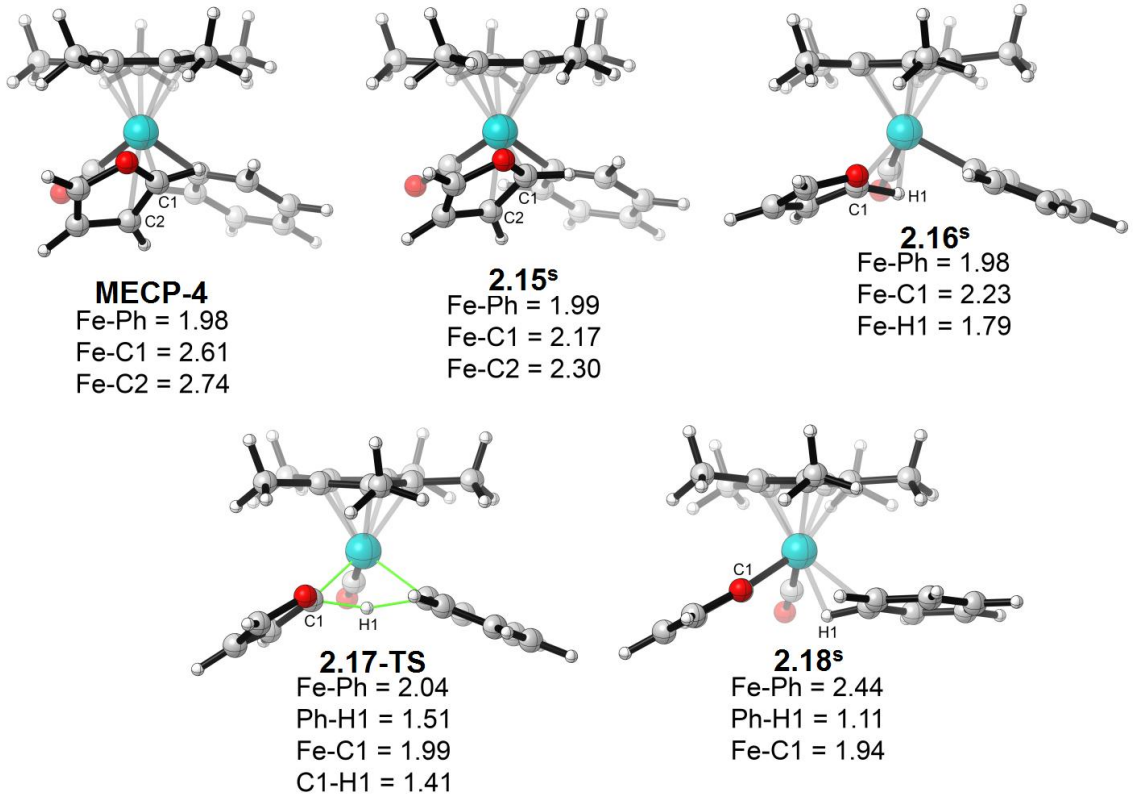


**Figure 2.25.** Calculated structures for furan C–H activation by Cp*Fe(CO)(NCMe)Ph (**2.6**). Bond lengths reported in Å.

On the enthalpy surface, the furan C–H bond cleavage transition state **2.17-TS** is higher in energy than **MECP-2** and **MECP-4** points. This suggests that the rate of Fe–Ph group transformation into a Fe–furyl group is controlled by **2.17-TS**, which is in accordance with the relatively large KIE value (~5) observed experimentally.

### 2.3.9 Discussion of Mechanism for Furan C–H Activation

Based on calculations and experimental results, a proposed mechanism and corresponding rate law for the C–H activation of furan by **2.6** is shown in Scheme 2.22. Reversible NCMe dissociation via a spin-forbidden pathway yields the coordinatively

unsaturated intermediate. After furan coordination and subsequent C–H bond cleavage with concomitant release of benzene, acetonitrile re-coordinates completing the transformation. The derived rate law contains [NCMe] in the denominator, which is consistent with the observed rate inhibition by added NCMe (Figure 2.23). Additionally, [furan] is present in both the numerator and denominator. As the concentration of furan increases, the [NCMe] terms become negligible. This gives a rate law of $k_1k_2k_3$[furan][**2.6**]/$k_2k_3$[furan]. The [furan] terms cancel out at high concentrations of furan to give a rate law of $k_1$[**2.6**]. This explains the saturation kinetics with regard to furan concentration observed experimentally (Figure 2.22), where there is a first order dependence at low concentrations and a zero order dependence at high concetrations.

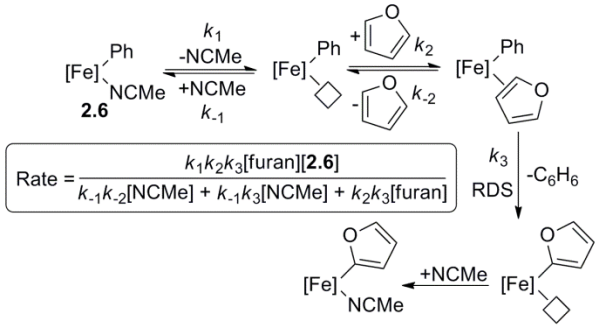


**Scheme 2.22.** Proposed mechanism and corresponding rate law for the C–H activation of furan by Cp*Fe(CO)(NCMe)Ph (**2.6**). [Fe] = Cp*Fe(CO), RDS = rate-determining step.

Using the proposed rate law, $k_1$ can be independently determined from the data in Figure 2.22 and Figure 2.23. Under saturation conditions (Figure 2.22), the rate law is reduced to rate = $k_1$[**2.6**] (see above) and using the data in Figure 2.22, $k_1 = 8.8 \times 10^{-4}$ $s^{-1}$. This value was determined by averaging the $k_{obs}$ values at saturation conditions. The value of $k_1$ can also be determined from the y-intercept of Figure 2.23. When concentration of NCMe in solution is negligible (i.e., under conditions when no excess NCMe is added), the rate law also reduces to $k_1$[**2.6**]. Thus, when [NCMe] = 0, $k_{obs} = k_1$.

Using the data from Figure 2.23, yields $k_1$ = 7.1 x $10^{-4}$ $s^{-1}$. Thus, the two independently determined values of $k_1$ are in good agreement. Since these $k_1$ values were determined indirectly and the value of $k_1$ from Figure 2.22 is an average of 3 independent data points, while the value of $k_1$ is from extrapolation of linear fit to the y-intercept, one might anticipate some deviation in the values.

Under saturation conditions in furan, $k_{obs} = k_1$, which provides the rate of NCMe dissociation from **2.6** (see above). Thus, an Eyring analysis of furan C–H activation by **2.6** was performed under saturation conditions (30 equiv of furan, –22 °C to 3 °C) in order to extract the activation parameters for the NCMe dissociation sequence (Figure 2.26). The amount of furan used in this experiment was determined from the horizontal portion of the plot in Figure 2.22, which would be when there is a zero order dependence on [furan]. Thus, for NCMe dissociation, $\Delta H^{\ddagger}$ = 20.2(3) kcal/mol and $\Delta S^{\ddagger}$ = 0(2) cal/mol·K. Scheme 2.21 shows the lowest energy pathway for NCMe dissociation results in **2.7$^{t}$**. Comparison of the enthalpy of **2.7$^{t}$** with the measured $\Delta H^{\ddagger}$ shows that the calculated value is ~10 kcal/mol too low. We examined the possibility that this discrepancy is due to the M06 density functional. However, all other functionals tested predicted lower enthalpy values for **2.7$^{t}$**. We note that $k_1$ values have been determined using an indirect method, and despite the discrepancy in experimental and calculated values, the comparison of overall energetics between theory and experiment are a good fit, and the predicted rate limiting C–H activation is in accord with the observed kinetic isotope effects.

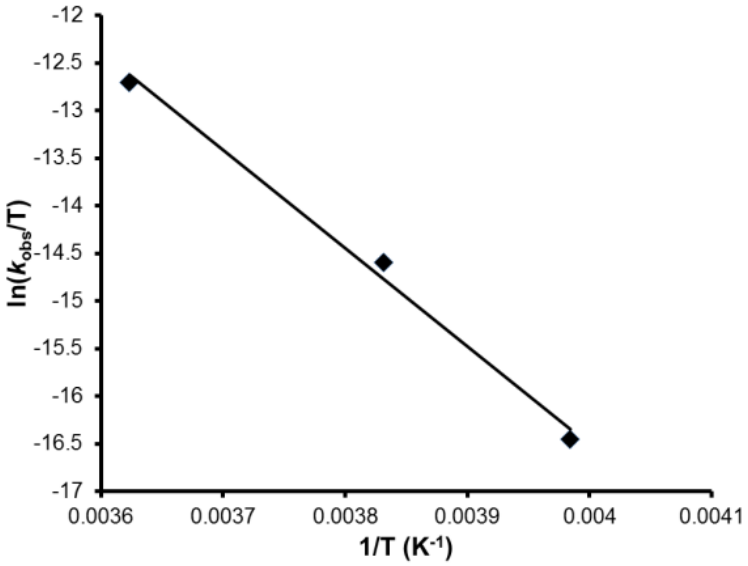


**Figure 2.26.** Eyring plot for furan (30 equiv relative to **2.6**) C–H activation by Cp*Fe(CO)(NCMe)Ph (**2.6**) ($R^2$ = 0.99; –22 °C to 3 °C).

### 2.3.10 Kinetic Analysis of Thiophene C–H Activation by Cp*Fe(CO)(NCMe)Ph (2.6)

We also explored the kinetics of thiophene activation by **2.6**. Using 20 equiv of thiophene at 3 ºC the $k_{obs}$ is 3.2(4) x $10^{-4}$ $s^{-1}$ (Figure 2.27). Comparing this rate constant to that from the reaction of **2.6** and 20 equiv of furan reveals that the C–H activation of furan is ~2.5 times quicker than the C–H activation of thiophene by **2.6**. The reason for the slower rate of thiophene C–H activation may be a result of the greater stability of analogous intermediates along the reaction pathway. For example, thiophene is a better Lewis base than furan, and, thus, the intermediacy of a Cp*Fe(CO)(*S*-thiophene)Ph intermediate may be responsible for the slower rate. Unlike in the reaction of **2.6** and thiazole, we have observed no intermediates by $^1$H NMR spectroscopy during the course of the reaction of **2.6** and thiophene. As such, we speculate that the decrease in rate from the reaction with furan might be explained from the smaller energy stabilization gained from the formation of the Fe–thienyl from the breaking C–H bond versus the analogous

transformation with furan. In the C–H activation transition states, the incipient Fe–thienyl bond may be weaker than the incipient Fe–furyl bond (Figure 2.28). This would have a destabilizing effect on the transition state and could be an explanation for why the rate of thiophene C–H activation is slower than the rate of furan C–H activation.

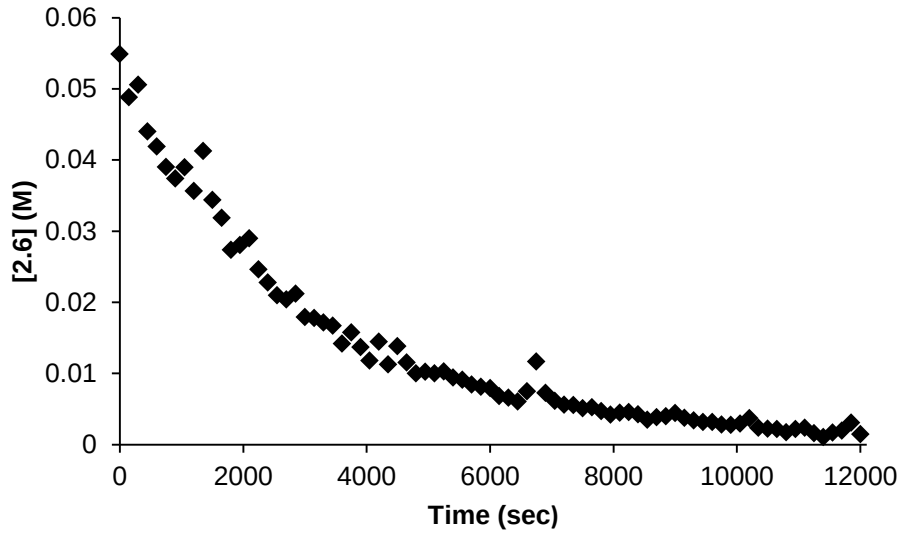


**Figure 2.27.** First order decay plot for the reaction of Cp*Fe(CO)(NCMe)Ph (**2.6**) and thiophene ($R^2$ = 0.99, [**2.6**] = 0.055 M, 20 equiv. (relative to **2.6**) thiophene, THF-$d_8$) at 3 °C.

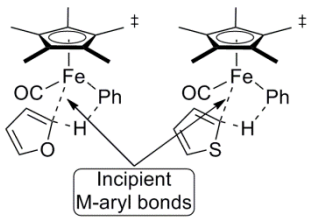


**Figure 2.28.** Comparison of transition states from C–H activation of furan and thiophene by Cp*Fe(CO)(NCMe)Ph (**2.6**).

### 2.3.11 Discussion of Regioselectivity of Furan C–H Activation

The ability to selectively activate C–H bonds on compounds with more than one type of C–H bond is of interest in synthetic chemistry. Therefore, the regioselective activation of furan prompted us to investigate the underlying reasons for this observed

selectivity.[18, 23, 60] Calculations show a $\Delta\Delta H^{\ddagger}$ of 3.8 kcal/mol between the **2.17-TS** and the regioisomeric transition state at the 3-position of furan (Figure 2.29). Again, the regioselectivity can be rationalized based on the relative stability gained by formation of an Fe–C2(furyl) bond versus an Fe–C3(furyl) bond in the transition state. The Fe–C2(furyl) intermediate **2.18**$^{s}$ generated from C–H bond cleavage has a $\Delta H$ value of 12.7 kcal/mol while the Fe–C3(furyl) intermediate generated from C–H bond activation has a $\Delta G$ value of 17.1 kcal/mol. Quantitative analysis of so-called "transition state bond energies" showed that in **2.17-TS** the Fe–C2(furyl) bond energy is 8 kcal/mol more stable than the Fe–C3(furyl) bond energy in the alternative regioisomeric C–H activation transition state.[59] Eisenstein, Perutz, and Jones have also suggested thermodynamic influence on the rates of metal-mediated C–H activation.[61-63]

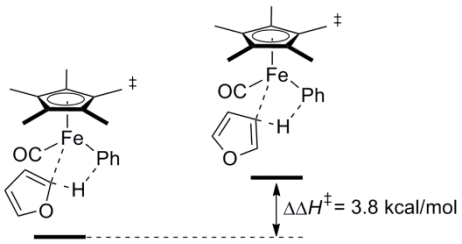


**Figure 2.29.** Comparison of regioisomeric transition states for the C–H activation of furan by Cp*Fe(CO)(NCMe)Ph (**2.6**).

## 2.4 Conclusions

In this chapter, the discovery of an Fe(II) complex, Cp*Fe(CO)(NCMe)Ph (**2.6**), that undergoes regioselective C–H activation with a range of aromatic substrates under mild conditions is reported. Starting from our previously reported TpRu hydroarylation catalysts, the progression from synthetic attempts to make TpFe complexes to experimental and synthetic studies of CpFe(CO)(py)Ph (**2.4**), and finally to the synthesis

and mechanistic studies of Cp*Fe(CO)(NCMe)Ph (**2.6**) toward the activation of aromatic C–H bonds has been demonstrated.

It has been shown that Cp*Fe(CO)(NCMe)Ph (**2.6**) can activate benzene C–H bonds at just 50 °C. Furthermore, Cp*Fe(CO)(NCMe)Ph (**2.6**) regioselectively activates the C–H bonds of furan, thiophene, thiazole and 2-methylfuran under very mild conditions. For instance, the furan 2-CH bond (calculated bond dissociation enthalpy = 118 kcal/mol) is readily broken below 0 ºC. In addition, we have disclosed a combined experimental and computational mechanistic study for the regioselective C–H activation of furan. The results herein demonstrate a relatively rare example of Fe(II)-mediated C–H activation by a non-radical pathway.

Importantly, the results reported in this chapter demonstrate the possible viability of Fe-based catalysts for the functionalization of inert hydrocarbons and other substrates with strong C–H bonds, such as olefin hydroarylation. The successful synthesis of Cp*Fe(CO)(NCMe)Ph (**2.6**) demonstrates the potential of synthesizing reactive Fe complexes with labile ligands. Additionally, Cp*Fe(CO)(NCMe)Ph (**2.6**) is able to mediate these C–H activations at mild temperatures (< 50 °C), which may help avoid Fe–C bond homolysis. By using the previously reported catalyst TpRu(CO)(NCMe)Ph as a starting point, we have been able to show that the similar Cp*Fe(CO)(NCMe)Ph (**2.6**) complex is active for aromatic C–H activation.

## 2.5 Experimental Methods

### 2.5.1 General Considerations

Unless otherwise noted, all synthetic procedures were performed under anaerobic conditions in a nitrogen-filled glovebox or by using standard Schlenk techniques.

Glovebox purity was maintained by periodic nitrogen purges and was monitored by an oxygen analyzer ($O_2$ < 15 ppm for all reactions). Tetrahydrofuran and *n*-pentane were dried by distillation from sodium/benzophenone and $P_2O_5$, respectively. Diethyl ether was distilled over $CaH_2$. Benzene, methylene chloride, and hexanes were purified by passage through a column of activated alumina. Benzene-$d_6$, acetone-$d_6$, $CD_3CN$, 1,4-dioxane-$d_8$, and THF-$d_8$ (for typical experiments) were used as received and stored under a $N_2$ atmosphere over 4 Å molecular sieves. For kinetic experiments, THF-$d_8$ was degassed by two conventional freeze-pump-thaw cycles and stored over 4 Å molecular sieves. $^1$H NMR spectra were recorded on a Varian Mercury 300 or Varian Inova 500 MHz spectrometer, and $^{13}$C NMR spectra were recorded on a Varian Inova 500 MHz spectrometer (operating frequency 125 MHz) or Bruker Avance III 800 MHz spectrometer (operating frequency 201 MHz) . All $^1$H and $^{13}$C spectra are referenced against residual proton signals ($^1$H NMR) or $^{13}$C resonances ($^{13}$C NMR) of the deuterated solvents. $^{31}$P NMR spectra were obtained on a Varian Mercury 300 MHz (operating frequency 121 MHz) spectrometer and referenced against an external standard of $H_3PO_4$ ($\delta = 0$). GC/MS was performed using a Shimadzu GCMS-QP2010 Plus system with a 30 m x 0.25 mm RTx-Qbond column with 8 μm thickness (for kinetic isotope effect experiments) or a 30 m x 0.25 mm SHRXI-5MS column with 0.25 μm thickness (for hydroarylation experiments) using electron impact ionization. IR spectra were obtained on a Shimadzu IRAffinity-1 Fourier transform infrared spectrometer. Samples were prepared in solution flow cells. Photolysis experiments were performed using UV-vis radiation generated by a 450 W power supply (Model #l7830, Ace Glass, Inc.) equipped with a water-cooled 450 W 5 inch arc IMMER UV-vis lamp (Model #7825-34, Ace

Glass, Inc.). Furan-$d_4$ was purchased from Aldrich and distilled prior to use. All other chemicals were used as purchased from commercial sources. Elemental analyses were performed by Atlantic Microlabs, Inc. $Fe(CO)_4I_2$ was prepared by the reaction of $Fe(CO)_5$ and $I_2$ in hexanes at room temperature in the dark.[39] $TpFe(CO)(PMe_3)Me$ (**2.1**),[36] $CpFe(CO)_2Ph$ (**2.3**),[43] and $Cp^*Fe(CO)_2I$[46] were prepared according to the literature procedures.

### 2.5.2 Experimental Section

**Observation of $TpFe(CO)_2I$ (2.2).** $Fe(CO)_4I_2$ (0.038 g, 0.090 mmol) and KTp (0.026 g, 0.11 mmol) were dissolved in $CH_2Cl_2$ and stirred for 3.5 h while monitoring the reaction progress by IR spectroscopy (appearance of two new peaks at 2060 and 2017 $cm^{-1}$). The resulting red reaction mixture was filtered through celite, and the volatiles were subsequently removed in vacuo to give 49 mg of a red solid. $^1H$ NMR (300 MHz, $CD_2Cl_2$): δ 8.47 (s, 2H, Tp 3/5), 7.83 (s, 2H, Tp 3/5), 7.73 (s, 1H, Tp 3/5), 7.47 (s, 1H, Tp 3/5), 6.39 (s, 2H, Tp 4), 6.20 (s, 1H, Tp 4). Note: There is likely fine splitting, but it was not resolved and the peaks have, therefore, been denoted as singlets. IR (DCM solution): $\nu_{CO}$ = 2060, 2017 $cm^{-1}$.

**Attempted Ethylene Hydrophenylation with $CpFe(CO)_2Ph$ (2.3).** In a glovebox, complex **2.3** (0.004 g, 0.02 mmol) was dissolved in benzene (5.0 mL, 0.056 mol, with 0.025 mol% hexamethylbenzene) in a reactor. The reactor was pressurized with 30 psi $C_2H_4$ and brought to a total pressure of 125 psi with $N_2$. The reactor was heated for 16 h at 120 °C. After cooling, the reactor was sampled under $N_2$ and analyzed by GC/MS. No products were observed. The reactor was subsequently re-sealed and pressurized to 125 psi with $C_2H_4$ and heated at 150 °C for an additional 4 h. After cooling to room

temperature, the reactor was sampled under $N_2$. Analysis of the aliquot by GC/MS revealed the formation of sub-stoichiometric amounts of ethylbenzene, styrene, propiophenone, and ferrocene. Attempts to obtain a $^1$H NMR spectrum of the resulting mixture by removal of the volatiles in vacuo and reconstitution in $C_6D_6$ was unsuccessful due to the apparent presence of paramagnetic decomposition products.

**Synthesis of CpFe(CO)(py)Ph (2.4).** Complex **2.3** (0.040 g, 0.16 mmol) was dissolved in ~5 mL pyridine in a thick-walled glass reaction vessel and sealed. The orange-yellow solution was photolyzed for 3 h during which time the solution turned purple. The volatiles were removed in vacuo, and the dark residue was rinsed with hexanes and pentane to give 30 mg of a brown solid in 62% yield. $^1$H NMR (300 MHz, $C_6D_6$): δ 8.24 (d, $^3J_{HH}$ = 4 Hz, 2H, py 2), 7.72 (d, $^3J_{HH}$ = 6 Hz, 2H, *ortho* phenyl), 7.11 (multiplet obscured by $C_6D_5H$ peak, *meta* phenyl and *para* phenyl), 6.41 ( t, $^3J_{HH}$ = 6 Hz, py 4), 5.89 (t, $^3J_{HH}$ = 6 Hz, py 3), 4.19 (s, 5H, Cp). IR (hexanes solution): $\nu_{CO}$ = 1928 cm$^{-1}$.

**Cp*Fe(CO)$_2$Ph (2.5).** A mixture of Cp*Fe(CO)$_2$I (0.533 g, 1.43 mmol), CuOTf (0.480 g, 1.91 mmol), $Bu_3SnPh$ (0.610 mL, 1.87 mmol) and 1,4-dioxane (~6 mL) was prepared. The mixture was stirred at 60 $^o$C for 4 hours during which time the mixture turned from dark brown to orange-beige. After cooling to room temperature, the mixture was filtered through a short plug of silica gel on a fine porosity frit followed by the *in vacuo* removal of the volatiles from the filtrate. The resulting residue was dissolved in a minimal amount of THF and chromatographed on silica gel eluting with 1:10 (v/v) diethyl ether/hexanes. A yellow band was collected and dried in vacuo. The resulting solid was triturated with a minimal amount of pentane to yield a yellow solid (0.311 g,

67%). A crystal suitable for single crystal X-ray diffraction was grown by the slow evaporation of a pentane solution of **2.5**. $^{1}$H NMR (300 MHz, $C_6D_6$): 7.58 (2H, d, $^{3}J_{HH}$ = 6 Hz, phenyl *ortho*), 7.16 (2H, t, $^{3}J_{HH}$ = 6 Hz, phenyl *meta*), 7.07 (1H, t, $^{3}J_{HH}$ = 6 Hz, phenyl *para*), 1.32 (15H, s, $C_5Me_5$). $^{13}$C NMR (75 MHz, $C_6D_6$): 218.3 (CO), 128.6, 143.4, 123.2 (Ph), 96.2 ($C_5Me_5$), 9.3 ($C_5Me_5$) (Note: 1 resonance of phenyl is missing presumably from coincidental overlap). IR (NCMe solution): $\nu_{CO}$ = 1994, 1937 cm$^{-1}$. Anal. Calcd for $C_{18}H_{20}O_2Fe$: C 66.69, H 6.22; found C 66.66, H 6.39.

**Cp*Fe(CO)(NCMe)Ph (2.6).** A solution of **2.5** (0.536 g, 1.67 mmol) in acetonitrile (~50 mL) was irradiated in an ice bath with stirring for a total of 3 h. After the first and second hour, photolysis was ceased and 2 conventional freeze-pump-thaw cycles were performed on the reaction flask. After 3 h, the volatiles were removed *in vacuo*. The resulting residue was extracted with diethyl ether (~50 mL) and filtered through Celite. Removal of volatiles produced a red solid, which was washed with pentane (~10 mL in portions) to yield a red-orange solid (0.450 g, 87% yield). This compound is moderately stable at room temperature in the solid state, but was typically stored at –35 $^{o}$C. A crystal suitable for single crystal X-ray diffraction was grown by the slow evaporation of a pentane solution of **2.6**. In order to obtain satisfactory elemental analysis, **2.6** was recrystallized from diethyl ether at –35 $^{o}$C. $^{1}$H NMR (300 MHz, dioxane-$d_8$): 7.34 (2H, d, $^{3}J_{HH}$ = 7 Hz, phenyl *ortho*), 6.82 (2H, t, $^{3}J_{HH}$ = 7 Hz, phenyl *meta*), 6.72 (1H, t, $^{3}J_{HH}$ = 7 Hz, phenyl *para*), 2.52 (3H, s, NCC$H_3$), 1.46 (15H, s, $C_5Me_5$). $^{13}$C NMR (125 MHz, THF-$d_8$): 223.9 (CO), 172.6, 143.0, 128.9, 126.5 (Ph), 121.4 ($CH_3CN$), 91.4 ($C_5Me_5$), 9.6 ($C_5Me_5$), 3.5 ($CH_3CN$). IR (NCMe solution): $\nu_{CO}$ =

1903 $cm^{-1}$. Anal. Calcd for $C_{19}H_{23}NOFe$: C 67.67, H 6.87, N 4.15; found C 67.52, H 6.85, N 4.07.

**Cp*Fe(CO)($PPh_3$)(2-furyl) (2.11)**. To a THF solution (~5 mL) of **2.6** (0.067 g, 0.20 mmol) was added furan (0.29 mL, 4.0 mmol). After stirring at room temperature for 1 h, $PPh_3$ (0.054 g, 0.21 mmol) dissolved in ~2 mL of THF was added. After stirring for an additional 1 h, the volatiles were removed under reduced pressure to leave a red residue. After transferring the residue to a vial with pentane (~3 mL) and subsequent removal of the volatiles under reduced pressure, a low density beige solid of **2.11** was obtained (0.105 g, 96% yield). A single crystal suitable for X-ray diffraction was grown from a saturated pentane solution of **2.11**. $^1$H NMR (300 MHz, acetone-$d_6$): 7.62 (1H, m, furyl 3), 7.35 (5H, br, $PPh_3$), 5.99 (1H, m, furyl 5), 5.64 (1H, m, furyl 4), 1.42(15H, s, $C_5Me_5$). $^{13}$C NMR (201 MHz, acetone-$d_6$): 224.6 (d, $^2J_{CP}$ = 28 Hz, CO), 177.3 (d, $^2J_{CP}$ = 40 Hz, furyl *ipso*), 148.1 (s, $PPh_3$), 134.6 (br, $PPh_3$), 130.3 (br s, $PPh_3$), 128.6 (s, furyl), 121.7 (s, furyl), 112.1 (s, furyl), 94.0 (s, $C_5Me_5$), 9.9 (s, $C_5Me_5$). Note: The *ipso* carbon for $PPh_3$ could not be located and may be obscured by the broad peaks for the remaining $PPh_3$ signals. $^{31}P\{^1H\}$ NMR (121 MHz, acetone-$d_6$): 77.8. IR ($C_6H_6$ solution): $\nu_{CO}$ = 1913 $cm^{-1}$. Anal. Calcd for $C_{30}H_{34}O_2PFe$: C 72.27, H 6.06; found C 72.42, H 6.19.

**Cp*Fe(CO)($PPh_3$)(2-thienyl) (2.12)**. Thiophene (0.31 mL, 3.9 mmol) was added to a THF solution (~7 mL) of **2.6** (0.065 g, 0.19 mmol). After stirring at room temperature for 1 h, $PPh_3$ (0.051 g, 0.19 mmol) dissolved in ~2 mL of THF was added. After stirring for an additional 30 min, the volatiles were removed under reduced pressure to leave a light brown residue. After transferring the residue to a vial with a small amount of pentane and diethyl ether and subsequent removal of the volatiles under reduced

pressure, a low-density red solid of **2.12** was obtained (0.109 g, 97% yield). $^{1}$H NMR (300 MHz, acetone-$d_6$): 7.39 (15H, br m, $PPh_3$), 7.19 (1H, d, $^{3}J_{HH}$ = 5 Hz, thienyl 3), 6.77 (dd, $^{3}J_{HH}$ = 5, 3 Hz, thienyl 5), 6.33 (br s, thienyl 4), 1.43 ($C_5Me_5$). Due to fluxionality, a clean $^{13}$C NMR spectrum could not be acquired. $^{31}P\{^{1}H\}$ NMR (121 MHz, acetone-$d_6$): 74.0. IR ($C_6H_6$ solution): $\nu_{CO}$ = 1913 cm$^{-1}$. Anal. Calcd for $C_{30}H_{34}OSPFe$: C 70.21, H 5.89; found C 69.92, H 6.05.

**Cp*Fe(CO)(*N*-thiazole)(2-thiazolyl) (2.13).** Thiazole (0.20 mL, 2.9 mmol) was added to a THF (~5 mL) solution of **2.6** (0.053 g, 0.16 mmol). The solution immediately became dark red and was stirred for 18 h after which time the volatiles were removed *in vacuo*. The residue was washed with 3 mL of pentane and collected on a fine porosity frit to give a red-brown solid of **2.13** (0.026 g, 36% yield). $^{1}$H NMR (300 MHz, acetone-$d_6$): 9.89 (1H, d, $^{3}J_{HH}$ = 3 Hz, thiazole 2), 8.04 (1H, d, $^{3}J_{HH}$ = 3 Hz, thiazole/thiazolyl 4), 7.91 (1H, d, $^{3}J_{HH}$ = 3 Hz, thiazole/thiazolyl 4) 7.65 (1H, dd, $^{3}J_{HH}$ = 3 Hz, $^{3}J_{HH}$ = 3 Hz, thiazole 5) 7.08 (1H, d, $^{3}J_{HH}$ = 3 Hz, thiazolyl 5), 1.42 (15H, s, $C_5Me_5$). $^{13}$C NMR (201 MHz, acetone-$d_6$): 223.1 (s, CO), 205.1 (s, thiazolyl *ipso*), 159.3 (s, thiazolyl/thiazole), 149.9 (s, thiazolyl/thiazole), 144.3 (s, thiazolyl/thiazole), 120.9 (s, thiazolyl/thiazole), 120.7 (s, thiazolyl/thiazole), 92.1 (s, $C_5Me_5$), 9.3 ($C_5Me_5$). IR (THF solution): $\nu_{CO}$ = 1910 cm$^{-1}$. Anal. Calcd for $C_{17}H_{17}N_2S_2OFe$: C 52.58, H 5.19, N 7.21; found C 52.16, H 5.06, N 7.04.

**Cp*Fe(CO)($PPh_3$)[2-(5-methylfuryl)] (2.14).** To a THF (~4 mL) solution of **2.6** (0.041 g, 0.12 mmol) was added 2-methylfuran (0.11 mL, 1.2 mmol). After stirring the red solution for 1 h, $PPh_3$ was dissolved in THF (.032 g, 0.12 mmol) and added to the reaction mixture. The volatiles were removed in vacuo. The subsequent solid was washed with pentane (~3 mL), and dried in vacuo to obtain a red solid of **2.14** (0.056 g, 82%

yield). $^{1}$H NMR (300 MHz, acetone-$d_6$): 7.36 (15H, br m, $PPh_3$), 5.52 (2H, overlapping, methylfuryl 3 and 4), 2.12 (3H, s, methyl), 1.43 (15H, s, $C_5Me_5$). $^{13}$C NMR (201 MHz, acetone-$d_6$) 224.8 (d, $^{2}J_{CP}$ = 27 Hz, CO), 173.5 (d, $^{2}J_{CP}$ = 32 Hz, thienyl *ipso*), 156.9 (s, $PPh_3$), 135.0 (br s, $PPh_3$), 130.3 (s, $PPh_3$), 128.5 (s, methyl*furyl*), 122.6 (s, methyl*furyl*), 108.3 (s, methyl*furyl*), 94.0 (s, $C_5Me_5$), 14.2 (s, *methyl*furyl), 10.1 (s, $C_5Me_5$). Note: The *ipso* carbon for $PPh_3$ could not be located likely due to coincidental overlap. $^{31}$P{$^{1}$H} NMR (121 MHz, acetone-$d_6$): 77.7. IR (THF solution): $\nu_{CO}$ = 1913 cm$^{-1}$. Anal. Calcd for $C_{31}H_{37}O_2PFe$: C 72.60, H 6.27; found C 72.61, H 6.26.

**Reaction of Cp*Fe(CO)(NCMe)Ph and $C_6D_6$.** In a screw-cap NMR tube, **2.6** (0.005 g, .02 mmol) and hexamethyldisilane (HMDS, internal standard, ~1 μL) were dissolved in $C_6D_6$ (0.25 mL). The NMR tube was heated to 50 °C in a temperature-controlled oil bath. The reaction was periodically monitored by $^{1}$H NMR spectroscopy until completion using a delay time of 5 s. During that time, the phenyl resonances decreased in intensity relative to HMDS. Using the integration of the Cp* methyl peaks versus the integration of HMDS, an approximate yield of 80% was determined for the formation of **2.6-*d*$_5$**.

**Determination of the Rate of Benzene C–D Activation.** A stock solution of **2.6** (0.024 g, 0.071 mmol) and HMDS (~3 μL) was prepared in 1.5 mL $C_6D_6$. Three 0.4 mL aliquots of this stock solution were added to three different screw-cap NMR tubes. The samples were frozen until it was time to collect data. Each sample was subsequently monitored by $^{1}$H NMR spectroscopy in a temperature-regulated probe (calibrated at 49 ºC) through 2 half-lives, collecting spectra every 5 minutes (5 s delay). The reaction was monitored through only 2 half-lives due to decomposition at longer reaction times. A plot

of [**2.6**] vs time was created and fitted to an exponential decay curve. The rate constants were extracted from these plots to yield $k_{obs}$ = 4.6(5) x $10^{-4}$ $s^{-1}$.

**Dependence on Furan Concentration of the C–H Activation of Furan by Cp*Fe(CO)(NCMe)Ph (2.6).** A representative experiment follows. Two stock solutions were prepared in 2 separate 1 mL volumetric flasks. In the first stock solution, complex **2.6** (0.027 g, 0.080 mmol) was dissolved in 1 mL of THF-$d_8$. In the second stock solution, furan (128 μL) and HMDS (8 μL) were added and diluted to 1 mL with THF-$d_8$. From the first stock solution, 275 μL (.022 mmol of **2.6**) aliquots were transferred to 3 separate screw-cap NMR tubes equipped with Teflon-lined septa. The second stock solution was transferred to a 1 dram vial with a Teflon-lined septum cap. Outside the glove box, one NMR tube was cooled in an ice-water bath. Using a microsyringe, a 125 μL (10 equiv of furan) aliquot of the second stock solution was injected through the cap of the NMR tube. The tube was vigorously shaken and placed in a temperature calibrated NMR probe (3 $^{o}$C). $^{1}$H NMR spectra (5 s delay, every 2.5 min) were acquired through at least 3 half-lives. By monitoring the disappearance of the *ortho*-phenyl protons of **2.6** versus HMDS, a plot of [**2.6**] vs time was created. Fitting the data to an exponential decay curve allowed the rate constant to be extracted. This was repeated for the two remaining NMR tubes. The whole procedure was performed for 7, 10, 15, 20, 25, 30, 35 equivalents of furan.

**Dependence on NCMe Concentration for the C–H Activation of Furan by Cp*Fe(CO)(NCMe)Ph (2.6).** A representative experiment follows. Two stock solutions were prepared in 2 separate 1 mL volumetric flasks. In the first stock solution, complex **2.6** (0.027 g, 0.080 mmol) was dissolved in 1 mL of THF-$d_8$. In the second stock

solution, furan (256 μL), NCMe (18.3 μL, 5% v:v in THF-$d_8$), HMDS (8 μL) were diluted to 1 mL with THF-$d_8$. From the first stock solution, 275 μL (.022 mmol of **2.6**) aliquots were transferred to 3 separate screw-cap NMR tubes equipped with Teflon-lined septa. The second stock solution was transferred to a 1-dram vial with a Teflon-lined septum cap. Outside the glove box, one NMR tube was cooled in an ice-water bath. Using a microsyringe, a 125 μL (20 equiv of furan, 0.1 equiv of NCMe) aliquot of the second stock solution was injected through the cap of the NMR tube. The tube was vigorously shaken and placed in a temperature calibrated NMR probe (3 $^{o}$C). $^{1}$H NMR spectra (5 s delay, every 5 min) were acquired through at least 3 half-lives. By monitoring the disappearance of the *ortho*-phenyl protons of .6**2** versus HMDS, a plot of [**2.6**] vs time was created. Fitting the data to an exponential decay curve allowed the rate constant to be extracted. This was repeated for the two remaining NMR tubes. The whole procedure was performed for 0.05, 0.1, and 0.2 equiv of NCMe. A plot of $1/k_{obs}$ vs [NCMe] showed an excellent linear correlation.

**Determination of Kinetic Isotope Effect for Furan C–H(D) Activation.** A representative experiment follows. In a 4-dram vial with a magnetic stir bar was prepared a THF solution (1.5 mL) of **2.6** (0.015 g, .045 mmol). To this solution was added a 1:1 (molar) mixture of furan and furan-$d_4$ (35 μL, ~10 eq arene). After ~20 min, an aliquot was removed and analyzed by GC/MS. The average mass spectrum for the peak representing benzene was analyzed. Using the relative ratios of m/z = 78 and 79 (adjusted for the natural abundance of $^{2}$H), the relative quantities of $C_6H_6$ and $C_6H_5D$ was determined to give a kinetic isotope effect of 5.43. The reported 5.0(4) is the average of 3 independent reactions as described above. Additionally, the above procedure was

performed using 50 equivalents of arene, which gave a kinetic isotope effect of 4.8(1). To ensure irreversibility of the reaction, multiple aliquots were analyzed throughout the course of the reaction (over ~2 h) with no significant deviation in the relative amounts of $C_6H_6$ and $C_6H_5D$.

**Eyring Plot for the C–H Activation of Furan by Cp*Fe(CO)(NCMe)Ph (2.6).** The procedure described above for measuring the dependence of rate of furan activation on furan concentration was repeated at –12, –6, and 13 °C using 10 equiv of furan (3 runs each, see Supporting Information). Plotting $\ln(k_{obs}/T)$ vs 1/T gave an excellent linear fit and allowed the determination of the activation parameters. The plotted $k_{obs}$ value is the value determined after dividing the experimentally determined $k_{obs}$ value by [furan].

**Determination of the Rate of Thiophene C–H Activation.** Two stock solutions were prepared in 2 separate 1 mL volumetric flasks. In the first stock solution, complex **2.6** (0.027 g, 0.080 mmol) was dissolved in 1 mL of THF-$d_8$. In the second stock solution, thiophene (281 μL) and HMDS (8 μL) were added and diluted to 1 mL with THF-$d_8$. From the first stock solution, 275 μL (.022 mmol **2.6**) aliquots were transferred to 3 separate screw-cap NMR tubes equipped with Teflon-lined septa. The second stock solution was transferred to a 1 dram vial with a Teflon-lined septum cap. Outside the glove box, one NMR tube was cooled in an ice-water bath. Using a microsyringe, a 125 μL (20 equiv of thiophene) aliquot of the second stock solution was injected through the cap of the NMR tube. The tube was vigorously shaken and placed in a temperature calibrated NMR probe (3 ºC). $^1$H NMR spectra (5 s delay, every 2.5 min) were acquired through at least 3 half-lives. By monitoring the disappearance of the *ortho*-phenyl protons of **2** versus HMDS, a plot of [**2.6**] vs time was created. Fitting the data to an exponential

decay curve allowed the rate constant to be extracted. This was repeated for the two remaining NMR tubes.

**Variable Temperature NMR for Cp*Fe(CO)($PPh_3$)(2-thienyl) (2.12).** An NMR sample of **2.12** dissolved in THF-$d_8$ was incrementally cooled in a 600 MHz NMR probe. Upon cooling, the resonance assigned to the Cp* methyl protons decoalesced into 2 singlets. Spectra were acquired at the following temperatures (not calibrated): 25 ºC, 0 ºC, –20 ºC, –40 ºC, –50 ºC, –60 ºC, –80 ºC.

**Monitoring Cp*Fe(CO)($PPh_3$)(2-thienyl) (2.12) in the presence of excess thiophene.** Complex **2.12** (11 mg, 0.020 mmol) was dissolved in THF-$d_8$ (0.4 mL) and transferred to an NMR tube sealed with a Teflon-lined screw cap. Following the acquisition of an initial $^1$H NMR spectrum, thiophene (0.8 μL, 0.010 mmol) was added. A $^1$H NMR spectrum of the resulting solution was acquired and revealed the presence of free thiophene and identical chemical shifts and peak shapes of the resonances assigned to **2.12** as observed in the initial spectrum.

**Experimental Evidence against the formation of a "tuck-in" complex during the reaction of Cp*Fe(CO)(NCMe)Ph (2.6) and $C_6D_6$.** While monitoring the reaction of **2.6** and $C_6D_6$, the total integration for the Cp* peaks relative to HMDS remained constant (within deviation), suggesting there is no H/D exchange into the methyl resonances of the Cp* ligand during the course of the reaction. The total deviation for the integrations of the Cp* region is ~4%.

**Eyring Plot for the C–H Activation of Furan by Cp*Fe(CO)(NCMe)Ph (2.6).** Two stock solutions were prepared in 2 separate 1 mL volumetric flasks. In the first stock solution, complex **2.6** (0.027 g, 0.080 mmol) was dissolved in 1 mL of THF-$d_8$. In the

second stock solution, furan (384 μL) and HMDS (8 μL) were added and diluted to 1 mL with THF-$d_8$. From the first stock solution, 275 μL (.022 mmol of **2.6**) aliquots were transferred to 3 separate screw-cap NMR tubes equipped with Teflon-lined septa. The second stock solution was transferred to a 1 dram vial with a Teflon-lined septum cap. Outside the glove box, one NMR tube was cooled in an ice-water bath. Using a microsyringe, a 125 μL (30 equiv of furan) aliquot of the second stock solution was injected through the cap of the NMR tube. The tube was vigorously shaken and placed in a temperature calibrated NMR probe (–22 $^{o}$C or –12 $^{o}$C). $^{1}$H NMR spectra (5 s delay, every 15 min or 25 min) were acquired through at least 2.5 half-lives. By monitoring the disappearance of the *ortho*-phenyl protons of **2.6** versus HMDS, a plot of [**2.6**] vs time was created. Fitting the data to an exponential decay curve allowed the rate constant to be extracted. Plotting ln($k_{obs}$/T) vs 1/T gave a very good linear fit and allowed the determination of the activation parameters.

### 2.5.3 Computational Details

All stationary points were optimized in the gas phase using either restricted or unrestricted M06 density functional theory with the 6-31G(d,p) basis set for all atoms except Fe. The LANL2DZ basis set and pseudopotential was utilized for Fe during optimization. Single point energies were further refined using the M06 functional with the 6-311++G(3df,3dp) basis set for light atoms and LANL2TZ(f) with an f exponent of 2.462 for Fe.[49, 50] Solvent energy corrections were calculated using the SMD solvent model of benzene and furan. Solvation calculations were performed on the gas-phase optimized structures.[51] Optimization, single point, and solvent calculations were all carried out in Gaussian 09.[64] Location of singlet-triplet intersystem crossing points, also

called minimum energy crossing points (MECPs), was done using the algorithm of Harvey in conjunction with Gaussian 09.[65, 66] Although MECPs are not stationary points, frequency calculations were carried out on these structures to obtain approximate enthalpy and free energy corrections.

## 2.6 References

(1) Goldberg, K. I.; Goldman, A. S., *Activation and Functionalization of C-H Bonds*. American Chemical Society: Washington, DC, 2004; Vol. 885.

(2) Goj, L. A.; Gunnoe, T. B. *Curr. Org. Chem.* **2005**, *9*, 671-685.

(3) Kuhl, N.; Hopkinson, M. N.; Wencel-Delord, J.; Glorius, F. *Angew. Chem. Int. Ed.* **2012**, *51*, 10236-10254.

(4) Stoutland, P. O.; Bergman, R. G.; Nolan, S. P.; Hoff, C. D. *Polyhedron* **1988**, *7*, 1429-1440.

(5) Hartwig, J. F., *Organotransition Metal Chemistry: From Bonding to Catalysis*. University Science Books: Sausalito, 2009.

(6) Bullock, R. M., *Catalysis without Precious Metals*. Wiley-VCH Verlag & Co.: Weinheim, Germany, 2010.

(7) Crabtree, R. H., *The Organometallic Chemistry of the Transition Metals*. 5th ed.; John Wiley and Sons: New York, 2009.

(8) Gunay, A.; Theopold, K. H. *Chem. Rev.* **2010**, *110*, 1060-1081.

(9) Wang, D.; Farquhar, E. R.; Stubna, A.; Munck, E.; Que, L. *Nature Chem.* **2009**, *1*, 145-150.

(10) Gamez, P.; Aubel, P. G.; Driessen, W. L.; Reedijk, J. *Chem. Soc. Rev.* **2001**, *30*, 376-385.

(11) Goldsmith, C. R.; Cole, A. P.; Stack, T. D. P. *J. Am. Chem. Soc.* **2005**, *127*, 9904-9912.

(12) Gephart, R. T.; Huang, D. L.; Aguila, M. J. B.; Schmidt, G.; Shahu, A.; Warren, T. H. *Angew. Chem. Int. Ed.* **2012**, *51*, 6488-6492.

(13) Mayer, J. M. *Acc. Chem. Res.* **1998**, *31*, 441-450.

(14) Wiese, S.; McAfee, J. L.; Pahls, D. R.; McMullin, C. L.; Cundari, T. R.; Warren, T. H. *J. Am. Chem. Soc.* **2012**, *134*, 10114-10121.

(15) Shilov, A. E.; Shul'pin, G. B. *Chem. Rev.* **1997**, *97*, 2879-2932.

(16) Bakac, A. *J. Am. Chem. Soc.* **2000**, *122*, 1092-1097.

(17) Jones, W. D.; Foster, G. P.; Putinas, J. M. *J. Am. Chem. Soc.* **1987**, *109*, 5047-5048.

(18) Hatanaka, T.; Ohki, Y.; Tatsumi, K. *Chem. Asian J.* **2010**, *5*, 1657-1666.

(19) Ittel, S. D.; Tolman, C. A.; English, A. D.; Jesson, J. P. *J. Am. Chem. Soc.* **1978**, *100*, 7577-7585.

(20) Tolman, C. A.; Ittel, S. D.; English, A. D.; Jesson, J. P. *J. Am. Chem. Soc.* **1979**, *101*, 1742-1751.

(21) Baker, M. V.; Field, L. D. *J. Am. Chem. Soc.* **1986**, *108*, 7433-7434.

(22) Baker, M. V.; Field, L. D. *J. Am. Chem. Soc.* **1986**, *108*, 7436-7438.

(23) Ohki, Y.; Hatanaka, T.; Tatsumi, K. *J. Am. Chem. Soc.* **2008**, *130*, 17174-17186.

(24) Lail, M.; Arrowood, B. N.; Gunnoe, T. B. *J. Am. Chem. Soc.* **2003**, *125*, 7506-7507.

(25) Foley, N. A.; Lail, M.; Lee, J. P.; Gunnoe, T. B.; Cundari, T. R.; Petersen, J. L. *J. Am. Chem. Soc.* **2007**, *129*, 6765-6781.

(26) Foley, N. A.; Lee, J. P.; Ke, Z. F.; Gunnoe, T. B.; Cundari, T. R. *Acc. Chem. Res.* **2009**, *42*, 585-597.

(27) Foley, N. A.; Gunnoe, T. B.; Cundari, T. R.; Boyle, P. D.; Petersen, J. L. *Angew. Chem. Int. Ed.* **2008**, *47*, 726-730.

(28) Joslin, E. E.; McMullin, C. L.; Gunnoe, T. B.; Cundari, T. R.; Sabat, M.; Myers, W. H. *Organometallics* **2012**, *31*, 6851-6860.

(29) Kalman, S. E.; Petit, A.; Gunnoe, T. B.; Ess, D. H.; Cundari, T. R.; Sabat, M. *Organometallics* **2013**, *32*, 1797-1806.

(30) Lail, M.; Bell, C. M.; Conner, D.; Cundari, T. R.; Gunnoe, T. B.; Petersen, J. L. *Organometallics* **2004**, *23*, 5007-5020.

(31) Foley, N. A.; Ke, Z. F.; Gunnoe, T. B.; Cundari, T. R.; Petersen, J. L. *Organometallics* **2008**, *27*, 3007-3017.

(32) Foley, N. A.; Lail, M.; Gunnoe, T. B.; Cundari, T. R.; Boyle, P. D.; Petersen, J. L. *Organometallics* **2007**, *26*, 5507-5516.

(33) Burgess, S. A.; Joslin, E. E.; Gunnoe, T. B.; Cundari, T. R.; Sabat, M.; Myers, W. H. *Chem. Sci.* **2014**, *5*, 4355-4366.

(34) King, R. B.; Bond, A. *J. Organomet. Chem.* **1974**, *73*, 115-118.

(35) King, R. B.; Bond, A. *J. Am. Chem. Soc.* **1974**, *96*, 1338-1343.

(36) Graziani, O.; Toupet, L.; Hamon, J. R.; Tilset, M. *J. Organomet. Chem.* **2003**, *669*, 200-206.

(37) Anderson, S.; Hill, A. F.; Slawin, A. M. Z.; Williams, D. J. *J. Chem. Soc., Chem. Comm.* **1993**, 266-267.

(38) Bruce, M. I.; Sharrock, D. N.; Stone, F. G. A. *J. Organomet. Chem.* **1971**, *31*, 269-273.

(39) Hieber, W.; Wirsching, A. *Z. Anorg. Allg. Chem.* **1940**, *245*, 35-58.

(40) Tellers, D. M.; Skoog, S. J.; Bergman, R. G.; Gunnoe, T. B.; Harman, W. D. *Organometallics* **2000**, *19*, 2428-2432.

(41) Yasuda, S.; Yorimitsu, H.; Oshima, K. *Organometallics* **2010**, *29*, 2634-2636.

(42) *The Chemistry of Organoiron Compounds*. John Wiley & Sons Ltd.: West Sussex, England, 2014.

(43) Yasuda, S.; Yorimitsu, H.; Oshima, K. *Organometallics* **2010**, *29*, 273-274.

(44) Yasuda, S.; Yorimitsu, H.; Oshima, K. *Organometallics* **2008**, *27*, 4025-4027.

(45) Kamitani, M.; Ito, M.; Itazaki, M.; Nakazawa, H. *Chem. Comm.* **2014**, *50*, 7941-7944.

(46) Diaz, C.; Cabezas, N.; Mendizabal, F. *Bol. Soc. Chil. Quim.* **2002**, *47*, 213-220.

(47) Jacobson, S. E.; Reichroh.P; Wojcicki, A. *Inorg. Chem.* **1973**, *12*, 717-723.

(48) Argouarch, G.; Grelaud, G.; Roisnel, T.; Humphrey, M. G.; Paul, F. *Tet. Lett.* **2012**, *53*, 5015-5018.

(49) Zhao, Y.; Truhlar, D. G. *Acc. Chem. Res.* **2008**, *41*, 157-167.

(50) Zhao, Y.; Truhlar, D. G. *Theor. Chem. Acc.* **2008**, *120*, 215-241.

(51) Marenich, A. V.; Cramer, C. J.; Truhlar, D. G. *J. Phys. Chem. B* **2009**, *113*, 6378-6396.

(52) Poli, R. *Chem. Rev.* **1996**, *96*, 2135-2204.

(53) Poli, R.; Harvey, J. N. *Chem. Soc. Rev.* **2003**, *32*, 1-8.

(54) Schroder, D.; Shaik, S.; Schwarz, H. *Acc. Chem. Res.* **2000**, *33*, 139-145.

(55) Lam, W. H.; Jia, G. C.; Lin, Z. Y.; Lau, C. P.; Eisenstein, O. *Chem. Eur. J.* **2003**, *9*, 2775-2782.

(56) Nakazawa, H.; Itazaki, M.; Owaribe, M. *Acta Cryst.* **2005**, *61*, M1275-M1276.

(57) Simmie, J. M.; Curran, H. J. *J. Phys. Chem. A* **2009**, *113*, 5128-5137.

(58) Brooks, B. C.; Gunnoe, T. B.; Harman, W. D. *Coord. Chem. Rev.* **2000**, *206*, 3-61.

(59) Petit, A.; Flygare, J.; Miller, A. T.; Winkel, G.; Ess, D. H. *Org. Lett.* **2012**, *14*, 3680-3683.

(60) Pittard, K. A.; Lee, J. P.; Cundari, T. R.; Gunnoe, T. B.; Petersen, J. L. *Organometallics* **2004**, *23*, 5514-5523.

(61) Balcells, D.; Clot, E.; Eisenstein, O. *Chem. Rev.* **2010**, *110*, 749-823.

(62) Jones, W. D.; Feher, F. J. *Acc. Chem. Res.* **1989**, *22*, 91-100.

(63) Clot, E.; Megret, C.; Eisenstein, O.; Perutz, R. N. *J. Am. Chem. Soc.* **2006**, *128*, 8350-8357.

(64) Frisch, M. J. T., G. W.; Schlegel, H. B.; Scuseria, G. E.; Robb,; A.;, M.; Cheeseman, J. R. S., G.; Barone, V.; Mennucci, B.; Petersson, G. A.; Nakatsuji,; H.; Caricato, M. L., X.; Hratchian, H. P.; Izmaylov, A. F.; Bloino, J.; Zheng, G.; Sonnenberg, J.; L.; Hada, M. E., M.; Toyota, K.; Fukuda, R.; Hasegawa, J.; Ishida,; M.; Nakajima, T.; Honda, Y. K., O.; Nakai, H.; Vreven, T.; Montgomery, Jr., J. A.; Peralta, J. E.; Ogliaro, F.;; Bearpark, M. H., J. J.; Brothers, E.; Kudin, K. N.; Staroverov, V. N.; Kobayashi, R.;; Normand, J. R., K.; Rendell, A.; Burant; , J. C. I., S. S.; Tomasi, J.; Cossi, M.;; Rega, N. M., N. J.; Klene, M.; Knox, J. E.; Cross, J. B.; Bakken, V.; Adamo, C.; Jaramillo,; J.; Gomperts, R. S., R. E.; Yazyev, O.; Austin, A. J.; Cammi, R.; Pomelli, C.; Ochterski,;

Martin, J. W.; , R. L. M., K.; Zakrzewski, V. G.; Voth, G. A.; Salvador, P.; Dannenberg,; J. J.; Dapprich, S. D., A. D.; Farkas, Ö.; Foresman, J. B.; Ortiz, J. V.; Cioslowski, J.; Fox,; J., D. *Gaussian 09, Revision B.01*, Gaussian, Inc.: Wallingford, CT, 2009.

(65) Harvey, J. N.; Aschi, M.; Schwarz, H.; Koch, W. *Theor. Chem. Acc.* **1998**, *99*, 95-99.

(66) Harvey, J. N.; Aschi, M. *Phys. Chem. Chem. Phys.* **1999**, *1*, 5555-5563.

# 3 The Reactivity of Cp*Fe(CO)(NCMe)Ph with Olefins and Internal Alkynes

## 3.1 Introduction

As discussed in Chapter 1, the development of an Fe catalyst for olefin hydroarylation is an important goal. The proposed olefin hydroarylation cycle involves two key steps, olefin insertion and aromatic C–H activation. A substantial challenge in developing Fe catalysts for olefin hydroarylation is that Fe mediated aromatic C–H activation is rare. In Chapter 2, we discovered that the Fe(II) complex Cp*Fe(CO)(NCMe)Ph (**3.1**) is highly active toward stoichiometric aromatic C–H activation (Scheme 3.1).[1] Indeed, C–H activation occurred at or below room temperature in some cases. With an Fe complex that can competently perform C–H activation in hand, the question remained whether this complex could mediate olefin insertion and catalyze olefin hydroarylation.

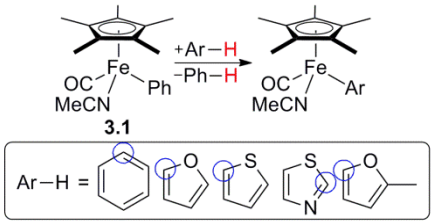


**Scheme 3.1.** Aromatic C–H activation by Cp*Fe(CO)(NCMe)Ph (**3.1**).

### 3.1.1 Olefin Insertion

In catalytic olefin hydroarylation, the insertion of the olefin into the M–aryl bond leads to the formation of a new C–C bond.[2] Specific features of this reaction were addressed in Chapter 1. At this point it should be noted that many transition metal complexes have been reported to mediate olefin insertion into M–R(H) (R = alkyl or aryl) bonds, both in stoichiometric reactions and catalytic reactions.[2-8] More relevant to this

work, there have been examples of Fe complexes that mediate this transformation (Figure 3.1). Brookhart and co-workers have reported highly active tridentate pyridinebisimine ligated Fe catalysts for olefin polymerization and oligomerization.[9, 10] Additionally, Chirik has reported Fe catalysts for olefin hydrogenation at room temperature, which involves olefin insertion into Fe–H bonds.[11] Peters and co-workers have also reported Fe olefin hydrogenation catalysts using trisphosphine ligands.[12] Holland and Cundari have reported olefin insertion using β-diketiminate Fe–H complexes, including catalytic defluorination of olefins.[13, 14] One study that is particularly relevant to our work is the report by Yorimitsu and Oshima of olefin insertion into Fe–aryl bonds by $CpFe(CO)_2(aryl)$ following CO dissociation.[15]

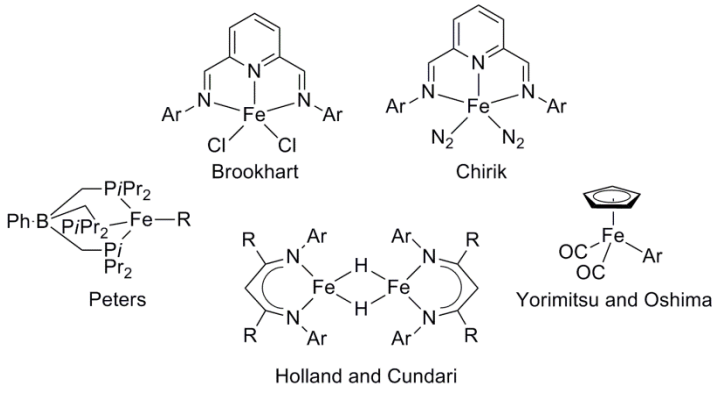


**Figure 3.1.** Select examples of Fe complexes capable of olefin insertion.

The olefin insertion step in catalytic olefin hydroarylation is at the center of several side reactions that could lead to catalyst deactivation or other undesired reactivity. As discussed in some detail in Chapter 1 (Section 1.3.3), these side reactions are olefin C–H activation, β-hydride elimination, and oligomerization/polymerization (Scheme 3.2). There is clearly a balancing act required to observe catalytic turnover, since these side

reactions are expected to have similar energetic profiles to the steps of the catalytic cycle.[2, 16-18]

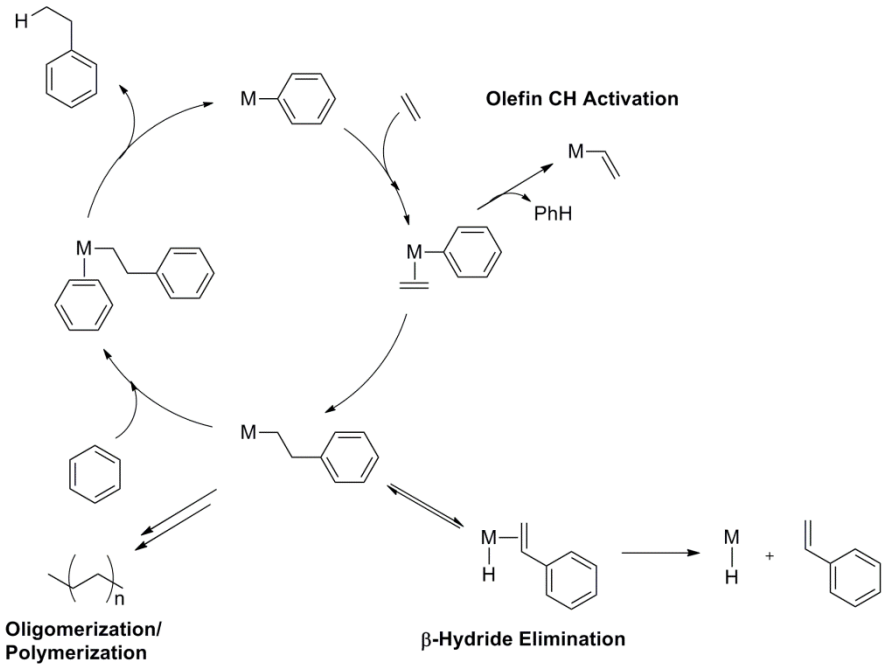


**Scheme 3.2.** Olefin hydroarylation catalytic cycle with possible side reactions involving olefin insertion.

### 3.1.3 Alkyne Hydroarylation

Besides a discussion of olefin hydroarylation using Cp*Fe(CO)(NCMe)Ph (**3.1**), this chapter will also include reactivity studies that were originally directed toward alkyne hydroarylation (Scheme 3.3). The hydroarylation of alkynes provides a means to synthesize vinyl arenes, which are important intermediates in the fine chemical industry.[19-21] Alkyne hydroarylation is more atom-economical and environmentally friendly compared to the Heck reaction (Scheme 3.4).[22, 23] Several examples of transition metal catalysts for alkyne hydroarylation are known, including catalysts based on Rh, Ni, Pt, Pd, Ir, Ru, and Re. While alkyne hydrophenylation has been reported,[20, 24] many examples involve heteroaromatic substrates or chelate assisted C–H activation.[20, 21] Iron

based catalysts for this transformation are unknown. Therefore, having an Fe complex that could perform C–H activation inspired us to broaden our study to alkyne hydroarylation.

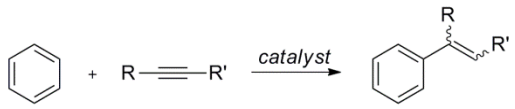


**Scheme 3.3**. Generic alkyne hydroarylation reaction.

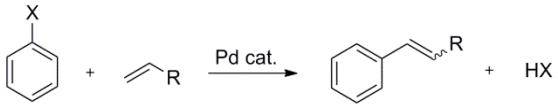


**Scheme 3.4.** Generic Heck reaction (X = halogen).

This chapter will describe the reactivity of Cp*Fe(CO)(NCMe)Ph (**3.1**) toward catalytic olefin hydroarylation and alkyne hydroarylation. A discussion of side reactivity accompanying both reactions will be included. In particular, the reactivity of Cp*Fe(CO)(NCMe)Ph (**3.1**) toward internal alkynes led to the formation of novel hydroxyindenyl and vinylidene ligands.[25] The hydroxyindenyl ligands are closely related to biologically relevant indenol compounds. The study of alkyne insertion with complex **3.1** has been previously published.[25] Dr. Michal Sabat (UVa) solved the X-ray crystal structures reported in that publication.

## 3.2 Results and Discussion

### 3.2.1 Application of Cp*Fe(CO)(NCMe)Ph (3.1) to Olefin Hydrophenylation

To explore the potential of complex **3.1** to catalyze olefin hydroarylation, catalytic ethylene hydrophenylation was attempted. A benzene solution of Cp*Fe(CO)(NCMe)Ph (**3.1**) (0.025 mol% relative to $C_6H_6$) was pressurized with 25 psi of $C_2H_4$ and heated at 30 °C for 20 h (Scheme 3.5). Analysis of the organic materials by

GC/MS revealed the formation of 0.6 TO of EtPh and 1.2 TO of styrene (average of 3 independent reactions). A low temperature was chosen due to decomposition of complex **3.1** upon thermolysis at elevated temperatures for an extended period of time. Despite this observation, ethylene hydrophenylation was also attempted at 100 °C and gave similar results with 0.6 TO of EtPh and 0.9 TO of styrene. Because we observe similar yields of functionalized products at different temperatures, it is likely that ethylene hydrophenylation and benzene vinylation occur rapidly, but catalyst deactivation is also rapid.

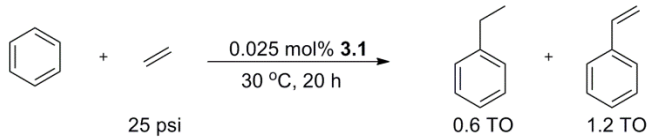


**Scheme 3.5.** Ethylene hydrophenylation mediated by Cp*Fe(CO)(NCMe)Ph (**3.1**).

In order to provide insight into the low catalytic turnover along with stoichiometric styrene formation, an NMR scale experiment was performed. In this experiment, Cp*Fe(CO)(NCMe)Ph (**3.1**) was dissolved in $C_6D_6$ and pressurized with 30 psi of $C_2H_4$ at room temperature. Within ~30 min, resonances corresponding to styrene and EtPh appeared, which demonstrates the fast rate of this reaction including evidence for benzene C–H activation at room temperature (Scheme 3.6, Figure 3.2). Previously reported ethylene hydrophenylation catalysts require elevated temperatures (>90 °C).[2, 16, 17, 26-35] In contrast, the appearance of ethylbenzene in this reaction demonstrates that ethylene insertion and benzene C–H activation occur at room temperature for the Fe system **3.1**. Along with the appearance of these organic products, a broad peak was observed around –17 ppm, which likely corresponds to an Fe–H complex consistent with

ethylene insertion and β-hydride elimination. Attempts to isolate the purported Fe–H complex were made. Stirring a THF solution of **3.1** under 50 psi of $C_2H_4$ followed by removal of the volatiles in vacuo gave a crude product that still has an Fe–H resonance (Figure 3.3). Further purification of this complex was challenging and eventually abandoned.

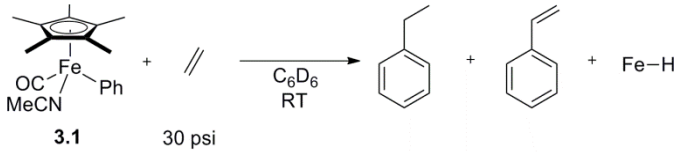


**Scheme 3.6.** Reaction of Cp*Fe(CO)(NCMe)Ph (**3.1**) and ethylene in $C_6D_6$.

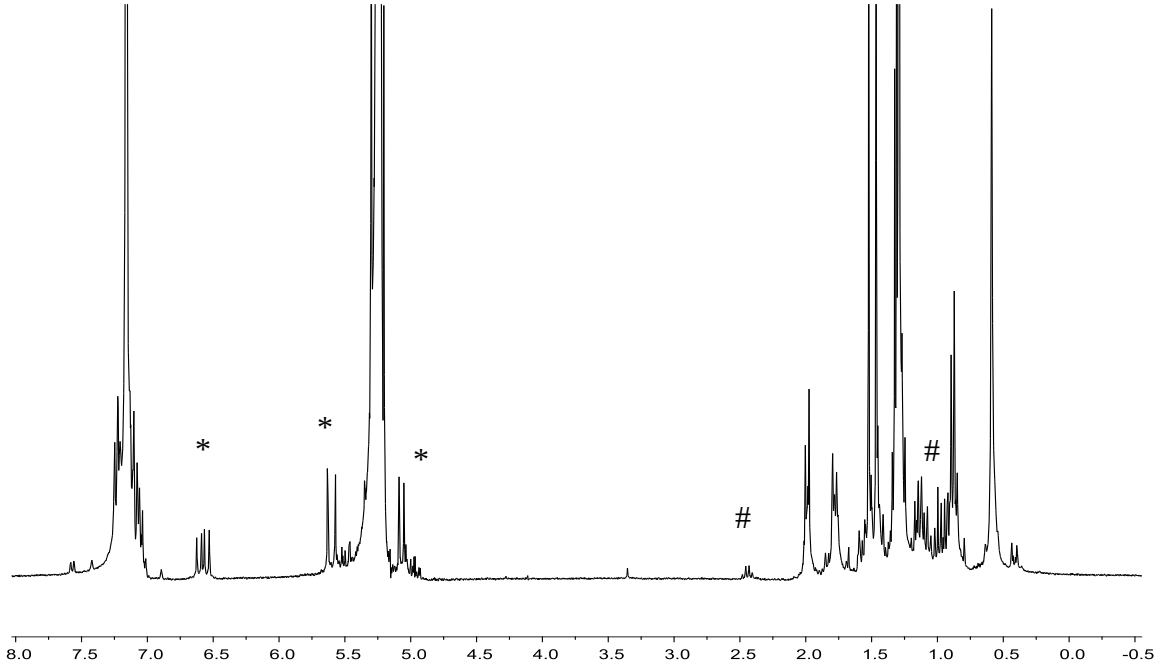


**Figure 3.2.** $^1$H NMR from the reaction of complex **3.1** and ethylene in $C_6D_6$ after 1 h at room temperature. Selected styrene (*) and ethylbenzene (#) resonances denoted.

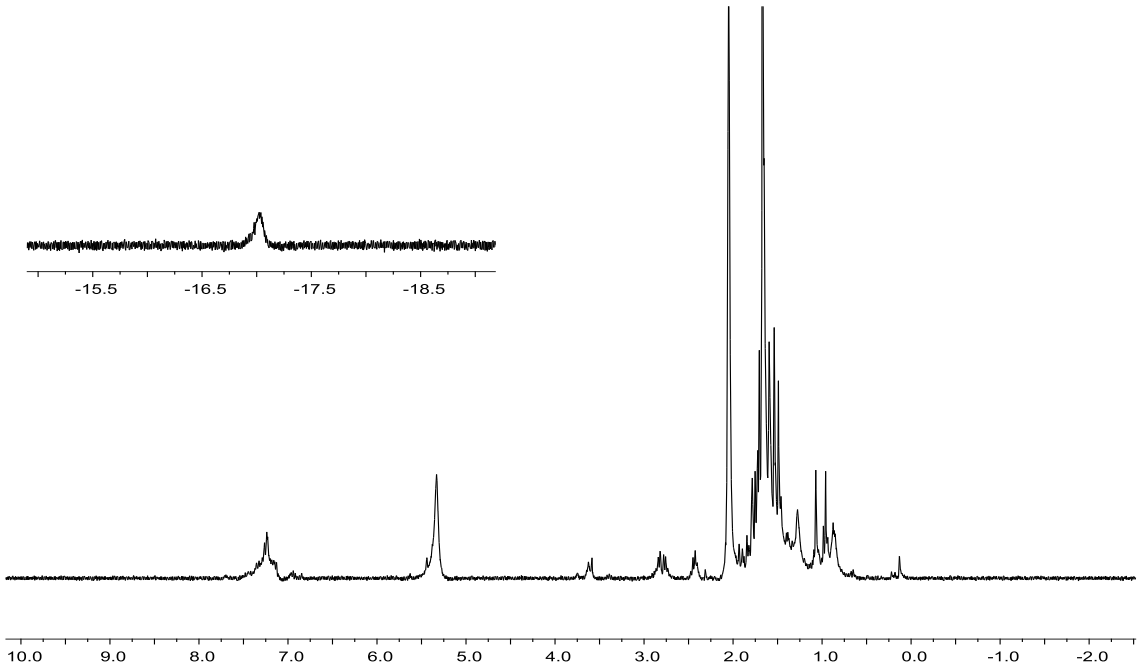


**Figure 3.3.** Crude $^{1}$H NMR spectrum of Fe–H complex from the reaction of Cp*Fe(CO)(NCMe)Ph (**3.1**) and ethylene in acetone-$d_6$. Inset is likely hydride resonance.

Based on these data, we suspect that β-hydride elimination to give an Fe–H complex is competitive with benzene C–H activation (Scheme 3.7). Irreversible β-hydride elimination to give an Fe–H complex likely removes Fe from the catalytic cycle. For example, benzene C–H activation across an Fe–H bond to give $H_2$ is thermodynamically unfavorable due to the strong Fe–H bond.[3, 36] In the presence of an oxidant, it is conceivable to make the styrene product catalytic (Scheme 3.8). Since benzene C–H activation by an Fe–H is thermodynamically unfavorable, an oxidant (e.g., $CuX_2$) can serve to oxidize the Fe–H to Fe–X and ½ $H_2$, in which the Fe–X can mediate C–H activation to regenerate the Fe–Ph complex. Some preliminary attempts were made (e.g., $IO_4^-$, Cu(II)), but these reactions gave diminished yields of styrene compared to the reactions without oxidant, which might suggest that the reaction of **3.1** and oxidant results in decomposition. Thus, these reactions were not pursued further.

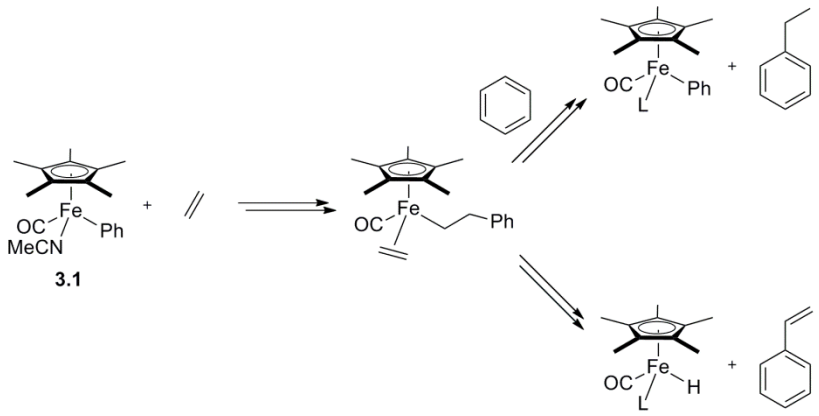


**Scheme 3.7.** Competitive benzene C–H activation and β-hydride elimination following ethylene insertion.

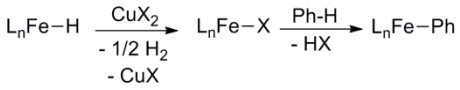


**Scheme 3.8.** Possible mechanism to regenerate Fe–Ph from Fe–H using a Cu(II) oxidant.

We explored the hydrophenylation of a few additional olefins to determine if improved selectivity and activity of Cp*Fe(CO)(NCMe)Ph (**3.1**) could be observed with different substrates. Therefore, the hydrophenylation of methyl acrylate, methyl methacrylate, and 1-pentene was attempted (Scheme 3.9). No efforts were made to optimize yields because in all cases stoichiometric amounts of products were observed. The hydrophenylation of methyl methacrylate was performed since this olefin would not have β-hydrogens if the expected 2,1-insertion occurred. Indeed, ~0.5 TO of the saturated product was observed. Methyl acrylate gave 0.9 TO of the unsaturated product with trace of the saturated product. For 1-pentene, we observed 0.4 TO of 1-phenylpentane as well as several isomers of the unsaturated product. Interestingly, no 2-phenylpentane was observed suggesting preference for the anti-Markovnikov product. The selectivity for the anti-Markovnikov product is encouraging since this product is not accessible using

Friedel-Crafts catalysis.[2, 24, 37, 38] However, with the low yields observed it is difficult to draw any definitive conclusions.

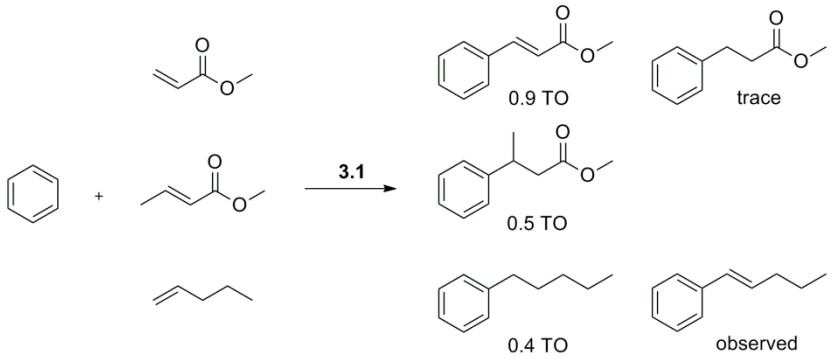


**Scheme 3.9.** Hydrophenylation of methyl acrylate, methyl methacrylate, and 1-pentene using Cp*Fe(CO)(NCMe)Ph (**3.1**).

### 3.2.2 Attempted Ethylene Hydroarylation with Furan and Thiophene

Since it was determined in Chapter 2 that the C–H activation of furan and thiophene have lower activation barriers than the C–H activation of benzene, we considered whether performing ethylene hydroarylation with heteroaromatics would make C–H activation more competitive with β-hydride elimination and thus lead to successful catalysis. Furan and thiophene are both present in many biologically relevant chemicals and,[39, 40] in the case of thiophene, also in materials.[19, 41, 42] Thus, an atom-economical way to form new C–C bonds with these substrates is an important area of study.

For ethylene hydroarylation with furan and thiophene, Cp*Fe(CO)(NCMe)Ar (Ar = 2-furyl or 2-thienyl) was generated in situ by stirring Cp*Fe(CO)(NCMe)Ph (**3.1**) with excess furan or thiophene and then treated with ethylene. The hydroarylation of ethylene using furan at room temperature with 25 psi of $C_2H_4$ gave no functionalized product as observed by GC/MS. Later, it was discovered that increasing the temperature to 120 °C

and the pressure to 100 psi resulted in ~0.3 TO of 2-ethylfuran (Scheme 3.10). The low yield of 2-ethylfuran was surprising at first. Therefore, we examined this reaction more closely.

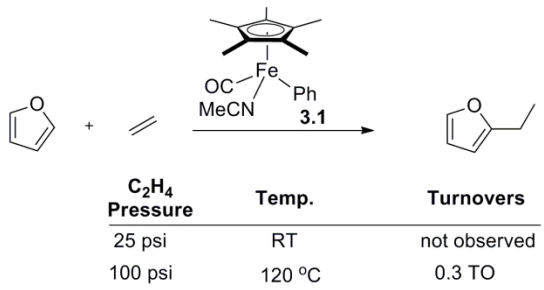


| $C_2H_4$ Pressure | Temp. | Turnovers |
|---|---|---|
| 25 psi | RT | not observed |
| 100 psi | 120 °C | 0.3 TO |

**Scheme 3.10.** Attempted ethylene hydroarylation using furan by Cp*Fe(CO)(NCMe)Ph (**3.1**).

An NMR scale experiment was performed that involved the reaction of Cp*Fe(CO)(NCMe)(2-furyl) (**3.2**) with ethylene (25 psi), which resulted in an immediate reaction to generate free NCMe (Scheme 3.11). Based on the $^1$H NMR data (see below), we suspect the new complex is Cp*Fe(CO)($\eta^2$-$C_2H_4$)(2-furyl) (**3.3**). Thermolysis of this solution at 60 °C eventually led to broadening of the $^1$H NMR resonances assignable to **3.3**, suggesting complex decomposition. There is no evidence for 2-ethylfuran formation. Therefore, it is likely that poor catalytic turnover of 2-ethylfuran is the result of very slow ethylene insertion (Scheme 3.11). The Fe–furyl bond of **3.2** is probably stronger than the Fe–Ph bond of **3.1**. The Fe–furyl bond may be stronger due to the more polar covalent bonding in the Fe–furyl bond in **3.2**.[43] Additionally, Prof. Daniel Ess (BYU) calculated the bond dissociation energies for the Fe–Ph bond of **3.1** and Fe–furyl bond of **3.2** to be 50.9 kcal/mol and 65.6 kcal/mol, respectively. As a result, there may be an increased enthalpic barrier for olefin insertion into the Fe–furyl bond versus the Fe–Ph bond.

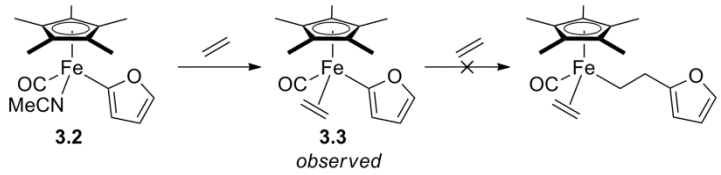


**Scheme 3.11.** Reaction of Cp*Fe(CO)(NCMe)(2-furyl) (**3.2**) results in no observed ethylene insertion.

In order to confirm the identity of the suspected Cp*Fe(CO)($\eta^2$-$C_2H_4$)(2-furyl) (**3.3**) complex, some attempts were made to isolate it. After stirring a THF solution of complex **3.2** (generated in situ) under ethylene pressure (40 - 70 psi) for 1-2 h, the volatiles were removed in vacuo to provide a crude $^1$H NMR spectrum of **3.3** as shown in Figure 3.4. One interesting feature of the $^1$H NMR spectrum of **3.3** is that one of the β protons on the 2-furyl ligand resonates upfield of its expected position at ~3.2 ppm. The reaction was repeated using furan-$d_4$ to prepare complex **3.2**, which confirmed that the resonance at 3.2 ppm is due to a furyl proton (Figure 3.5). The coordinated ethylene peak shows up as doublet (one resonance observed likely due to coincidental overlap), which suggests rapid rotation about the Fe–ethylene bond. To help confirm that a 2-furyl ligand was on the Fe complex, HCl was added to a $C_6D_6$ solution of complex **3.3**. Rather than observing furan, 2-ethylfuran was observed by $^1$H NMR spectroscopy and GC/MS (Scheme 3.12). Thus, the expected protonation of the 2-furyl ligand in **3.3** did not occur. Tentatively, we believe that protonation involves oxidation of Fe(II) to Fe(III) or Fe(IV), which facilitates insertion (Scheme 3.12).

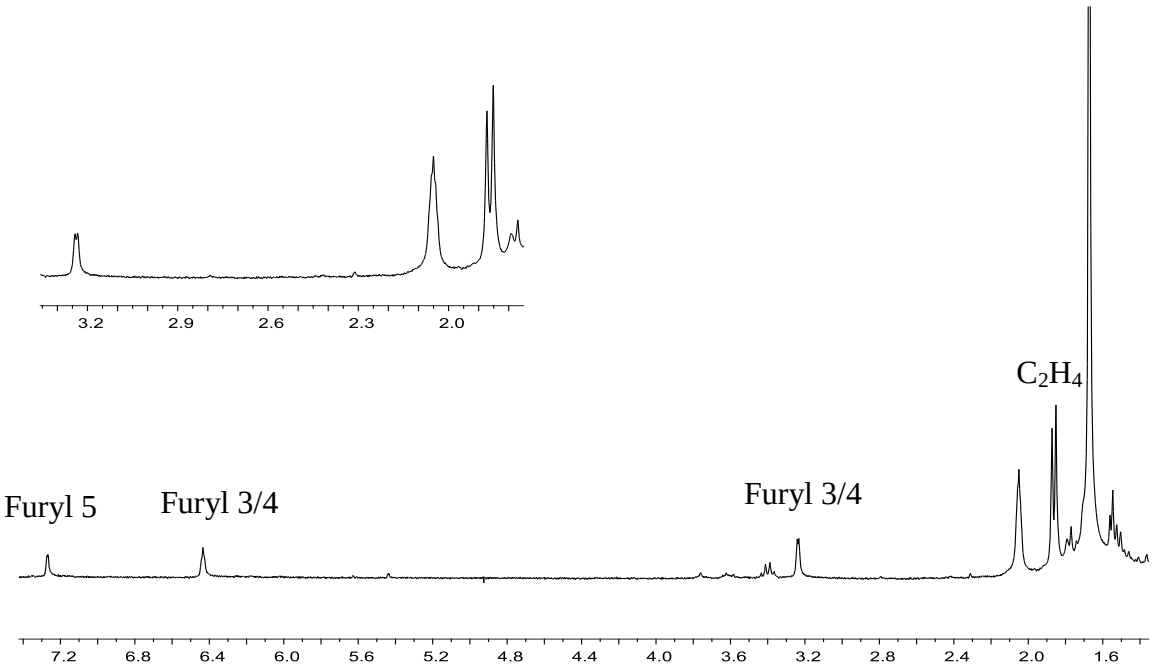


**Figure 3.4.** $^{1}$H NMR spectrum of Cp*Fe(CO)($\eta^2$-$C_2H_4$)(2-furyl) (**3.3**) in acetone-$d_6$ with key resonances assigned.

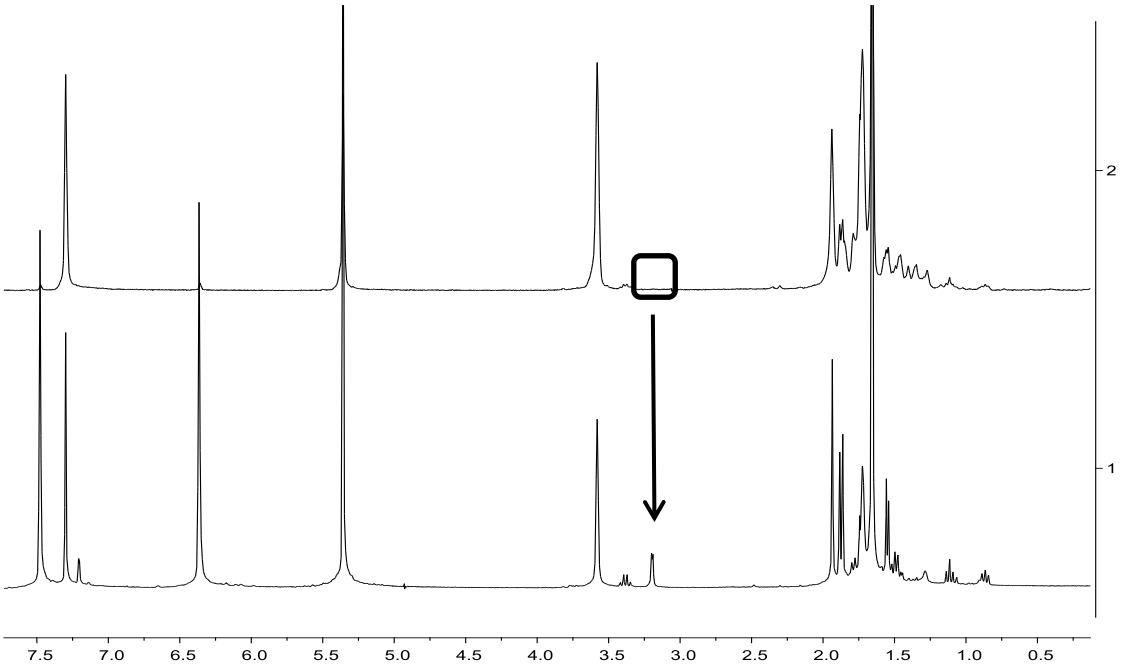

**Figure 3.5.** $^{1}$H NMR spectra of complex **3.3**-$d_3$ (top) and complex **3.3** (bottom) generated in situ in THF-$d_8$.

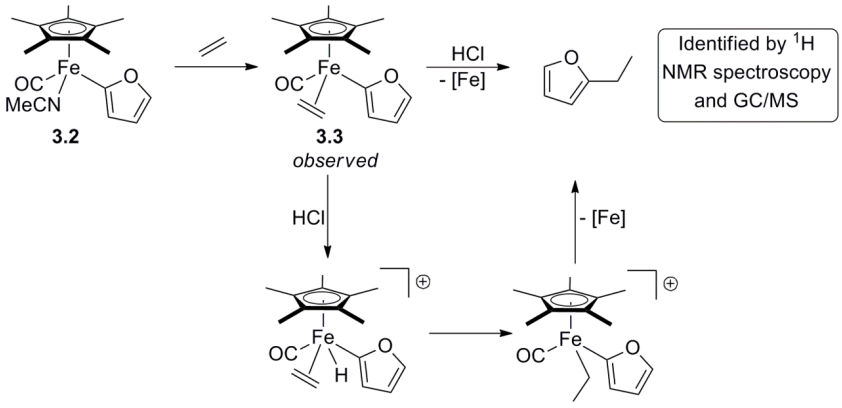


**Scheme 3.12.** Observation of 2-ethylfuran upon protonation of complex **3.3**.

Similar to the reactivity of furan and ethylene, we observe no evidence for 2-ethylthiophene formation from the reaction of thiophene and ethylene mediated by **3.1**. The reaction of Cp*Fe(CO)(NCMe)Ph (**3.1**) with thiophene followed by $C_2H_4$ (50 psi) in THF for 1 h at room temperature gave a $^1$H NMR spectrum (Scheme 3.13, Figure 3.6) with similar features as that of complex **3.3**. Thus, by analogy, we propose that the product is Cp*Fe(CO)($\eta^2$-$C_2H_4$)(2-thienyl) (**3.4**).

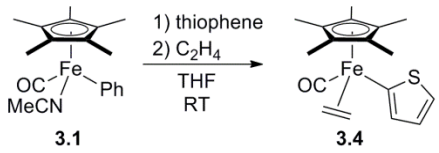


**Scheme 3.13.** Reaction of Cp*Fe(CO)(NCMe)Ph (**3.1**) with thiophene then ethylene.

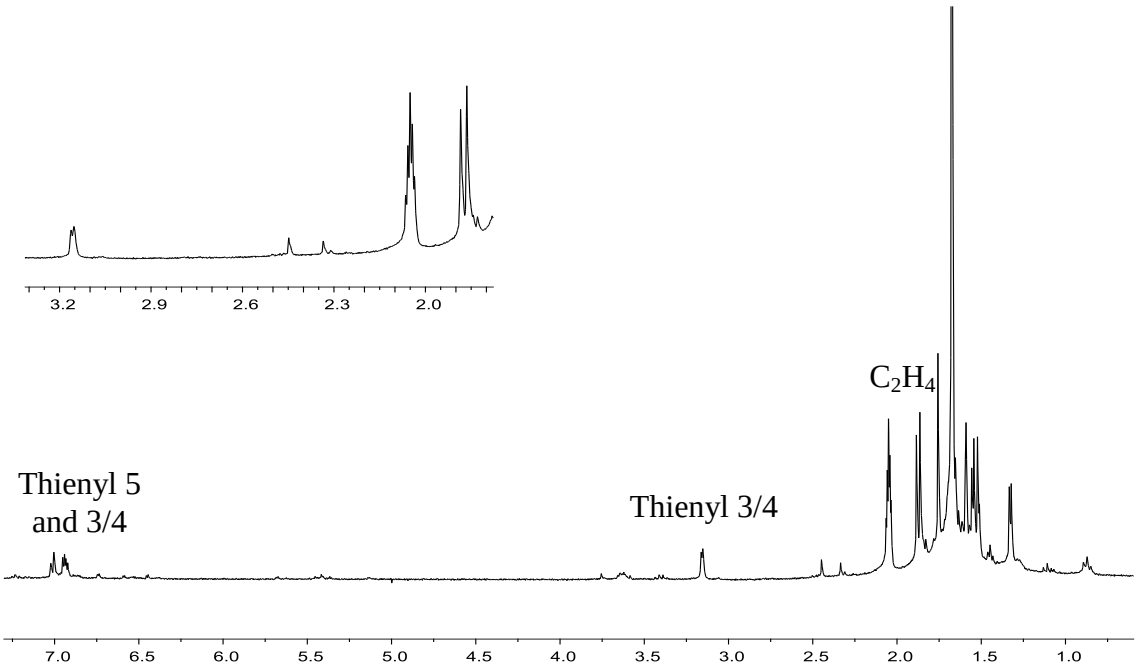


**Figure 3.6.** $^1$H NMR spectrum of Cp*Fe(CO)($\eta^2$-$C_2H_4$)(2-thienyl) (**3.4**) in acetone-$d_6$ with assignments of key resonances.

The results with the heteroaromatics are actually relatively consistent with what was observed for catalytic ethylene hydroarylation using TpRu(CO)(NCMe)Ph.[44] For the TpRu(CO)(NCMe)Ph catalyst, catalytic ethylene hydroarylation using furan produced only 17 TO of 2-ethylfuran using 40 psi of ethylene. In contrast, using 10 psi ethylene gave only 9 TO of 2-ethylfuran. For ethylene hydrophenylation catalyzed by TpRu(CO)(NCMe)Ph, an inverse dependence on catalytic activity was observed with increased ethylene pressures.[44] While there is no mechanistic analysis for the hydroarylation using furan catalyzed by TpRu(CO)(NCMe)Ph, it may very well be that the rate-determining step switches from C–H activation to olefin insertion when heteroaromatics are used in place of benzene. As mentioned above, this is probably related to the increased bond energy of M–heteroaryl bonds compared to M–Ph bonds.

### 3.2.3 Attempted Hydrophenylation of Internal Alkynes

Due to many of the challenges associated with developing catalytic reactions using Cp*Fe(CO)(NCMe)Ph (**3.1**) and olefins, we pursued the hydrophenylation of internal alkynes. Because β-hydride elimination was observed for the reactions of olefins and benzene using Cp*Fe(CO)(NCMe)Ph (**3.1**), it appeared that internal alkynes may be a suitable substrate to avoid this undesired reactivity. After insertion of the alkyne into the Fe–Ph bond, no β-hydrogens would be present and should therefore lead to benzene C–H activation to release the desired vinyl arene (Scheme 3.14).

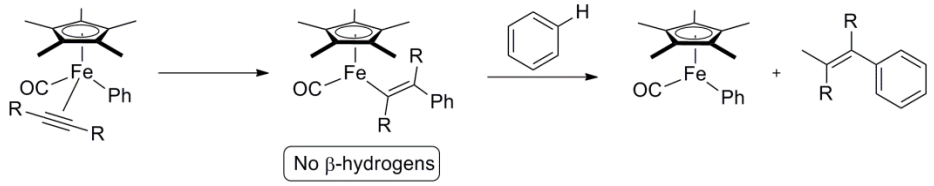


**Scheme 3.14.** No β-hydrogens after alkyne insertion is rationale for using internal alkynes as unsaturated substrate for hydroarylation.

The hydrophenylation reactions of 2-butyne and bis(TMS)acetylene (TMS = trimethylsilyl) were examined at room temperature and 100 °C (Scheme 3.15). In both cases, no functionalized arenes were observed by GC/MS. One observation was that the reaction solutions remained homogeneous throughout the reaction, even at 100 °C, which is atypical for other reactions with **3.1**. We initially considered that alkyne insertion might not be occurring, although we anticipated that it would be facile with complex **3.1**.

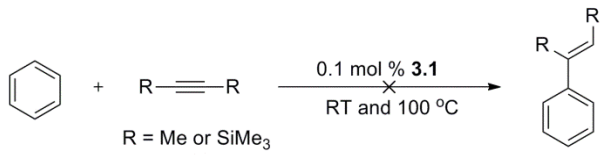


**Scheme 3.15.** Attempted hydrophenylation of 2-butyne and bis(TMS)acetylene by Cp*Fe(CO)(NCMe)Ph (**3.1**).

### 3.2.4 Stoichiometric Reactions of Cp*Fe(CO)(NCMe)Ph (3.1) and Internal Alkynes

#### 3.2.4.1 Reaction of Cp*Fe(CO)(NCMe)Ph (3.1) with 2-Butyne

In order to understand the lack of catalytic activity in the attempted hydrophenylation of alkynes, Cp*Fe(CO)(NCMe)Ph (**3.1**) was treated with excess 2-butyne in THF at room temperature (Scheme 3.16). Upon addition of the alkyne, an immediate color change from red to deep purple was observed. Monitoring the reaction by $^1$H NMR spectroscopy revealed the complete conversion of starting material to a new product with concomitant release of NCMe. The absence of any terminal or bridging carbonyl stretches in the infrared spectrum of the product indicates that the CO ligand was consumed in the reaction. After work-up, the complex Cp*Fe($\eta^5$-1-hydroxy-2,3-dimethylindenyl) (**3.5**) was isolated in 60% yield as a purple crystalline solid. The aromatic region of the $^1$H NMR spectrum (acetone-$d_6$) of complex **3.5** exhibits a pair of doublets at 7.43 and 7.23 ppm as well as a complex multiplet at 6.90 ppm that integrates for two protons, consistent with the unbound portion of the indenyl fragment. The hydroxyl proton is visible as a sharp singlet at 6.33 ppm (Figure 3.7). The methyl resonances for the indenyl fragment are broad, but the line width can vary from sample to sample. It is unclear why this broadening is observed, although it may be related to a fluctional process.

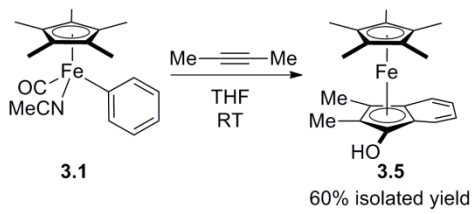


**Scheme 3.16.** The reaction of Cp*Fe(CO)(NCMe)Ph (**3.1**) to give Cp*Fe($\eta^5$-1-hydroxy-2,3-dimethylindenyl) (**3.5**).

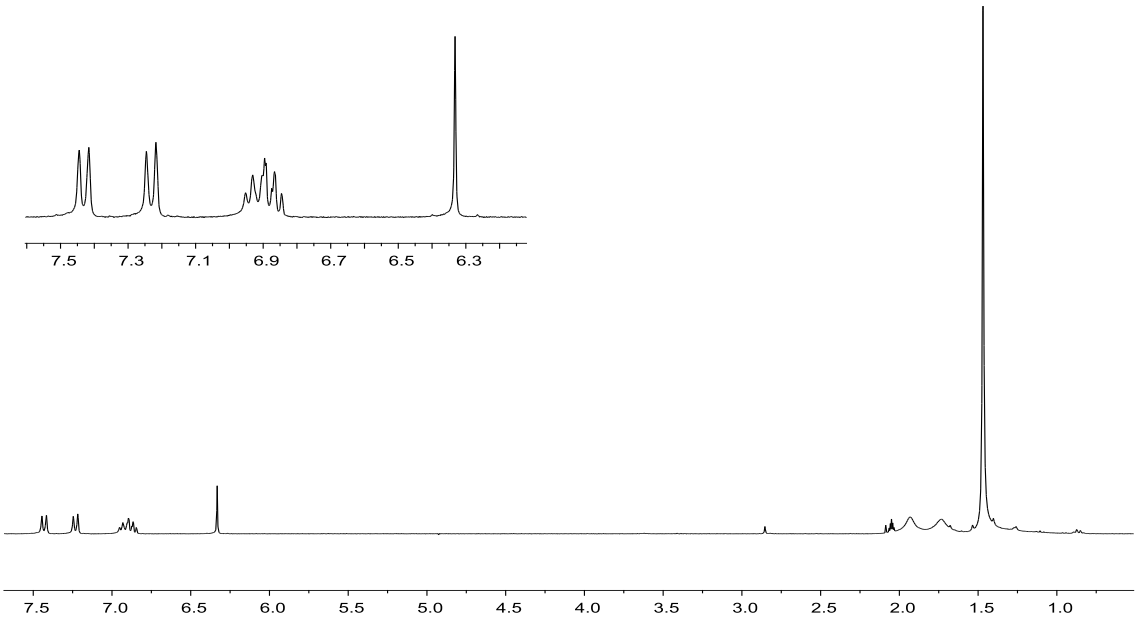


**Figure 3.7.** $^{1}$H NMR spectrum of Cp*Fe($\eta^{5}$-1-hydroxy-2,3-dimethylindenyl) (**3.5**) in acetone-$d_6$.

A crystal suitable for a single crystal X-ray diffraction study was grown from the slow evaporation of a saturated pentane solution of **3.5** (Figure 3.8). To the best of our knowledge, complex **3.5** is only the second example of a structurally characterized transition metal ligated by a hydroxyindenyl ligand. Previously, Jones and co-workers isolated and structurally characterized a related Ru sandwich compound from their studies on carbene migratory insertion.[45] Notably, the –OH of complex **3.5**, where the hydrogen placement has been calculated, is in the α-position relative to the indenyl ring junction while the –OH group is in the β-position for the previously reported Ru complex (Figure 3.9). The average Fe–indenyl bond distance is ~2.07 Å, which is consistent with other structurally characterized Fe–indenyl fragments.[46-48] The C22–O2 bond length is 1.374(2) Å, which is consistent with C–O bond lengths for other hydroxycyclopentadienyl and hydroxyindenyl ligands.[45, 49, 50]

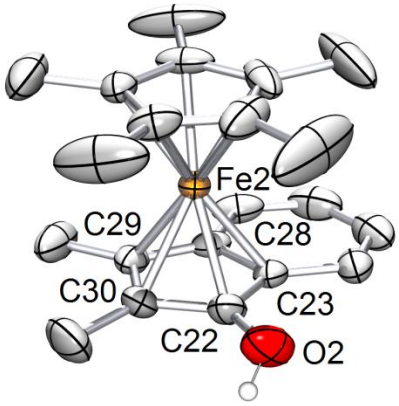


**Figure 3.8.** ORTEP of Cp*Fe($\eta^5$-1-hydroxy-2,3-dimethylindenyl) (**3.5**) (50% probability ellipsoids). Most H atoms omitted and one independent molecule shown for clarity. Selected bond angles (Å): Fe2–C22 2.058(2); Fe2–C23 2.088(2); Fe2–C28 2.070(2); Fe2–C29 2.051(2); Fe2–C30 2.067(2); C22–O2 1.374(2). Selected bond angles (deg): O2–C22–C23 122.8(2); O2–C22–C30 128.1(2).

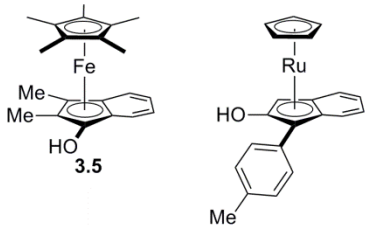


**Figure 3.9.** Comparison of connectivity between two known structurally characterized hydroxyindenyl complexes.

The formation of the hydroxyindenyl ligand from the attempted hydrophenylation of 2-butyne is intriguing. First, the hydroxyindenyl ligand resembles a class of molecules known as indenols (Figure 3.10). Indenols have been shown to have analgesic and anti-inflammatory properties,[51, 52] and they are intermediates in the synthesis of compounds with insecticidal properties.[53, 54] As a result of these important applications, a survey of the literature reveals interest among the synthetic chemistry community in developing new methods for the preparation of these compounds. Among the variety of synthetic strategies, transition metal mediated reactions have shown promise, with many

methodologies involving the carbocyclization of aryl ketones and alkynes (Scheme 3.17).[55-64] One strategy involves the pre-functionalization of an aryl ketone with a halide or boronic acid, and catalytic systems based on palladium, cobalt, and nickel have been reported.[58-63] The groups of Cheng and Glorious have independently developed Rh catalysts, and Jeganmohan has developed a Ru catalyst for a reaction that does not require pre-functionalization but rather proceeds via aromatic C–H activation.[55-57]

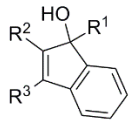


**Figure 3.10.** Structure of substituted indenol.

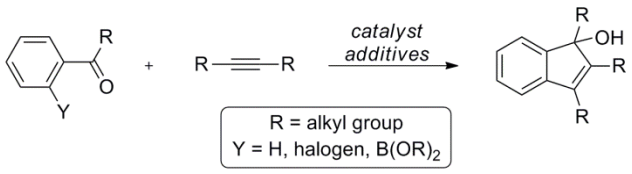


**Scheme 3.17.** General transition metal catalyzed carbocyclization of aryl ketones and alkynes.

The reason that the formation of the hydroxyidnenyl ligand in complex **3.5** is relevant to indenol synthesis is that it can be thought of as the coupling of a phenyl ligand, a CO ligand, and 2-butyne. While it is outside the scope of this Dissertation, one may consider a strategy for indenol synthesis that involves the coupling of benzene, CO, and an alkyne (Scheme 3.18).

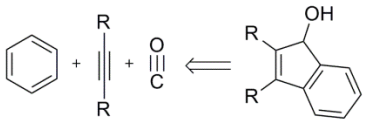


**Scheme 3.18.** Retrosynthesis of indenols from benzene, CO, and an alkyne.

More relevant to this body of work, the formation of the hydroxyindenyl ligand reveals a potential flaw in the design of **3.1** as a catalyst for alkyne hydroarylation. During the formation of the hydroxyindenyl ligand, CO insertion occurs. Thus, in the case of the hydrophenylation of 2-butyne, CO is not simply an ancillary ligand and results in undesired reactivity.

While the mechanism of the formation of the hydroxyindenyl ligand is not clear, it is worth considering potential mechanisms. The overall transformation bares similarities to the work of Butler and co-workers on indenone synthesis from $CpFe(CO)_2Ph$ and alkynes and Allison and co-workers' study of electrocyclic ring closures in $CpFe(CO)_2(\eta^1$-1,3-butadienyl) complexes to give hydroxyferrocenes (Scheme 3.19).[65-67] A possible mechanism for the transformation of Cp*Fe(CO)(NCMe)Ph (**3.1**) and 2-butyne to Cp*Fe($\eta^5$-1-hydroxy-2,3-dimethylindenyl) (**3.5**) is shown in Scheme 3.20. After initial ligand exchange between NCMe and 2-butyne, the alkyne likely inserts into the Fe–Ph bond to give a vinyl intermediate. For simplicity, a *cis* insertion is shown, which has been demonstrated to be more likely based on experimental and theoretical predictions.[3, 68] We have previously shown that Cp*Fe(CO)(NCMe)Ph (**3.1**) performs facile aromatic C–H activation, thus cyclometalation via intramolecular aromatic C–H activation appears viable.[1] Subsequent CO insertion would give a pentadienoyl fragment. Allison and co-workers have been able to observe a similar intermediate in their work.[67] From the pentadienoyl intermediate, electrocyclic ring closure and subsequent tautomerization would give complex **3.5**.

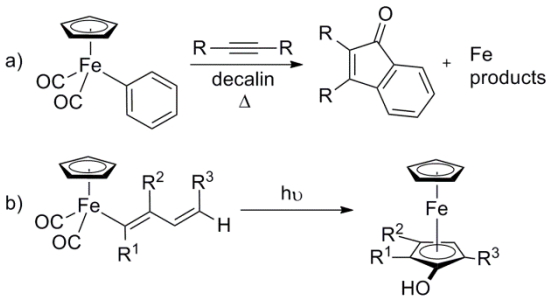


**Scheme 3.19.** Formation of indenones and hydroxycyclopentadienyl ligands mediated by CpFe complexes.[65-67]

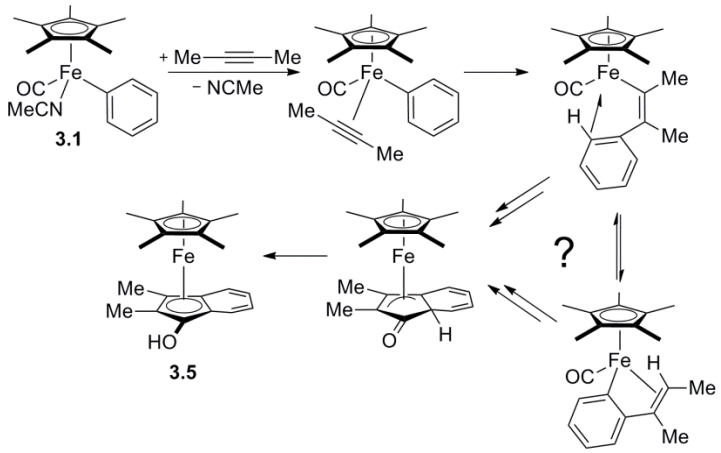


**Scheme 3.20.** Possible mechanism for the formation of Cp*Fe($\eta^5$-1-hydroxy-2,3-dimethylindenyl) (**3.5**) from Cp*Fe(CO)(NCMe)Ph (**3.1**) and 2-butyne.

While the mechanism shown in Scheme 3.17 is possible, the intimate details following alkyne insertion in the mechanism giving the hydroxyindenyl ligand cannot be known due to the lack of experimental data. Other mechanisms that are also plausible include a concerted deprotonation-metalation to give an Fe(IV) intermediate from which the CO ligand can insert into either the Fe–phenyl or Fe–vinyl bond. Here, a reductive coupling may occur to form the five-membered ring portion of the indenyl ligand. It is also possible that in the mechanism shown in Scheme 3.20, the CO inserts into the Fe–vinyl bond prior to the proposed cyclometalation step. A recent publication using a Ru(II)

complex demonstrated the feasibility that our mechanism involves C–H activation by 1,4-migration (Scheme 3.21).[69]

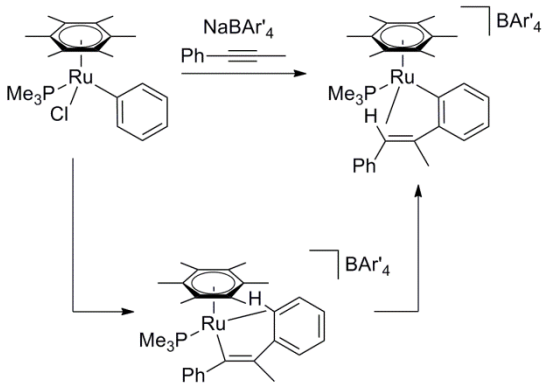


**Scheme 3.21.** Ru(II) 1,4-migration following alkyne insertion into Ru–Ph bond.

### 3.2.4.2 Reaction of Cp*Fe(CO)(NCMe)Ph (3.1) with Bis(TMS)acetylene

Knowing that attempted catalysis with 2-butyne led to the formation of a hydroxyindenyl ligand, we investigated the reaction of **3.1** with bis(TMS)acetylene. Treating complex **3.1** with excess bis(TMS)acetylene led to slow conversion to a new species at room temperature. Using an elevated temperature (60 °C) allowed for the reaction to proceed to completion within 4 h (Scheme 3.22). Contrary to the reaction with 2-butyne, this reaction turned from red-orange to dark yellow. Examining the infrared spectrum revealed the persistence of a terminal CO stretching frequency at 1938 $cm^{-1}$, suggesting a reaction pathway for bis(TMS)acetylene that is distinct from that of 2-butyne. The $\nu_{CO}$ of the product is ~30 $cm^{-1}$ greater in energy than the starting complex **1**, suggesting a less π-basic Fe center for the product. After work-up, the vinylidene complex Cp*Fe(CO)(TMS)(=C=C(TMS)Ph) (**3.6**) was isolated in 50% yield. Resonances at 333.1 ppm and 120.3 ppm in the $^{13}C$ NMR spectrum (THF-$d_8$) are assigned to the $C_\alpha$ and the $C_\beta$ of the vinylidene, respectively (Figure 3.11). The $^{1}H$ NMR spectrum has a

triplet at 7.26 ppm and two overlapping signals at 7.11 ppm for the monosubstituted phenyl ring and three singlets upfield at 1.88 ppm, 0.17 ppm, and 0.12 ppm for the Cp* methyl groups, the vinylidene TMS, and the Fe–TMS, respectively. The peak for the Fe–TMS group is somewhat broad, which may be a result of hindered rotation due to steric congestion about the metal center (Figure 3.12).

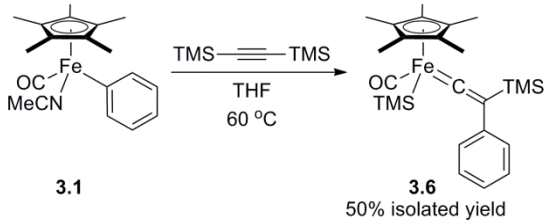


**Scheme 3.22.** Reaction of Cp*Fe(CO)(NCMe)Ph (**3.1**) and bis(TMS)acetylene to give Cp*Fe(CO)(TMS)(=C=C(TMS)Ph) (**3.6**).

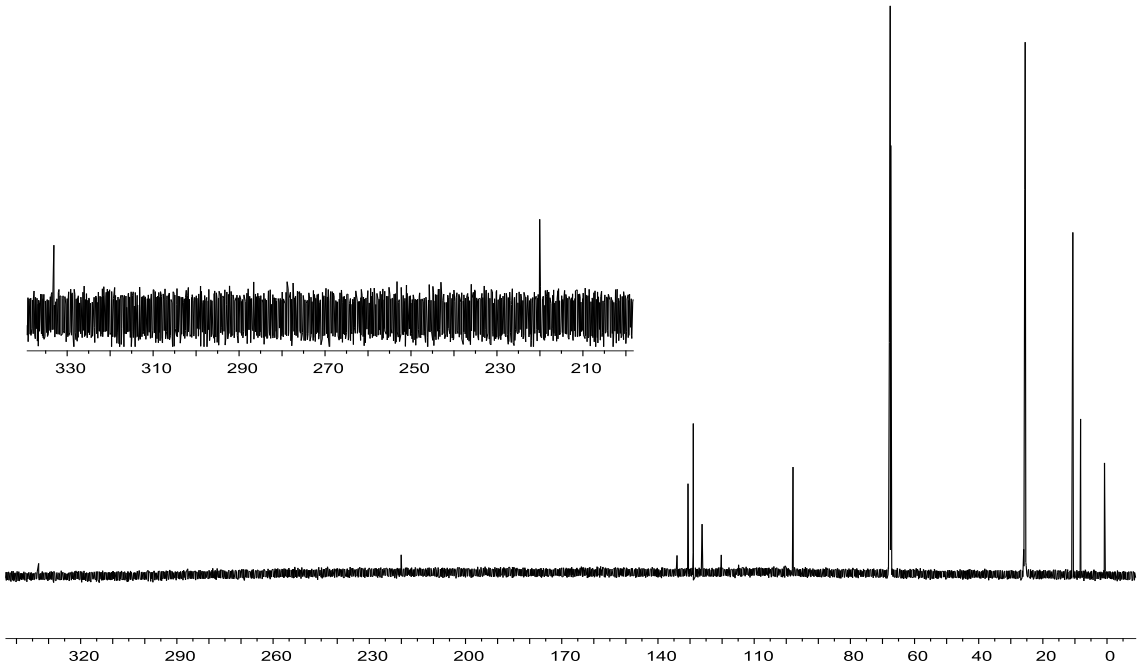


**Figure 3.11.** $^{13}$C NMR spectrum of Cp*Fe(CO)(TMS)(=C=C(TMS)Ph) (**3.6**) in THF-$d_8$.

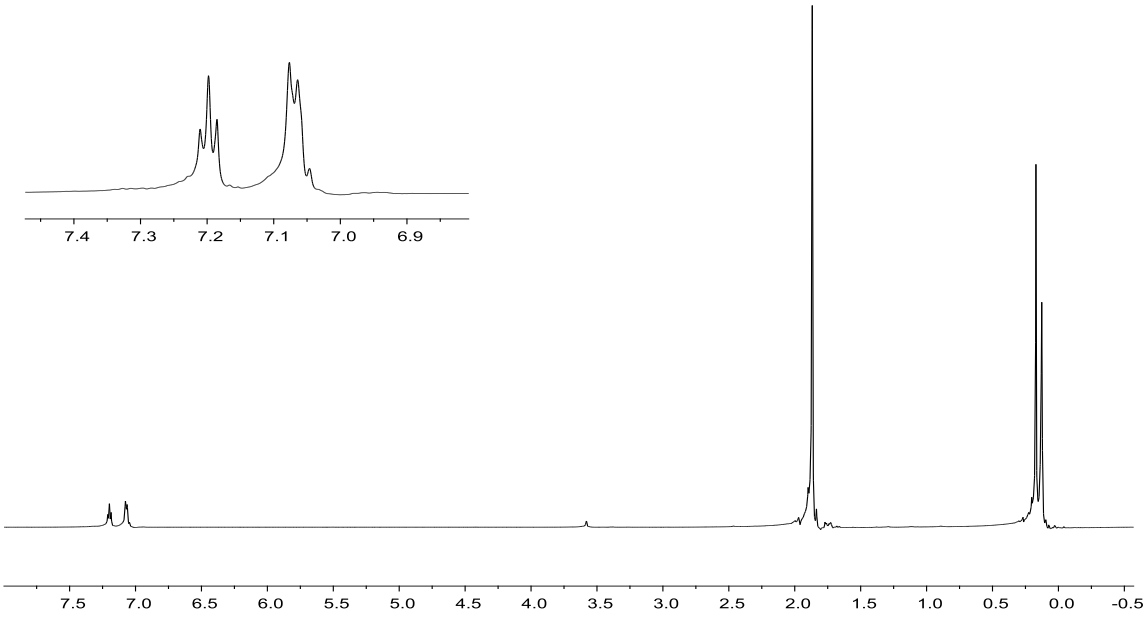


**Figure 3.12.** $^{1}$H NMR spectrum of Cp*Fe(CO)(TMS)(=C=C(TMS)Ph) (**3.6**) in THF-$d_8$.

Single crystals suitable for an X-ray diffraction study were grown from slow evaporation of a pentane solution of **3.6**, and the ORTEP diagram is shown in Figure 3.13. This structure represents the second example of a neutral half-sandwich Fe vinylidene.[70] The phenyl group is *syn* to the Fe–TMS group, possibly for steric reasons. The Fe–C1 bond length is 1.744(9) Å, and the C1–C2 bond length is 1.29(1) Å. The vinylidene is slightly distorted from linearity with the Fe–C1–C2 bond angle being 175.3(9)°, which is consistent with other vinylidene complexes.[70-72]

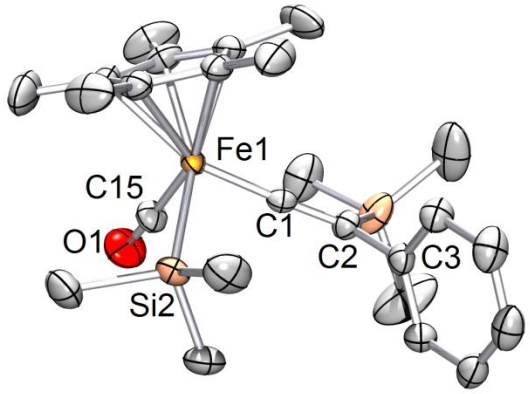


**Figure 3.13.** ORTEP drawing for Cp*Fe(CO)(TMS)(=C=C(TMS)Ph) (**3.6**) (50% probability ellipsoids). H atoms omitted and one independent molecule shown for clarity. Selected bond lengths (Å): Fe–C15 1.73(1); Fe–C1 1.744(9); Fe–Si2 2.330(3); C1–C2 1.29(1). Selected bond angles (deg): C1–Fe–Si2 84.1(3); C15–Fe–Si2 82.0(4); Fe–C1–C2 175.3(9).

Vinylidene complexes play an important role as both catalysts and intermediates in many chemical transformations. For example, vinylidene complexes have been used as alkyne polymerization, dimerization, and enyne metathesis catalysts among many other reactions.[73-75] The synthesis of half-sandwich iron vinylidene complexes generally occurs by treating an Fe–alkynyl complex with an electrophile, halide abstraction followed by coordination and re-arrangement of a terminal alkyne, or by treating an Fe–acyl complex with an electrophile.[75] Thus, the formation of neutral vinylidene **3.6** appears to occur via a mechanism distinct from the pathways reported for other cationic half-sandwich Fe vinylidenes.

A viable mechanism for the formation of vinylidene complex **3.6** is shown in Scheme 3.23. After ligand exchange with NCMe, the alkyne can insert into the Fe–Ph bond giving a vinyl intermediate. Subsequent β-TMS elimination would regenerate coordinated alkyne and give an Fe–TMS bond. The proposed β-TMS elimination is

known for several transition metals,[76-81] but β-TMS elimination from vinyl complexes is less common.[76] The newly formed alkyne ligand can rearrange to the final observed vinylidine via a net 1,2-TMS-shift.[75] It is also conceivable that vinylidene **3.6** could form directly by α-TMS elimination from the vinyl intermediate, although we are not aware of any reported examples of such a transformation. Additionally, the reactivity of complex **3.1** with alkynes bearing a single TMS substituent (see below) seems to preclude this mechanism as well.

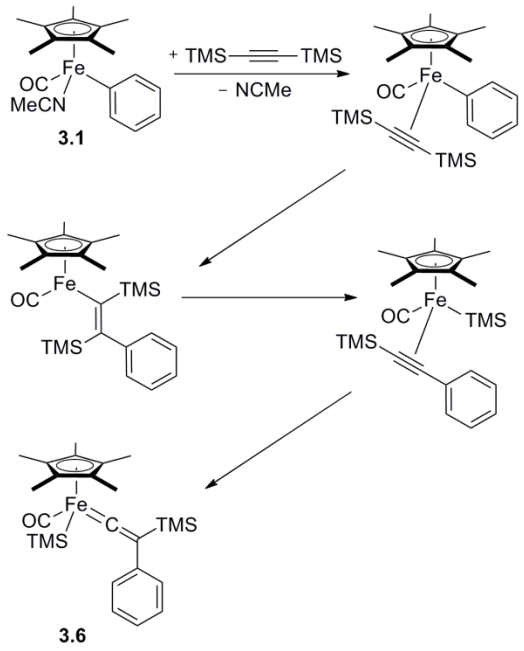


**Scheme 3.23.** Proposed mechanism for the transformation of Cp*Fe(CO)(NCMe)Ph (**3.1**) to Cp*Fe(CO)(TMS)(=C=C(TMS)Ph) (**3.6**).

The implication of this reactivity for catalytic hydroarylation is that the substrate scope could restricted from substrates that contain TMS groups. This potential functional group incompatibility is worth noting since substrates with $R_3Si$– substituents could be used in future transformations by the Hiyama reaction.[22]

### 3.2.4.3 Alkyne Substrate Scope

Having observed two different reaction pathways based on the identity of the alkyne and understanding the importance of these ligand moieties in synthetic chemistry (see above), we were inspired to investigate this reactivity more thoroughly by evaluating the substrate scope of the reaction. One question we had was whether the insertion reaction had any regioselectivity when using asymmetric alkynes. Additionally, we wondered whether the reactivity is compatible with carbonyl functionality. Finally, we wanted to investigate the reactivity patterns of alkynes containing a single TMS group to determine whether β-TMS elimination could be observe for these substrates.

To assess the regioselectivity of this reaction, we next turned our attention to asymmetric internal alkynes. The reaction of complex **3.1** with excess 1-phenylpropyne in THF at room temperature gave the expected hydroxyindenyl product **3.7a** in 49% isolated yield (Scheme 3.24). Monitoring the reaction by $^{1}$H NMR spectroscopy revealed the formation of one major product with a small amount (~15%) of a second product, presumably the regioisomer (**3.7b**) (Table 3.1). Upon work-up by washing with cold pentane or hexanes, a single isomer can be isolated; however, trace amounts (<5%) of the minor isomer may be observed depending on the reaction and the sensitivity of the NMR spectrometer. Consistent with the hydroxyindenyl ligand, the $^{1}$H NMR spectrum (acetone-$d_6$) of **3.7a** shows a pair of doublets at 7.58 ppm and 7.36 ppm (overlaps with a phenyl resonance) and a complex multiplet at 7.03 ppm that integrates for 2 protons. The hydroxyl proton resonates at 6.63 ppm. Additional aryl resonances are observed that correspond to the phenyl group that is appended to the indenyl ring (Figure 3.14).

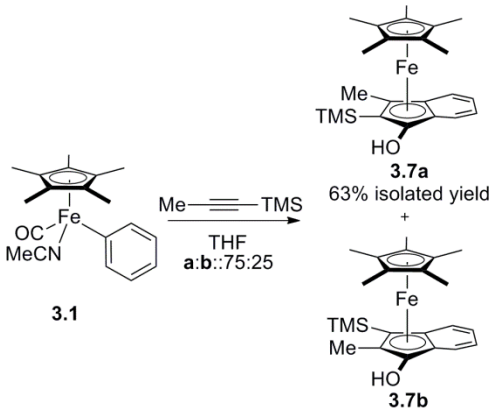


**Scheme 3.24.** Reaction of Cp*Fe(CO)(NCMe)Ph (**3.1**) and 1-phenylpropyne to give Cp*Fe($\eta^5$-1-hydroxy-2-methyl-3-phenylindenyl) (**3.7a**)

**Table 3.1.** Ratio of regioisomers observed in the crude reaction mixtures for the reactions of Cp*Fe(CO)(NCMe)Ph (**3.1**) with asymmetric alkynes.

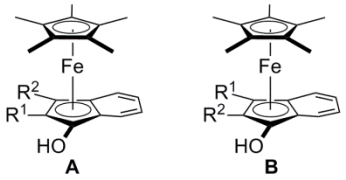


| # | $R^1$ | $R^2$ | **A** : **B** (%) |
|---|---|---|---|
| **3.7** | Ph | Me | 85 : 15 |
| **3.8** | $CO_2Me$ | Me | 80 : 20 |
| **3.9** | TMS | Me | 75 : 25 |
| **3.10** | TMS | Ph | 50 : 50 |

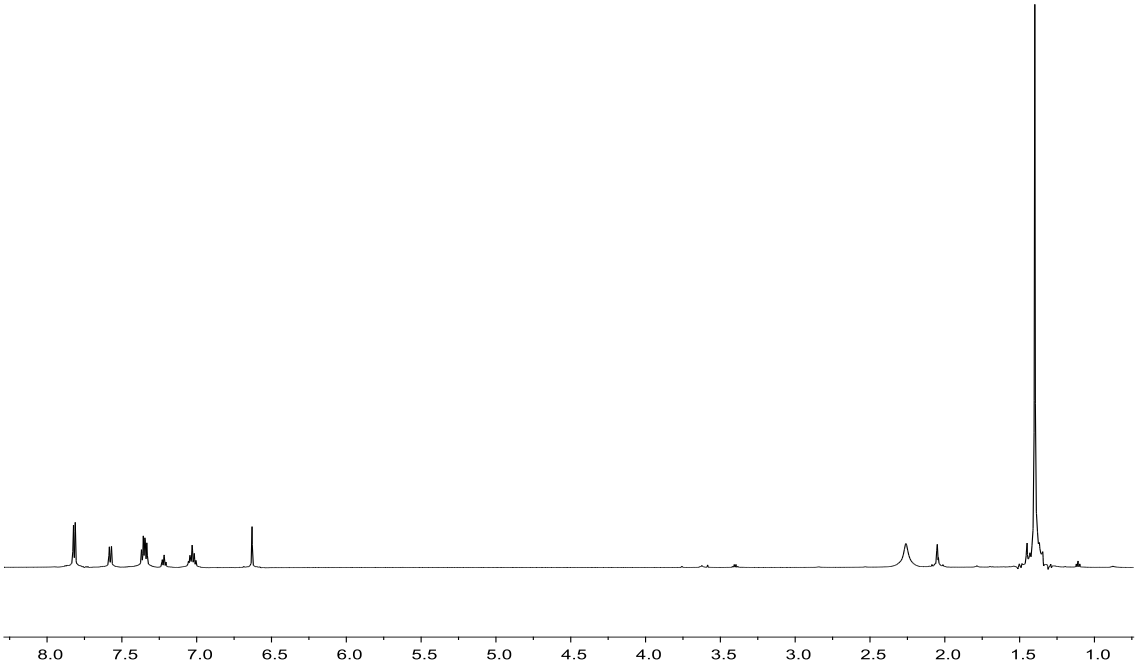


**Figure 3.14.** $^{1}$H NMR spectrum of Cp*Fe($\eta^{5}$-1-hydroxy-2-methyl-3-phenylindenyl) (**3.7a**) in acetone-$d_6$.

The cyclization reaction proceeds similarly with an alkynyl ester, demonstrating the reaction's compatibility with ester functionality. As in the synthesis of complex **3.7**, the reaction of **3.1** with excess methyl-2-butynoate gave the cyclized product **3.8a** in 49% isolated yield (Scheme 3.25). Like **3.7**, complex **3.8** forms as a regioisomeric mixture with the minor isomer (**3.8b**) constituting ~20% of the product ($^{1}$H NMR) (Table 3.1). The major isomer can be isolated after washing with cold pentane. Like complex **3.7**, at times <5% of the minor isomer may be detected depending on the reaction and spectrometer used in analysis. As expected, the $^{1}$H NMR spectrum (acetone-$d_6$) of the major isomer has two doublets at 7.39 ppm and 7.31 ppm with a multiplet at 7.06 ppm for the unbound ring and a singlet at 7.00 ppm for the hydroxyl proton (Figure 3.15).

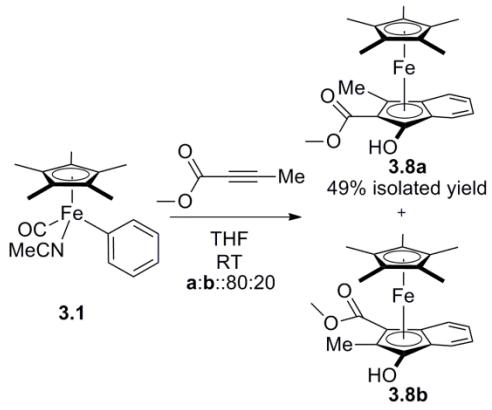


**Scheme 3.25.** Reaction of Cp*Fe(CO)(NCMe)Ph (**3.1**) to give Cp*Fe($\eta^5$-1-hydroxy-2-methyl-3-methylester-indenyl) (**3.8a**).

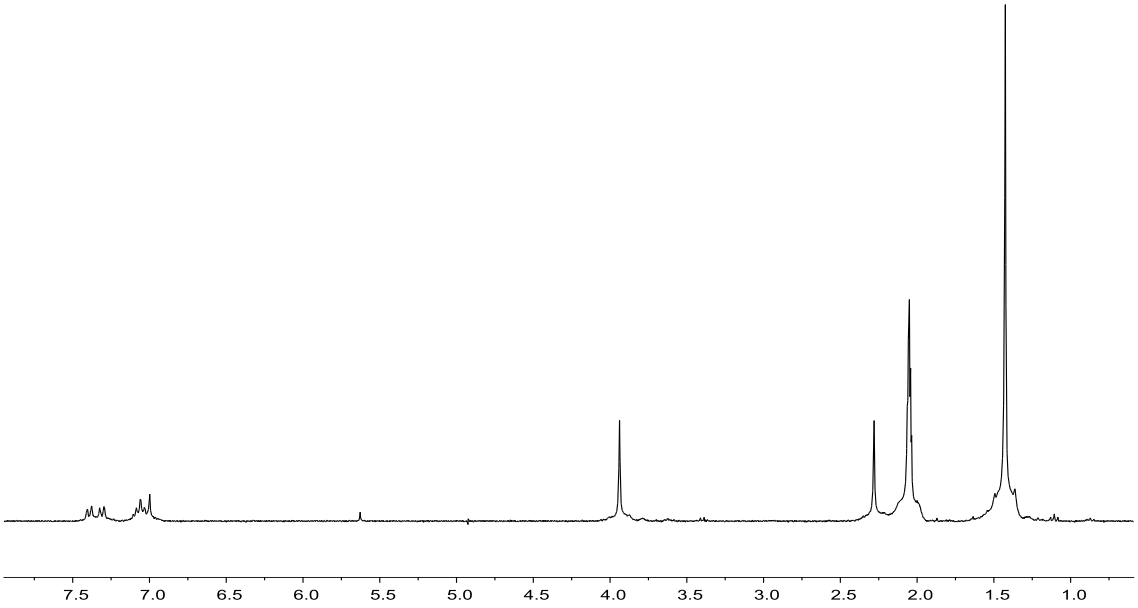


**Figure 3.15.** $^1$H NMR spectrum of Cp*Fe(η5-1-hydroxy-2-methyl-3-methylester-indenyl) (**3.8a**) in acetone-$d_6$.

In order to determine the regiochemistry of the major isomers for complexes **3.7** and **3.8**, two-dimensional NOESY spectra were obtained. Figure 3.16 shows representations of the cross peaks observed, while the two-dimensional spectra can be seen in Figures 3.24 and 3.25 for complexes **3.7** and **3.8**, respectively. For complex **3.7a**, cross peaks are observed between the *ortho* phenyl resonances and the resonance for the

hydroxyl proton as well as between the methyl resonance and a resonance associated with the unbound indenyl ring (Figure 3.17). This interaction suggests that the phenyl ring is proximal to the alcohol as shown in Figure 3.16. For complex **3.8a**, a cross peak was observed between the methyl group directly attached to the indenyl ligand and a proton on the unbound ring (Figure 3.18). No cross peaks were observed between the hydroxyl proton and the methyl group of the ester; however, that interaction may be too weak to be observed. Nonetheless, these data provide evidence that the ester functionality is adjacent to the alcohol group.

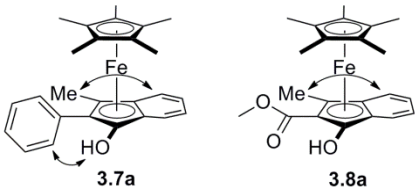


**Figure 3.16.** Representations showing important cross peaks from NOESY spectra of Cp*Fe(1-hydroxy-2-phenyl-3-methylindenyl) (**3.7a**) and Cp*Fe(1-hydroxy-2-methylester-3-methylindenyl) (**3.8a**).

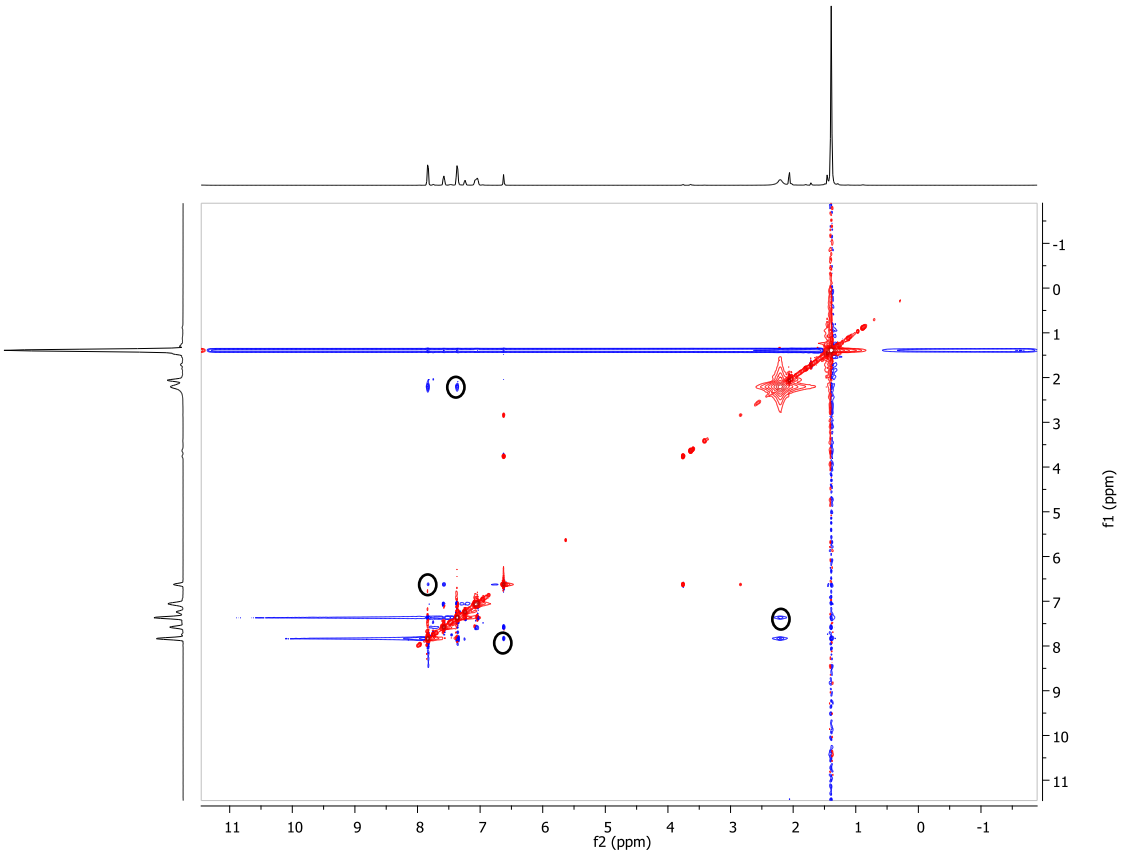


**Figure 3.17.** Two-dimensional NOESY spectrum for Cp*Fe(1-hydroxy-2-phenyl-3-methylindenyl) (**3.7a**) in acetone-$d_6$. Important cross peaks are circled.

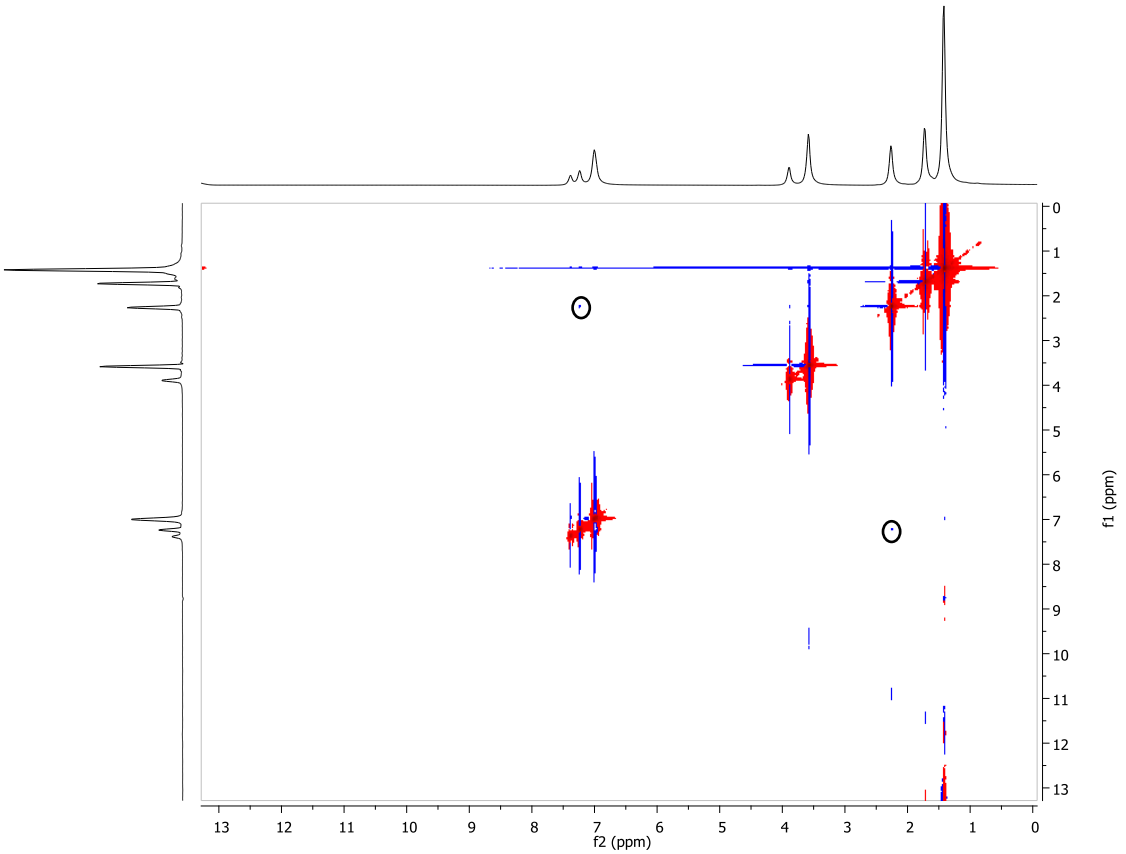


**Figure 3.18.** Two-dimensional NOESY spectrum for Cp*Fe(1-hydroxy-2-methylester-3-methylindenyl) (**3.8a**) in THF-$d_8$. Important cross peaks are circled.

Since the proposed mechanism for the formation of the vinylidene in complex **3.6** involves β-elimination of the TMS group from the alkyne insertion intermediate, we investigated the reactivity of **3.1** with other TMS-substituted alkynes. Treatment of **3.1** with 1-TMS-1-propyne in THF at room temperature gave a purple solution. Monitoring the reaction by $^1$H NMR spectroscopy showed the presence of a major (**3.9a**) and a minor isomer (**3.9b**) (~3:1 ratio, Table 3.1). The spectra are consistent with the cyclized products **3.9a** and **3.9b** (Scheme 3.26). Complexes **3.9** have excellent solubility in all common organic solvents. The complex was purified by chromatography and was isolated in 63% yield as a single isomer with the TMS group proximal to the hydroxyl

group (**3.9a**). The regiochemistry of this complex has been determined by a NOESY experiment (Figure 3.19) with a summary of the observed cross peaks shown in Figure 3.20. The $^{1}$H NMR spectrum (acetone-$d_6$) of **3.9a** shows two doublets at 7.50 and 7.26 ppm, a multiplet at 6.95 ppm, and singlet at 6.35 ppm, which is consistent with the hydroxyindenyl ligand (Figure 3.21).

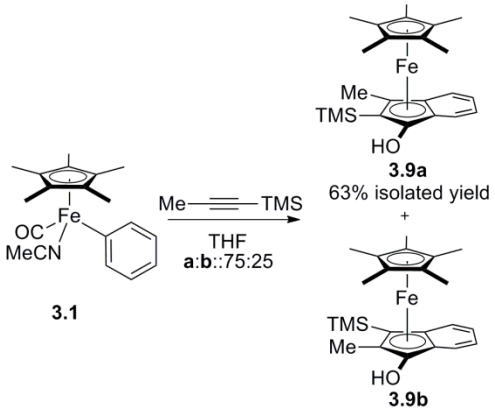


**Scheme 3.26.** Reaction of Cp*Fe(CO)(NCMe)Ph (**3.1**) and 1-TMS-1-propyne to give Cp*Fe($\eta^5$-1-hydroxy-2-methyl-3-trimethylsilylindenyl) (**3.9a**).

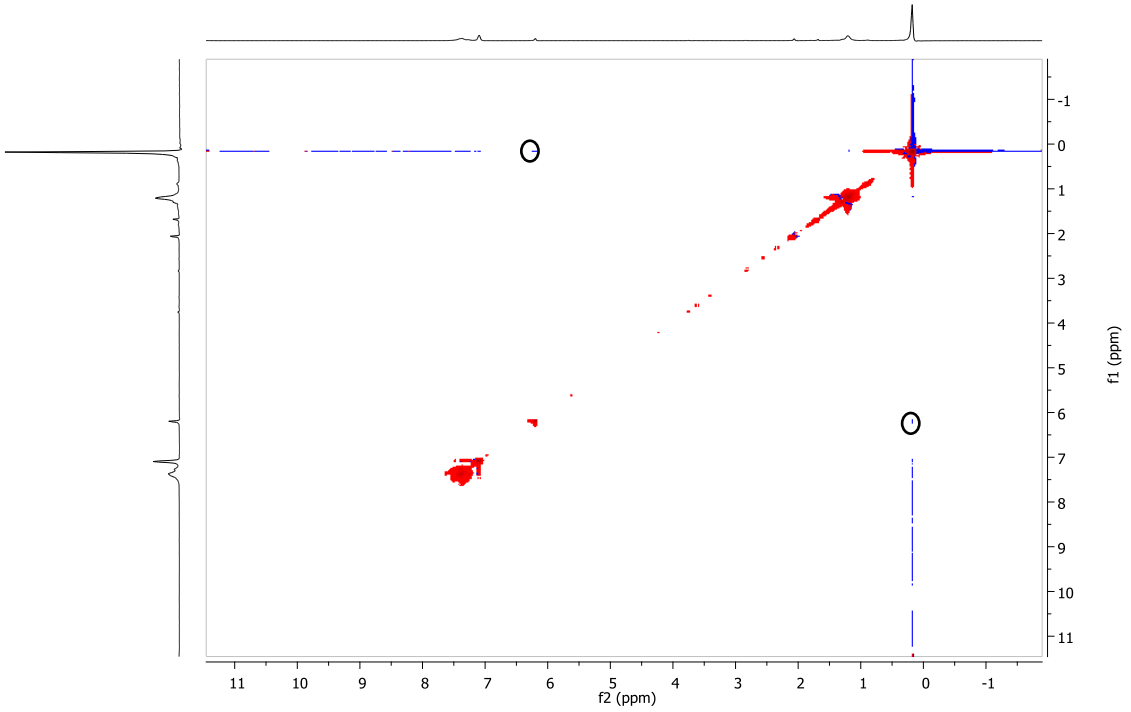


**Figure 3.19.** Two-dimensional NOESY spectrum for Cp*Fe($\eta^5$-1-hydroxy-2-trimethylsilyl-3-methylindenyl) (**3.9a**) in acetone-$d_6$. Important cross peaks are circled.

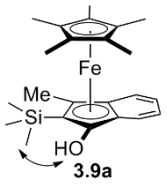


**Figure 3.20.** Representation showing the important cross peaks observed from the NOESY spectrum of Cp*Fe($\eta^5$-1-hydroxy-2-trimethylsilyl-3-methylindenyl) (**3.9a**).

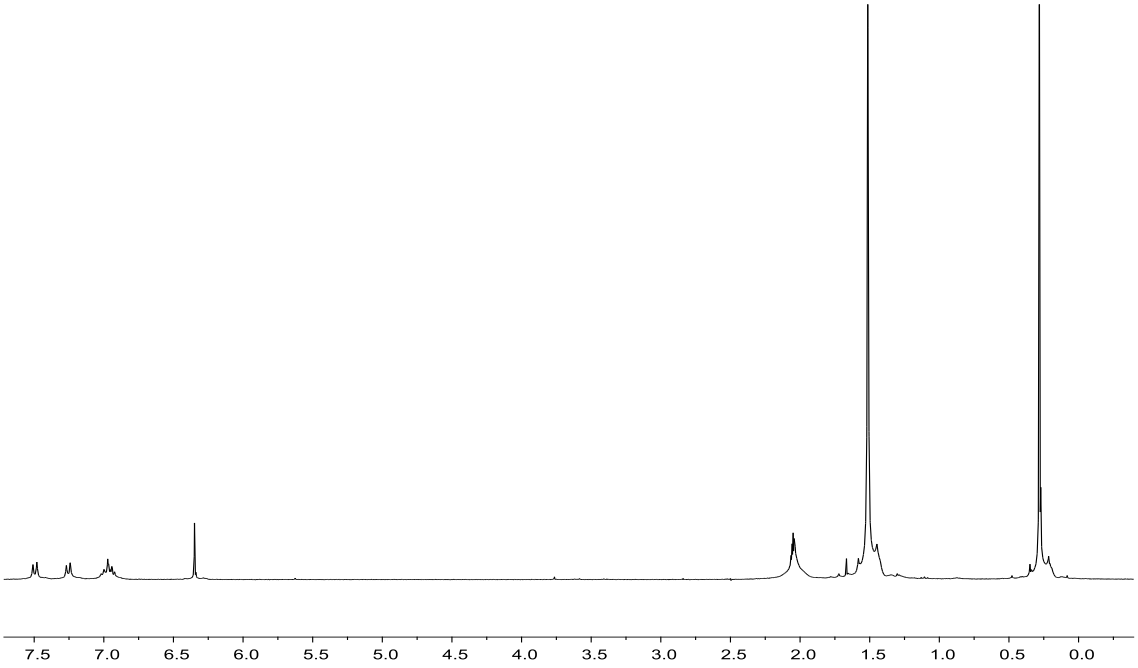


**Figure 3.21.** $^{1}$H NMR spectrum of Cp*Fe(η5-1-hydroxy-2-trimethylsilyl-3-methylindenyl) (**3.9a**) in acetone-$d_6$.

We explored the reactivity of complex **3.1** with another alkyne bearing a single TMS group. Heating **3.1** with excess 1-TMS-2-phenylacetylene in THF at 60 °C gave a purple solution. The phenyl group of 1-TMS-2-phenylacetylene required slightly elevated temperatures when compared to the reaction of 1-TMS-1-propyne. Similar to the other asymmetric alkynes studied thus far, the cyclized products **3.10a** and **3.10b** forms as a mixture of isomers (~1:1) (Scheme 3.27). Complexes **3.10a** and **3.10b** were isolated in 70% yield as a mixture of isomers. Complexes **3.10a** and **3.10b** are a purple-red viscous oil with high solubility in all common organic solvents. The $^{1}$H NMR spectrum (acetone-$d_6$) of **3.10a** and **3.10b** shows several aryl resonances for the phenyl protons and the unbound indenyl protons. A single resonance is observed at 6.80 ppm that integrates for 2 protons, likely a result of chemical exchange between the hydroxyl protons for both isomers. The Cp* protons for both isomers appear to resonate as a single broad resonance

at 1.48 ppm, likely due to coincidental overlap. The two signals for the TMS protons appear as two singlets at 0.23 ppm and 0.13 ppm (Figure 3.22).

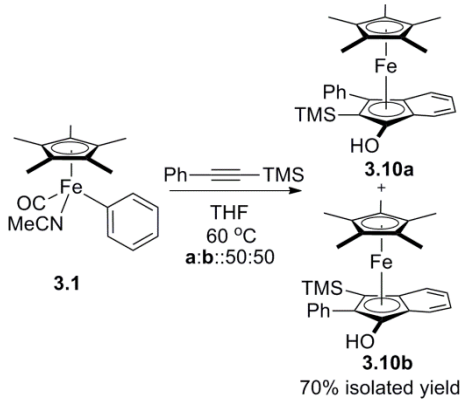


**Scheme 3.27.** Reaction of Cp*Fe(CO)(NCMe)Ph (**3.1**) to give Cp*Fe($\eta^5$-1-hydroxy-2-trimethylsilyl-3-phenylindenyl) (**3.10a**) and Cp*Fe($\eta^5$-1-hydroxy-2-phenyl-3-trimethylsilylindenyl) (**3.10b**).

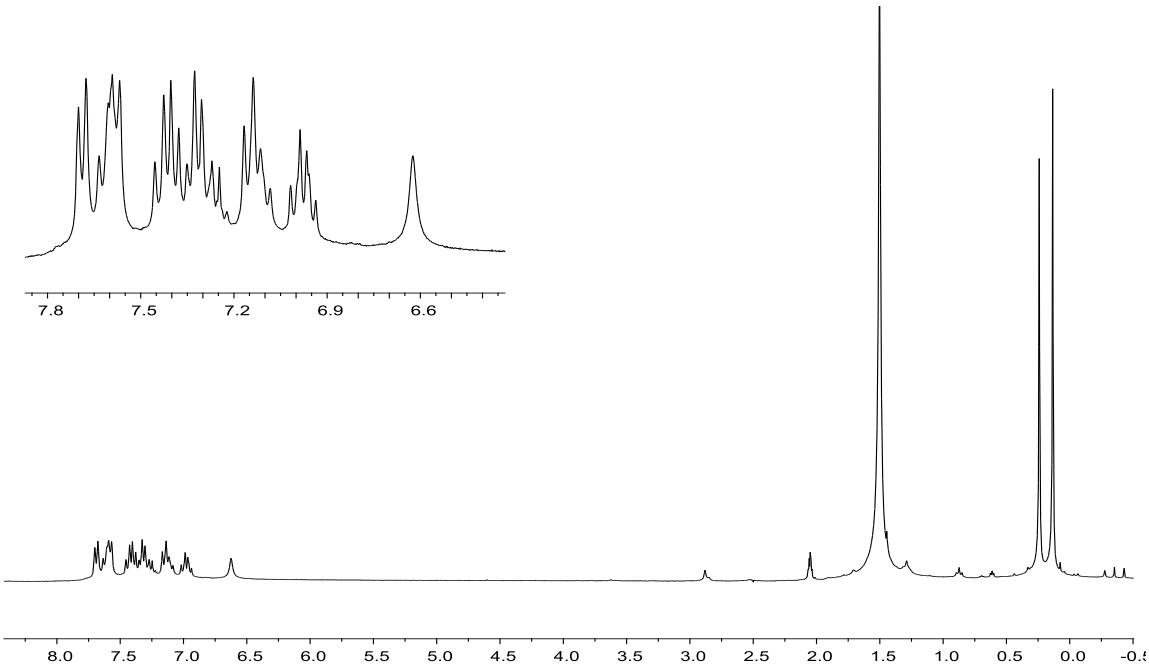


**Figure 3.22.** $^1$H NMR spectrum of Cp*Fe($\eta^5$-1-hydroxy-2-trimethylsilyl-3-phenylindenyl) (**3.10a**) and Cp*Fe($\eta^5$-1-hydroxy-2-phenyl-3-trimethylsilylindenyl) (**3.10b**) in acetone-$d_6$.

There is no evidence for β-TMS elimination during the formation of complexes **3.9** and **3.10,** and we sought to rationalize this observation. The insertion of either 1-

trimethylsilylpropyne or 1-TMS-2-phenylacetylene can produce two regioisomers –one with the TMS group on the α-carbon and one with the TMS group on the β-carbon (Scheme 3.28). The regioisomer with the TMS group on the α-carbon cannot undergo β-TMS elimination and therefore is unlikely to form a vinylidene complex. However, the regioisomer with the TMS group on the β-carbon can either undergo the cyclization reaction or undergo β-TMS elimination (Scheme 3.25). For the β-TMS vinyl complexes that form from 1-trimethylsilylpropyne or 1-TMS-2-phenylacetylene it seems likely that β-TMS elimination is kinetically accessible; however, the respective vinylidene complexes are not observed experimentally. We assume that this is due to a large kinetic barrier for the rearrangement of the coordinated alkyne of the putative complexes Cp*Fe(CO)($\eta^2$-RC≡CPh)(TMS) (R = Ph, Me) to Cp*Fe(CO)(=C=C(R)Ph). Thus, if β-TMS elimination is kinetically accessible to form Cp*Fe(CO)($\eta^2$-RC≡CPh)(TMS) (R = Ph, Me), it is reversible under the reaction conditions to ultimately yield complexes **3.9** and **3.10**.

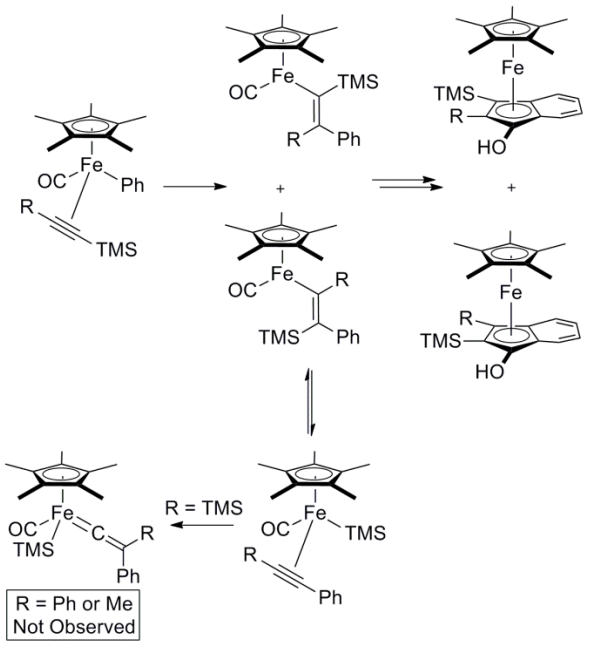


**Scheme 3.28.** Two possible reaction pathways for trimethylsilyl-substituted alkynes.

## 3.3 Conclusions

In this chapter, attempted catalysis with Cp*Fe(CO)(NCMe)Ph (**3.1**) with olefins and alkynes was studied (Scheme 3.29). It was determined that complex **3.1** is a poor catalyst for ethylene hydrophenylation, providing only 0.6 TO of ethylbenzene and 1.2 TO of styrene. The reason for this poor catalytic activity was determined to likely be a result of competitive β-hydride elimination versus benzene C–H activation from the Cp*Fe(CO)($CH_2CH_2Ph$) intermediate, which leads to the formation of styrene and an Fe–H complex. Studying catalytic ethylene hydroarylation using furan gave different results. Only under relatively forcing conditions was any 2-ethylfuran observed. Studies indicated that ethylene insertion into the Fe–furyl bond is prohibitively slow, possibly a result of the increased bond strength of the Fe–furyl bond over the Fe–Ph bond. A similar result was obtained for ethylene hydroarylation using thiophene.

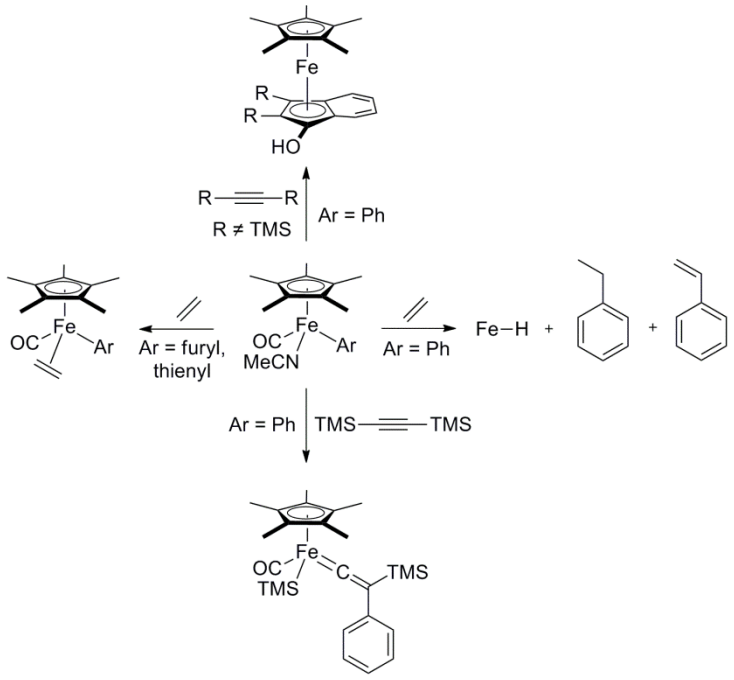


**Scheme 3.29.** Summary of results from attempted catalytic hydroarylation of ethylene and alkynes.

Considering the possibility that complex **3.1** might be better suited for the hydrophenylation of internal alkynes, the catalytic addition of 2-butyne and bis(TMS)acetylene with benzene was evaluated (Scheme 3.29). These reactions led to the formation of a hydroxyindenyl ligand and a vinylidene ligand in the case of 2-butyne and bis(TMS)acetylene, respectively. The reaction with several other alkynes was studied, even those bearing one TMS group, which demonstrated that formation of the hydroxyindenyl ligand is general. An exception is the reaction of **3.1** with bis(TMS)acetylene. For the reactions of Cp*Fe(CO)(NCMe)Ph (**3.1**) with alkynes, the reactivity appears to be dictated by the high thermodynamic stability of the Cp*Fe($\eta^5$-hydroxyndenyl) sandwich compounds and the Fe–vinylidene complex.

The studies presented in this chapter reveal several salient points regarding the design of Fe-based catalysts for hydroarylation. First, irreversible β-hydride elimination

appears to be more problematic than was the case for our group's Ru(II) catalysts.[16, 17, 26-29] It should be noted that associative displacement of $\eta^2$-styrene may be accessible with the Cp* ligand when compared to the Tp (or trispyrazolylalkane) ligand, which could render β-hydride elimination irreversible (Scheme 3.30). Alternatively, the rate of dissociative displacement of $\eta^2$-styrene by ethylene from Cp*Fe(CO)($\eta^2$-syrene)H may be faster than re-insertion. For our group's Ru(II) catalysts, experimental and computational studies suggest that β-hydride elimination is rapidly occurring under catalytic conditions; however, it is also reversible.[17, 18] Consistent with the hypothesis that the ring slip of the cyclopentadienyl ligand may be responsible for styrene formation during ethylene hydrophenylation with **3.1**, we have previously studied ethylene hydrophenylation with $CpRu(PPh_3)_2Ph$ and found that it was a poor catalyst due to styrene formation.[17] In this study, ring slip of the Cp ligand was proposed to be responsible for the formation of styrene.[17] Additionally, the use of heteroaromatics as substrates is potentially complicated by the increased Fe–aryl bond strengths, which may hinder olefin insertion. These studies seem to agree with the trends in reactivity observed for our previously reported TpRu(CO)(NCMe)Ph catalyst.[44] Finally, as noted through the study of alkyne hydroarylation with complex **3.1**, CO insertion is problematic in this Fe complex. While TpRu(CO)(NCMe)Ph is proposed to decompose through a bimetallic pathway that may involve the CO ligand,[17, 82] CO insertion has not been observed with this complex. Comparison of the IR stretching frequency for the CO ligands in Cp*Fe(CO)(NCMe)Ph (**3.1**) (1903 $cm^{-1}$) and TpRu(CO)(NCMe)Ph (1935 $cm^{-1}$) reveals that the CO ligand in TpRu(CO)(NCMe)Ph is more electrophilic. As a result, one might expect CO insertion to be more favorable for the TpRu(CO)(NCMe)Ph complex since the

phenyl group would be more likely to migrate to the carbonyl. However, the thermodynamics from forming the hydroxyindenyl sandwich complexes may provide the driving force for CO insertion from complex **3.1**. Reactivity studies of TpRu(CO)(NCMe)Ph with alkynes have not been performed.

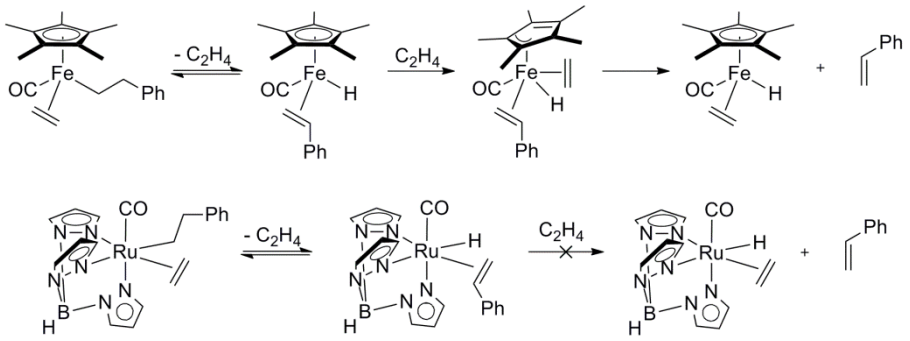


**Scheme 3.30.** Comparison of proposed mechanisms for styrene displacement from Cp*Fe(CO)($\eta^2$-$C_2H_4$)($CH_2CH_2Ph$) and TpRu(CO)($\eta^2$-$C_2H_4$)($CH_2CH_2Ph$). It is also possible that styrene displacement by ethylene for Cp*Fe occurs by a dissociative mechanism in which the rate is faster than re-insertion.

## 3.4 Experimental Section

### 3.4.1 General Considerations

Unless otherwise noted, all synthetic procedures were performed under anaerobic conditions in a nitrogen-filled glovebox or by using standard Schlenk techniques. Glovebox purity was maintained by periodic nitrogen purges and was monitored by an oxygen analyzer ($O_2$ < 15 ppm for all reactions). Tetrahydrofuran, diethyl ether and pentane were dried by distillation from sodium/benzophenone. Hexanes and benzene were purified by passage through a column of activated alumina. Deuterated solvents were used as received and stored under a $N_2$ atmosphere over 4 Å molecular sieves. $^1$H NMR spectra were recorded on a Varian Mercury 300 MHz or a Bruker DRX 600 MHz spectrometer. $^{13}$C NMR spectra were obtained on a Bruker DRX 600 MHz (operating

frequency 150 MHz) or a Bruker Avance III 800 MHz spectrometer (operating frequency 201 MHz). NOESY spectra were obtained on a Bruker Avance 600 MHz spectrometer. All $^{1}H$ and $^{13}C$ spectra are referenced against residual proton signals ($^{1}H$ NMR) or $^{13}C$ resonances ($^{13}C$ NMR) of the deuterated solvents and are reported in ppm. GC/MS was performed using a Shimadzu GCMS-QP2010 Plus system with a 30 m x 0.25 mm RTx-Qbond column with 8 μm thickness (for kinetic isotope effect experiments) or a 30 m x 0.25 mm SHRXI-5MS column with 0.25 μm thickness (for hydroarylation experiments) using electron impact ionization. IR spectra were obtained on a Shimadzu IRAffinity-1 Fourier transform infrared spectrometer. Samples were prepared in solution flow cells. Ethylene was purchased from GTS-Welco. All other reagents were purchased from commercial sources and used as received. Elemental analyses were performed by Atlantic Microlabs, Inc. Cp*Fe(CO)(NCMe)Ph (**3.1**) was prepared as previously reported.[1]

### 3.4.2 Experimental Procedures

**Ethylene Hydrophenylation using Cp*Fe(CO)(NCMe)Ph (3.1).** Complex **3.1** (0.006 g, 0.02 mmol) was dissolved in benzene (6 mL) containing 0.025 mol% hexamethylbenzene as an internal standard and placed in a stainless steel pressure reactor. The reactor was sealed and pressurized to 25 psi with ethylene and left stirring at 30 °C for 20 h. After the reaction was complete, an aliquot was removed for analysis by GC/MS. This reaction was performed three times to give 0.6 TO of ethylbenzene and 1.2 TO of styrene. The reaction at higher temperature was performed similarly.

**Monitoring the reaction between Cp*Fe(CO)(NCMe)Ph (3.1) and ethylene in $C_6D_6$ by $^{1}H$ NMR spectroscopy.** Complex **3.1** (0.003 g, 0.01 mmol) was dissolved in $C_6D_6$ (~0.25 mL) in a high pressure NMR tube. After degassing the sample by conventional freeze-pump-thaw cycles, the tube was pressurized with 30 psi of ethylene

at room temperature and then brought to 120 psi with $N_2$. The sample was kept at room temperature and periodically monitored by $^1$H NMR spectroscopy revealing the formation of ethyl benzene, styrene, and an unidentified Fe–H complex.

**Attempted ethylene hydroarylation of furan using Cp*Fe(CO)(NCMe)Ph (3.1).** Complex **3.1** (0.010 g, 0.03 mmol) was dissolved in furan (2 mL) containing 0.1 mol% hexamethylbenzene as an internal standard and placed in a stainless steel pressure reactor. The reactor was sealed and subsequently pressurized with 100 psi of $C_2H_4$. After heating at 120 °C for 17 h, the reactor was cooled in ice. An aliquot was taken and analyzed by GC/MS to reveal 0.3 TO of ethyl furan. Other hydroarylation reactions were performed similarly.

**Observation of purported Cp*Fe(CO)($\eta^2$-$C_2H_4$)(2-furyl) (3.3) from the reaction between Cp*Fe(CO)(NCMe)(2-furyl) (3.2) and $C_2H_4$.** Complex **3.1** was (0.007 g, 0.02 mmol) and furan (8 μL, 0.11 mmol) were dissolved in THF-$d_8$ and transferred to a thick walled J-Young NMR tube. After ~30 min, the tube was pressurized with 50 psi $C_2H_4$ and monitored by $^1$H NMR. After several hours, the volatiles were removed in vacuo, and residue was reconstituted in $C_6D_6$. To this solution HCl (22 μL, 0.02 mmol, 1 M solution in diethyl ether) was added and analyzed by $^1$H NMR spectroscopy and GC/MS. The reaction to produce **3.3-*d*$_3$** was performed in a similar fashion.

**Isolation of purported Cp*Fe(CO)($\eta^2$-$C_2H_4$)(2-furyl) (3.3).** In a round bottom flask, complex **3.1** (0.060 g, 0.18 mmol) was combined with furan (0.26 mL, 3.6 mmol) in THF (6 mL) and stirred at room temperature. After 1 h, the volatiles were removed in vacuo and the residue was reconstituted in THF (8 mL) and transferred to a stainless steel

high pressure reactor and pressurized with 70 psi of $C_2H_4$. After 1 h, the reactor was brought into a glove box and the volatiles were removed in vacuo to give a red oil. The oil was analyzed by $^1$H NMR spectroscopy. $^1$H NMR (300 MHz, acetone-$d_6$): δ 7.27 (d, $^3J_{HH}$ = 2 Hz, 1H, furyl 5 position), 6.43 (t, $^3J_{HH}$ = 2 Hz, 1H, furyl 3 or 4 position), 3.24 (d, $^3J_{HH}$ = 2 Hz, 1H, furyl 3 or 4 position), 1.86 (d, $^2J_{HH}$ = 6 Hz, 4H, $\eta^2$-$C_2H_4$), 1.67 (15H, s, Cp*).

**Isolation of purported Cp*Fe(CO)($\eta^2$-$C_2H_4$)(2-thienyl) (3.4).** Complex **3.1** (0.039 g, 0.12 mmol) was combined with thiophene (0.19 mL, 0.24 mmol) in THF (4 mL). After stirring at room temperature for 1 h, the volatiles were removed in vacuo. The residue was reconstituted in THF (5 mL) and transferred to a stainless steel pressure reactor. The reactor was pressurized with 50 psi of $C_2H_4$ and stirred at room temperature for ~ 45 min. The reactor was brought back into the glove box and the volatiles were removed in vacuo to give a red residue. The residue was analyzed by $^1$H NMR spectroscopy. $^1$H NMR (300 MHz, acetone-$d_6$): δ 7.00 (m, 1H, thienyl 5 position), 6.94 (m, 1H, thienyl 3 or 4 position), 3.16 (d, $^3J_{HH}$ = 3 Hz, thienyl 3 or 4 position), 1.87 (d, $^2J_{HH}$ = 6 Hz, 4H, $\eta^2$-$C_2H_4$), 1.68 (s, 15H, Cp*).

**Attempted alkyne hydrophenylation by Cp*Fe(CO)(NCMe)Ph (3.1).** To a 4 dram vial with a stir bar was added complex **3.1** (0.007 g, 0.02 mmol), benzene (2 mL, 20 mmol), and an internal alkyne (1.2 mmol). The vial was sealed with a teflon-lined cap and heated in an oil bath at the appropriate temperature for the given amount of time. After cooling to room temperature an aliquot was removed and analyzed by GC/MS.

**Cp*Fe($\eta^5$-1-hydroxy-2,3-dimethylindenyl) (3.5).** To a solution of **3.1** (0.076 g, 0.23 mmol) in THF (~7 mL) was added 2-butyne (0.35 mL, 4.5 mmol). The solution

immediately changed from red-orange to dark purple. After stirring for 1 hour, the volatiles were removed in vacuo. The resulting crude purple solid was extracted with pentane (~3 mL) and filtered. The filtrate was stored in the glovebox freezer (–35 °C) overnight to afford a dark purple crystalline solid that was separated by decantation and dried under vacuum (0.047 g, 60% yield). A crystal suitable for single crystal X-ray diffraction was grown by slow evaporation of a pentane solution of **3.5**. $^{1}$H NMR (300 MHz, acetone-$d_6$): 7.43 (d, $^{3}J_{HH}$ = 8.5 Hz, 1H, indenyl), 7.23 (d, $^{3}J_{HH}$ = 8.5 Hz, 1H, indenyl), 6.90 (m, 2H, indenyl), 6.33 (s, 1H, OH), 1.93 (br s, 3H, indenyl methyl), 1.73 (br s, 3H, indenyl methyl), 1.47 (s, 15H, Cp*). $^{13}$C NMR (150 MHz, $C_6D_6$): 126.5 (indenyl unbound), 124.8 (indenyl unbound), 122.2 (indenyl unbound), 121.9 (indenyl unbound), 112.5 (C–OH), 82.3 (indenyl bound), 78.0 (indenyl bound), 77.6 (s, $C_5Me_5$), 75.8 (indenyl bound), 68.0 (indenyl bound), 9.4 (indenyl methyl), 9.0 ($C_5(CH_3)_5$), 8.3 (indenyl methyl). Anal. Calcd. for $C_{21}H_{26}FeO$: C, 72.01; H, 7.48. Found: C, 72.28; H, 7.64.

**Cp*Fe(CO)(=C=C(Ph)TMS)(TMS) (3.6).** Complex **3.1** (0.070 g, 0.21 mmol), bis(TMS)acetylene (0.45 mL, 2.1 mmol), and THF (~5 mL) were combined in a thick-walled pressure tube. The pressure tube was sealed and stirred at 60 °C for 4 h during which time the solution changed from red-orange to dark yellow. The resulting solution was cooled to RT and the volatiles were removed in vacuo. The resulting yellow residue was loaded onto a plug of silica gel in a 15 mL frit and eluted with a diethyl ether/hexanes (1:10) mixture. A yellow band was collected and dried in vacuo. The resulting yellow solid was washed with pentane (2 x ½ mL) and dried (0.048 g, 50%). A crystal suitable for a single crystal X-ray diffraction study was grown by the slow

evaporation of a pentane solution of **3.6**. $^{1}$H NMR (600 MHz, THF-$d_8$): δ 7.20 (t, $^{3}J_{HH}$ = 7 Hz, 2H, phenyl *meta*), 7.06 (m, 3H, phenyl *ortho* and *para*), 1.80 (s, 15H, Cp*), 0.17 (s, 9H, C–TMS), 0.13 (br s, 9H, Fe–TMS). $^{13}$C NMR (THF-$d_8$): 333.1 ($C_\alpha$ vinylidene), 220.1 (CO), 134.1 (phenyl *ipso*), 130.6 (phenyl *ortho*), 129.0 (phenyl *meta*), 126.3 (phenyl *para*), 120.3 ($C_\beta$ vinylidene), 97.9 ($C_5Me_5$), 10.7 ($C_5(CH_3)_5$), 8.2 (C–TMS), 0.8 (Fe–TMS). IR (THF solution): $\nu_{CO}$ = 1938 cm$^{-1}$. Anal. Calcd. For $C_{25}H_{38}FeOSi_2$: C, 64.35; H, 8.21. Found: C, 64.60; H, 8.37.

**Cp*Fe(η$^5$-1-hydroxy-2-methyl-3-phenylindenyl) (3.7a).** To a THF solution (~6 mL) of **3.1** (0.113 g, 0.335 mmol) was added 1-phenyl-1-propyne (0.21 mL, 1.7 mmol). The red-orange solution changed to dark red and was stirred for 16 h at room temperature. The volatiles were removed in vacuo. The resulting purple residue was treated with ~1 mL hexanes and cooled to –35 °C in the glovebox freezer. After several hours, a dark purple solid was collected on a fine porosity frit and dried in vacuo (0.067 g, 49% yield). $^{1}$H NMR (600 MHz, acetone-$d_6$): 7.82 (d, $^{3}J_{HH}$ = 7.3 Hz, 2H, phenyl *ortho*), 7.58 (d, $^{3}J_{HH}$ = 8.3 Hz, 1H, indenyl), 7.38 – 7.30 (overlapping, 3H, 2 x phenyl *meta* and indenyl), 7.22 (t, $^{3}J_{HH}$ = 7.4 Hz, 1H, phenyl *para*), 7.03 (m, 2H, indenyl), 6.63 (s, 1H, hydroxyl), 2.29 (br s, 3H, methyl), 1.38 (s, 15H, Cp*). $^{13}$C NMR (201 MHz, acetone-$d_6$): 137.4 (phenyl *ipso*), 130.6, 128.3, 127.2, 126.2, 126.1, 123.2, 123.1 (phenyl/indenyl unbound), 113.0 (C–OH), 83.6, 79.7, 79.0 (indenyl bound), 78.1 ($C_5Me_5$), 66.6 (indenyl bound), 12.2 (indenyl methyl), 9.1 ($C_5(CH_3)_5$). Anal. Calcd. for $C_{26}H_{28}FeO$: C, 75.73; H, 6.84. Found: C, 75.56; H, 6.96.

**Cp*Fe(η$^5$-1-hydroxy-2-methyl-3-methylester-indenyl) (3.8a).** To a THF solution (~6 mL) of complex **3.1** (0.104 g, 0.309 mmol) was added methyl-2-butynoate

(0.31 mL, 3.1 mmol). The resulting solution was stirred for ~19 h at room temperature during which time the solution changed from red-orange to a deep red color. The volatiles were removed in vacuo, and ~1.5 mL of hexanes was added to the residue. After storing in the glove box freezer at –35 °C, a dark red solid was collected on a fine porosity frit and washed with 1 mL hexanes and dried in vacuo (0.060 g, 49%). $^{1}$H NMR (300 MHz, acetone-$d_6$) δ 7.39 (d, $^{3}J_{HH}$ = 9 Hz, 1H, indenyl), 7.31 (d, $^{3}J_{HH}$ = 9 Hz, 1H, indenyl), 7.06 (m, 2H, indenyl), 7.00 (s, 1H, hydroxyl), 3.94 (s, 3H, -OMe), 2.28 (s, 3H, Me), 1.43 (s, 15H, Cp*). $^{13}$C NMR (201 MHz, acetone-$d_6$): 175.9 (C=O), 125.9, 124.44, 124.39, 124.12 (indenyl unbound), 118.1 (C–OH), 85.2 (indenyl bound), 79.6 ($C_5Me_5$), 79.1, 68.6, 60.3 (indenyl bound), 51.7 ($OCH_3$) 10.7 ($CH_3$), 8.6 ($C_5(CH_3)_5$). Anal. Calcd. for $C_{22}H_{26}FeO_3$: C, 67.02; H, 6.65. Found: C, 67.25; H, 6.68.

**Cp*Fe(η$^5$-1-hydroxy-2-methyl-3-trimethylsilylindenyl) (3.9a).** 1-Trimethylsilylpropyne (0.23 mL, 1.8 mmol) was added to a THF solution (~4 mL) of complex **3.1** (0.061 g, 0.18 mmol). The solution was stirred for ~16 h. The volatiles were removed from the resulting purple solution in vacuo. The purple oil was extracted with pentane and filtered through Celite. The filtrate was dried in vacuo, and the resulting residue was loaded onto a plug of silica gel in a 15 mL frit. A mixture of benzene/hexanes (1:20) eluted a pale yellow band that was collected and discarded. Using a mixture of benzene/hexanes (1:1) eluted a purple band that was collected and dried in vacuo to give a purple solid of the desired product (0.047 g, 63%). $^{1}$H NMR (600 MHz, acetone-$d_6$):) δ 7.47 (d, $^{3}J_{HH}$ = 9 Hz, 1H, indenyl), 7.27 (d, $^{3}J_{HH}$ = 9 Hz, 1H, indenyl), 7.02 (m, 1H, indenyl), 6.95 (m, 1H, indenyl), 1.92 (br s, 3H, Me), 1.48 (s, 15H, Cp*), 0.29 (m, 9H, TMS). $^{13}$C NMR (201 MHz, acetone-$d_6$): 127.1, 125.8, 122.9, 122.8

(indenyl unbound), 120.3 (C–OH), 86.5, 80.0 (indenyl bound), 78.0 ($C_5Me_5$), 73.2, 66.5 (indenyl bound), 12.5 ($CH_3$), 9.9 ($C_5(CH_3)_5$, 1.7 ($Si(CH_3)_3$). Anal. Cald. for $C_{23}H_{32}FeOSi$: C, 67.64; H, 7.90. Found: C, 67.56; H, 7.90.

**Cp*Fe(η$^5$-1-hydroxy-2-trimethylsilyl-3-phenylindenyl) (3.10a) and Cp*Fe(η$^5$-1-hydroxy-2-phenyl-3-trimethylsilylindenyl) (3.10b).** Complex **3.1** (0.037 g, 0.11 mmol), 1-TMS-2-phenylpropyne (0.11 mL, 0.56 mmol), and THF (~3 mL) were combined in a thick-walled pressure tube. The vessel was sealed and stirred at 60 °C for ~4.5 h during which time the solution turned from red-orange to purple. The reaction mixture was cooled to RT, and the volatiles were removed in vacuo. The resulting purple residue was loaded onto a plug of silica gel in a 15 mL frit. The plug was washed with a benzene/hexanes (1:20) mixture to elute the free alkyne and a light pink band, which was collected and discarded. Eluting with diethyl ether/hexanes (1:1) allowed the collection of a purple band that was subsequently dried in vacuo to give a sticky purple oil (0.036 g, 70%). $^1$H NMR (300 MHz, acetone-$d_6$) δ 7.69 (d, $^3J_{HH}$ = 7 Hz, 2H, 2 x indenyl/phenyl), 7.60 (m, 4H, 4 x indenyl/phenyl), 7.34 (overlapping m, 6H, 6 x indenyl/phenyl), 7.13 (m, 4H, 4 x indenyl/phenyl), 6.98 (m, 2H, 2 x indenyl/phenyl), 6.62 (s, 2H, 2 x –OH), 1.47 (s, 30H, 2 x Cp*), 0.24 (s, 9H, TMS), 0.11 (s, 9H, TMS). Anal. Cald. for $C_{28}H_{34}FeOSi$: C, 71.48; H, 7.28. Found: C, 71.21; H, 7.31.

## 3.5 References

(1) Kalman, S. E.; Petit, A.; Gunnoe, T. B.; Ess, D. H.; Cundari, T. R.; Sabat, M. *Organometallics* **2013**, *32*, 1797-1806.

(2) Andreatta, J. R.; McKeown, B. A.; Gunnoe, T. B. *J. Organomet. Chem.* **2011**, *696*, 305-315.

(3) Hartwig, J. F., *Organotransition Metal Chemistry: From Bonding to Catalysis*. University Science Books: Sausalito, 2009.

(4) Cui, X. H.; Burgess, K. *Chem. Rev.* **2005**, *105*, 3272-3296.

(5) Harmon, R. E.; Gupta, S. K.; Brown, D. J. *Chem. Rev.* **1973**, *73*, 21-52.

(6) Ittel, S. D.; Johnson, L. K.; Brookhart, M. *Chem. Rev.* **2000**, *100*, 1169-1203.

(7) Gibson, V. C.; Spitzmesser, S. K. *Chem. Rev.* **2003**, *103*, 283-315.

(8) Beletskaya, I. P.; Cheprakov, A. V. *Chem. Rev.* **2000**, *100*, 3009-3066.

(9) Small, B. L.; Brookhart, M. *J. Am. Chem. Soc.* **1998**, *120*, 7143-7144.

(10) Small, B. L.; Brookhart, M.; Bennett, A. M. A. *J. Am. Chem. Soc.* **1998**, *120*, 4049-4050.

(11) Bart, S. C.; Lobkovsky, E.; Chirik, P. J. *J. Am. Chem. Soc.* **2004**, *126*, 13794-13807.

(12) Daida, E. J.; Peters, J. C. *Inorg. Chem.* **2004**, *43*, 7474-7485.

(13) Yu, Y.; Sadique, A. R.; Smith, J. M.; Dugan, T. R.; Cowley, R. E.; Brennessel, W. W.; Flaschenriem, C. J.; Bill, E.; Cundari, T. R.; Holland, P. L. *J. Am. Chem. Soc.* **2008**, *130*, 6624-6638.

(14) Vela, J.; Smith, J. M.; Yu, Y.; Ketterer, N. A.; Flaschenriem, C. J.; Lachicotte, R. J.; Holland, P. L. *J. Am. Chem. Soc.* **2005**, *127*, 7857-7870.

(15) Yasuda, S.; Yorimitsu, H.; Oshima, K. *Organometallics* **2010**, *29*, 2634-2636.

(16) Foley, N. A.; Lee, J. P.; Ke, Z. F.; Gunnoe, T. B.; Cundari, T. R. *Acc. Chem. Res.* **2009**, *42*, 585-597.

(17) Lail, M.; Bell, C. M.; Conner, D.; Cundari, T. R.; Gunnoe, T. B.; Petersen, J. L. *Organometallics* **2004**, *23*, 5007-5020.

(18) Oxgaard, J.; Goddard, W. A. *J. Am. Chem. Soc.* **2004**, *126*, 442-443.

(19) Yamamoto, Y. *Chem. Soc. Rev.* **2014**, *43*, 1575-1600.

(20) Wang, X. L.; Zhou, L. H.; Lu, W. J. *Curr. Org. Chem.* **2010**, *14*, 289-307.

(21) Kitamura, T. *Eur. J. Org. Chem.* **2009**, 1111-1125.

(22) *Metal-catalyzed Cross-coupling Reactions*. Wiley-VCH: Weinheim, 1998.

(23) Corbet, J. P.; Mignani, G. *Chem. Rev.* **2006**, *106*, 2651-2710.

(24) Goj, L. A.; Gunnoe, T. B. *Curr. Org. Chem.* **2005**, *9*, 671-685.

(25) Kalman, S. E.; Gunnoe, T. B.; Sabat, M. *Organometallics* **2014**, *33*, 5457-5463.

(26) Lail, M.; Arrowood, B. N.; Gunnoe, T. B. *J. Am. Chem. Soc.* **2003**, *125*, 7506-7507.

(27) Foley, N. A.; Ke, Z. F.; Gunnoe, T. B.; Cundari, T. R.; Petersen, J. L. *Organometallics* **2008**, *27*, 3007-3017.

(28) Burgess, S. A.; Joslin, E. E.; Gunnoe, T. B.; Cundari, T. R.; Sabat, M.; Myers, W. H. *Chem. Sci.* **2014**, *5*, 4355-4366.

(29) Joslin, E. E.; McMullin, C. L.; Gunnoe, T. B.; Cundari, T. R.; Sabat, M.; Myers, W. H. *Organometallics* **2012**, *31*, 6851-6860.

(30) McKeown, B. A.; Foley, N. A.; Lee, J. P.; Gunnoe, T. B. *Organometallics* **2008**, *27*, 4031-4033.

(31) McKeown, B. A.; Gonzalez, H. E.; Friedfeld, M. R.; Brosnahan, A. M.; Gunnoe, T. B.; Cundari, T. R.; Sabat, M. *Organometallics* **2013**, *32*, 2857-2865.

(32) McKeown, B. A.; Gonzalez, H. E.; Friedfeld, M. R.; Gunnoe, T. B.; Cundari, T. R.; Sabat, M. *J. Am. Chem. Soc.* **2011**, *133*, 19131-19152.

(33) McKeown, B. A.; Gonzalez, H. E.; Gunnoe, T. B.; Cundari, T. R.; Sabat, M. *ACS Catal.* **2013**, *3*, 1165-1171.

(34) McKeown, B. A.; Gonzalez, H. E.; Michaelos, T.; Gunnoe, T. B.; Cundari, T. R.; Crabtree, R. H.; Sabat, M. *Organometallics* **2013**, *32*, 3903-3913.

(35) McKeown, B. A.; Prince, B. M.; Ramiro, Z.; Gunnoe, T. B.; Cundari, T. R. *ACS Catal.* **2014**, *4*, 1607-1615.

(36) Labinger, J. A.; Bercaw, J. E. *Organometallics* **1988**, *7*, 926-928.

(37) Olah, G.; Molnar, A., *Hydrocarbon Chemistry*. 2nd ed.; Wiley-Interscience: New York, 2003.

(38) Olah, G. A., *Friedel-Crafts Chemistry*. John Wiley & Sons: New York, 1973.

(39) Gramec, D.; Masic, L. P.; Dolenc, M. S. *Chem. Res. Toxicol.* **2014**, *27*, 1344-1358.

(40) Dalvie, D. K.; Kalgutkar, A. S.; Khojasteh-Bakht, S. C.; Obach, R. S.; O'Donnell, J. P. *Chem. Res. Toxicol.* **2002**, *15*, 269-299.

(41) Yamamoto, T. *NPG Asia Mater.* **2010**, *2*, 54-60.

(42) Zhang, L.; Colella, N. S.; Cherniawski, B. P.; Mannsfeld, S. C. B.; Briseno, A. L. *ACS Appl. Mater. Interfaces* **2014**, *6*, 5327-5343.

(43) Petit, A.; Flygare, J.; Miller, A. T.; Winkel, G.; Ess, D. H. *Org. Lett.* **2012**, *14*, 3680-3683.

(44) Pittard, K. A.; Lee, J. P.; Cundari, T. R.; Gunnoe, T. B.; Petersen, J. L. *Organometallics* **2004**, *23*, 5514-5523.

(45) Yang, J.; Yin, J. G.; Abboud, K. A.; Jones, W. M. *Organometallics* **1994**, *13*, 971-978.

(46) Curnow, O. J.; Fern, G. M. *Organometallics* **2002**, *21*, 2827-2829.

(47) Thimmaiah, M.; Luck, R. L.; Fang, S. Y. *J. Organomet. Chem.* **2007**, *692*, 1956-1962.

(48) Bradley, C. A.; Flores-Torres, S.; Lobkovsky, E.; Abruna, H. D.; Chirik, P. J. *Organometallics* **2004**, *23*, 5332-5346.

(49) Kirchner, K.; Kwan, K. S.; Taube, H. *Inorg. Chem.* **1993**, *32*, 4974-4975.

(50) Wang, X. W.; Frohlich, R.; Daniliuc, C. G.; Rieger, B.; Jonovic, A.; Kehr, G.; Erker, G. *Organometallics* **2012**, *31*, 6741-6752.

(51) Samula, K.; Cichy, B. *Acta Pol. Pharm.* **1985**, *42*, 256-262.

(52) Sheridan, H.; Walsh, J. J.; Cogan, C.; Jordan, M.; McCabe, T.; Passante, E.; Frankish, N. H. *Biorg. Med. Chem. Let.* **2009**, *19*, 5927-5930.

(53) Kuraray Co. Ltd. Jpn. Kokai Tokkyo Koho. JP 56113740, 1981.

(54) Kuraray Co. Ltd. Jpn. Kokai Tokkyo Koho. JP 57004945, 1982.

(55) Chinnagolla, R. K.; Jeganmohan, M. *Eur. J. Org. Chem.* **2012**, 417-423.

(56) Muralirajan, K.; Parthasarathy, K.; Cheng, C. H. *Angew. Chem. Int. Ed.* **2011**, *50*, 4169-4172.

(57) Patureau, F. W.; Besset, T.; Kuhl, N.; Glorius, F. *J. Am. Chem. Soc.* **2011**, *133*, 2154-2156.

(58) Yang, M.; Zhang, X. M.; Lu, X. Y. *Org. Lett.* **2007**, *9*, 5131-5133.

(59) Matsuda, T.; Makino, M.; Murakami, M. *Chem. Lett.* **2005**, *34*, 1416-1417.

(60) Shintani, R.; Okamoto, K.; Hayashi, T. *Chem. Lett.* **2005**, *34*, 1294-1295.

(61) Chang, K. J.; Rayabarapu, D. K.; Cheng, C. H. *Org. Lett.* **2003**, *5*, 3963-3966.

(62) Rayabarapu, D. K.; Cheng, C. H. *Chem. Comm.* **2002**, 942-943.

(63) Rayabarapu, D. K.; Yang, C. H.; Cheng, C. H. *J. Org. Chem.* **2003**, *68*, 6726-6731.

(64) Gevorgyan, V.; Quan, L. G.; Yamamoto, Y. *Tet. Lett.* **1999**, *40*, 4089-4092.

(65) Butler, I. R.; Cullen, W. R.; Lindsell, W. E.; Preston, P. N.; Rettig, S. J. *J. Chem. Soc., Chem. Comm.* **1987**, 439-441.

(66) Butler, I. R.; Elliott, J. E.; Houde, J. *Can. J. Chem.* **1989**, *67*, 1308-1311.

(67) Dawson, D. P.; Yongskulrote, W.; Bramlett, J. M.; Wright, J. B.; Durham, B.; Allison, N. T. *Organometallics* **1994**, *13*, 3873-3880.

(68) Thorn, D. L.; Hoffmann, R. *J. Am. Chem. Soc.* **1978**, *100*, 2079-2090.

(69) Takano, K.; Ikeda, T.; Kodama, S.; Ishii, Y. *Chem. Comm.* **2015**, *51*, 4981-4984.

(70) Adams, H.; Broughton, S. G.; Walters, S. J.; Winter, M. J. *Chem. Comm.* **1999**, 1231-1232.

(71) Mansuy, D.; Battioni, J. P.; Lavallee, D. K.; Fischer, J.; Weiss, R. *Inorg. Chem.* **1988**, *27*, 1052-1056.

(72) Yen, Y. S.; Lin, Y. C.; Liu, Y. H.; Wang, Y. *Organometallics* **2007**, *26*, 1250-1255.

(73) Bruneau, C.; Dixneuf, P. H. *Acc. Chem. Res.* **1999**, *32*, 311-323.

(74) Trost, B. M.; McClory, A. *Chem. Asian J.* **2008**, *3*, 164-194.

(75) *Metal Vinylidenes and Allenylidenes in Catalysis: From Reactivity to Applications in Synthesis*. Wiley-VCH: Weinheim, Germany, 2008.

(76) Edelbach, B. L.; Lachicotte, R. J.; Jones, W. D. *Organometallics* **1999**, *18*, 4660-4668.

(77) Randolph, C. L.; Wrighton, M. S. *J. Am. Chem. Soc.* **1986**, *108*, 3366-3374.

(78) Wakatsuki, Y.; Yamazaki, H.; Nakano, M.; Yamamoto, Y. *J. Chem. Soc., Chem. Comm.* **1991**, 703-704.

(79) Marciniec, B.; Pietraszuk, C. *J. Chem. Soc., Chem. Comm.* **1995**, 2003-2004.

(80) LaPointe, A. M.; Rix, F. C.; Brookhart, M. *J. Am. Chem. Soc.* **1997**, *119*, 906-917.

(81) Kakiuchi, F.; Yamada, A.; Chatani, N.; Murai, S.; Furukawa, N.; Seki, Y. *Organometallics* **1999**, *18*, 2033-2036.

(82) Joslin, E. E. Synthesis and Characterization of Ru(II) Complexes as Potential Catalysts in Olefin Hydroarylation. University of Virginia, 2013.

# 4 The Reactivity of Cp*Fe[P(OCH$_2$)$_3$CEt]$_2$Ph toward Aromatic C–H Bonds and Unsaturated Substrates

## 4.1 Introduction

In the previous two chapters (Chapter 2 and Chapter 3), we have demonstrated the reactivity of Cp*Fe(CO)(NCMe)Ph toward aromatic C–H bonds and unsaturated substrates.[1, 2] Despite being highly active for aromatic C–H bond activation, Cp*Fe(CO)(NCMe)Ph is a poor catalyst for both olefin hydroarylation and alkyne hydroarylation. It was determined that side reactions dominate over the preferred reactions in the catalytic cycle shown in Scheme 1.32.[3-5] For instance, ethylene hydrophenylation is hindered by competitive β-hydride elimination leading to the formation of styrene and, likely, catalyst deactivation. Moreover, ethylene hydroarylation with furan was not successful, apparently due to the prohibitively slow ethylene insertion into the Fe–furyl bond. Finally, we did not observe any catalytic turnover for alkyne hydrophenylation as a result of intramolecular activity involving either CO insertion or β-TMS elimination.

Knowing that the Cp*Fe motif is promising for aromatic C–H bond activation,[2, 6-8] we probed the impact of replacing the CO ligand.[9, 10] Our motivation for this study can be summarized by the following two points. First, removal of CO would eliminate intramolecular reactivity associated with CO, which could result in more robust Fe complexes. Additionally, changing the electronics of the Fe system could facilitate C–H activation over the undesired β-hydride elimination. If β-hydride elimination did occur, it would be expected that the resulting Fe–H complex could be more stable since no CO is present to potentially insert into the Fe–H bond.[11, 12] A stable Fe-hydride intermediate may provide the opportunity to develop Fe-catalyzed vinylation reactions. Therefore, in

this chapter we demonstrate the synthesis and characterization of a new Fe(II) complex, Cp*Fe[P($OCH_2$)$_3$CEt]$_2$Ph (**4.2**), and study its reactivity toward aromatic C–H bonds and unsaturated substrates.

## 4.2 Results and Discussion

### 4.2.1 Rationale for the Bicyclic Phosphite P($OCH_2$)$_3$CEt

While many phosphine and phosphite ligands are known, we initially chose to study Fe complexes with the ligand P($OCH_2$)$_3$CEt based on the success of the TpRu[P($OCH_2$)$_3$CEt](NCMe)Ph complex for catalytic olefin hydroarylation.[13, 14] The P($OCH_2$)$_3$CEt ligand P–O–C angles are reduced compared to P(OR)$_3$ so that intramolecular C–H activation is unlikely. Additionally, the cone angle for P($OCH_2$)$_3$CEt is relatively small compared to the many other phosphines and phosphites, and thus should be suitable for the smaller Fe(II) metal center.[15, 16]

### 4.2.2 Synthesis of Cp*Fe[P($OCH_2$)$_3$CEt]$_2$Ph (4.2)

The synthesis of Cp*Fe[P($OCH_2$)$_3$CEt]$_2$Ph (**4.2**) has been reported in a publication from our group for a study that was focused on oxygen atom insertion into Fe–Ph bonds,[17] but since the synthesis of **4.2** was born out of the project discussed in this Dissertation, it will be discussed here.

As we began investigating Cp*Fe complexes without CO ligands, a general synthetic procedure was sought that would enable to the synthesis of a variety of related complexes. We found that the complex [(tmeda)$FeCl_2$]$_x$ (x = 1,2; tmeda = *N*,*N*,*N'*,*N'*-tetramethylethylenediamine)[18] provided a reasonable starting point where the addition of 2 equivalents of a neutral two-electron donor would displace the tmeda ligand and coordinate the desired ligands. Subsequent reaction with LiCp* would give the desired Cp*Fe(L)$_2$Cl complex. Thus, the sequential treatment of [(tmeda)$FeCl_2$]$_x$ with 2

equivalents of $P(OCH_2)_3CEt$ followed by LiCp* in THF provides $Cp^*Fe[P(OCH_2)_3CEt]_2Cl$ (**4.1**) in 74% yield after work-up as a red-brown solid (Scheme 4.1).

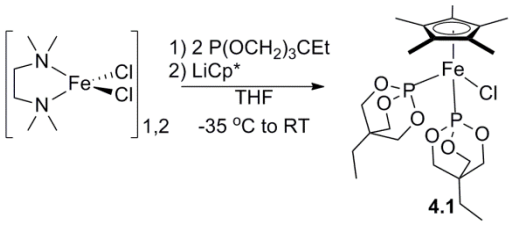


**Scheme 4.1.** Synthesis of $Cp^*Fe[P(OCH_2)_3CEt]_2Cl$ (**4.1**).

The $^1H$ NMR spectrum for complex **4.1** shows a broad singlet at 4.20 ppm for the $–OCH_2$ of $P(OCH_2)_3CEt$ and a singlet at 1.49 ppm for the Cp* methyl protons. The ethyl group of the phosphite shows up as a quartet at 1.22 ppm and a triplet ($^3J_{HH}$ = 7 Hz) at 0.81 ppm (Figure 4.1). Coordination of the phosphite is confirmed by a singlet at 162.9 ppm in the $^{31}P$ NMR spectrum.

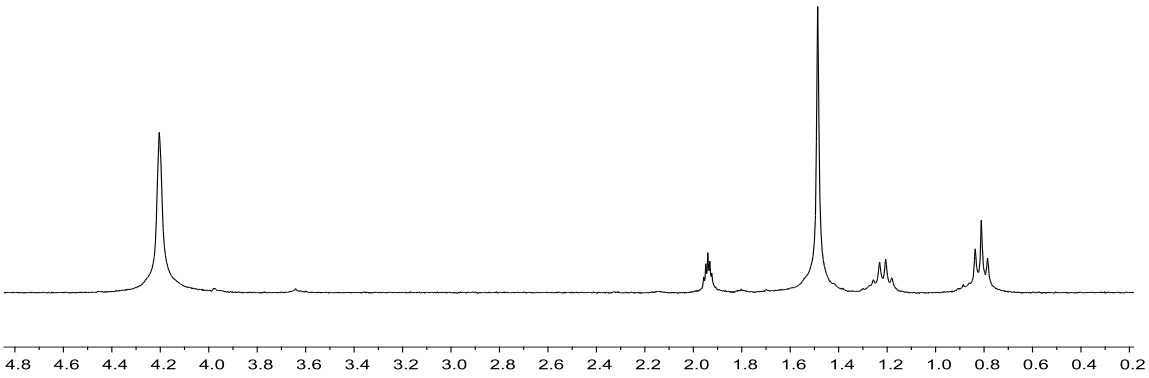


**Figure 4.1.** $^1H$ NMR spectrum of $Cp^*Fe[P(OCH_2)_3CEt]_2Cl$ (**4.1**) in $CD_3CN$.

The reaction of complex **4.1** with excess PhLi (1.5-2 equiv.) in THF at –78 °C followed by warming to room temperature results in a color change of dark red to yellow over the course of approximately 1 h. Filtration through silica gel followed by washing with hexanes or *n*-pentane affords Cp*Fe[P(OCH$_2$)$_3$CEt]$_2$Ph (**4.2**) in 72% yield as a yellow solid (Scheme 4.2). The phenyl protons appear as a doublet at 7.58 ppm, a triplet at 6.75 ppm, and a triplet ($^3J_{HH}$ = 7 Hz for each) at 6.66 ppm in a 2:2:1 ratio (Figure 4.2). The resonance in the $^{31}$P NMR shifts slightly downfield to 166.2 ppm from 162.9 ppm.

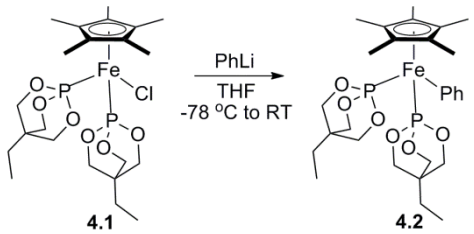


**Scheme 4.2.** Synthesis of Cp*Fe[P(OCH$_2$)$_3$CEt]$_2$Ph (**4.2**).

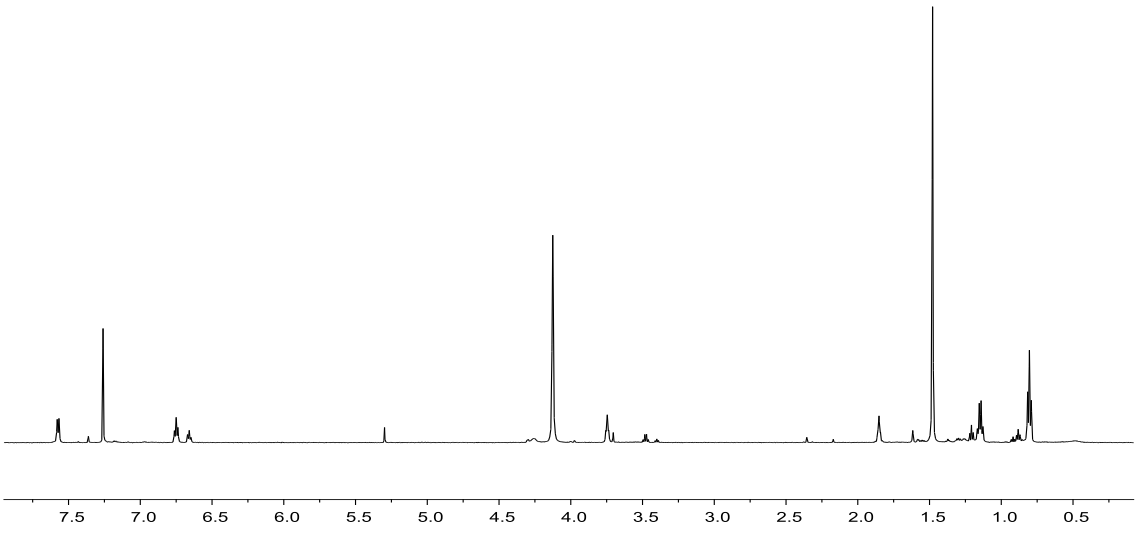


**Figure 4.2.** $^1$H NMR spectrum of Cp*Fe[P(OCH$_2$)$_3$CEt]$_2$Ph (**4.2**) in $CDCl_3$.

X-ray quality crystals were grown by the diffusion of *n*-pentane into a THF solution of **4.2**, and a single crystal X-ray diffraction study allowed for determination of the structure (Figure 4.3). The overall structure is typical have a half-sandwich complex with an Fe–Ph bond measuring 1.9993(2) Å. Despite the expected $C_{2v}$ symmetry, complex **4.2** crystallizes asymmetric with Fe–P bonds of 2.0854(4) Å and 2.0996(4) Å. The Fe–$P(OCH_2)_3CEt$ bond distance in the reported complex $[Fe(C_2H_3O)(CO)_2(P(OCH_2)_3CEt)(C_{10}H_{16}As_2]BF_4$ is 2.217(4) Å, which is slightly elongated compared to those of **4.2**.[19]

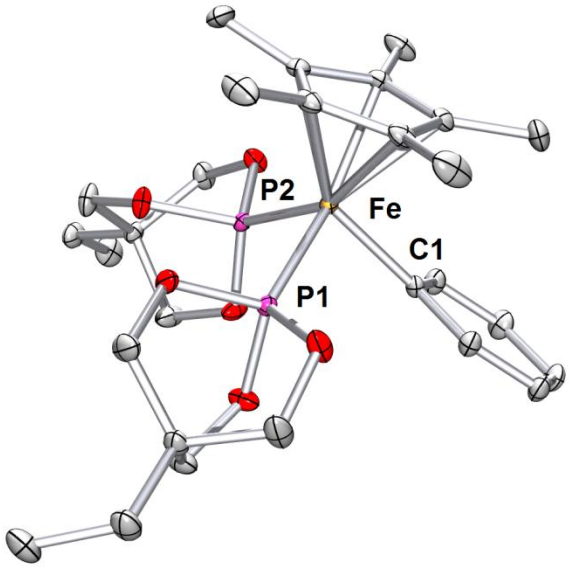


**Figure 4.3.** ORTEP drawing of $Cp^*Fe[P(OCH_2)_3CEt]_2Ph$ (**4.2**) (50% probability ellipsoids; H atoms omitted). Selected bond lengths (Å): Fe–C1 1.9993(2), Fe–P1 2.0854(4), Fe–P2 2.0996(4). Selected bond angles (deg): C1–Fe–P1 92.91(4), C1–Fe–P2 92.73(4), P1–Fe–P2 91.65(2).

### 4.2.3 Reactivity of Cp*Fe[P(OCH$_2$)$_3$CEt]$_2$Ph (4.2) under Thermal Conditions

In order to react with C–H bonds or unsaturated substrates, it is important for the Fe complex **4.2** to generate a coordination site. However, the P(OCH$_2$)$_3$CEt ligands in complex **4.2** are strongly coordinated to the Fe center (see below). The stability of this Fe complex is observed by its thermolysis in $C_6D_6$ (Scheme 4.3). Thermolysis at 70° for ~1 day resulted in no reaction. Repeating thermolysis of complex **4.2** at 100 °C results in no changes to the $^1$H NMR spectrum after 1.5 h, including no evidence for $C_6D_6$ C–D activation. Only after raising the temperature to 140 °C broadening of the $^1$H NMR resonances is observed, likely indicating decomposition to a paramagnetic species. Additionally, heating Cp*Fe[P(OCH$_2$)$_3$CEt]$_2$Ph (**4.2**) in THF-$d_8$ in the presence of $C_2H_4$ (50 psi) resulted in no productive reaction (Scheme 4.3). After heating at 100 °C for approximately 4 days, some broadening of the $^1$H NMR spectrum was observed with starting material and free P(OCH$_2$)$_3$CEt as the only two species observed in the $^{31}$P NMR spectrum. An attempted catalytic reaction using 0.1 mol% of **4.2** and heating to 125 °C in $C_6H_6$ with 25 psi $C_2H_4$ resulted in the observation of 0.25 TO of styrene and trace ethylbenzene by GC/MS (Scheme 4.4). In addition, biphenyl was observed but not quantified.

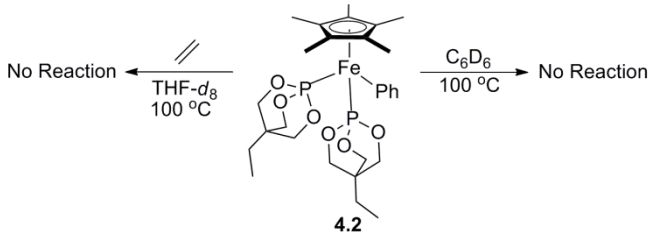


**Scheme 4.3.** No reaction observed during thermolysis of Cp*Fe[P(OCH$_2$)$_3$CEt]$_2$Ph (**4.2**) with $C_6D_6$ or $C_2H_4$.

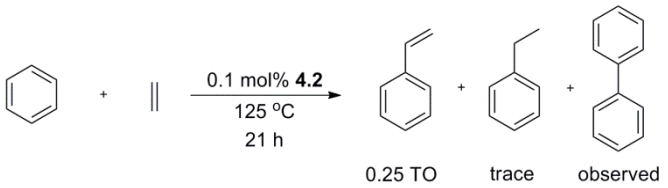


**Scheme 4.4.** Attempted ethylene hydrophenylation using 0.1 mol% **4.2** in $C_6H_6$ (3 mL) at 125 °C with 25 psi $C_2H_4$ for 21 h.

To further explore the lability of $P(OCH_2)_3CEt$, complex **4.2** was combined in $CD_3CN$ with excess $PMe_3$ and heated at 70 °C over the course of ~2 days (Scheme 4.5). Partial conversion (~30%) to $Cp^*Fe[P(OCH_2)_3CEt](PMe_3)Ph$ was observed by $^{31}P$ NMR spectroscopy. $Cp^*Fe[P(OCH_2)_3CEt](PMe_3)Ph$ is characterized by two doublets ($^2J_{PP}$ = 104 Hz) at 165.9 ppm for $P(OCH_2)_3CEt$ and 33.4 ppm for $PMe_3$.[17] Clearly, the substitution was quite slow under these conditions. We later discovered that this reaction is promoted by visible light photolysis (see below).[17]

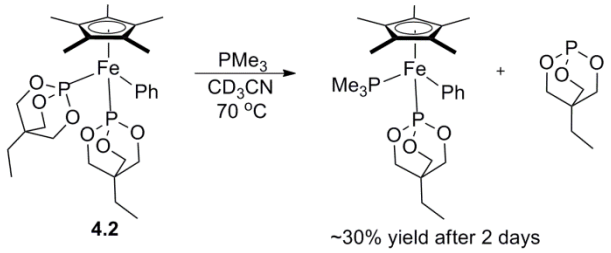


**Scheme 4.5.** Reaction of $Cp^*Fe[P(OCH_2)_3CEt]_2Ph$ (**4.2**) with excess $PMe_3$.

### 4.2.4 Attempted Synthesis of $Cp^*Fe[P(OCH_2)_3CEt](L)R$ (L = labile ligand, R = Me, Ph)

Due to the strong coordinating ability of the $P(OCH_2)_3CEt$ ligand, we investigated procedures to access a complex of the type $Cp^*Fe[P(OCH_2)_3CEt](L)R$ (L = labile ligand, R = Me, Ph). Scheme 4.6 summarizes the three synthetic approaches studied: 1) Photolytic or thermal substitution of $P(OCH_2)_3CEt$ in complex **4.2** with a labile ligand; 2) sequential addition of a labile ligand and $P(OCH_2)_3CEt$ to $[(tmeda)FeCl_2]_x$ then alkylation

to give the desired complex; and 3) synthesis of Cp*Fe[P(OCH$_2$)$_3$CEt](acac) (acac = acetylacetonate) followed by addition of labile ligand and methylation to give Cp*Fe[P(OCH$_2$)$_3$CEt](L)Me.[12]

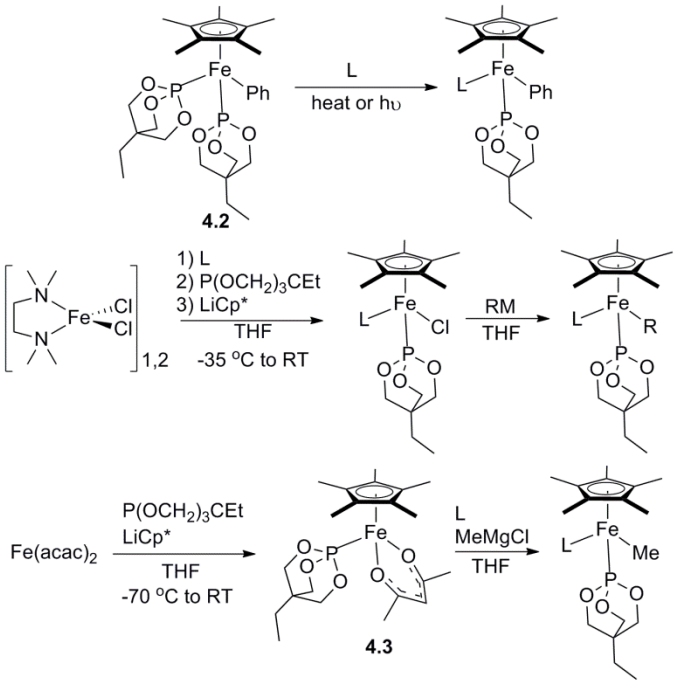


**Scheme 4.6.** Synthetic pathways for Cp*Fe[P(OCH$_2$)$_3$CEt](L)R (L = labile ligand, R = Me, Ph).

We found that heating or photolyzing complex **4.2** in NCMe or pyridine resulted in no evidence of ligand substitution. Under prolonged reaction times, gradual decomposition of the starting material is observed, as evidenced by broadening of the $^1$H NMR spectrum, observation of solid in the NMR tube, and/or observation of free P(OCH$_2$)$_3$CEt with no new $^{31}$P NMR resonances. Additionally, attempts to treat [(tmeda)FeCl$_2$]$_x$ with a labile ligand (e.g., NCMe, pyridine, PPh$_3$) followed by the addition of P(OCH$_2$)$_3$CEt results in the coordination of 2 equivalents of P(OCH$_2$)$_3$CEt, which is confirmed by comparison of the NMR data with that of complex **4.1**.

Bercaw and co-workers have previously reported the synthesis of Cp*Fe($PMe_3$)(acac) that reacts with $PMe_3$ and MeMgCl to yield Cp*Fe($PMe_3$)$_2$Me.[12] It seemed reasonable that generation of Cp*Fe[$P(OCH_2)_3CEt$](acac) followed by the sequential addition of a labile ligand and MeMgCl might allow for the synthesis of Cp*Fe[$P(OCH_2)_3CEt$](L)Me.

Thus, the low temperature (–70 °C) reaction of Fe(acac)$_2$ with LiCp* and $P(OCH_2)_3CEt$ in THF followed by warming to room temperature produced Cp*Fe[$P(OCH_2)_3CEt$](acac) (**4.3**). The $^1$H NMR spectrum of **4.3** shows two singlets at 5.14 and 1.88 ppm for the acac ligand. The resonances for $P(OCH_2)_3CEt$ are observed at 3.77 ppm for the –$OCH_2$ groups and 0.24 ppm and 0.08 ppm for the ethyl group (Figure 4.4). Due to challenges consistently isolating pure material, which is a result for the very high solubility of **4.3**, this synthetic route was eventually abandoned. The crude reaction product is typically contaminated with excess free $P(OCH_2)_3CEt$. If the methylation is performed with any free $P(OCH_2)_3CEt$, Cp*Fe[$P(OCH_2)_3CEt$]$_2$Me is the major product.

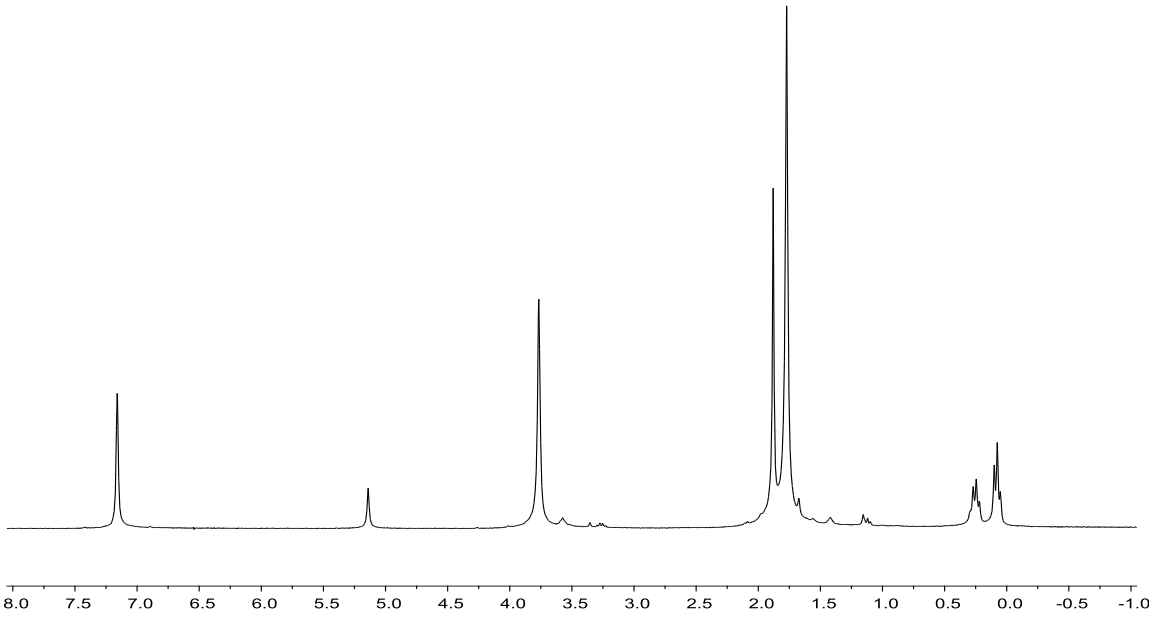


**Figure 4.4.** $^{1}$H NMR spectrum of Cp*Fe[P(OCH$_2$)$_3$CEt](acac) (**4.3**) in $C_6D_6$. This highly pure sample is not consistently obtained.

### 4.2.5 Reactivity of Cp*Fe[P(OCH$_2$)$_3$CEt]$_2$Ph (4.2) under Photolytic Conditions

During the course of our studies on oxygen atom insertion into the Fe–Ph bond of Cp*Fe[P(OCH$_2$)$_3$CEt]$_2$Ph (**4.2**), Dr. Jiajun Mei discovered that the oxy-insertion reaction is facilitated by photolysis.[17] Successful oxygen atom insertion produced phenol, but in the absence of light, the generation of phenol is not observed. Also, phenol production is accelerated under photolysis (compared to under ambient light). It has been hypothesized that photolysis aids in the dissociation of P(OCH$_2$)$_3$CEt. Evidence for this hypothesis was obtained by photolyzing Cp*Fe[P(OCH$_2$)$_3$CEt]$_2$Ph (**4.2**) in the presence of excess PMe$_3$ (Scheme 4.7). Within 1 h, complete conversion to Cp*Fe[P(OCH$_2$)$_3$CEt](PMe$_3$)Ph was observed. Kinetic studies indicated that dissociation of P(OCH$_2$)$_3$CEt is rate limiting during the ligand substitution reaction.[17] The photolytic reaction of **4.2** and PMe$_3$

provides rationale for why the thermal reaction of **4.2** and $PMe_3$ mentioned above was so sluggish—ambient light, not heat, was responsible for the observed reaction.

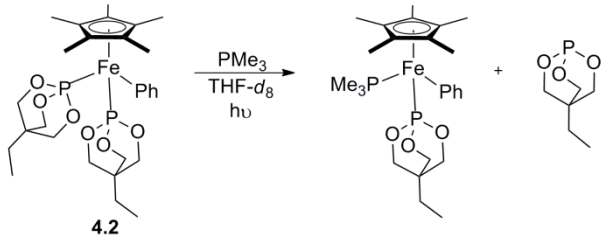


**Scheme 4.7.** Photolytic reaction of $Cp^*Fe[P(OCH_2)_3CEt]_2Ph$ (**4.2**) with $PMe_3$.[17]

Photolysis of **4.2** in the presence of labile ligands such as NCMe or pyridine results in no reaction. It is possible that the photolytic reactions of **4.2** with NCMe or pyridine are not thermodynamically favorable. Thus, we wondered whether photolysis would generate a coordinatively unsaturated Fe complex that could react with aromatic C–H bonds or olefin and alkynes and ultimately catalyze olefin or alkyne hydroarylation. To test the possibility that photolysis of complex **4.2** could generate the coordinatively unsaturated intermediate $Cp^*Fe[P(OCH_2)_3CEt]Ph$ and react with aromatic C–H bonds in order to determine feasibility of olefin hydroarylation, $Cp^*Fe[P(OCH_2)_3CEt]_2Ph$ (**4.2**) was photolyzed in $C_6D_6$ (Scheme 4.8). Unfortunately, no evidence for $C_6D_6$ activation was observed by $^1H$ NMR spectroscopy. One explanation for the lack of reactivity is that the rate of benzene coordination and C–D activation is slower than the rate of re-coordination of $P(OCH_2)_3CEt$ (i.e., $k_2 << k_{-1}$ in Scheme 4.8).

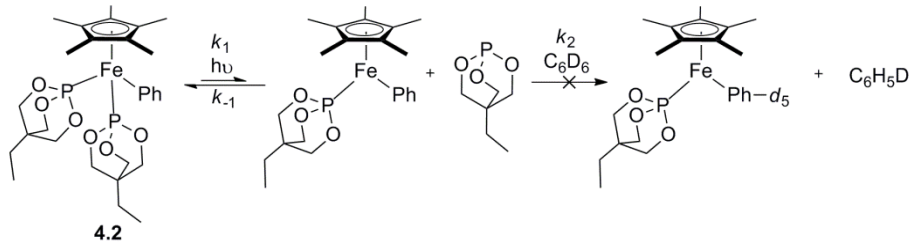


**Scheme 4.8.** Photolysis of Cp*Fe[P(OCH$_2$)$_3$CEt]$_2$Ph (**4.2**) in $C_6D_6$ does not results in $C_6D_6$ activation.

Given our hypothesis that the slower rate of benzene coordination and C–H activation compared to phosphite re-coordination was responsible for the lack of benzene C–H activation, it was hoped that furan would provide a better ligand than benzene.[20] Harman and co-workers have shown that in π-basic metal fragments, furan coordinates more strongly in an $\eta^2$ fashion than benzene does.[20] This is exemplified in the half-lives of $[Os(NH_3)_5(L)]^+$ (L = $\eta^2$-benzene or $\eta^2$-furan) complexes in NCMe. The half-life for substitution of $\eta^2$-benzene by NCMe is 5.5 h at 25 °C, while the half-life for substitution with $\eta^2$-furan is 4 h at 100 °C. The reason for this is the more significant π-back bonding from the metal to the furan π* orbital compared to that to the benzene π* orbital.[20] Additionally, in our study of aromatic C–H activation by Cp*Fe(CO)(NCMe)Ph (see Chapter 2), we observed a significantly faster rate for the activation of the furan C–H bond over the benzene C–H bond.[2] Thus, we reasoned that the rate of furan C–H activation by Cp*Fe[P(OCH$_2$)$_3$CEt]$_2$Ph (**4.2**) might be observed under photolytic conditions.

Photolysis of Cp*Fe[P(OCH$_2$)$_3$CEt]$_2$Ph (**4.2**) with excess furan results in the liberation of $C_6H_6$ and the generation of a new complex identified as Cp*Fe[P(OCH$_2$)$_3$CEt]$_2$(2-furyl) (**4.4**) (Scheme 4.9). This result, where Cp*Fe[P(OCH$_2$)$_3$CEt]$_2$Ph (**4.2**) has been shown to activate aromatic C–H bonds, adds this

complex to the short list of Fe complexes capable of aromatic C–H activation. Scaling up the reaction and purifying by re-crystallization from diethyl ether and *n*-pentane at –35 °C gave the desired complex **4.4** in 39% isolated yield. The modest yields are a result of purifying the product as opposed to low conversion of the starting material. Complex **4.4** is characterized by three broad singlets in the downfield region of the $^{1}$H NMR spectrum at 7.58 ppm, 6.07 ppm, and 5.97 ppm for the furyl resonances (Figure 4.5). The presence of one resonance downfield at 7.58 ppm is consistent with one proton that is adjacent to the oxygen, which suggests selective activation of the furan 2-position. The $^{31}$P NMR spectrum of **4.4** has a singlet at 168.1 ppm, which demonstrates the persistence of the coordinated phosphite ligands.

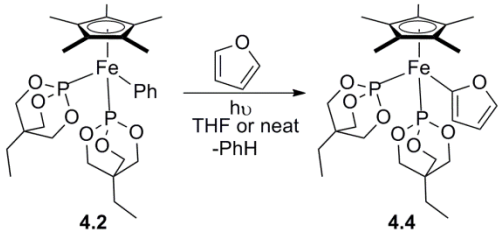


**Scheme 4.9.** Synthesis of Cp*Fe[P(OCH$_2$)$_3$CEt]$_2$(2-furyl) (**4.4**).

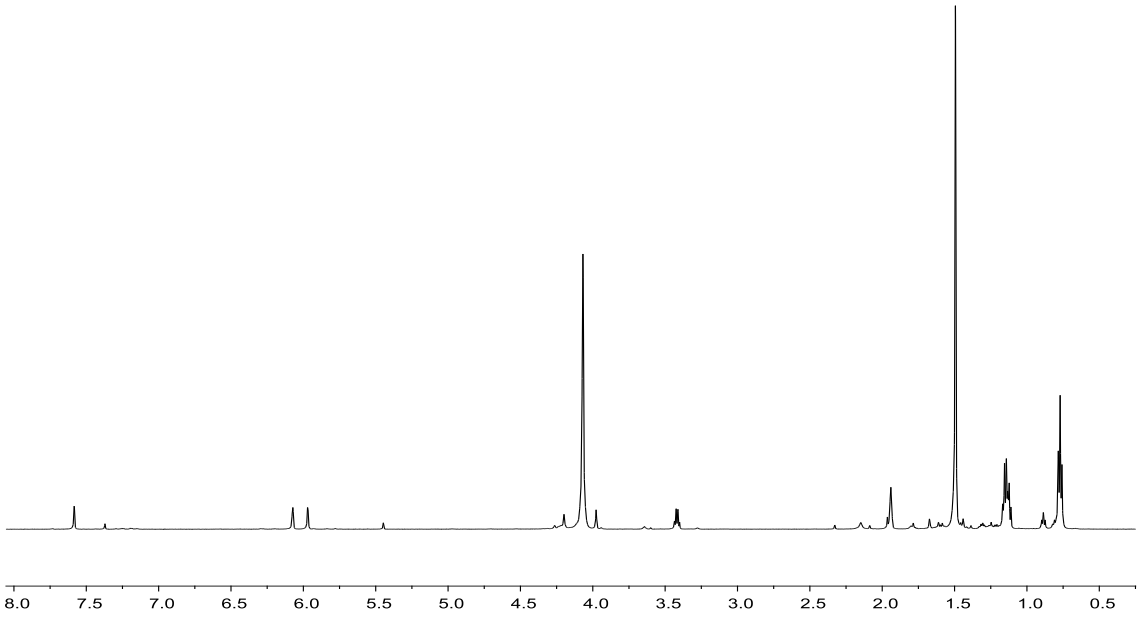


**Figure 4.5.** $^{1}$H NMR spectrum of Cp*Fe[P(OCH$_2$)$_3$CEt]$_2$(2-furyl) (**4.4**) in CD$_3$CN.

Cooling a saturated solution of **4.4** in a 1:1 mixture of diethyl ether and *n*-pentane resulted in the formation of crystals that were suitable for an X-ray diffraction study (Figure 4.6). Like complex **4.2**, the structure of **4.4** is piano stool with the ~90° bond angles for the non-Cp* ligands. The Fe–C$_{furyl}$ bond is 1.930(5) Å, which is approximately 0.07 Å shorter than the Fe–Ph bond of **4.2**. This may be a reflection of the stronger Fe–C bond of the Fe–furyl over the Fe–Ph.[2]

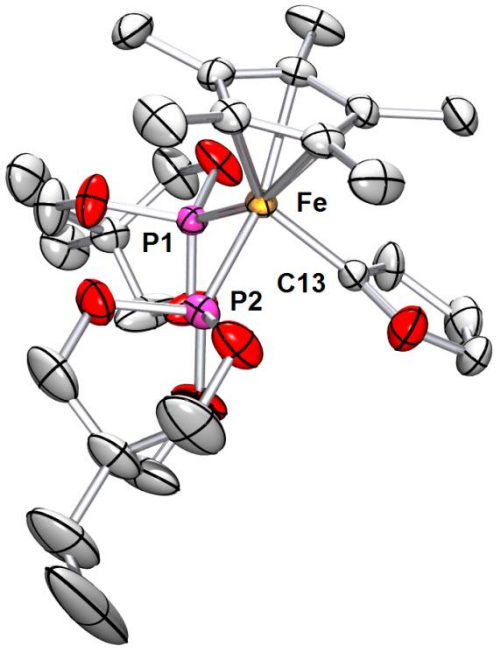


**Figure 4.6.** ORTEP diagram of Cp*Fe[P(OCH$_2$)$_3$CEt]$_2$(2-furyl) (**4.4**) (30% probability ellipsoids, H atoms omitted). Selected bond lengths (Å): Fe–C13 1.930(5), Fe–P1 2.096(1), Fe–P2 2.075(1). Selected bond angles (deg): C13–Fe–P1 90.8(2), C13–Fe–P2 91.1(1), P1–Fe–P2 92.27(5).

Since photolysis can generate free radicals via M–L bond homolysis (e.g., possible Fe–Ph bond homolysis from **4.2**), we probed whether free radicals were involved in the photolytic C–H activation of furan. Cp*Fe[P(OCH$_2$)$_3$CEt]$_2$Ph (**4.2**) was photolyzed with excess 2-methylfuran. As explained in Chapter 2, the selectivity of the C–H bond activation of 2-methylfuran provides insight into whether or not free radicals are involved. If free radicals are involved, one would expect activation of the weaker C–H bond of the methyl group (BDE = 86 kcal/mol)[21] over the activation of an aromatic C–H bond (BDE = 120 kcal/mol).[21]

Indeed, the photolytic reaction of Cp*Fe[P(OCH$_2$)$_3$CEt]$_2$Ph (**4.2**) and 2-methylfuran results in the isolation of Cp*Fe[P(OCH$_2$)$_3$CEt]$_2$[2-(5-methylfuryl)] (**4.5**) in 60% yield (Scheme 4.10). The diagnostic peak in the $^1$H NMR spectrum that indicates the

selectivity for activation of the aromatic C–H bond is the presence of a singlet that integrates for three protons at 2.19 ppm, which corresponds to the methyl group on the furyl ring (Figure 4.7). Additionally, two furyl resonances are observed at 5.80 ppm and 5.60 ppm, which are likely due to the furyl 3- and 4-positions. The $^{31}$P NMR spectrum has a singlet at 168.1 ppm, demonstrating that the phosphite ligands are still coordinated to the Fe center.

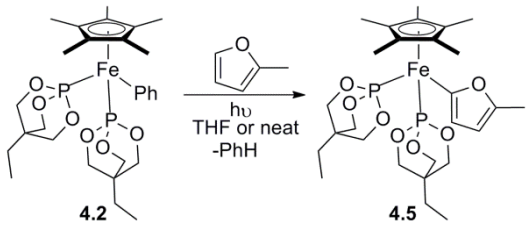


**Scheme 4.10.** Synthesis of Cp*Fe[P(OCH$_2$)$_3$CEt]$_2$[2-(5-methylfuryl)] (**4.5**).

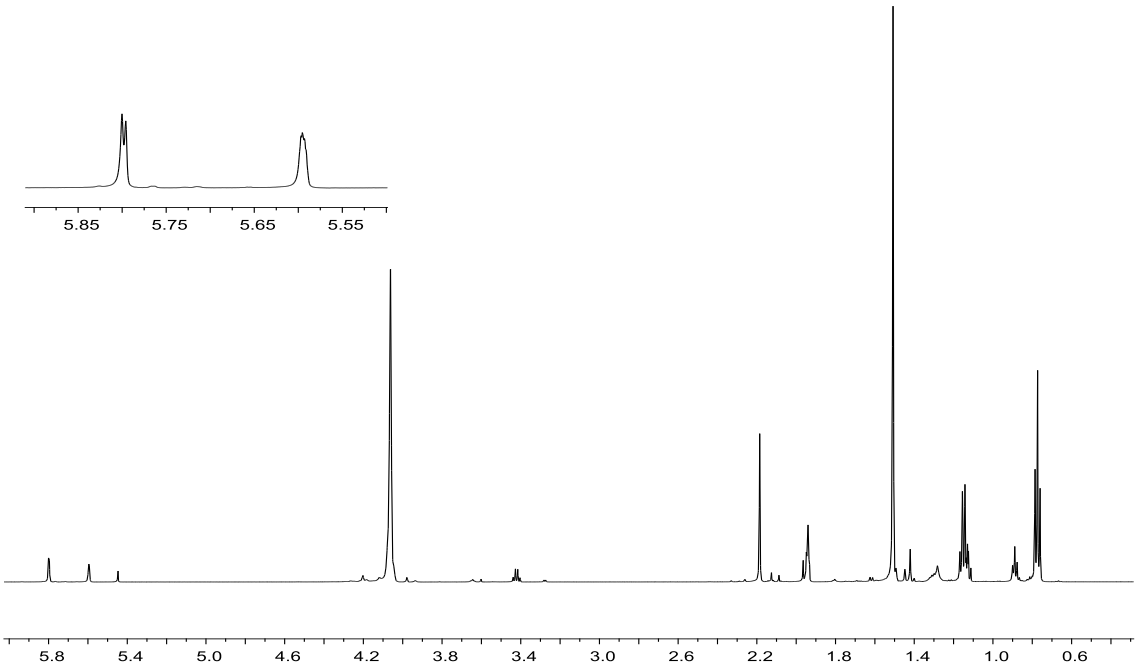


**Figure 4.7.** $^{1}$H NMR spectrum of Cp*Fe[P(OCH$_2$)$_3$CEt]$_2$[2-(5-methylfuryl)] (**4.5**) in CD$_3$CN.

A mixture of **4.2** and excess thiophene was photolyzed. In contrast to the reactions with furan and 2-methylfuran, rather than staying yellow, the reaction mixture turned deep purple. Monitoring the reaction by $^{31}$P NMR spectroscopy revealed the presence of at least two products. The ratio of these two products varied significantly from reaction to reaction. For instance, when the reaction was performed in neat thiophene, we consistently observed a purple reaction solution with one product that is characterized by a $^{31}$P NMR resonance at 159 ppm. According to $^{31}$P NMR spectroscopy, approximately one equivalent of $P(OCH_2)_3CEt$ is liberated during the course of the reaction. Based on these preliminary observations, we hypothesized that this product was not a result of thiophene C–H activation (see below).

The purple product from the reaction of **4.2** and neat thiophene has excellent solubility in common organic solvents. The $^1$H NMR spectrum shows resonances consistent with a phenyl ligand at 7.84 ppm, 7.39 ppm, and 7.28 ppm in a 2:1:2 ratio (Figure 4.8). The only other ligands apparent by $^1$H NMR spectroscopy are one $P(OCH_2)_3CEt$ ligand and the Cp* ligand. Single crystals suitable for an X-ray diffraction study were grown by cooling an *n*-pentane solution of the product, allowing it to be unambiguously assigned as Cp*Fe[$P(OCH_2)_3CEt$]($\kappa^2$-SC(S)Ph) (**4.6**) (Figure 4.9). The C–S bond lengths of **4.6** are nearly identical [1.687(4) Å and 1.683(4) Å], which are consistent with delocalized π-electrons in the $CS_2$ fragment. In the complex $Fe(CO)_3Br(S_2CNEt_2)$ the C–S bond lengths both measure 1.712(2) Å.[22] The Fe–S bond distances are 2.265(1) Å and 2.264(1) Å, which is also consistent with the reported $Fe(CO)_3Br(S_2CNEt_2)$ complex (Fe–S bond distances = 2.3119(4) Å and 2.3127(5) Å).[22]

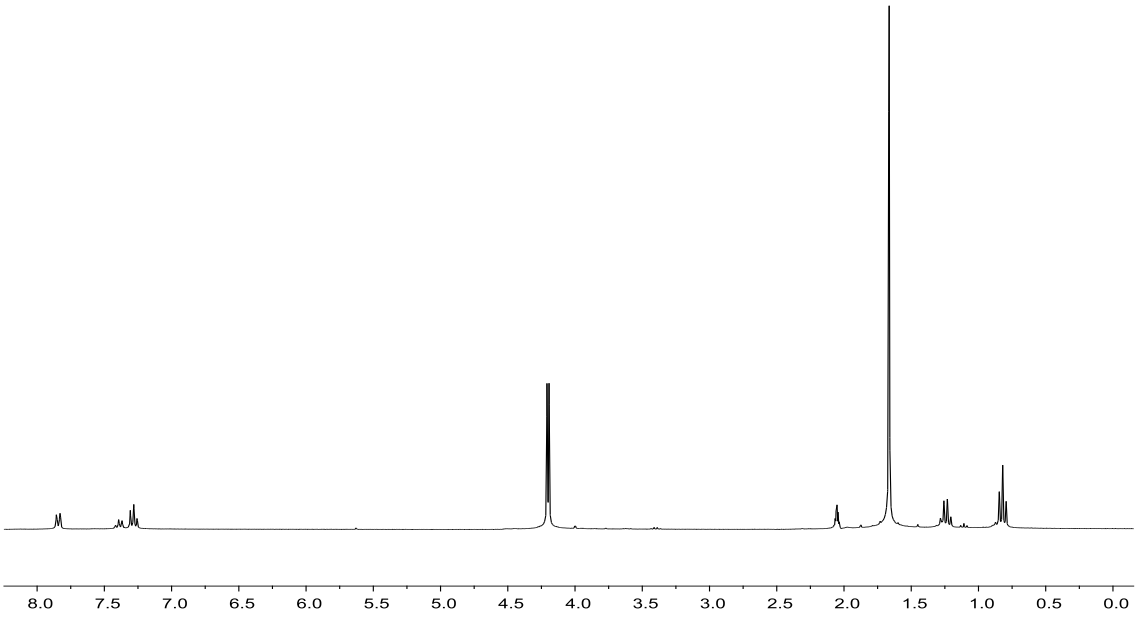


**Figure 4.8.** $^{1}$H NMR spectrum of Cp*Fe[P(OCH$_2$)$_3$CEt](κ$^2$-SC(S)Ph) (**4.6**) in acetone-$d_6$.

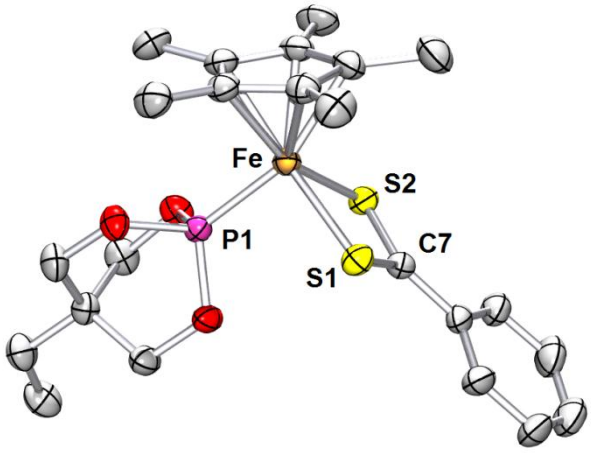


**Figure 4.9.** ORTEP diagram of Cp*Fe[P(OCH$_2$)$_3$CEt](κ$^2$-SC(S)Ph) (**4.6**) (50% probability ellipsoids; H atoms omitted). Selected bond lengths (Å): Fe–P1 2.108(1), Fe–S1 2.265(1), Fe–S2 2.264(1), S1–C7 1.687(4), S2–C7 1.683(4). Selected bond angles (deg): S1–Fe–P1 97.09(4), P1–Fe–S2 91.36(4), S1–Fe–S2 74.57(4).

For the formation of **4.6**, we initially considered that Cp*Fe[P(OCH$_2$)$_3$CEt]$_2$Ph (**4.2**) could be mediating C–S bond cleavages, but the complexity of the reaction and the inability to find organic by-products suggested another explanation. Also, several

observations provided evidence *against* Fe-mediated desulfurization of thiophene as the pathway to **4.6**. First, we did not observe analogous reactivity with other thiophenes, including benzothiophene, 2-methylthiophene, 2,5-dimethylthiophene, 3-methylthiophene, and 2-acetylthiophene. In these cases, low conversion to suspected C–H bond activated products was typically observed. In addition, depending on the reaction, varying amounts of $S{=}P(OCH_2)_3CEt$ were identified by $^{31}P$ NMR spectroscopy.[23] Photolyzing $P(OCH_2)_3CEt$ in thiophene confirmed that $S{=}P(OCH_2)_3CEt$ was forming from the reaction of free $P(OCH_2)_3CEt$ with either thiophene or an impurity in the thiophene. A sample $^{31}P$ NMR spectrum of the crude reaction can be seen in Figure 4.10. Because the product **4.6** appears to be the result of a net insertion of $CS_2$, the reaction of $Cp^*Fe[P(OCH_2)_3CEt]_2Ph$ (**4.2**) and $CS_2$ was performed under photolytic conditions. The major product from this reaction is complex **4.6**. Therefore, it seemed likely that the formation of **4.6** from complex **4.2** in thiophene was resulting from the presence of $CS_2$ impurity in the thiophene. Additionally, we have confirmed that $S{=}P(OCH_2)_3CEt$ forms from the reaction of $P(OCH_2)_3CEt$ and $CS_2$ (Scheme 4.11). GC/MS analysis of the thiophene used in the above reactions confirmed the presence of a $CS_2$ impurity. Thus, the actual reaction is the insertion of $CS_2$ into the Fe–Ph bond of complex **4.2** (Scheme 4.12).

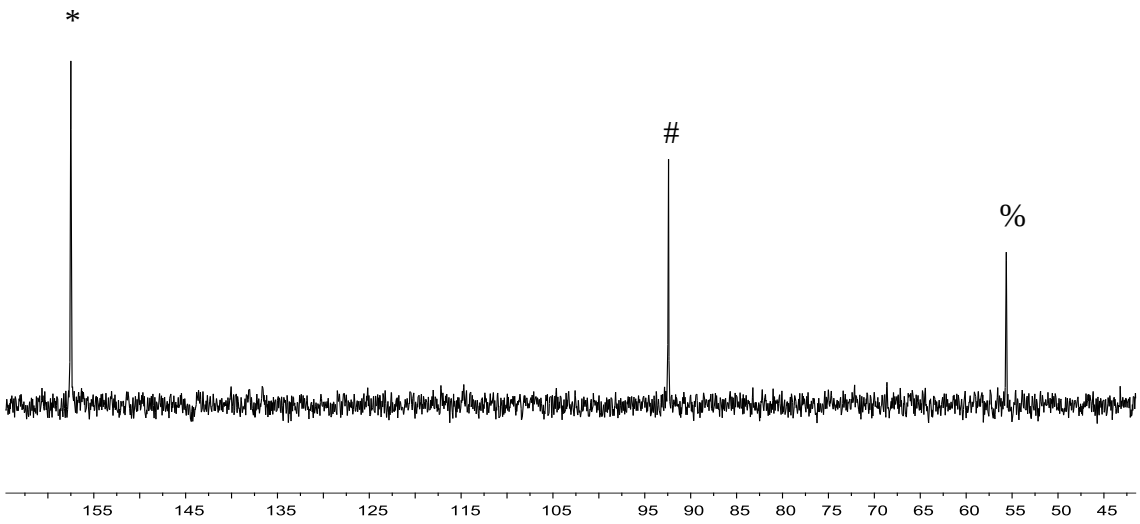


**Figure 4.10.** $^{31}$P NMR spectrum from the reaction of Cp*Fe[P(OCH$_2$)$_3$CEt]$_2$Ph (**4.2**) and thiophene showing resonances for Cp*Fe[P(OCH$_2$)$_3$CEt](κ$^2$-SC(S)Ph) (**4.6**) (*), free P(OCH$_2$)$_3$CEt (#) and S=P(OCH$_2$)$_3$CEt (%).

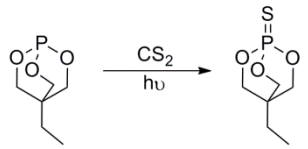


**Scheme 4.11.** The reaction of P(OCH$_2$)$_3$CEt and CS$_2$.

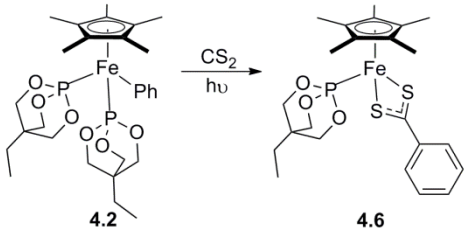


**Scheme 4.12.** The reaction of Cp*Fe[P(OCH$_2$)$_3$CEt]$_2$Ph (**4.2**) and CS$_2$ to give Cp*Fe[P(OCH$_2$)$_3$CEt](κ$^2$-SC(S)Ph) (**4.6**).

The insertion of CS$_2$ into the Fe–Ph bond of Cp*Fe[P(OCH$_2$)$_3$CEt]$_2$Ph (**4.2**) occurs much more readily than the C–H activation of thiophene (i.e., a couple hours vs 2 days). In order to probe whether complete conversion of **4.2** to Cp*Fe[P(OCH$_2$)$_3$CEt]$_2$(2-

thienyl) (**4.7**) could occur under photolytic conditions, we utilized analytical grade thiophene instead of the reagent grade that had been used previously. By using a higher purity thiophene, we find that the C–H activation of the 2-position of thiophene by **4.2** occurs with high selectivity; however, we typically still observe trace formation of complex **4.6** by $^{31}$P NMR spectroscopy (Scheme 4.13). Conveniently, complexes **4.6** and **4.7** can be separated using silica gel chromatography. By this method, we have been able to isolate Cp*Fe[P(OCH$_2$)$_3$CEt]$_2$(2-thienyl) (**4.7**) in 46% yield with relatively good purity by $^{1}$H NMR spectroscopy (Figure 4.11). A multiplet at 7.12 ppm that integrates for one proton and overlapping multiplets at 6.80 ppm that integrate for two protons are evidence for selective activation of the 2-position of thiophene. The $^{31}$P NMR spectrum has a singlet at 167.6 ppm, which is consistent with coordinated P(OCH$_2$)$_3$CEt. Unfortunately, due to the slow reaction, inconsistent conversions, and challenges separating the starting material **4.2** from the product **4.7**, the isolated product is typically contaminated with the starting material Cp*Fe[P(OCH$_2$)$_3$CEt]$_2$Ph (**4.2**). We have observed that from reaction to reaction, the rate can vary significantly. For example, in some cases the reaction is complete within 2 days of photolysis, while other times the reaction has not even reached 50% conversion during the same time period. Currently, we are still studying how to increase conversions of this reaction and isolate consistently pure material (see Chapter 7 for more information).

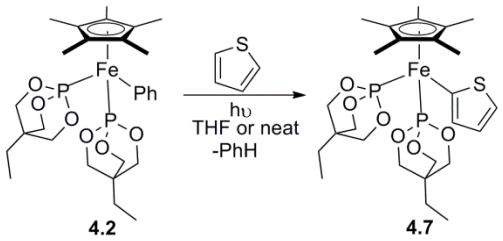


**Scheme 4.13.** Synthesis of Cp*Fe[P(OCH$_2$)$_3$CEt]$_2$(2-thienyl) (**4.7**).

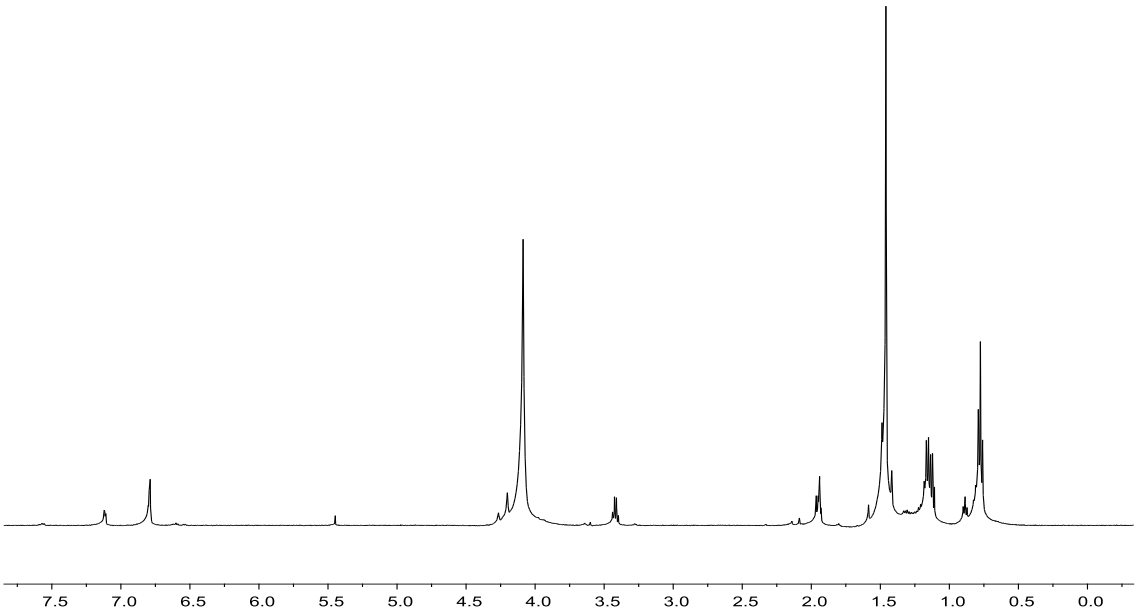


**Figure 4.11.** $^{1}$H NMR spectrum of Cp*Fe[P(OCH$_2$)$_3$CEt]$_2$(2-thienyl) (**4.7**) in CD$_3$CN.

Work has also been directed to more fully understanding the substrate scope of these photolytic C–H activations by Cp*Fe[P(OCH$_2$)$_3$CEt]$_2$Ph (**4.2**). Thus far, we have only observed clean C–H activation reactions with furan, 2-methylfuran and thiophene. Other substrates studied that were not activated include benzene, pentafluorobenzene, thiazole, *N*-methylpyrazole and 2,5-dimethylfuran (Figure 4.12). In each of these cases, over prolonged reaction times gradual decomposition of the starting material **4.2** is observed with no evidence for the formation of a new phosphite containing product. It is worth highlighting that C–H activation was not observed with 2,5-dimethylfuran. This substrate was chosen to probe whether C–H activation at the 3-position was possible. The lack of C–H activation of 2,5-dimethylfuran might be a result of the more hindered 3-position from the presence of the methyl groups.

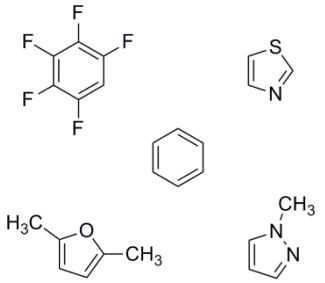

**Figure 4.12**. Substrates where no photolytic C–H activation was observed using Cp*Fe[P(OCH$_2$)$_3$CEt]$_2$Ph (**4.2**).

Since furan C–H activation using Cp*Fe[P(OCH$_2$)$_3$CEt]$_2$Ph (**4.2**) has been observed under photolytic conditions, it is reasonable that catalytic ethylene hydroarylation with furan might be achieved using photolysis. Thus, Cp*Fe[P(OCH$_2$)$_3$CEt]$_2$(2-furyl) (**4.4**) was generated in situ in THF-$d_8$, treated with excess furan (50 equiv.) and $C_2H_4$ (30 psi), and the solution was photolyzed while periodically monitoring by NMR spectroscopy (Scheme 4.14). 2-Ethylfuran was not observed under these conditions, which is consistent with the lack of reactivity observed for Cp*Fe(CO)(NCMe)(2-furyl) toward ethylene (see Chapter 3). Instead, gradual decomposition of the starting material was observed, as evidenced by substantial solid formation and broadening of the NMR resonances.

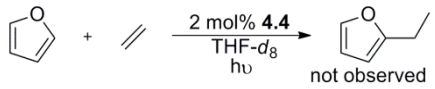


**Scheme 4.14.** Attempted ethylene hydroarylation with furan by Cp*Fe[P(OCH$_2$)$_3$CEt]$_2$(2-furyl) (**4.4**) with 30 psi $C_2H_4$ in THF-$d_8$.

We have also begun to investigate the potential of Cp*Fe[P(OCH$_2$)$_3$CEt]$_2$(2-furyl) (**4.4**) to serve as a catalyst for alkyne hydroarylation with furan. Based on the results reported in Chapter 3, where the reactivity of Cp*Fe(CO)(NCMe)Ph with alkynes results

in hydroxyindenyl formation involving CO insertion, we hoped that the absence of a CO ligand would enable catalytic turnover.[1] Unfortunately, this is not the case. It should be noted that this work is ongoing, but preliminary studies indicate that, again, intramolecular reactivity is dominant for the reactions of Cp*Fe[$P(OCH_2)_3CEt]_2$(2-furyl) (**4.4**) with alkynes.

The photolytic reaction of Cp*Fe[$P(OCH_2)_3CEt]_2$(2-furyl) (**4.4**), which is generated in situ, and excess 2-butyne leads to the formation of a deep red solution even in the presence of excess furan. While monitoring the reaction by $^{31}$P NMR spectroscopy, it is apparent that the reaction leads to an Fe complex without $P(OCH_2)_3CEt$ coordinated. Figure 4.13 shows a $^1$H NMR spectrum of the product after workup. Based on NMR spectroscopy, with the aid of two-dimensional NMR spectroscopy (HMQC and HMBC, Figures 4.14 and 4.15), the product is assigned as Cp*Fe[$\eta^5$-$C_5Me_4$(CH=CHCHO)] (**4.8**) (Scheme 4.15).

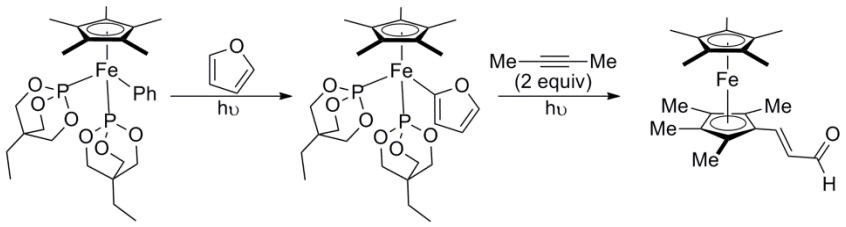


**Scheme 4.15.** Formation of Cp*Fe[$\eta^5$-$C_5Me_4$(CH=CHCHO)] (**4.8**) from the reaction of Cp*Fe[$P(OCH_2)_3CEt]_2$Ph (**4.2**) and furan followed by 2-butyne under photolytic conditions.

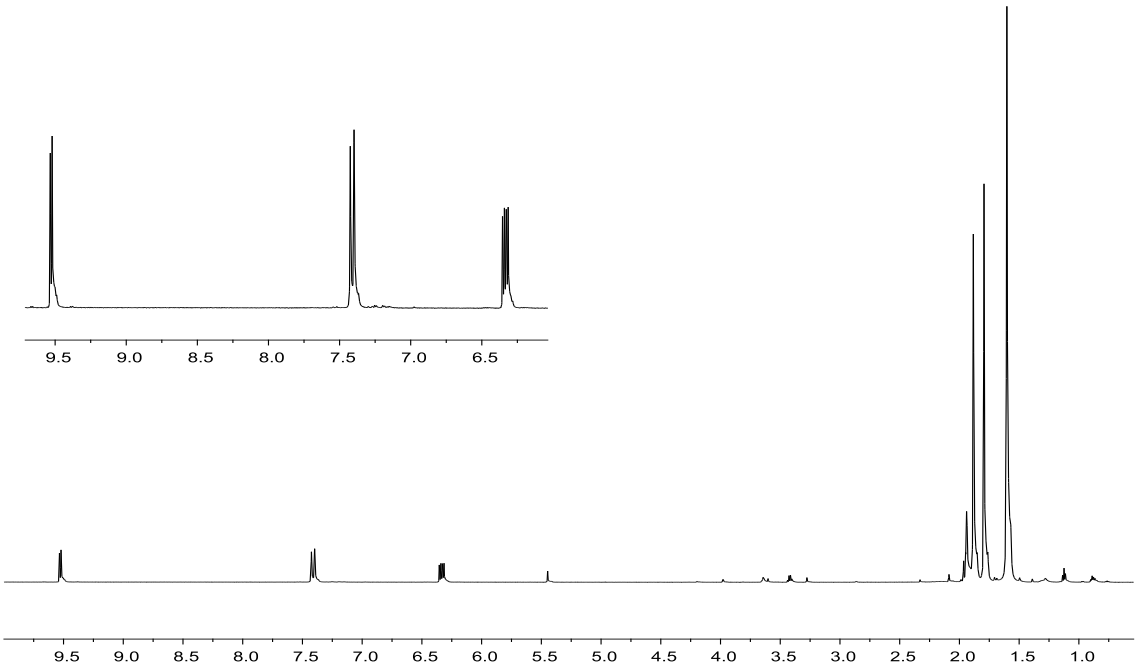


**Figure 4.13.** $^{1}$H NMR spectrum of Cp*Fe[$\eta^5$-$C_5Me_4$(CH=CHCHO)] (**4.8**) in $CD_3CN$.

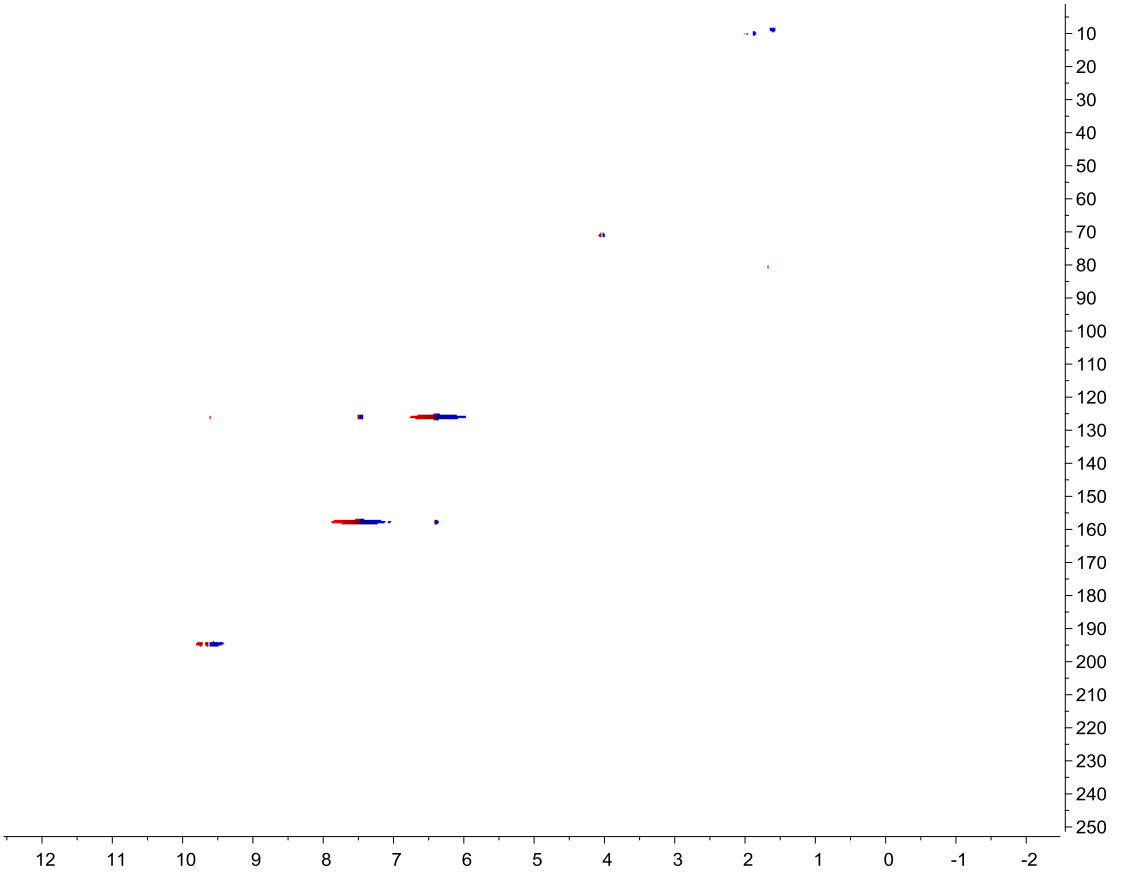


**Figure 4.14.** HMQC spectrum of Cp*Fe[$\eta^5$-$C_5Me_4$(CH=CHCHO)] (**4.8**) in $CD_3CN$. Small amount of $P(OCH_2)_3CEt$ is present in this sample (>90% pure).

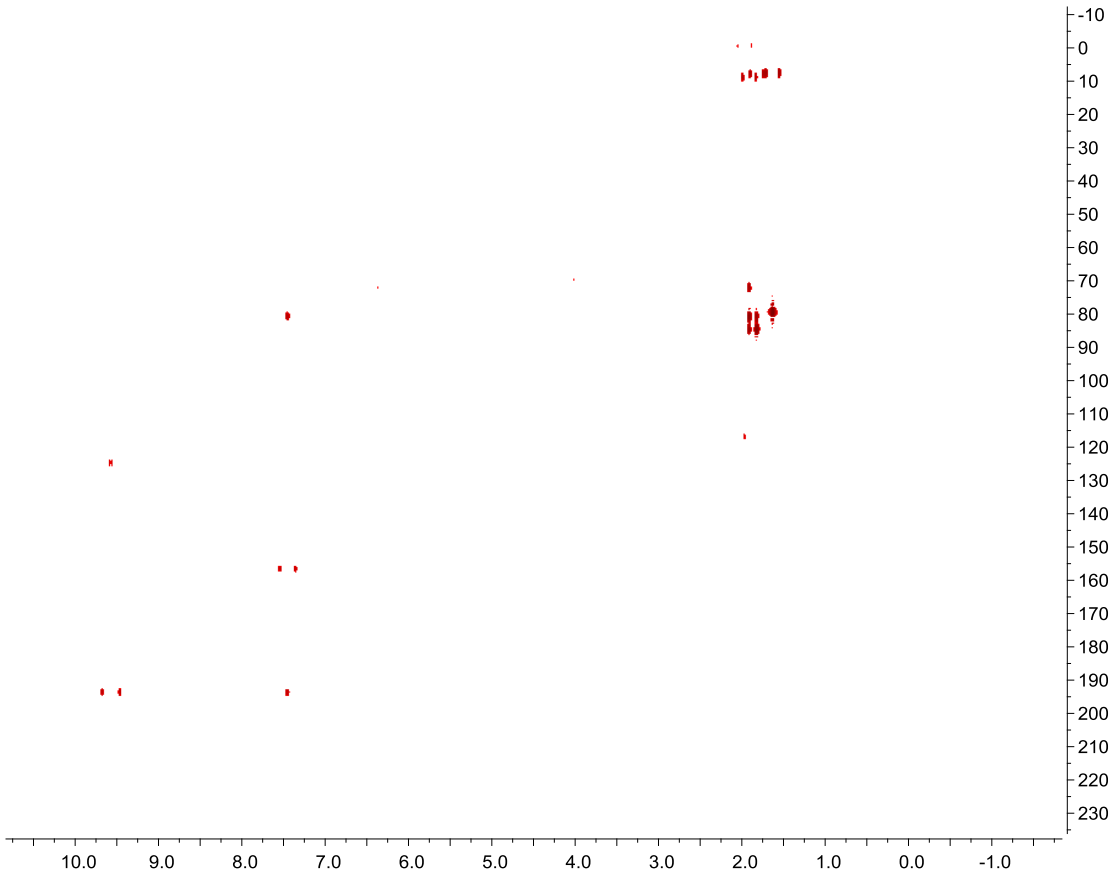


**Figure 4.15.** HMBC spectrum of Cp*Fe[$\eta^5$-$C_5Me_4$(CH=CHCHO)] (**4.8**) in $CD_3CN$. Small amount of $P(OCH_2)_3CEt$ is present in this sample (>90% pure).

The $^1$H NMR spectrum shows a doublet ($^3J_{HH}$ = 8 Hz) at 9.53 ppm, which is assigned as the proton of the aldehyde. Consistent with an aldehyde, the $^{13}$C NMR spectrum has a peak at 194.5 ppm for the carbonyl carbon. Additional evidence for this assignment is found in the HMQC spectrum (Figure 4.14), which shows a correlation between the proton that resonates at 9.53 ppm and the carbon that resonates at 194.5 ppm, demonstrating that the proton at 9.53 ppm is one bond away from the carbon at 194.5 ppm. The olefinic protons resonate as a doublet at 7.41 ppm ($^3J_{HH}$ = 16 Hz) and a doublet of doublets at 6.34 ppm ($^3J_{HH}$ = 16 Hz, 8 Hz) in the $^1$H NMR spectrum. The symmetry of the cyclopentadienyl ring that forms from the two alkynes can be seen by the presence of

two methyl resonances at 1.88 ppm and 1.79 ppm that each integrate for six protons (Figure 4.13).

Single crystals suitable for a single crystal X-ray diffraction study were grown by the slow evaporation of an *n*-pentane/diethyl ether solution of **4.8** (Figure 4.16). The O1–C8 bond measures 1.205(5) Å, which is consistent with a C=O moiety.[24] The olefin C–C bond (C7–C6) has a bond length of 1.324(5) Å, as expected for a conjugated C=C bond.[24] The Fe–C(C1-C5) bond lengths for the cyclopentadienyl fragment range from 2.042(3) Å to 2.060(3) Å. This is similar to the Fe–C bond lengths of Ohki and Tatsumi's ferrocenyl-diimine complex formed from alkyne induced ring opening of an NHC (NHC = *N*-heterocyclic carbene) ligand [2.041(2) - 2.054(2) Å] (Scheme 4.16).[25]

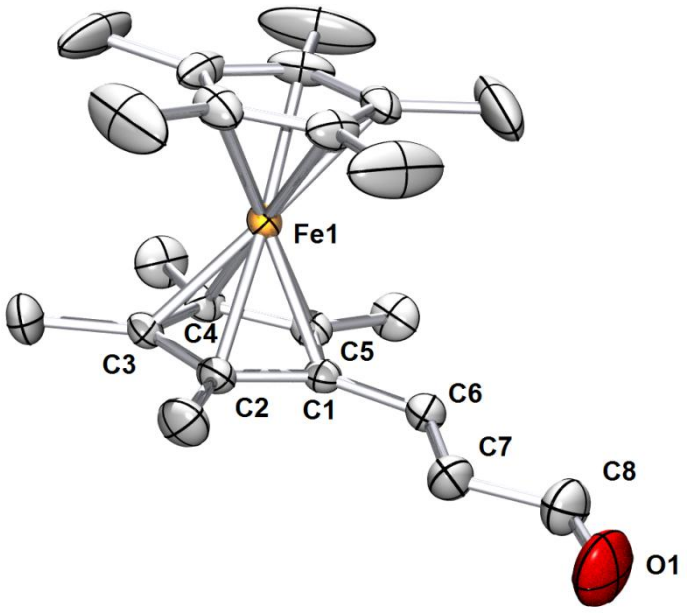


**Figure 4.16.** ORTEP drawing of Cp*Fe[$\eta^5$-$C_5Me_4$(CH=CHCHO)] (**4.8**) (50% probability ellipsoids; H atoms omitted; one independent molecule shown). Selected bond lengths (Å): O1–C8 1.205(5), C8–C7 1.428(5), C7–C6 1.324(5), C6–C1 1.442(4), Fe1–C1 2.051(3), Fe1–C2 2.049(3), Fe1–C3 2.060(3), Fe1–C4 2.059(3), Fe1–C5 2.042(3). Selected bond angles (deg): O1–C8–C7 127.0(5), C8–C7–C6 121.2(4), C7–C6–C1 130.2(3).

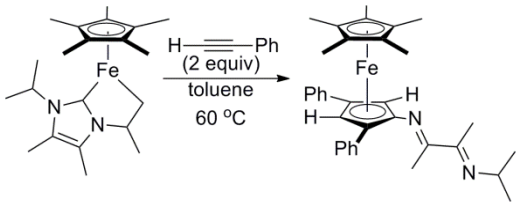


**Scheme 4.16.** Previously reported NHC ring opening to give a ferrocenyl-diimine complex.

While the intimate details of the mechanism of the transformation of Cp*Fe[P(OCH$_2$)$_3$CEt]$_2$(2-furyl) (**4.4**) and 2-butyne to Cp*Fe[$\eta^5$-C$_5$Me$_4$(CH=CHCHO)] (**4.8**) are not known, it appears to involve insertion of two equivalents of 2-butyne into the Fe–furyl bond of **4.4** followed by furyl ring opening that eventually leads to the formation of **4.8** (Scheme 4.17). The ring opening of furans is relevant for the conversion of biomass into liquid fuels,[26, 27] and to the best of our knowledge, furyl ring opening is unprecedented with an Fe complex. Therefore, further studies elucidating the mechanism and scope of the reaction are currently underway.

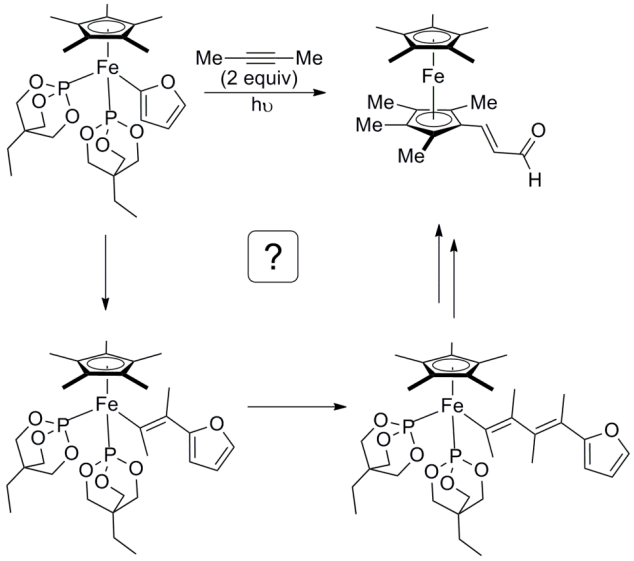


**Scheme 4.17.** Possible partial mechanism for the the transformation of Cp*Fe[P(OCH$_2$)$_3$CEt]$_2$(2-furyl) (**4.4**) and 2-butyne to Cp*Fe[$\eta^5$-C$_5$Me$_4$(CH=CHCHO)] (**4.8**).

## 4.3 Conclusions and Future Work

In this chapter, we have reported the synthesis and characterization of a new Fe–Ph complex, Cp*Fe[P($OCH_2$)$_3$CEt]$_2$Ph (**4.2**). Under thermal conditions, complex **4.2** does not activate aromatic C–H bonds. Attempts to develop Fe–Ph complexes bearing the P($OCH_2$)$_3$CEt and a labile ligand of the type Cp*Fe[P($OCH_2$)$_3$CEt](L)Ph (L = labile ligand) were unsuccessful. However, it was discovered that under photolytic conditions, Cp*Fe[P($OCH_2$)$_3$CEt]$_2$Ph (**4.2**) is active for aromatic C–H activation of furan, 2-methylfuran, and thiophene. During the investigations of the reactivity of **4.2** toward thiophene, we have observed $CS_2$ insertion into the Fe–Ph bond of **4.2** as a result of an impurity in thiophene. Under photolytic conditions, Cp*Fe[P($OCH_2$)$_3$CEt]$_2$(2-furyl) (**4.4**) is inactive for ethylene hydroarylation with furan. Extending reactivity studies toward alkynes has led to the observation that, like Cp*Fe(CO)(NCMe)Ph in Chapter 3, the reaction of Cp*Fe[P($OCH_2$)$_3$CEt]$_2$(2-furyl) (**4.4**) with 2-butyne leads to a sandwich complex, Cp*Fe[$\eta^5$-$C_5Me_4$(CH=CHCHO)] (**4.8**). Future work will be directed toward expanding the substrate scopes of C–H activation by Cp*Fe[P($OCH_2$)$_3$CEt]$_2$Ph (**4.2**) and alkyne insertion by Cp*Fe[P($OCH_2$)$_3$CEt]$_2$(2-furyl) (**4.4**) as well as elucidating the mechanisms of these transformations (see Chapter 7 for more details).

## 4.4 Experimental Section

### 4.4.1 General Considerations

Unless otherwise noted, all synthetic procedures were performed under anaerobic conditions in a nitrogen-filled glovebox or by using standard Schlenk techniques. Glovebox purity was maintained by periodic nitrogen purges and was monitored by an oxygen analyzer ($O_2$ < 15 ppm for all reactions). Tetrahydrofuran and *n*-pentane were dried by distillation from sodium/benzophenone and $P_2O_5$, respectively. Diethyl ether

was distilled over $CaH_2$. Benzene, methylene chloride, and hexanes were purified by passage through a column of activated alumina. Benzene-$d_6$, acetone-$d_6$, $CD_3CN$, 1,4-dioxane-$d_8$, and THF-$d_8$ were used as received and stored under a $N_2$ atmosphere over 4 Å molecular sieves. $^1H$ NMR spectra were recorded on a Varian 300, Varian 500 MHz or a Bruker 600 MHz spectrometer, and $^{13}C\{^1H\}$ NMR spectra were recorded on a Varian 500 (operating frequency 125 MHz), Bruker 600 MHz (operating frequency = 150 MHz) or a Bruker 800 MHz spectrometer (operating frequency 201 MHz) . All $^1H$ and $^{13}C$ spectra are referenced against residual proton signals ($^1H$ NMR) or $^{13}C$ resonances ($^{13}C$ NMR) of the deuterated solvents. $^{31}P\{^1H\}$ NMR spectra were obtained on a Varian 300 MHz (operating frequency 121 MHz), Varian 500 MHz (operating frequency = 201 MHz) or Varian 600 MHz (operating frequency = 243 MHz) spectrometer and referenced against an external standard of $H_3PO_4$ ($\delta = 0$). GC/MS was performed using a Shimadzu GCMS-QP2010 Plus system with a 30 m x 0.25 mm RTx-Qbond column with 8 μm thickness or a 30 m x 0.25 mm SHRXI-5MS column with 0.25 μm thickness using electron impact ionization. Photolysis experiments were performed using UV-vis radiation generated by a 450 W power supply (Model #l7830, Ace Glass, Inc.) equipped with a water-cooled 450 W 5 inch arc IMMER UV-vis lamp (Model #7825-34, Ace Glass, Inc.). The complex $[(tmeda)FeCl_2]_x$ was prepared according to the literature procedure.[18] Analytical grade thiophene was purchased from Sigma-Aldrich. All other reagents were used as purchased from commercial sources. Elemental analyses were performed by Atlantic Microlabs, Inc.

### 4.4.2 Experimental Procedures

**Synthesis of $Cp^*Fe[P(OCH_2)_3CEt]_2Cl$ (4.1**). In one flask, $[(tmeda)FeCl_2]_x$ (0.583 g, 2.40 mmol) and $P(OCH_2)_3CEt$ (0.789 g, 4.87 mmol) were dissolved in THF (25

mL). In another flask, a suspension of LiCp* (0.353 g, 2.49 mmol) was made in THF (5 mL). After cooling both flasks to –35 °C, the solution of $[(tmeda)FeCl_2]_x$ and $P(OCH_2)_3CEt$ was added to a rapidly stirred suspension of the LiCp*. The reaction mixture turned red-brown in color and was allowed to stir at room temperature for ~2 h. After this time, the volatiles were removed in vacuo, and the residue was reconstituted in THF and filtered through a plug of silica gel rinsing with THF. A red-brown band was collected and dried in vacuo. Washing with copious amounts of hexanes afforded complex **4.1** as a red-brown solid (0.985 g, 74% yield). $^1$H NMR (300 MHz, acetone-$d_6$): δ 4.20 (br s, 12H, $P(OCH_2)_3CEt$), 1.49 (s, 15H, Cp*), 1.22 (q, $^3J_{HH}$ = 7 Hz, 4H, $P(OCH_2)_3CCH_2CH_3$), 0.81 (t, $^3J_{HH}$ = 7 Hz, 6H, $P(OCH_2)_3CCH_2CH_3$). $^{31}$P NMR (243 MHz, $CD_3CN$): δ 162.9 (s). $^{13}$C NMR data and elemental analysis were reported in a previous publication.[17]

**Synthesis of Cp*Fe[P(OCH$_2$)$_3$CEt]$_2$Ph (4.2).** A THF solution of **4.1** (0.381 g, 0.688 mmol) was cooled to –78 °C. To the chilled solution was added excess PhLi (0.58 mL, 1.8 M in dibutyl ether, 1.0 mmol). The reaction solution was allowed to warm to room temperature and stirred for 1 h. During this time, the solution changed from deep red to dark yellow. After this time, the reaction mixture was filtered through a plug of silica gel, and the resulting yellow filtrate was dried in vacuo. Washing the resulting residue with hexanes afforded complex **4.2** as a yellow solid (0.293 g, 72% yield). Single crystals suitable for an X-ray diffraction study were grown by the slow diffusion of *n*-pentane into a THF solution of **4.2**. $^1$H NMR (600 MHz, $CDCl_3$): δ 7.57 (d, $^3J_{HH}$ = 7 Hz, 2H, *ortho* phenyl), 6.75 (t, $^3J_{HH}$ = 7Hz, 2H, *meta* phenyl), 6.66 (t, $^3J_{HH}$ = 7.0 Hz, 1H, *para* phenyl), 4.13 (s, 12H, $P(OCH_2)_3CEt$), 1.48 (s, 15H, Cp*), 1.14 (q, $^3J_{HH}$ = 8 Hz, 4H,

$P(OCH_2)_3CCH_2CH_3$), 0.80 (t, $^3J_{HH}$ = 8 Hz, 6H, $P(OCH_2)_3CCH_2CH_3$). ). $^{31}$P NMR (243 MHz, $CD_3CN$): δ 166.2 (s). $^{13}$C NMR data and elemental analysis were reported in a previous publication.[17]

**Synthesis of Cp*Fe[P(OCH$_2$)$_3$CEt](acac) (4.3).** A mixture of $Fe(acac)_2$ (0.198 g, 0.780 mmol) and LiCp* (0.110 g, 0.775 mmol) in a round bottom flask was cooled to –70 °C. Additionally, a THF solution (3 mL) of $P(OCH_2)_3CEt$ (0.142 g, 0.877 mmol) was cooled to the same temperature. The THF solution of $P(OCH_2)_3CEt$ was added to $Fe(acac)_2$/LiCp* mixture. The resulting red mixture was allowed to stir at room temperature for ~0.5 h when the volatiles were removed in vacuo. The residue was extracted with diethyl ether and filtered through celite. The filtrate was dried in vacuo and then reconstituted in a minimal amount of diethyl ether. After storing at –35 °C, the supernatant was decanted, the resulting solid was dried and the remaining solid was reconstituted in $C_6D_6$ and analyzed by NMR spectroscopy. $^1$H NMR (300 MHz, $C_6D_6$): δ 5.14 (s, 1H, acac methyne), 3.77 (s, 6H, $P(OCH_2)_3CEt$), 1.85 (s, 6H, acac methyl), 1.72 (s, 15H), 0.25 (q, $^3J_{HH}$ = 7 Hz, 2H, $P(OCH_2)_3CCH_2CH_3$), 0.08 (t, $^3J_{HH}$ = 7Hz, 3H, $P(OCH_2)_3CCH_2CH_3$).

**Synthesis of Cp*Fe[P(OCH$_2$)$_3$CEt]$_2$(2-furyl) (4.4).** $Cp^*Fe[P(OCH_2)_3CEt]_2Ph$ (**4.2**) (0.037 g, 0.062 mmol) was dissolved in furan (~1 mL) and placed in a J-young NMR tube. The reaction mixture was photolyzed for a total of 4 h with the reaction progress being monitored by $^{31}$P NMR spectroscopy. The reaction solution was dried in vacuo and then reconstituted in $C_6H_6$. The resulting solution was loaded on a plug of silica gel and eluted with THF. A yellow band was collected, which was dried in vacuo. The resulting yellow solid was reconstituted in ~3 mL of a 1:1 mixture of *n*-pentane and

diethyl ether. The solution was stored at –35 °C to give a yellow crystalline solid. The supernatant was decanted from the solid and the resulting solid was washed with *n*-pentane to give **4.4** as a yellow crystalline solid (0.014 g, 39% yield). Single crystals suitable for an X-ray diffraction study were grown from a saturate;d solution of **4.4** in *n*-pentane and diethyl ether at –35 °C. $^{1}$H NMR (600 MHz, $CD_3CN$) δ 7.59 (br s, 1H, furyl 5), 6.07 (br s, 1H, furyl 3/4), 5.97 (br s, 1H, furyl 3/4), 4.07 (s, 12H, P(OC$H_2$)$_3$CEt), 1.47 (s, 15H, Cp*), 1.16 (q, 4H, $^{3}J_{HH}$ = 7 Hz, P(OCH$_2$)$_3$CC$H_2$CH$_3$), 0.77 (t, $^{3}J_{HH}$ = 7 Hz, 6H, P(OCH$_2$)$_3$CCH$_2$C$H_3$). $^{31}$P NMR (201 MHz, $CD_3CN$): δ 168.1 (s).

**Synthesis of Cp*Fe[P(OCH$_2$)$_3$CEt]$_2$[2-(5-methylfuryl)] (4.5).** A mixture of Cp*Fe[P(OCH$_2$)$_3$CEt]$_2$Ph (**4.2**) (0.038 g, 0.064 mmol), 2-methylfuran (0.30 mL, 3.4 mmol) and THF (1 mL) were placed in a J-young NMR tube. The reaction solution was photolyzed for a total of 22 h while monitoring by $^{31}$P NMR spectroscopy. After the reaction was complete, the resulting mixture was dried in vacuo. The residue was extracted with diethyl ether and filtered through celite. The filtrate was dried in vacuo, reconstituted in ~2 mL of a 1:1 mixture of *n*-pentane and diethyl ether and stored at –35 °C. The resulting yellow solid was collected and washed with *n*-pentane and dried in vacuo to give **4.5** as a yellow-orange solid (0.023 g, 60% yield). $^{1}$H NMR (600 MHz, $CD_3CN$): δ 5.80 (d, $^{3}J_{HH}$ = 3 Hz, 1H, furyl 3), 5.60 (m, 1H, furyl 4), 4.06 (s, 12H, P(OC$H_2$)$_3$CEt), 2.19 (s, 3H, furyl methyl), 1.50 (s, 15H, Cp*), 1.14 (q, $^{3}J_{HH}$ = 8 Hz, 4H, P(OCH$_2$)$_3$CC$H_2$CH$_3$), 0.79 (t, $^{3}J_{HH}$ = 8 Hz, 6H, P(OCH$_2$)$_3$CCH$_2$C$H_3$). $^{31}$P NMR (201 MHz, $CD_3CN$): δ 168.1 (s).

**NMR analysis of Cp*Fe[P(OCH$_2$)$_3$CEt](κ$^2$-SC(S)Ph) (4.6).** Cp*Fe[P(OCH$_2$)$_3$CEt]$_2$Ph (**4.2**) (0.065 g, 0.11 mmol) was combined with thiophene (0.18

mL, 2.3 mmol) and THF (5 mL) in a 4 dram vial with a stir bar. The vial was sealed with a Teflon lined cap and photolyzed for 16 h. The resulting purple solution was dried under vacuum. The resulting residue was chromatographed on plug of silica gel using a 1:1 mixture of diethyl ether and hexanes as eluent. A purple band was collected and dried in vacuo. The resulting residue was reconstituted in ~1 mL of *n*-pentane and stored at –35 °C. The supernatant was decanted from a purple crystalline solid, which was subsequently dried. This solid was reconstituted in acetone-$d_6$ and analyzed by NMR spectroscopy. A similar procedure was repeated, excepted crystallization at –35 °C in *n*-pentane afforded crystals suitable for an X-ray diffraction study. $^1$H NMR (300 MHz, acetone-$d_6$): δ 7.84 (d, 2H, $^3J_{HH}$ = 9 Hz, phenyl *ortho*), 7.39 (t, 1H, $^3J_{HH}$ = 9 Hz, phenyl *para*), 7.28 (t, 2H, $^3J_{HH}$ = 9 Hz, phenyl *meta*), 4.20 (d, $^3J_{HP}$ = 5 Hz, 6H, P(OC$H_2$)$_3$CEt), 1.67 (s, 15H, Cp*), 1.24 (q, $^3J_{HH}$ = 8 Hz, 2H, P(OCH$_2$)$_3$CC$H_2$CH$_3$), 0.83 (t, $^3J_{HH}$ = 8Hz, 3H, P(OCH$_2$)$_3$CCH$_2$C$H_3$). $^{31}$P NMR (125 MHz, acetone-$d_6$): δ 159.2 (s).

**Synthesis of Cp*Fe[P(OCH$_2$)$_3$CEt]$_2$(2-thienyl) (4.7).** Cp*Fe[P(OCH$_2$)$_3$CEt]$_2$Ph (**4.2**) (0.041 g, 0.069 mmol) was combined with thiophene (0.28 mL, 3.5 mmol) and THF (1 mL) in a J-young NMR tube. The reaction was photolyzed for a total of 43 h while monitoring by $^{31}$P NMR spectroscopy. After this time, the resulting dark yellow solution was dried in vacuo, and the residue was chromatographed on a plug of silica gel with 25% THF in hexanes. A yellow band was collected and dried under reduced pressure. The yellow residue was dissolved in ~1 mL of a 1:1 mixture of *n*-pentane and diethyl ether and stored at –35 °C. Yellow microcrystals formed and were collected and washed with *n*-pentane to give **4.7** (0.019 g, 32% yield). $^1$H NMR (500 MHz, CD$_3$CN): δ 7.11 (m, 1H, thienyl 5), 6.79 (overlapping, 2H, thienyl 3 and 4), 4.09 (s, 12H, P(OC$H_2$)$_3$CEt), 1.45

(s, 15H, Cp*), 1.16 (q, $^{3}J_{HH}$ = 8 Hz, 4H, $P(OCH_2)_3CCH_2CH_3$), 0.79 (t, $^{3}J_{HH}$ = 8 Hz, 6H, $P(OCH_2)_3CCH_2CH_3$). $^{31}$P NMR (201 MHz, $CD_3CN$): δ 167.6 (s).

**Synthesis of Cp*Fe[η$^5$-$C_5Me_4$(CH=CHCHO)] (4.8).** $Cp^*Fe[P(OCH_2)_3CEt]_2Ph$ (**4.2**) (0.031 g, 0.052 mmol) was dissolved in furan (1 mL) and placed in a J-young NMR tube. The reaction was photolyzed for 21 h until complex conversion to $Cp^*Fe[P(OCH_2)_3CEt]_2$(2-furyl) (**4.4**) was observed by $^{31}$P NMR spectroscopy. At this point, the NMR tube was brought back into the glove box and 2-butyne (0.08 mL, 1 mmol) was added. The resulting mixture was photolyzed for an additional 6 h until the reaction was complete by $^{31}$P NMR spectroscopy. The purple solution was brought back into the glove box, and the volatiles were removed in vacuo. The purple reside was chromatographed on a plug of silica gel in a 15 mL frit, eluting with a 10:1 mixture of hexanes and THF. A purple band was collected, and the volatiles were removed in vacuo. To this solid was added ~1/2 mL of hexanes and the vial was placed in the freezer at –35 °C (Note: not all of the solid dissolves). After sitting overnight, the supernatant was decanted from the purple solid, and the solid was dried to give **4.8** as a purple solid (0.011 g, 58% yield). Single crystals suitable for an X-ray diffraction study were grown by slow evaporation of an *n*-pentane/diethyl ether solution of **4.8**. $^{1}$H NMR (600 MHz, $CD_3CN$): δ 9.53 (d, *J* = 8 Hz, 1H, –C*H*O), 7.41 (d, *J* = 16 Hz, 1H, $C_5Me_4CH$=CH), 6.33 (dd, *J* = 16, 8 Hz, 1H, $C_5Me_4CH$=C*H*), 1.88 (s, 6H, 2 of $C_5Me_4$ adjacent to olefin), 1.79 (s, 6H, 2 of $C_5Me_4$ not adjacent to olefin), 1.60 (s, 15H, Cp*). $^{13}$C NMR (201 MHz, $CD_3CN$): δ 194.5 (*C*HO), 157.7 ($C_5Me_4$*C*H=CH), 126.1 ($C_5Me_4$CH=*C*H), 86.1 (2 of $C_5Me_4$ β to olefin), 82.2 (2 of $C_5Me_4$ γ to olefin), 80.9 ($C_5Me_5$), 73.7 ($C_5Me_4$ α to olefin), 10.7 (Me's on $C_5Me_4$ $C_\beta$), 9.6 (Me's on $C_5Me_4$ $C_\gamma$), 9.4 ($C_5Me_5$).

**Thermal Reaction of Cp*Fe[P(OCH$_2$)$_3$CEt]$_2$Ph (4.2) with C$_6$D$_6$.** A solution of ~5 mg of complex **4.2** in $C_6D_6$ (~0.4 mL) in a screw-cap NMR tube was heated at 80 °C, 100 °C and 140 °C while being monitored by $^1$H NMR spectroscopy. No reaction was observed up to 100 °C and decomposition was observed at 140 °C.

**Thermal Reaction of Cp*Fe[P(OCH$_2$)$_3$CEt]$_2$Ph (4.2) with C$_2$H$_4$.** Cp*Fe[P(OCH$_2$)$_3$CEt]$_2$Ph (**4.2**) (0.060 g, 0.01 mmol) was dissolved in THF-$d_8$ (0.4 mL) and transferred to a high pressure NMR tube. The NMR tube was pressurized with 50 psi of $C_2H_4$. $^1$H NMR spectra were periodically taken while heating at 70 °C and then 100 °C. After heating at 100 °C, broadening of the NMR resonances was observed with solid being deposited on the bottom of the NMR tube.

**Attempted Ethylene Hydrophenylation with Cp*Fe[P(OCH$_2$)$_3$CEt]$_2$Ph (4.2) under Thermal Conditions.** Cp*Fe[P(OCH$_2$)$_3$CEt]$_2$Ph (**4.2**) (0.020 g, 0.034 mmol) was dissolved in 3 mL of a 0.1 mol% hexamethylbenzene/benzene solution in a stainless steel pressure reactor. The reactor was purged with $C_2H_4$, pressurized to 25 psi with $C_2H_4$ and then brought to a total of 120 psi with $N_2$. The reactor was heated at 125 °C for 21 h. After cooling to room temperature, the mixture was analyzed by GC/MS, which showed 0.25 TO styrene and 0.01 TO ethylbenzene. Biphenyl was also identified by GC/MS.

**Attempted Ethylene Hydroarylation with Furan by Cp*Fe[P(OCH$_2$)$_3$CEt]$_2$(2-furyl) (4.4).** Cp*Fe[P(OCH$_2$)$_3$CEt]$_2$Ph (**4.2**) (0.003 g, 0.005 mmol) was combined with furan (18 μL, 0.25 mmol) in THF-$d_8$ in a J-young NMR tube. The mixture was photolyzed for ~3 h to generate Cp*Fe[P(OCH$_2$)$_3$CEt]$_2$(2-furyl) (**4.4**) in situ. Ethylene (30 psi) was introduced to the NMR tube, and the reaction was photolyzed

for an additional 3 h. Analysis by NMR spectroscopy revealed no evidence for 2-ethylfuran and decomposition of the Fe complex was noted.

## 4.5 References

(1) Kalman, S. E.; Gunnoe, T. B.; Sabat, M. *Organometallics* **2014**, *33*, 5457-5463.

(2) Kalman, S. E.; Petit, A.; Gunnoe, T. B.; Ess, D. H.; Cundari, T. R.; Sabat, M. *Organometallics* **2013**, *32*, 1797-1806.

(3) Andreatta, J. R.; McKeown, B. A.; Gunnoe, T. B. *J. Organomet. Chem.* **2011**, *696*, 305-315.

(4) Foley, N. A.; Lail, M.; Lee, J. P.; Gunnoe, T. B.; Cundari, T. R.; Petersen, J. L. *J. Am. Chem. Soc.* **2007**, *129*, 6765-6781.

(5) Goj, L. A.; Gunnoe, T. B. *Curr. Org. Chem.* **2005**, *9*, 671-685.

(6) Waltz, K. M.; Hartwig, J. F. *Science* **1997**, *277*, 211-213.

(7) Hatanaka, T.; Ohki, Y.; Tatsumi, K. *Chem. Asian J.* **2010**, *5*, 1657-1666.

(8) Ohki, Y.; Hatanaka, T.; Tatsumi, K. *J. Am. Chem. Soc.* **2008**, *130*, 17174-17186.

(9) Hartwig, J. F., *Organotransition Metal Chemistry: From Bonding to Catalysis*. University Science Books: Sausalito, 2009.

(10) Crabtree, R. H., *The Organometallic Chemistry of the Transition Metals*. 5th ed.; John Wiley and Sons: New York, 2009.

(11) Green, M. L. H.; Leach, J. B.; Kelland, M. A. *J. Organomet. Chem.* **2007**, *692*, 4147-4156.

(12) Paciello, R. A.; Manriquez, J. M.; Bercaw, J. E. *Organometallics* **1990**, *9*, 260-265.

(13) Foley, N. A.; Ke, Z. F.; Gunnoe, T. B.; Cundari, T. R.; Petersen, J. L. *Organometallics* **2008**, *27*, 3007-3017.

(14) Burgess, S. A.; Joslin, E. E.; Gunnoe, T. B.; Cundari, T. R.; Sabat, M.; Myers, W. H. *Chem. Sci.* **2014**, *5*, 4355-4366.

(15) Hutteman, T. J.; Foxman, B. M.; Sperati, C. R.; Verkade, J. G. *Inorg. Chem.* **1965**, *4*, 950-953.

(16) Tolman, C. A. *Chem. Rev.* **1977**, *77*, 313-348.

(17) Mei, J. J.; Pardue, D. B.; Kalman, S. E.; Gunnoe, T. B.; Cundari, T. R.; Sabat, M. *Organometallics* **2014**, *33*, 5597-5605.

(18) Davies, S. C.; Hughes, D. L.; Leigh, G. J.; Sanders, J. R.; deSouza, J. S. *J. Chem. Soc. Dalt. Trans.* **1997**, 1981-1988.

(19) Newlands, M. J.; Mackay, M. F. *Acta Cryst.* **1986**, *42*, 677-679.

(20) Harman, W. D. *Chem. Rev.* **1997**, *97*, 1953-1978.

(21) Simmie, J. M.; Curran, H. J. *J. Phys. Chem. A* **2009**, *113*, 5128-5137.

(22) Hewison, L.; Crook, S. H.; Mann, B. E.; Meijer, A. J. H. M.; Adams, H.; Sawle, P.; Motterlini, R. A. *Organometallics* **2012**, *31*, 5823-5834.

(23) Robien, W., University of Vienna. In Scifinder (spectra data obtained from Wiley Subsciption Services, Inc.).

(24) Allen, F. H.; Kennard, O.; Watson, D. G.; Brammer, L.; Orpen, A. G.; Taylor, R. *J. Chem. Soc. Perkin Trans. II* **1987**, S1-S19.

(25) Hatanaka, T.; Ohki, Y.; Tatsumi, K. *Angew. Chem. Int. Ed.* **2014**, *53*, 2727-2729.

(26) Sutton, A. D.; Waldie, F. D.; Wu, R. L.; Schlaf, M.; Silks, L. A.; Gordon, J. C. *Nature Chem.* **2013**, *5*, 428-432.

(27) Chatterjee, M.; Matsushima, K.; Ikushima, Y.; Sato, M.; Yokoyama, T.; Kawanami, H.; Suzuki, T. *Green Chem.* **2010**, *12*, 779-782.

# 5 The Synthesis of Iron Complexes with Functional Group Appended Cyclopentadienyl, Pincer, and Tetraamine Ligands and Evaluation for Olefin Hydroarylation

## 5.1 Introduction

In the previous chapters, the reactivity of Cp*Fe complexes toward aromatic C–H bonds and unsaturated substrates has been discussed. The motivation for these studies has been the development of Fe catalysts for olefin hydroarylation.[1-3] In Chapter 2, it was demonstrated that Cp*Fe(CO)(NCMe)Ph is very active for stoichiometric aromatic C–H activation. Extending Cp*Fe(CO)(NCMe)Ph to catalytic alkyne or olefin hydroarylation in Chapter 3 was unsuccessful, as a result of β-hydride elimination in olefin hydrophenylation and hydroxyindenyl or vinylidene ligand formation in alkyne hydrophenylation. Chapter 4 highlighted the reactivity of Cp*Fe[P(OCH$_2$)$_3$CEt]$_2$Ph, which was not a catalyst for olefin hydroarylation or alkyne hydroarylation. Here, we had challenges accessing a vacant coordination site on the Fe center, which limited the substrate scope for aromatic C–H activation. Additionally, we have evidence that an alkyne cyclization reaction is also problematic for Cp*Fe[P(OCH$_2$)$_3$CEt]$_2$Ph as it was for Cp*Fe(CO)(NCMe)Ph.

Based on the work described in the previous chapters, it became apparent that while half-sandwich iron complexes based on the pentamethylcyclopentadienyl ligand were effective complexes for mediating C–H activation and C–C bond forming reactions, these complexes were ineffective at catalytically producing C–H functionalized products.[4, 5] Because of the problems mentioned in the previous paragraph, we undertook an investigation into several Fe complexes with different ligand motifs. These ligands were studied due to the anticipated thermal robustness of the desired Fe complexes and their propensity to retain an octahedral coordination environment, which would hopefully

lead to low spin Fe complexes with a well-defined coordination environment for selective reactivity with aromatic C–H bonds and unsaturated substrates. Thus, we report here initial synthetic efforts to make Fe complexes with functional group appended cyclopentadienyl, pincer, and tetraamine ligands and preliminary reactivity studies with these complexes.

## 5.2 Results and Discussion

### 5.2.1 Tethered Cyclopentadienyl Ligands

Because of the success of the Cp* ligand for aromatic C–H activation, but difficulties with stability, we considered that appending a two electron-donor ligand to the cyclopentadienyl ring may give more robust systems. Additionally, in Chapter 3, we hypothesized that β-hydride elimination from Cp*Fe(CO)($CH_2CH_2Ph$) may be irreversible due to associative displacement of styrene. Based on previous studies with TpRu(CO)(NCMe)Ph, the fact that styrene does not dissociate from the metal center renders β-hydride elimination reversible in this system.[6, 7] If the ability for the Cp* ligand in the purported Cp*Fe(CO)($\eta^2$-CH=CHPh)H intermediate to ring slip is contributing to the irreversibility of β-hydride elimination, having an additional donor appended to the cyclopentadienyl ligand may stabilize the $\eta^5$ coordination mode. This class of ligand has been previously used on Fe complexes.[8, 9] In fact, an *N*-heterocyclic carbene tethered cyclopentadienyl ligated Fe complex has served as hydrosilylation and transfer hydrogenation catalyst.[8] Therefore, we targeted several Fe complexes of the general structure shown in Figure 5.1.

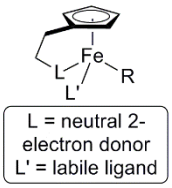


**Figure 5.1.** General structure of tethered cyclopentadienyl iron complexes.

One of the first ligands we targeted contained a pyridyl functionality, namely 2-picolylcyclopentadienyl ([$CpCH_2Py$]$^-$). The [$CpCH_2Py$]$^-$ ligand was studied because of the good coordinating ability of the pyridyl group and its resistance to oxidation in the case of pursuing oxidative olefin hydroarylation reactions. The [$CpCH_2Py$]$^-$ ligand was synthesized according to modification of the literature procedures as outlined in Scheme 5.1. Treatment of 2-chloromethylpyridine with NaCp affords two isomers of the picolyl substituted cyclopentadiene compound. Deprotonation with MeLi gives the desired Li[$CpCH_2Py$] pro-ligand.[10]

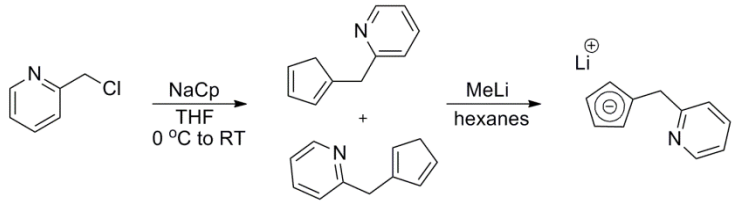


**Scheme 5.1.** Synthesis of Li[$CpCH_2Py$].

Several attempts at complexing the [$CpCH_2Py$]$^-$ ligand to Fe were unsuccessful. For example, stirring $(py)_4FeCl_2$ (py = pyridine) with the pro-ligand Li[$CpCH_2Py$] resulted in a brown intractable mixture that exhibited very broad resonances in the $^1$H NMR spectrum. One likely reason is that the –$CH_2Py$ chain is not long enough to coordinate to the Fe center. Relevant to this hypothesis, the sandwich complex ($\eta^5$-$CpCH_2Py)_2Fe$ has been observed in the crude reaction mixture of the reaction of $FeCl_2$,

Li[$CpCH_2Py$], and $P(OCH_2)_3CEt$, providing evidence that the pyridyl group does not coordinate to the Fe center.[11] While the addition of another methylene linker might increase the propensity for the pyridyl group to coordinate, we chose to pursue other functional groups that would be better donors and not have as much rigidity as the pyridine ring.

The most synthetic success to date has been achieved with the diphenyl phosphine ligand, 1-diphenylphosphino-2-cyclopentadienylethane ($[Cp(CH_2)_2PPh_2]^-$). The nucleophilic attack of $KPPh_2$ to spiro[2,4]hepta-4,6-diene in THF yields the desired pro-ligand $K[Cp(CH_2)_2PPh_2]$ (Scheme 5.2).[12] According to the literature, aqueous work-up followed by a second deprotonation allows for isolation of the clean pro-ligand. However, we found the direct reaction of spiro[2,4]hepta-4,6-diene and $KPPh_2$ gives the desired compound in suitable purity.[12]

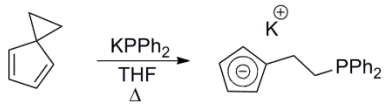


**Scheme 5.2.** Synthesis of $K[Cp(CH_2)_2PPh_2]$.

The ligand $[Cp(CH_2)_2PPh_2]^-$ has previously been used to make the complex $[Cp(CH_2)_2PPh_2]Fe(CO)Cl$.[9] Since CO has been shown to be problematic in our chemistry, complexes with other ancillary ligands were pursued. Adaptation of the synthetic procedure to make $[Cp(CH_2)_2PPh_2]Fe(CO)Cl$ provided a suitable means to make a variety of new Fe complexes (see below).[9] Unfortunately, attempts to synthesize a complex of the type $[Cp(CH_2)_2PPh_2]Fe(L)Ph$ (L = labile ligand) were unsuccessful, leading to a mixture of intractable products (Table 5.1, entries 1,2,4, and 6). It was found that using more strongly coordinating ligands than those shown in entries 1,2,4, and 6 in

Table 5.1 allowed for the isolation of stable complexes. In a typical procedure, $[(tmeda)FeCl_2]_x$ (x = 1,2) (tmeda = *N*,*N*,*N*′,*N*′-tetramethylethylenediamine) was treated with $K[Cp(CH_2)_2PPh_2]$ to generate a purple solution. Addition of one equivalent of a monodentate ligand, such as $P(OCH_2)_3CEt$, affords $[Cp(CH_2)_2PPh_2]Fe(L)Cl$ (L = $P(OCH_2)_3CEt$, $PMe_3$, $CN^tBu$) (Scheme 5.3). Table 5.1 summarizes the variety of complexes made by this procedure along with those ligands that did not provide isolable complexes. In most cases, spectroscopically clean material could be obtained, although rigorous efforts to give analytically pure material were not pursued. Nonetheless, for illustrative purposes the $^1H$ NMR spectra of these compounds are shown in Figures 5.3 - 5.5. The complexes are characterized by four multiplets between 1.5 and 3.5 ppm that correspond to the inequivalent protons on the alkyl linker, which contrasts with the two resonances observed for the pro-ligand salt. Additionally, the coordinated $PPh_2$ moiety shows up ~70 ppm in the $^{31}P$ NMR spectra as a doublet for complexes **5.1** and **5.2** and a singlet for complex **5.3**. The resonance for the $PPh_2$ moiety is shifted significantly downfield of the pro-ligand salt.[12]

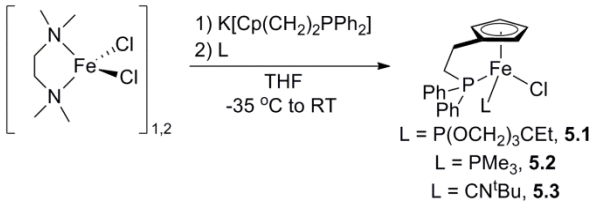


**Scheme 5.3.** Synthesis of $[Cp(CH_2)_2PPh_2]Fe(L)Cl$ complexes.

**Table 5.1.** Results from synthesis of $[Cp(CH_2)_2PPh_2]Fe(L)Cl$ complexes.

| Entry | Ligand (L) | Result (Cpd #) |
|---|---|---|
| 1 | NCMe | Not isolable |
| 2 | $PPh_3$ | Not isolable |
| 3 | $P(OCH_2)_3CEt$ | Isolated (**5.1**) |
| 4 | $C_2H_4$ | Not isolable |
| 5 | $PMe_3$ | Isolated (**5.2**) |
| 6 | Pyridine | Not isolable |
| 7 | $PPh_2Me$ | Isolated – Low Purity |
| 8 | $CN^tBu$ | Isolated (**5.3**) |

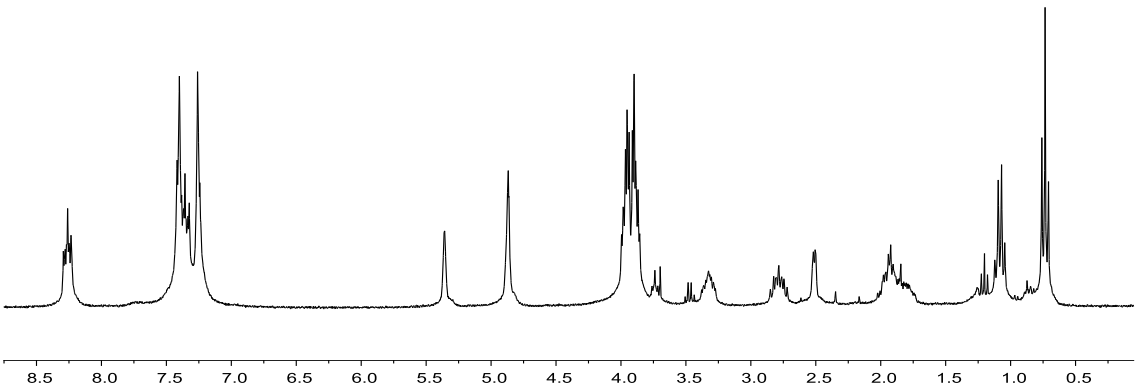


**Figure 5.2.** $^1H$ NMR spectrum of $[Cp(CH_2)_2PPh_2]Fe[P(OCH_2)_3CEt]Cl$ (**5.1**) in $CDCl_3$.

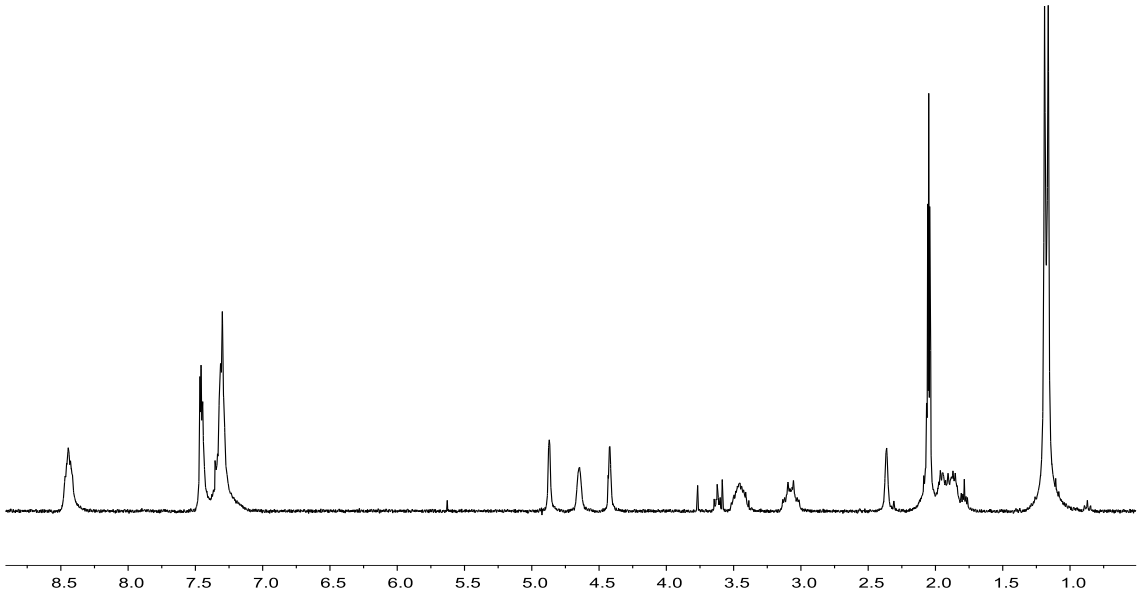


**Figure 5.3.** $^{1}$H NMR spectrum of [Cp(CH$_2$)$_2$PPh$_2$]Fe(PMe$_3$)Cl (**5.2**) in acetone-$d_6$.

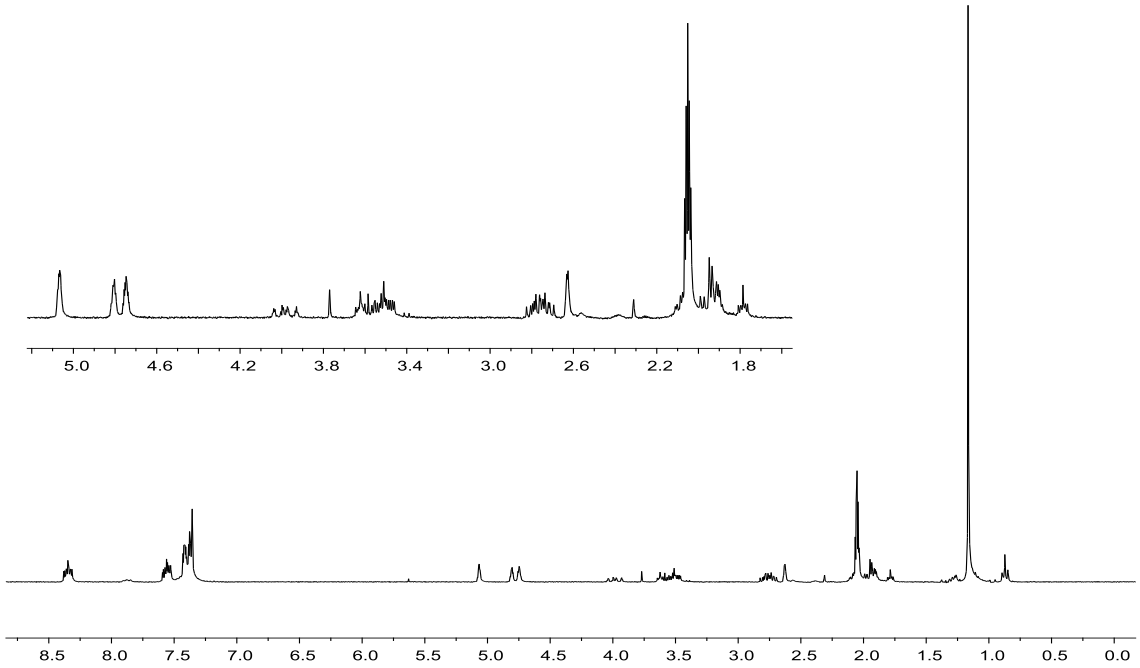


**Figure 5.4.** $^{1}$H NMR spectrum of [Cp(CH$_2$)$_2$PPh$_2$]Fe(CN$^{t}$Bu)Cl (**5.3**) in acetone-$d_6$.

Reaction of the corresponding [Cp(CH$_2$)$_2$PPh$_2$]Fe(L)Cl complexes with MeLi at –35 °C followed by warming to room temperature gives the corresponding methyl

complexes $[Cp(CH_2)_2PPh_2]Fe(L)Me$ (Scheme 5.4).[9] The $^1H$ NMR spectra for complexes **5.4**-**5.6** contain the diagnostic upfield methyl peaks between 0.25 ppm and –1.0 ppm. A virtual triplet is observed for the methyl ligand of **5.4** while the methyl peak for complex **5.5** resonates as a doublet of doublets. As expected, the methyl peak for complex **5.6** is a doublet in the $^1H$ NMR spectrum (Figures 5.6-5.8).

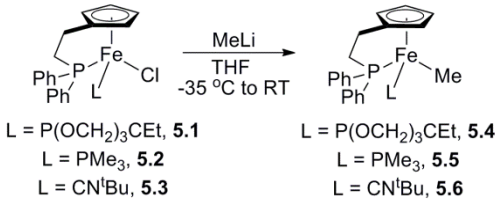


**Scheme 5.4.** Synthesis of $[Cp(CH_2)_2PPh_2]Fe(L)Me$ complexes (**5.4-5.6**).

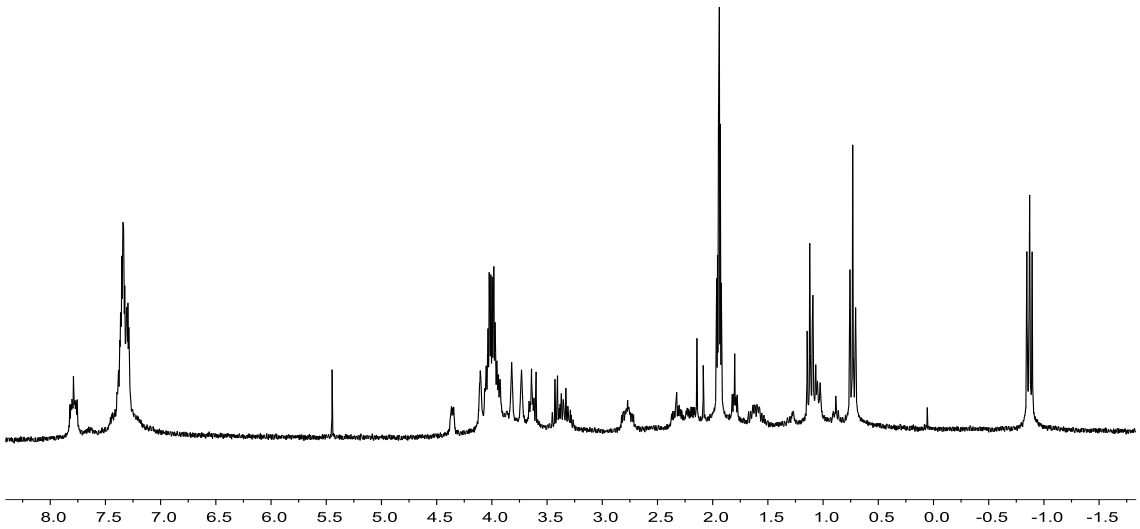


**Figure 5.5.** $^1H$ NMR spectrum of $[Cp(CH_2)_2PPh_2]Fe[P(OCH_2)_3CEt]Me$ (**5.4**) in $CD_3CN$.

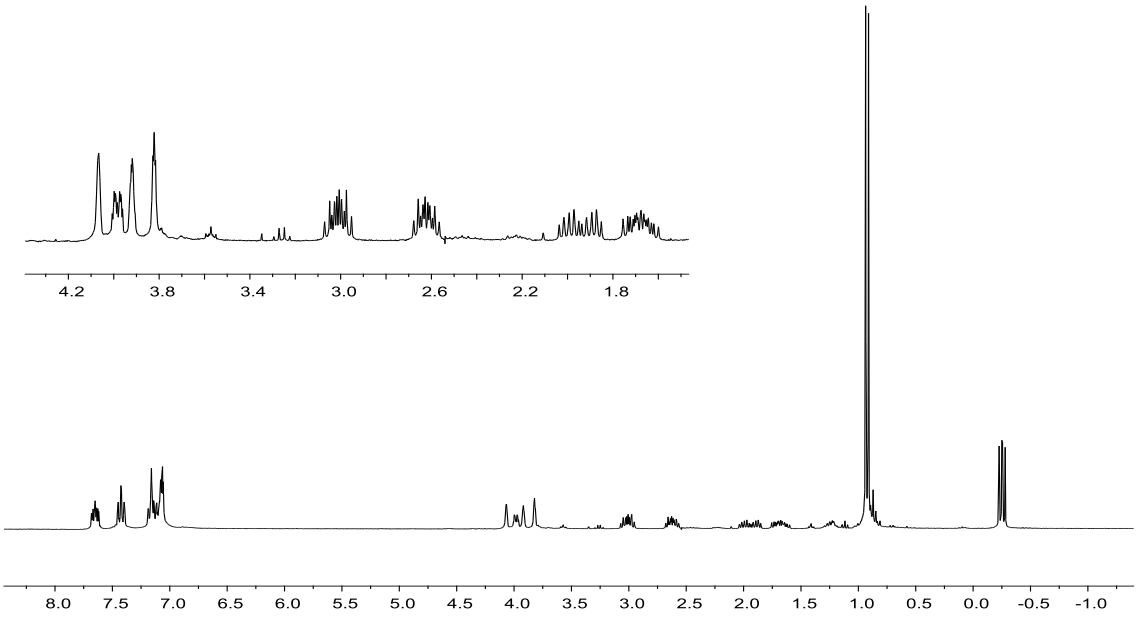


**Figure 5.6.** $^{1}$H NMR spectrum of $[Cp(CH_2)_2PPh_2]Fe(PMe_3)Me$ (**5.5**) in $C_6D_6$.

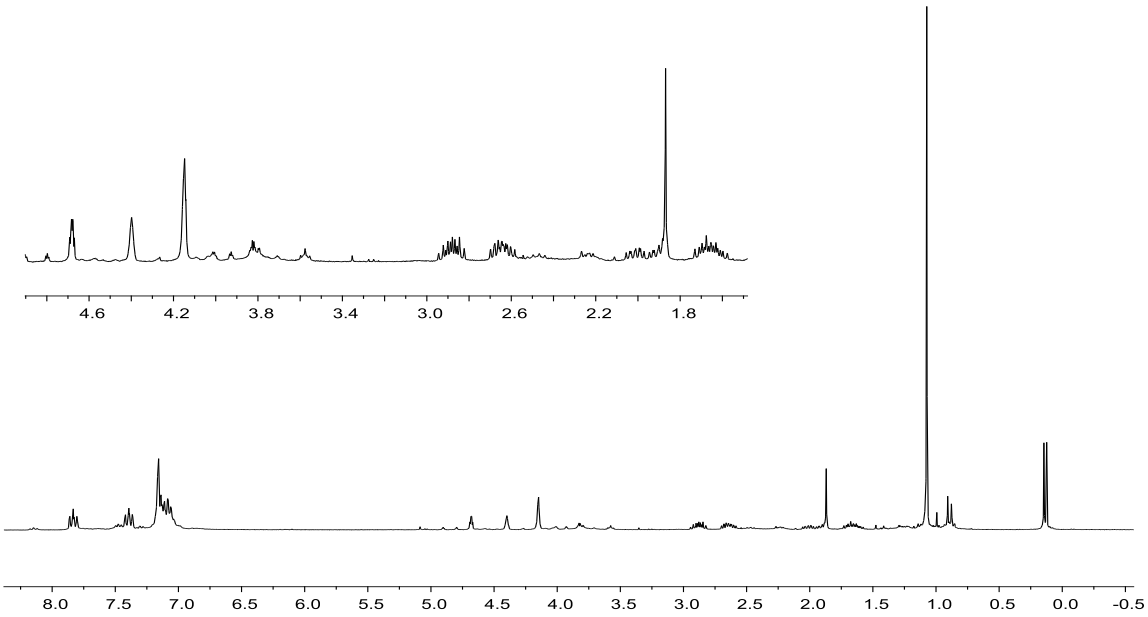


**Figure 5.7.** $^{1}$H NMR spectrum of $[Cp(CH_2)_2PPh_2]Fe(CN^{t}Bu)Me$ (**5.6**) in $C_6D_6$.

.

Despite the fact that we were unable to directly synthesize complexes of the type $[Cp(CH_2)_2PPh_2]Fe(L)Me$ (L = NCMe or pyridine) and could only cleanly isolate

complexes with strongly coordinating ligands, we still performed a few experiments with complexes **5.4**-**5.6** to determine the potential of this class of Fe complexes to mediate C–H activation and whether these Fe complexes could serve as synthetic precursors to the desired Fe complexes with labile ligands (NCMe of pyridine). For instance, we hoped that photolyzing $[Cp(CH_2)_2PPh_2]Fe[P(OCH_2)_3CEt]Me$ (**5.4**) in NCMe or pyridine would lead to $[Cp(CH_2)_2PPh_2]Fe(L)Me$ (L = NCMe or pyridine). Table 5.2 provides a summary of the reactions investigated with complexes **5.4**-**5.6**. In all cases, either no reaction was observed or the complexes decomposed under the reaction conditions.

**Table 5.2.** Summary of reactions performed with complexes **5.4**-**5.6**.

| Entry | Complex | Reactants/Conditions | Result |
|---|---|---|---|
| 1 | **5.4** | Thermolysis in $C_6D_6$ | No reaction |
| 2 | **5.4** | Photolysis in $C_6D_6$ | Decomposition |
| 3 | **5.4** | Photolysis in pyridine | Decomposition |
| 4 | **5.4** | Photolysis in acetonitrile | Decomposition |
| 5 | **5.4** | Reaction with $(^tBuO)_2$ | No reaction |
| 6 | **5.4** | Reaction with pyridine-N-oxide | No reaction, decomposition upon heating |
| 7 | **5.5** | Thermolysis in $C_6D_6$ | Decomposition |
| 8 | **5.5** | Thermolysis in pyridine | Decomposition |
| 9 | **5.6** | Photolysis in $C_6D_6$ | Slow reaction, no $CH_3D$ observed |

We next considered the possibility that a coordinatively unsaturated complex $[Cp(CH_2)_2PPh_2]Fe(Me)$ could be synthesized directly. The reaction of $[(tmeda)FeCl_2]_x$ with $K[Cp(CH_2)_2PPh_2]$ followed by MeLi resulted in the formation of a diamagnetic Fe complex (Scheme 5.5). NMR data suggest the formation of $K[Cp(CH_2)_2PPh_2]Fe(\eta^1\text{-}PPh_2(CH_2)_2Cp)Me$ (**5.7**) (Figure 5.9 and Figure 5.10). We observe two doublets centered at 85.2 ppm and 70.2 ppm ($^2J_{PP}$ = 38 Hz). Zooming in on these doublets reveals that another pair of doublets with $^2J_{PP}$ = 38 Hz with nearly identical chemical shifts as the previous doublets (Figure 5.10). While we have not definitively determined the reason for

the observed of two sets of doublets, we hypothesize that this may be explained by isomers, especially considering that the chemical shifts and coupling constants between the two sets are nearly identical. The formation of $K[Cp(CH_2)_2PPh_2]Fe(\eta^1\text{-}PPh_2(CH_2)_2Cp)Me$ (**5.7**) indicates that the pro-ligand salt likely reacts with the coordinatively unsaturated $[Cp(CH_2)_2PPh_2]FeCl$ intermediate, and hence, prevents the synthesis of complexes of the type $[Cp(CH_2)_2PPh_2]Fe(L)Cl$ (L = NCMe, pyridine, $PPh_3$, etc.) since these ligands cannot outcompete $K[Cp(CH_2)_2PPh_2]$ for coordination. It also potentially explains the reason for the low yields (20-30%) in the synthesis of complexes **5.1**-**5.3** since two equivalents of ligand salt may be involved in the reaction.

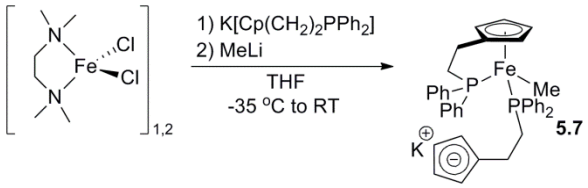


**Scheme 5.5.** Synthesis of purported $K[Cp(CH_2)_2PPh_2]Fe(\eta^1\text{-}PPh_2(CH_2)_2Cp)Me$ (**5.7**).

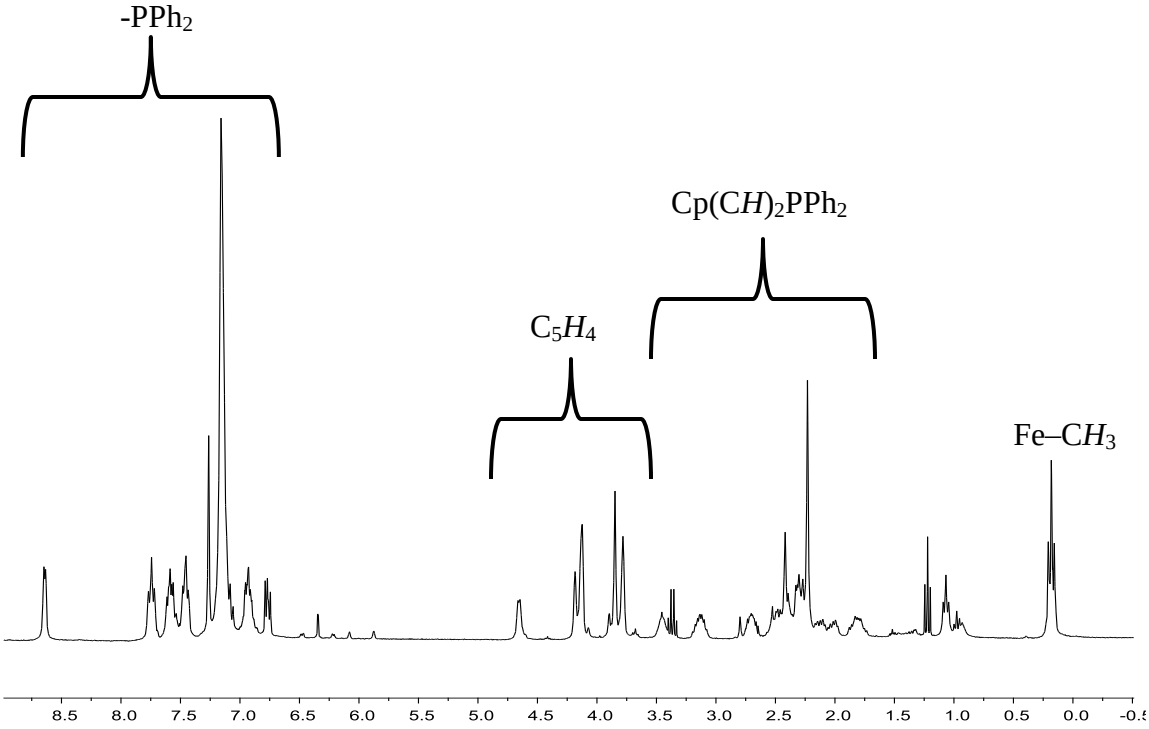


**Figure 5.8.** $^{1}$H NMR spectrum (with assignments) of purported K[Cp(CH$_2$)$_2$PPh$_2$]Fe(η$^1$-PPh$_2$(CH$_2$)$_2$Cp)Me (**5.7**) in C$_6$D$_6$.

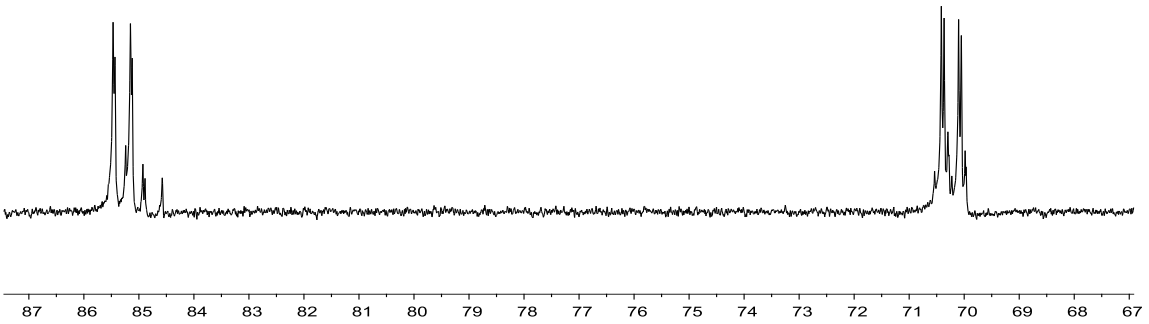


**Figure 5.9.** $^{31}$P NMR spectrum of purported K[Cp(CH$_2$)$_2$PPh$_2$]Fe(η$^1$-PPh$_2$(CH$_2$)$_2$Cp)Me (**5.7**) in C$_6$D$_6$.

Efforts were made to synthesize Fe complexes using the $[Cp(CH_2)_2PMe_2]^-$ ligand. The $Li[Cp(CH_2)_2PMe_2]$ pro-ligand was synthesized by in situ generation of $LiPMe_2$ by reaction of $PPhMe_2$ with Li followed by reaction with spiro[2,4]hepta-4,6-diene to give the desired product in ~90% purity (Scheme 5.6).[12] Following a similar procedure for the synthesis of complexes **5.1**-**5.3**, we attempted to make complexes of the type $[Cp(CH_2)_2PPh_2]Fe(L)Cl$ (L = neutral, two-electron donor) (Scheme 5.7). The results of these synthetic attempts are shown in Table 5.3.

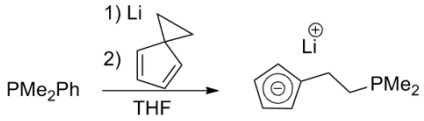


**Scheme 5.6.** Synthesis of $Li[Cp(CH)_2PMe_2]$.

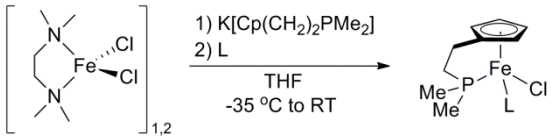


**Scheme 5.7.** Synthesis of $[Cp(CH_2)_2PPh_2]Fe(L)Cl$ (L = neutral, two-electron donor) complexes.

**Table 5.3.** Results from attempted synthesis of $[Cp(CH_2)_2PMe_2]Fe(L)Cl$ complexes.

| Entry | Ligand (L) | Result (Cpd #) |
|---|---|---|
| 1 | $PPh_3$ | Not isolable |
| 2 | $PMe_3$ | Multiple products |
| 3 | $P(OCH_2)_3CEt$ | Isolated (**5.8**) |
| 4 | $CN^tBu$ | Multiple products |
| 5 | cyclohexene | Not isolable |

In the case of entries 1 and 5, it seems likely that we are forming $Li[Cp(CH_2)_2PMe_2]Fe(\eta^1\text{-}PMe_2(CH_2)_2Cp)Cl$ based on spectral data of crude products. For instance, the reaction of $[(tmeda)FeCl_2]_x$ with $Li[Cp(CH_2)_2PMe_2]$ followed by $PPh_3$ led to

the formation of a product characterized by two doublets at 58.6 ppm and 36.4 ppm ($^2J_{PP}$ = 63 Hz) in the $^{31}$P NMR spectrum. Additionally, we observe no resonances in the $^1$H NMR spectrum consistent with coordinated $PPh_3$. Thus, the product is formulated as Li[Cp$(CH_2)_2$PMe$_2$]Fe($\eta^1$-PMe$_2(CH_2)_2$Cp)Cl. The only complex obtained in reasonable purity was with the bicyclic phosphite (entry 3). For the other ligands that provided stable complexes with the [Cp$(CH_2)_2$PPh$_2$]$^-$ ligand (entries 2 and 4), we observed multiple products. The complex [Cp$(CH_2)_2$PPh$_2$]Fe[P$(OCH_2)_3$CEt]Cl (**5.8**) was synthesized and isolated as a green solid. To our knowledge, this is the first example of [Cp$(CH_2)_2$PMe$_2$] coordinated to Fe. The expected resonances for the coordinated phosphite are observed in the $^1$H NMR spectrum along with diastereotopic methylene protons of [Cp$(CH_2)_2$PMe$_2$]$^-$ (Figure 5.10). The $^{31}$P NMR spectrum shows 2 doublets ($^2J_{PP}$ = 118 Hz) at 167.9 ppm for the phosphite and at 65.6 for the –PMe$_2$ group.

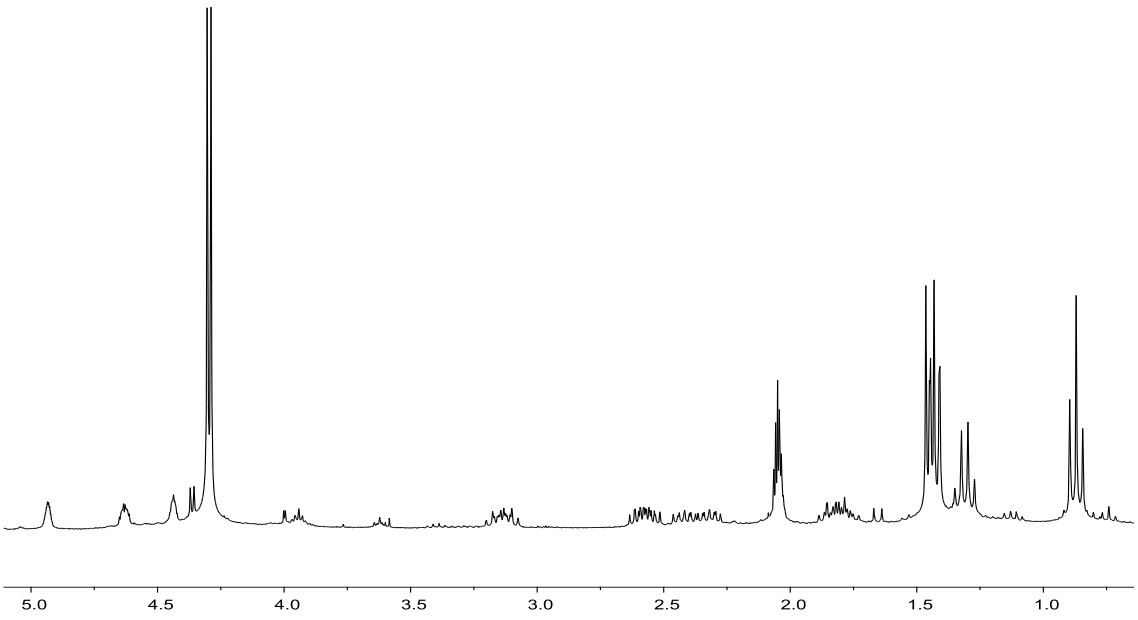


**Figure 5.10.** $^1$H NMR spectrum of [Cp$(CH_2)_2$PMe$_2$]Fe[P$(OCH_2)_3$CEt]Cl (**5.8**) in acetone-$d_6$.

Treating $[Cp(CH_2)_2PMe_2]Fe[P(OCH_2)_3CEt]Cl$ (**5.8**) with MeLi at –35 °C followed by warming to room temperature formed the expected complex $[Cp(CH_2)_2PMe_2]Fe[P(OCH_2)_3CEt]Me$ (**5.9**) (Scheme 5.8). For complex **5.9**, we performed the synthesis on a small scale and used the product directly in subsequent NMR scale reactions. Complex **5.9** is characterized by a virtual triplet at 0.03 ppm for the Fe–Me and two doublets, 170.5 ppm and 70.4 ppm, in the $^{31}P$ NMR spectrum for the coordinated phosphite and the $–PMe_2$ group (Figure 5.11 and 5.12). Complex **5.9** was photolyzed in pyridine with the hope of producing $[Cp(CH_2)_2PMe_2]Fe(py)Me$. However, this reaction only led to decomposition of the starting material. From these preliminary investigations, we found that the synthesis of Fe complexes of the type $[Cp(CH_2)_2PR_2]Fe(L)Me$ [R = Ph or Me, L = labile ligand (e.g, NCMe or pyridine)] to be challenging. Thus, we opted to refocus our efforts on ligand motifs that would allow greater accessibility to Fe complexes with labile ligands.

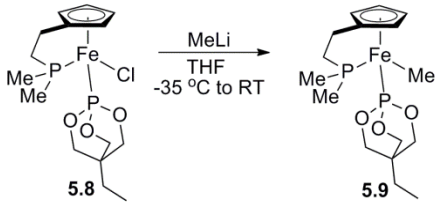


**Scheme 5.8.** Synthesis of $[Cp(CH_2)_2PMe_2]Fe[P(OCH_2)_3CEt]Me$ (**5.9**).

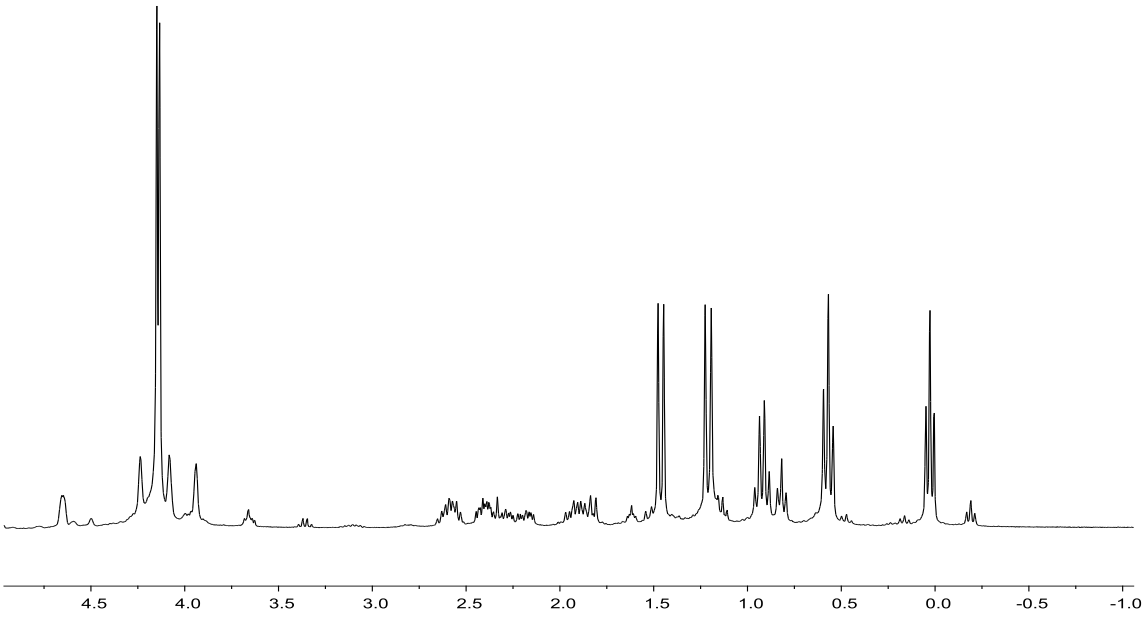


**Figure 5.11.** $^{1}$H NMR spectrum of $Cp(CH_2)_2PMe_2]Fe[P(OCH_2)_3CEt]Me$ (**5.9**) in pyridine-$d_5$.

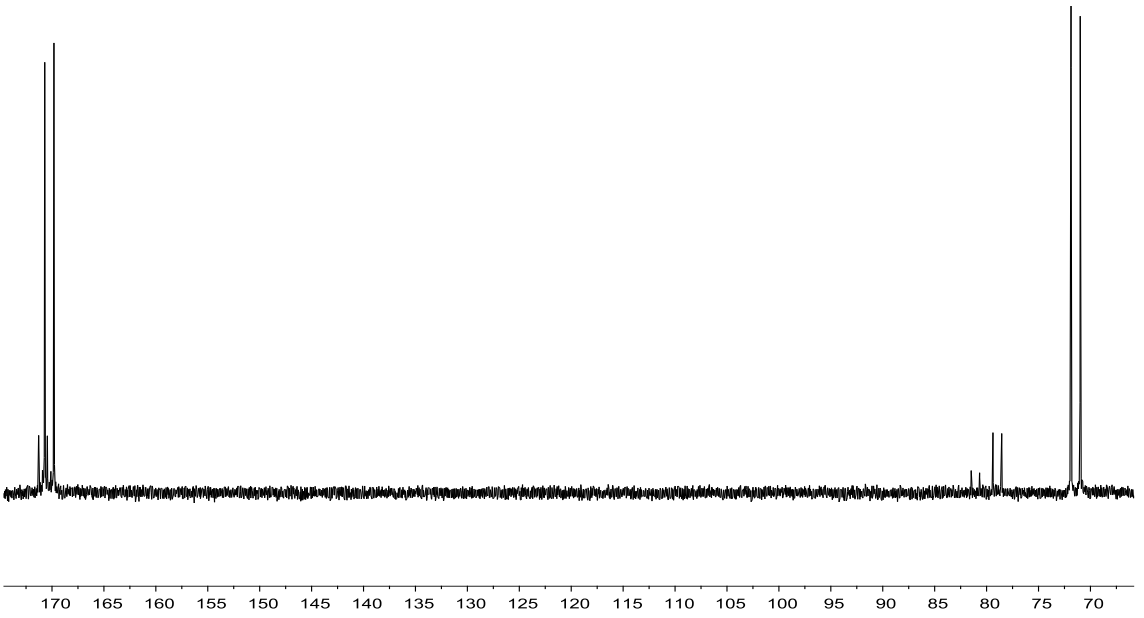


**Figure 5.12.** $^{31}$P NMR spectrum of $[Cp(CH_2)_2PMe_2]Fe[P(OCH_2)_3CEt]Me$ (**5.9**) in pyridine-$d_5$. Peaks at 78.8 ppm, 80.1 ppm, and 170.7 ppm are from unidentified by-products.

### 5.2.2 Complexes of 2,5-Bis(dihydrocarbylphosphinomethyl)pyridine

Based on the results from the preceding section (Section 5.2.1) and Chapters 2-4, we considered that half sandwich Fe complexes based on facially coordinating anionic ligands, such as Tp, Cp, Cp*, and [$Cp(CH_2)_2PR_2$] (R = Ph or Me) would not be suitable catalysts for olefin hydroarylation. One significant challenge we had was producing complexes with a labile ligand. A labile ligand is needed so that it can dissociate and generate a vacant coordination site that would allow the Fe center to react with either C–H bonds or unsaturated substrates (e.g., olefins or alkynes) to enter the catalytic cycle. Thus, we reasoned that using a formally neutral ligand would allow us to abstract a halide to generate a coordinatively unsaturated Fe(II) complex (Scheme 5.9) or an Fe(II) complex with a labile ligand. Consequently, we began studying the synthesis of Fe complexes based on neutral chelates that would still maintain an overall octahedral coordination environment.

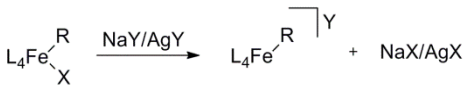


**Scheme 5.9.** Halide abstraction to generate Fe(II) complex with vacant coordination site (L = neutral, two-electron donor ligand, R = Me or Ph, X = halide, Y = non-coordinating anion).

One class of ligand that we were interested in was 2,6-bis(dihydrocarbylphosphinomethyl)pyridines (PNP) (Figure 5.13). The electronics and sterics can be tuned based on the identity of the dialkyl(aryl)phosphine groups.[13] Moreover, substituents can be appended to the pyridine ring to adjust the donor ability of the ligand. There have also been examples of Fe complexes with these ligands being

active catalysts for hydrogenation of carbon dioxide and ketones.[14-16] However, there are no examples of (PNP)Fe complexes with an alkyl or aryl ligand.

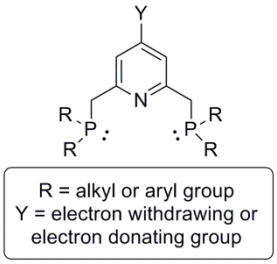


**Figure 5.13.** General structure of 2,6-bis(dihydrocarbylphosphinomethyl)pyridine (PNP) ligands.

Our study began with the 2,6-bis(diphenylphosphinomethyl)pyridine ligand ($^{Ph}$PNP). Because of the small Fe(II) center, a ligand with smaller phosphine substituents might be more suitable for the types of complexes we were interested in studying. The chemistry of ($^{Ph}$PNP)Fe complexes is largely unexplored, with the only known Fe complexes of this ligand being ($^{Ph}$PNP)$FeX_2$ (where X is a halide or pseudo-halide).[17] A general structure for the target complex [($^{Ph}$PNP)Fe(L)(L')R]$^+$ (L = neutral two-electron donor, L' = labile ligand) is shown in Figure 5.14.

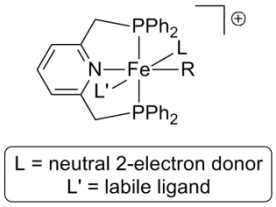


**Figure 5.14.** Structure of target complex [($^{Ph}$PNP)Fe(L)(L')R]$^+$.

The $^{Ph}$PNP ligand was synthesized by modification of literature procedures. This synthesis involves treating 2,6-bis(chloromethyl)pyridine with $KPPh_2$ in THF (Scheme 5.10).[18] While rigorous purification could be performed in order to obtain the desired

ligand in high purity, it was determined that the crude ligand could be used directly and did not affect the outcome of the complexation reaction. Thus, stirring a mixture of $FeCl_2$ and $^{Ph}$PNP in THF precipitated the known yellow $[(^{Ph}PNP)FeCl_2]_x$ (**5.10**) (Scheme 5.11).[19] Complex **5.10** is not soluble in common organic solvents, which suggests a polymeric nature. Alternatively, the formulation of complex **5.10** could be $[(^{Ph}PNP)_2)Fe][FeCl_4]$. As a result of the poor solubility of **5.10**, we could not obtain any solution characterization data and attempts to obtain elemental analysis were not made. This yellow solid was used in subsequent reactions.


**Scheme 5.10.** Synthesis of $^{Ph}$PNP ligand.

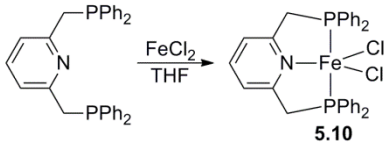


**Scheme 5.11.** Synthesis of $(^{Ph}PNP)FeCl_2$ (**5.10**).

Treating complex **5.10** with $P(OCH_2)_3CEt$ or $PMe_3$ results in no reaction, likely due to the poor solubility of the starting material **5.10**. We found, however, that treating complex **5.10** with 2 equivalents of a halide abstracting reagent (NaY; Y = $BAr'_4$ or $PF_6$) in NCMe furnished the complex $[(^{Ph}PNP)Fe(NCMe)_3]Y_2$ (**5.11-BAr'$_4$** and **5.11-PF$_6$**) in very good yields (>85%) (Scheme 5.12). The $[(^{Ph}PNP)Fe(NCMe)_3]^{2+}$ dication is characterized by two singlets in a 1:2 ratio at 2.48 ppm and 1.50 ppm in the $^1$H NMR spectrum corresponding to the NCMe ligands. The upfield shift relative to free NCMe for the coordinated NCMe ligands in the coordination site perpendicular to the PNP plane

may be a result of shielding from the $PPh_2$ groups of the PNP ligand. A virtual triplet is observed at 4.45 ppm for the methylene linker of the $^{Ph}$PNP ligand (Figure 5.15). A singlet is observed in the $^{31}$P NMR at 59.5 ppm, which is significantly downfield of free $^{Ph}$PNP. Typically, ~1 equivalent of diethyl ether is observed in the $^{1}$H NMR spectrum of **5.11-Y**. Complex **5.11-PF$_6$** is soluble in polar solvents such as $CH_2Cl_2$ and NCMe, while complex **5.11-BAr'$_4$** has better solubility in less polar solvents such as diethyl ether.

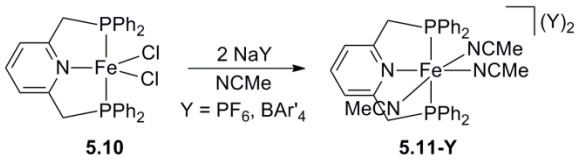


**5.10** **5.11-Y**

**Scheme 5.12.** Synthesis of [($^{Ph}$PNP)Fe(NCMe)$_3$]Y$_2$ (**5.11-Y**).

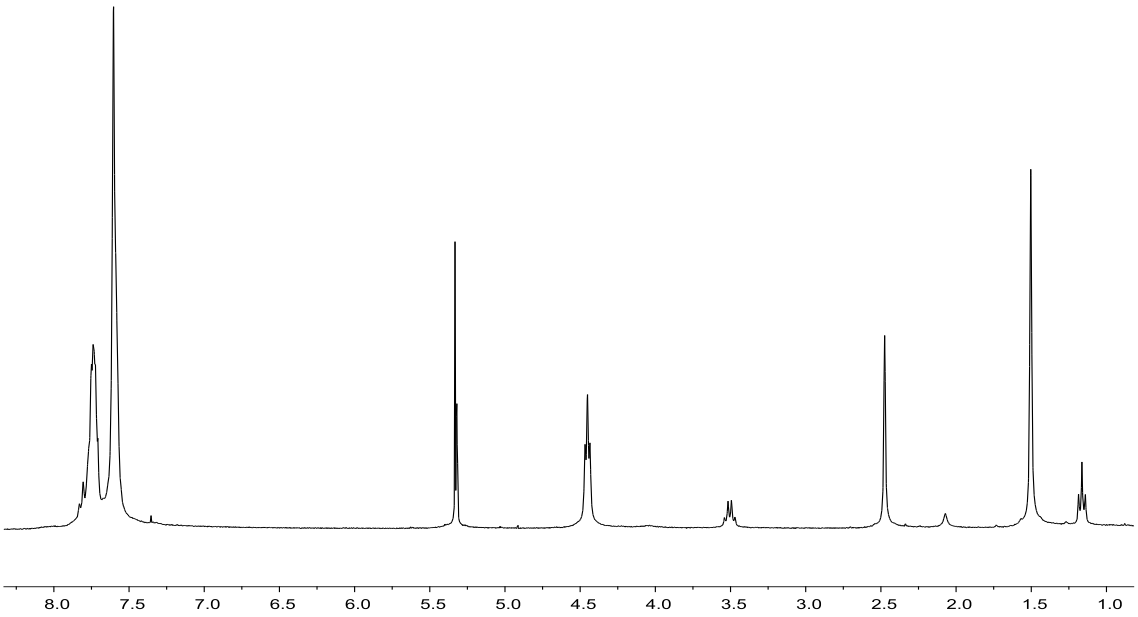


**Figure 5.15.** $^{1}$H NMR spectrum of [($^{Ph}$PNP)Fe(NCMe)$_3$](PF$_6$)$_2$ (**5.11-PF$_6$**) in $CD_2Cl_2$. Residual diethyl ether and dichloromethane are observed.

The NCMe ligands of complexes **5.11** are labile, making these complexes excellent precursors for subsequent syntheses. For instance, the addition of one

equivalent of $PMe_3$ to a DCM solution of complex **5.11** displaces one NCMe ligand to give *trans*-[($^{Ph}$PNP)Fe($PMe_3$)($NCMe)_2$]$(Y)_2$ (**5.12-Y**) (Y = $BAr'_4$ or $PF_6$) (Scheme 5.13). Complexes **5.12-Y** are isolated as red solids in excellent yield (98%). The $^1$H NMR spectrum for cation **5.12** shows a singlet that integrates for 6H at 1.67 ppm for the coordinated NCMe ligands, indicative of a *trans* relationship of the nitrile ligands. The coordinated $PMe_3$ resonates as a doublet at 1.25 ppm in the $^1$H NMR spectrum of complexes **5.12-Y** (Figure 5.16). Evidence for the coordinated $PMe_3$ is apparent in the $^{31}$P NMR spectrum, which reveals a doublet and a triplet ($^2J_{PP}$ = 47 Hz) at 56.7 ppm and 15.9 ppm for the $^{Ph}$PNP ligand and the $PMe_3$ ligand, respectively. The addition of excess $PMe_3$ during the synthesis of cation **5.12** does not result in the coordination of two $PMe_3$ ligands, which could be an indication of the sterically congested coordination sphere.

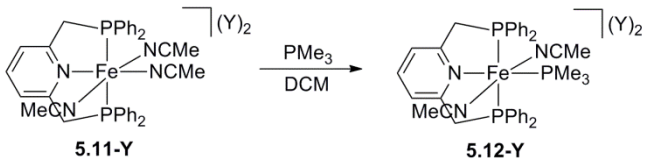


5.11-Y 5.12-Y

**Scheme 5.13.** Synthesis of *trans*-[($^{Ph}$PNP)Fe($PMe_3$)($NCMe)_2$]$(Y)_2$ (**5.12-Y**) (Y = $BAr'_4$ or $PF_6$).

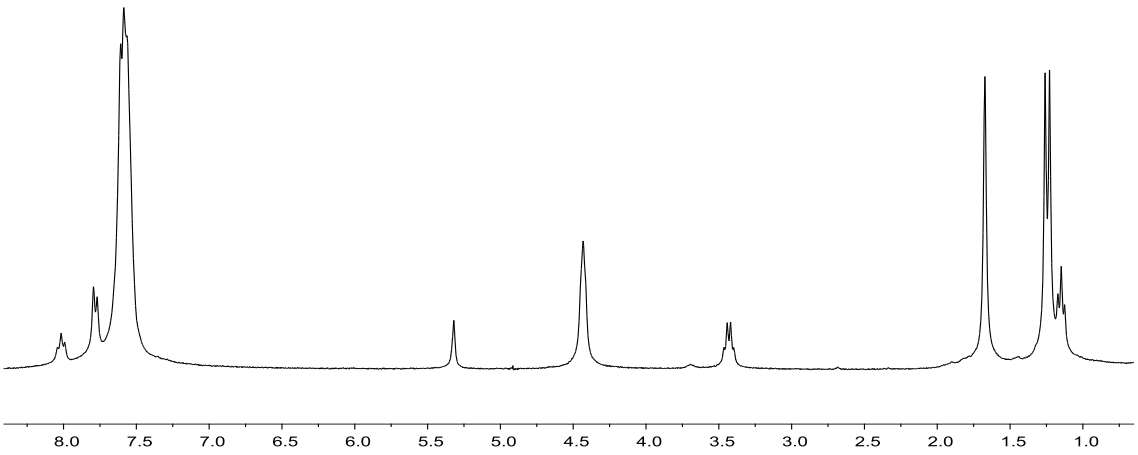


**Figure 5.16.** $^{1}$H NMR spectrum of *trans*-[($^{Ph}$PNP)Fe(PMe$_3$)(NCMe)$_2$](PF$_6$)$_2$ (**5.12-PF$_6$**) in $CD_2Cl_2$. Residual diethyl ether is present in the sample.

Reaction of the smaller ligand P(OCH$_2$)$_3$CEt with complex **5.11-PF$_6$** gives a different result. Treating a DCM solution of **5.11-PF$_6$** with one equivalent of P(OCH$_2$)$_3$CEt resulted in a color change from red to orange. As indicated by $^{31}$P NMR spectroscopy, the reaction results in the formation of two isomers, likely the *cis* and *trans* coordination isomers. The complexes *cis*-[($^{Ph}$PNP)Fe(P(OCH$_2$)$_3$CEt)(NCMe)$_2$](PF$_6$)$_2$ (***cis*-5.13-PF$_6$**) and *trans*-[($^{Ph}$PNP)Fe(P(OCH$_2$)$_3$CEt)(NCMe)$_2$](PF$_6$)$_2$ (***trans*-5.13-PF$_6$**) were isolated as light orange solids in 85% yield (Scheme 5.14). The –OCH$_2$ groups for each coordinated phosphite show up as doublets at 4.26 ppm and 3.70 ppm. The resonances for the NCMe ligands for ***cis*-5.13-Y** appear at 2.53 ppm and 1.25 ppm, while a resonance for the coordinated NCMe ligand for ***trans*-5.13-Y** appears at 1.48 ppm (Figure 5.17).

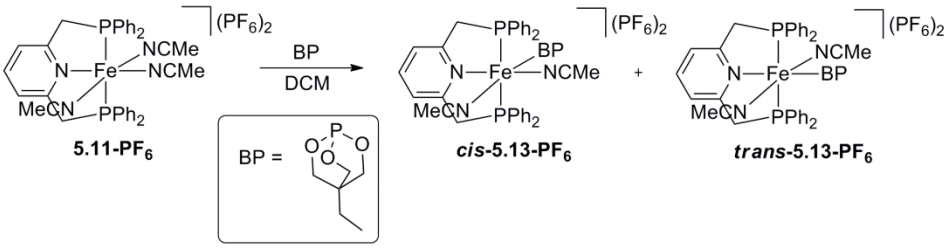


**Scheme 5.14.** Synthesis of *cis*-[($^{Ph}$PNP)Fe(P(OCH$_2$)$_3$CEt)(NCMe)$_2$](PF$_6$)$_2$ (***cis*-5.13-PF$_6$**) and *trans*-[($^{Ph}$PNP)Fe(P(OCH$_2$)$_3$CEt)(NCMe)$_2$](PF$_6$)$_2$ (***trans*-5.13-PF$_6$**).

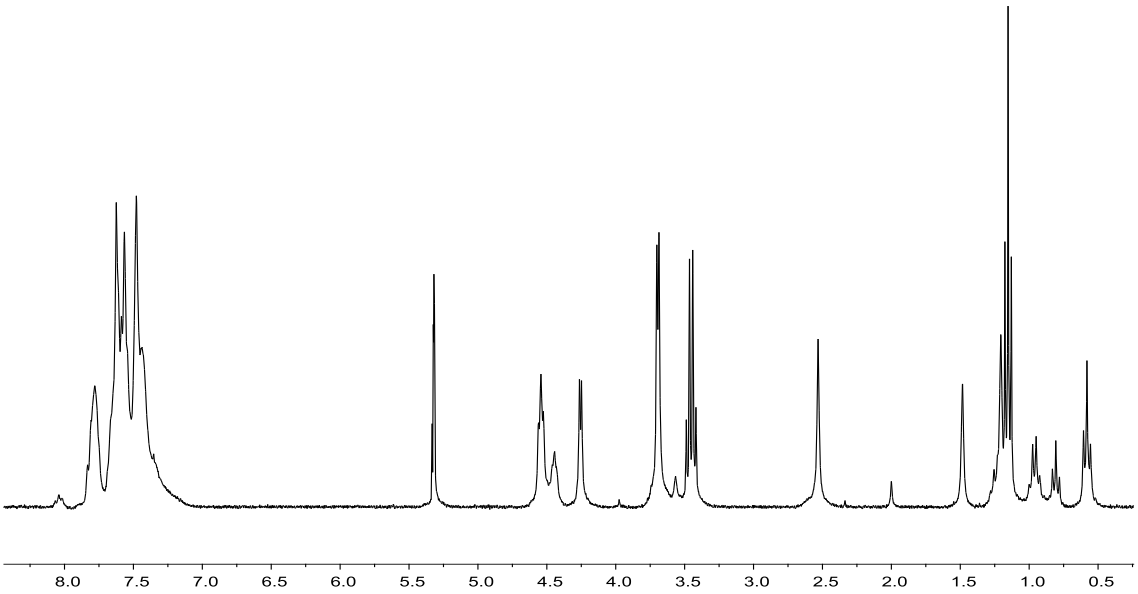


**Figure 5.17.** $^1$H NMR spectrum of *cis*-[($^{Ph}$PNP)Fe(P(OCH$_2$)$_3$CEt)(NCMe)$_2$](PF$_6$)$_2$ (***cis*-5.13**-PF$_6$) and *trans*-[($^{Ph}$PNP)Fe(P(OCH$_2$)$_3$CEt)(NCMe)$_2$](PF$_6$)$_2$ (***trans*-5.13**-PF$_6$) in CD$_2$Cl$_2$. Residual diethyl ether present in sample.

Based on $^1$H NMR integrations, the ratio of ***cis*-5.13-PF$_6$** to ***trans*-5.13-PF$_6$** is ~2.5:1. In order to gain insight into which isomer is thermodynamically preferred, a solution of a mixture of ***cis*-5.13-PF$_6$** and ***trans*-5.13-PF$_6$** was gently heated and monitored by NMR spectroscopy (Scheme 5.15, Figure 5.18). Over the course of approximately one day, the distribution changed from 2.5:1 (*cis*:*trans*) to 1:5. This suggests that the kinetic isomer is ***cis*-5.13-PF$_6$** while the thermodynamic isomer is ***trans*-**

**5.13-PF$_6$**. The pyridine group on the $^{Ph}$PNP ligand likely has a weaker *trans* effect than a coordinated NCMe ligand, resulting in the favorability of dissociating an NCMe ligand *cis* to the pyridine over the NCMe ligand *trans* to the pyridine. The result of the NCMe *cis* to the pyridine group dissociating first in the reaction of complex **5.11-PF$_6$** with P(OCH$_2$)$_3$CEt appears to be in contrast with the reaction of **5.11-Y** and PMe$_3$ where only the *trans* NCMe appears to dissociate. However, in the case of PMe$_3$, this result is likely dictated by sterics. We believe that the PMe$_3$ ligand is too large to coordinate to the Fe center perpendicular to the PNP plane, which is why this *cis* isomer is not observed for complex **5.12**.

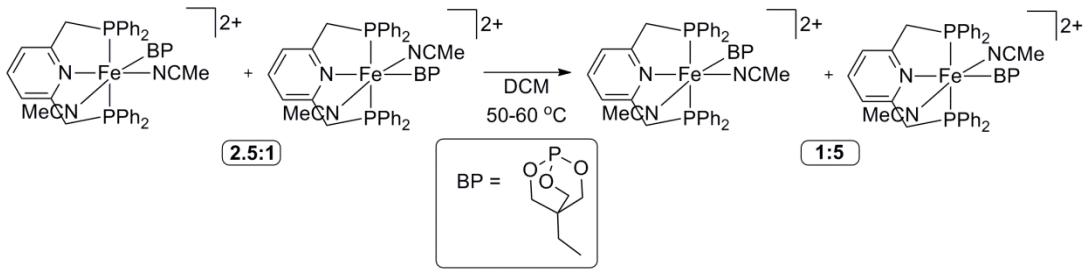


**Scheme 5.15.** Thermal isomerization of *cis*-[($^{Ph}$PNP)Fe(P(OCH$_2$)$_3$CEt)(NCMe)$_2$](PF$_6$)$_2$ (***cis*-5.13-PF$_6$**) and *trans*-[($^{Ph}$PNP)Fe(P(OCH$_2$)$_3$CEt)(NCMe)$_2$](PF$_6$)$_2$ (***trans*-5.13-PF$_6$**).

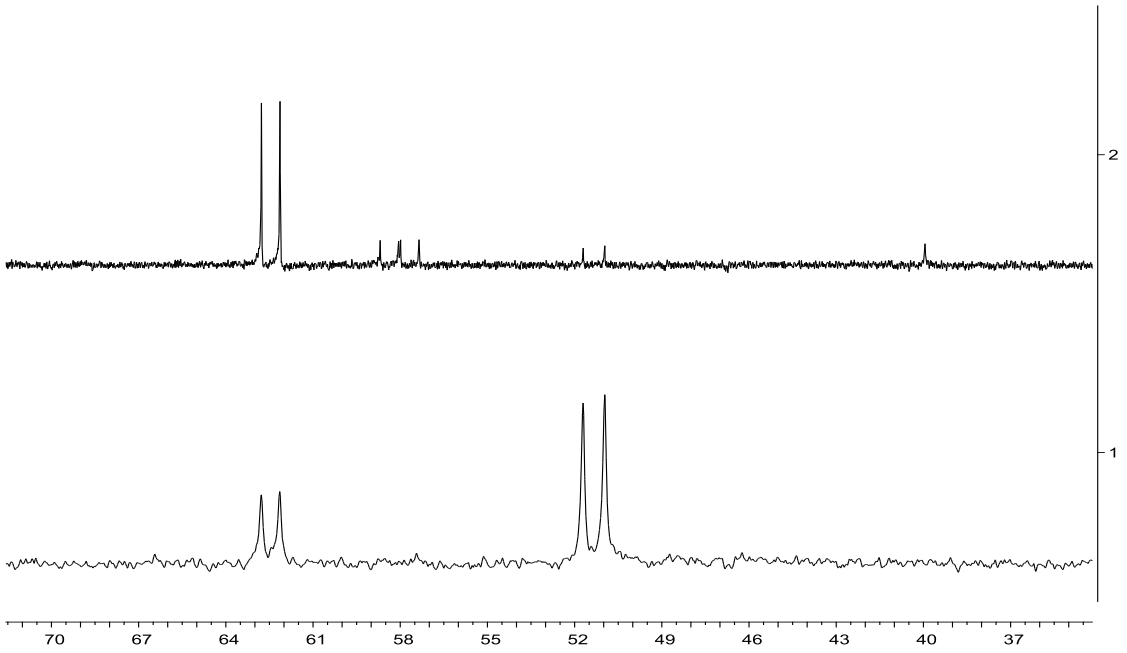


**Figure 5.18.** $^{31}$P NMR spectra showing isomerization of *cis*-[($^{Ph}$PNP)Fe(P(OCH$_2$)$_3$CEt)(NCMe)$_2$](PF$_6$)$_2$ (***cis*-5.13-PF$_6$**) and *trans*-[($^{Ph}$PNP)Fe(P(OCH$_2$)$_3$CEt)(NCMe)$_2$](PF$_6$)$_2$ (***trans*-5.13-**PF$_6$). Bottom spectrum is initial, and top is after heating at 50 - 60 °C for ~1 day. $^{Ph}$PNP region of spectra shown for clarity.

During the course of this experiment, a second phosphite containing species appears along with another species exhibiting broadened peaks. Based on the $^{31}$P NMR data, the first species appears to contain two P(OCH$_2$)$_3$CEt ligands and is likely *cis*-[($^{Ph}$PNP)Fe(P(OCH$_2$)$_3$CEt)$_2$(NCMe)](PF$_6$)$_2$ (Figure 5.18). The second species shows a singlet in the $^{31}$P NMR spectrum at ~40 ppm, suggesting that it does not contain a phosphite ligand. This second species appears to be a common thermal decomposition product, as it has formed in other reactions with ($^{Ph}$PNP)Fe complexes (see below). Based on the relatively small size of the $^{Ph}$PNP ligand, we considered that the identity of this species could be the homoleptic complex [($^{Ph}$PNP)$_2$Fe](Y)$_2$. Indeed, stirring a DCM solution of [($^{Ph}$PNP)Fe(NCMe)$_3$](PF$_6$)$_2$ (**5.11-PF$_6$**) with $^{Ph}$PNP resulted in a product with spectral data consistent with the observed decomposition product (Scheme 5.16).

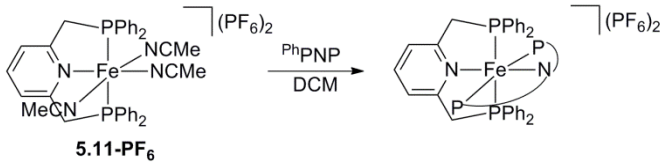


5.11-PF$_6$

**Scheme 5.16.** Synthesis of proposed decomposition product [($^{Ph}$PNP)$_2$Fe](PF$_6$)$_2$. Second ligand abbreviated for clarity.

With the complexes *trans*-[($^{Ph}$PNP)Fe(PMe$_3$)(NCMe)$_2$](Y)$_2$ (**5.12-Y**) and *cis*-[($^{Ph}$PNP)Fe(P(OCH$_2$)$_3$CEt)(NCMe)$_2$](PF$_6$)$_2$ (***cis*-5.13-PF$_6$**) and *trans*-[($^{Ph}$PNP)Fe(P(OCH$_2$)$_3$CEt)(NCMe)$_2$](PF$_6$)$_2$ (***trans*-5.13-PF$_6$**) in hand, we explored alkylation. Due to the simplicity of the single isomer for **5.12-Y**, initial synthetic attempts focused on this complex. The small scale reaction of complex **5.12- BAr'$_4$** with MeLi at –35 °C in diethyl ether resulted in a crude product with $^1$H NMR data consistent with the desired methyl complex [($^{Ph}$PNP)Fe(PMe$_3$)(NCMe)Me](BAr'$_4$)$_2$ (**5.14-BAr'$_4$)**. We found, however, that the reaction proceeded more cleanly with thermolysis (60 °C) of *trans*-[($^{Ph}$PNP)Fe(PMe$_3$)(NCMe)$_2$](BAr'$_4$)$_2$ (**5.12-BAr'$_4$**) and AlMe$_3$ in THF (Scheme 5.17). To the best of our knowledge, complex **5.14-BAr'$_4$** is the first example of an Fe–methyl complex ligated by a PNP ligand.

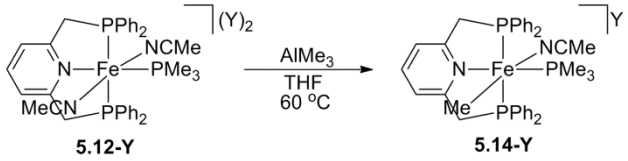


5.12-Y 5.14-Y

**Scheme 5.17.** Synthesis of [($^{Ph}$PNP)Fe(PMe$_3$)(NCMe)Me](Y) (**5.14-Y)**.

A significant challenge with this reaction protocol was the isolation and purification of complex **5.14-BAr'$_4$**. Following the reaction by $^{31}$P NMR spectroscopy indicated that the reaction proceeded relatively cleanly with a small amount of

[($^{Ph}$PNP)$_2$Fe](Y)$_2$ forming from decomposition. As a result of the challenges with purification, isolated yields were typically low (~15%). The $^1$H NMR spectrum of the desired product can be seen in Figure 5.19. The diagnostic resonance for the methyl ligand at –1.10 ppm resonates as an apparent quartet in the $^1$H NMR spectrum. A classic AB pattern for the methylene linkers of the $^{Ph}$PNP ligand is seen between 4.20-3.92 ppm. The coordinated NCMe resonates at 1.62 ppm in the $^1$H NMR spectrum, suggesting it is in the position perpendicular to the PNP plane, consistent the methyl ligand *trans* to the NCMe ligand. A doublet at 69.7 ppm and a triplet at 26.6 ppm are observed in the $^{31}$P NMR spectrum for the $^{Ph}$PNP ligand and the $PMe_3$ ligand, respectively. This stereochemistry is important to note since C–H activation and olefin insertion require that a vacant coordination site be available *cis* to the alkyl ligand.[20] Nonetheless, if isomerization is kinetically accessible, the desired reactivity might still be observed.

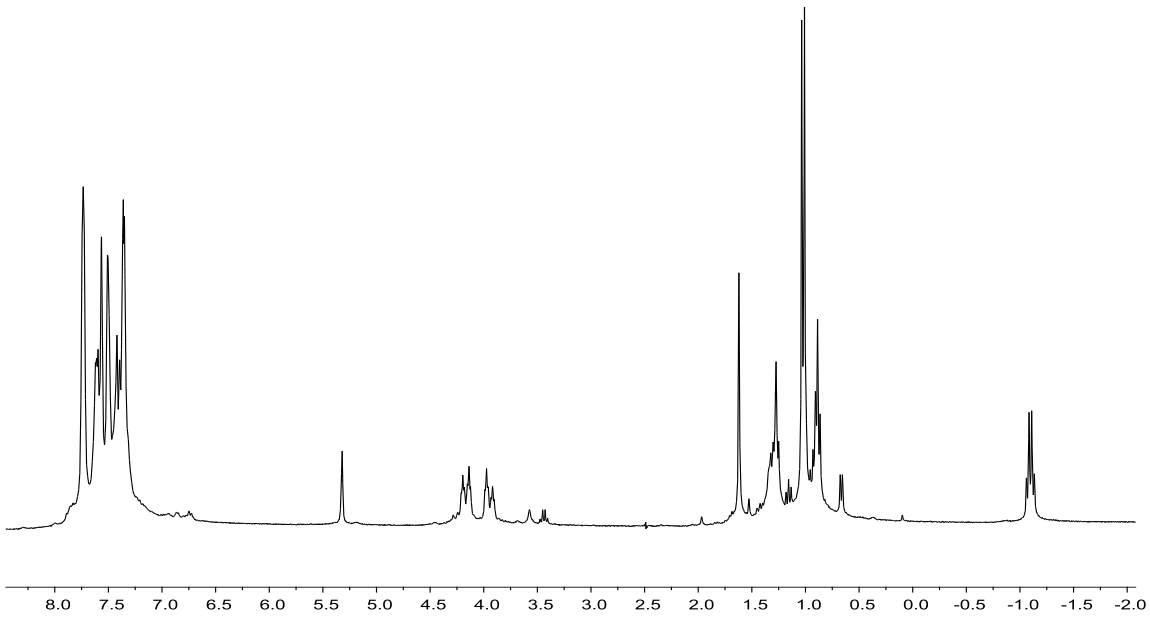


**Figure 5.19.** $^1$H NMR spectrum of [($^{Ph}$PNP)Fe($PMe_3$)(NCMe)Me](BAr'$_4$) (**5.14-BAr'$_4$**) in $CD_2Cl_2$. Pentane as well as trace impurities are observed in this sample.

It is worth noting that the reaction proceeds similarly starting from complex **5.12-$PF_6$**. Because of the challenges purifying complex **5.14-BAr'$_4$**, it was hoped that the $PF_6^-$ counterion would allow for re-crystallization. However, complex **5.12-$PF_6$** was not soluble in the THF reaction solvent. While the reaction did proceed, it resulted in very viscous reaction solutions, which made isolation of the product challenging. In fact, this phenomenon was also observed occasionally in the synthesis of **5.14-BAr'$_4$**. It is possible that THF is polymerizing under the reaction conditions. Unfortunately, other solvents did not prove to be suitable for this reaction (e.g., dioxane, DCM, etc.).

A full array of reactivity studies was not performed with complex **5.14-Y** due to the problems mentioned above, but additional efforts cleanly synthesizing **5.14-Y** and studying its reactivity will be performed in the Gunnoe lab. However, some preliminary experiments were performed. For example, complex **5.14-BAr'$_4$** was dissolved in $C_6D_6$ and heated between 60-90 °C to probe for benzene C–H activation. Over time, the signal-to-noise in the $^1$H NMR spectrum decreased along with the formation of precipitate in the tube. While not definitively determined, we suspect that complex **5.14-BAr'$_4$** precipitates out of solution since, other than the formation of a solid and the decrease in the signal-to-noise in the $^1$H NMR spectrum, no other significant changes were observed. No evidence for $CH_3D$ was detected by $^1$H NMR spectroscopy. As a result of the apparent solubility issues in $C_6D_6$, complex **5.14-BAr'$_4$** was heated in $CD_2Cl_2$ with excess $C_6D_6$ at 90 °C. This resulted in decomposition with the formation of multiple products as detected by $^{31}$P NMR spectroscopy without evidence for $CH_3D$ generation. A similar outcome was observed with THF-$d_8$ as the solvent. Additionally, complex **5.14-$PF_6$** was heated in *o*-dichlorobenzene-$d_4$ with excess furan to potentially observed furan C–H activation, but

this also resulted in decomposition to uncharacterized products. One final reaction was performed in which an acetone-$d_6$ solution of complex **5.14-PF$_6$** was treated with excess $C_6D_6$ and $C_2H_4$. After heating up to 90 °C, broad resonances were observed in the $^1$H NMR spectrum and substantial solid formed. While it is impossible to make any broad conclusions from these experiments, considering the questionable purity of some of the samples and the limited number of conditions examined, it is reasonable that complex **5.14-Y** is not sufficiently stable, resulting in decomposition before isomerization and productive reactivity is observed. Further experiments would need to be performed to confirm this hypothesis.

We examined methylating conditions to make [($^{Ph}$PNP)Fe(P(OCH$_2$)$_3$CEt)(NCMe)Me](PF$_6$) from [($^{Ph}$PNP)Fe(P(OCH$_2$)$_3$CEt)(NCMe)$_2$Me](PF$_6$)$_2$ (***cis/trans*-5.13-PF$_6$)**. Using a variety of methylating reagents (e.g., AlMe$_3$, Me$_2$Mg, MeLi), the desired complex was not able to be made in suitable purity. While a methyl complex could be observed in the crude reaction mixture from the reaction with AlMe$_3$, as evidenced by a doublet of triplets at ~ –1.4 ppm, attempts at cleanly isolating this complex have thus far been futile. The crude $^1$H NMR spectrum contains at least two other methyl resonances. Efforts to cleanly make [($^{Ph}$PNP)Fe(P(OCH$_2$)$_3$CEt)(NCMe)Me](PF$_6$) will likely be the subject of future studies in the Gunnoe lab.

In order to potentially increase the thermal stability of this class of Fe complex, investigations into ($^{Cy}$PNP)Fe complexes ($^{Cy}$PNP = 2,6-bis(dicyclohexylphosphinomethyl)pyridine) commenced. Because of the larger steric profile of the cyclohexyl substituents, we believed that they would better protect the Fe

center. The ligand $^{Cy}$PNP was synthesized by modification of the literature procedure as outlined in Scheme 5.18.[18] The reaction of $Cy_2PH$ and *n*-BuLi at low temperature generates $LiPCy_2$, which was reacted with 2,6-bis(chloromethyl)pyridine. In our hands, the $LiPCy_2$ mixture had to be further diluted with THF to ~1/2 the concentration reported in the literature procedure in order to successfully make the desired ligand. Treating the $^{Cy}$PNP with $FeCl_2$ in THF resulted in a yellow reaction mixture. After work-up, the yellow solid ($^{Cy}$PNP)$FeCl_2$ (**5.15**) was isolated in 41% yield (Scheme 5.19). Interestingly, complex **5.15** is soluble in polar solvents, while complex **5.10** with phenyl substituents is not. Other ($^{R}$PNP)$FeX_2$ (R = *i*Pr or *t*Bu) complexes are also soluble in polar solvents (e.g., NCMe and DCM), which likely suggests that the small phenyl substituents of $^{Ph}$PNP result in either a polymeric structure or form [($^{Ph}$PNP)$_2$Fe][$FeCl_4$].[21] The $^1$H NMR spectrum of **5.15** exhibits broadened resonances with a large chemical shift window (–5 ppm to 100 ppm), which is consistent with a paramagnetic complex (Figure 5.20).

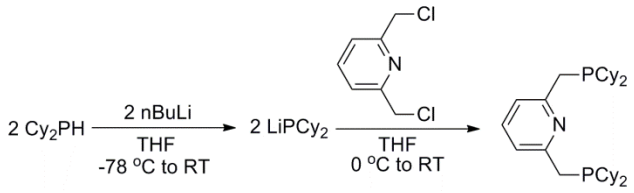


**Scheme 5.18.** Synthesis of $^{Cy}$PNP.

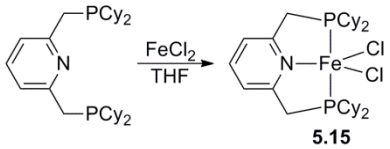


**Scheme 5.19.** Synthesis of ($^{Cy}$PNP)$FeCl_2$ (**5.15**).

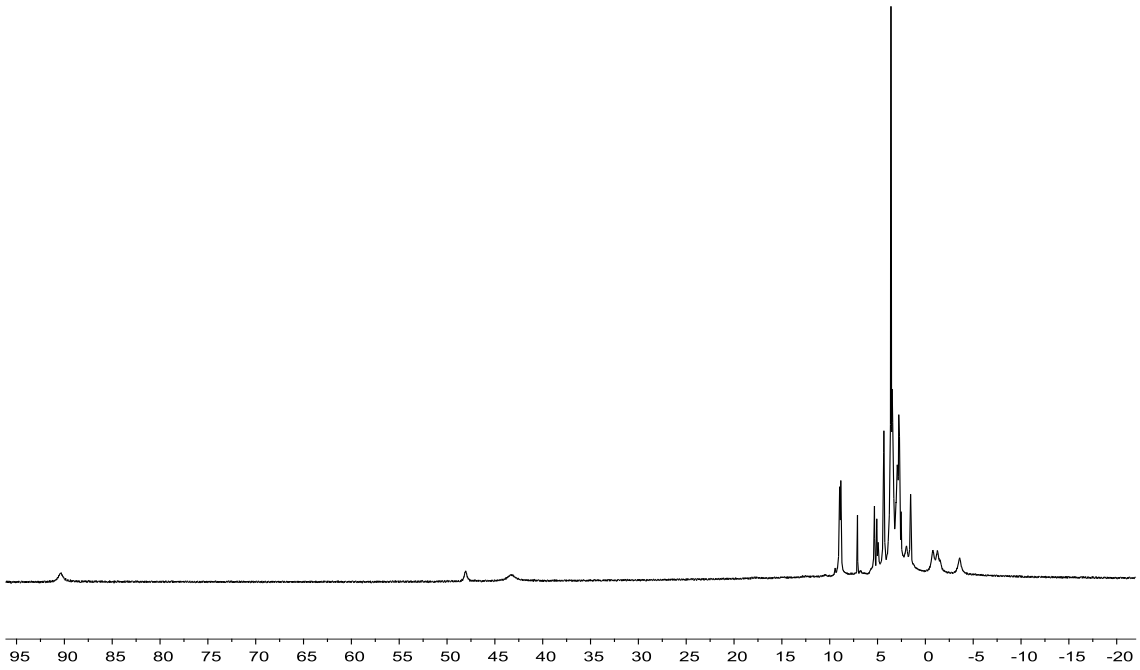


**Figure 5.20.** $^{1}$H NMR spectrum of ($^{Cy}$PNP)FeCl$_2$ (**5.15**) in $CD_3CN$.

Attempts were made to coordinate a phosphine or phosphite directly to complex **5.15** without going through [($^{Cy}$PNP)Fe(NCMe)$_3$](Y)$_2$. Combining complex **5.15** with $PMe_3$ resulted in no reaction based on no evidence for $PMe_3$ coordination in the $^{31}$P NMR spectrum. Thus, the increased steric profile of the cyclohexyl groups may be preventing coordination to ($^{Cy}$PNP)FeCl$_2$ (**5.15**). The reaction of complex **5.15** with P(OCH$_2$)$_3$CEt in NCMe results in the formation of multiple products as detected by $^{31}$P NMR spectroscopy (Figure 5.21, Scheme 5.20), which reflect the small size of P(OCH$_2$)$_3$CEt compared to $PMe_3$.[22] Initially, the predominant species appears to have two equivalents of P(OCH$_2$)$_3$CEt coordinated, as evidenced by a triplet in the $^{31}$P NMR spectrum at ~58 ppm, likely due to the formation of an isomer of [($^{Cy}$PNP)Fe(P(OCH$_2$)$_3$CEt)$_2$Cl]Cl. There is a second minor species that also has two equivalents of P(OCH$_2$)$_3$CEt coordinated (a triplet at ~62 ppm in the $^{31}$P NMR spectrum), which is likely another isomer of [($^{Cy}$PNP)Fe(P(OCH$_2$)$_3$CEt)$_2$Cl]Cl. It is difficult to assign which isomer is *cis* and *trans*

since the $P(OCH_2)_3CEt$ region of the $^{31}P$ NMR spectrum contains many overlapping signals, making it challenging to determine the splitting of the resonances in that region. Additionally, the desired complex *trans*-($^{Cy}$PNP)Fe($P(OCH_2)_3CEt)Cl_2$ also forms in minor amounts based on a doublet at 66.4 ppm and a triplet at 163.8 ppm ($^2J_{PP}$ = 70 Hz) for the $^{Cy}$PNP ligand and the two $P(OCH_2)_3CEt$ ligands, respectively. Heating this reaction solution to 60 °C results in the gradual conversion to the ($^{Cy}$PNP)Fe($P(OCH_2)_3CEt)Cl_2$ complex (Figure 5.21). Apparently, ($^{Cy}$PNP)Fe($P(OCH_2)_3CEt)Cl_2$ is thermodynamically preferred. Further heating at 60 °C did not change the product distribution. The final product distribution is ~1:1 [sum of bis(phosphite) isomers:mono(phosphite) isomer]. Due the formation of multiple products, alternative synthetic procedures were examined that involved direct methylation of complex **5.15** with and without added $P(OCH_2)_3CEt$. However, these attempts were unsuccessful. Additional experiments would need to be performed to conclude whether ($^{Cy}$PNP)Fe complexes are promising candidates as pre-catalysts for olefin hydroarylation.

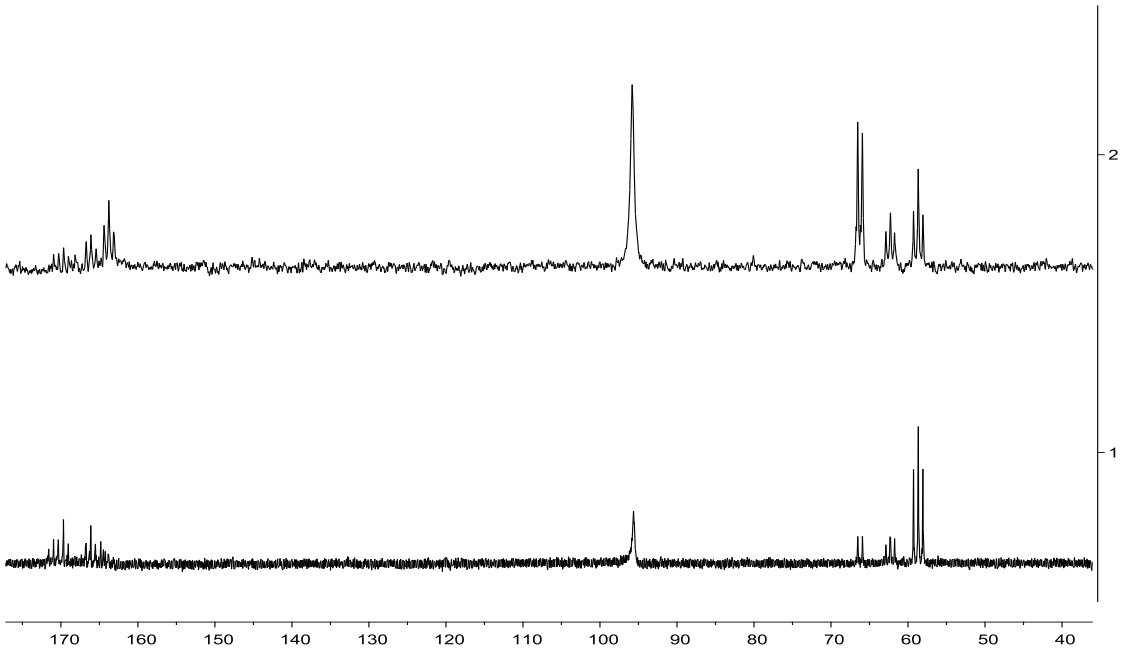


**Figure 5.21.** $^{31}$P NMR spectra showing the reaction of ($^{Cy}$PNP)FeCl$_2$ (**5.15**) with P(OCH$_2$)$_3$CEt in CD$_3$CN. Bottom spectrum is after stirring at room temperature for 4 h. Top spectrum is after heating at 60 °C for an additional 4 h. Peak at ~96 ppm is free P(OCH$_2$)$_3$CEt.

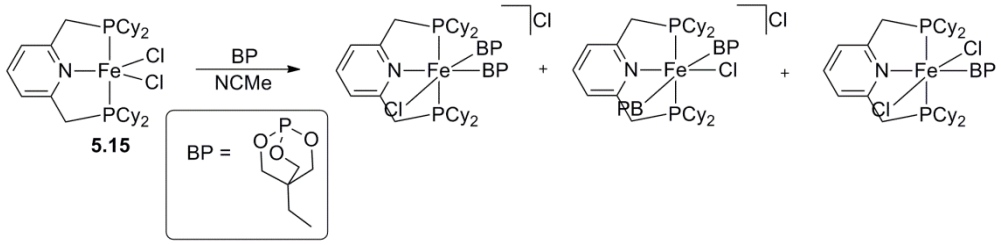


**Scheme 5.20.** Reaction of ($^{Cy}$PNP)FeCl$_2$ (**5.15**) and P(OCH$_2$)$_3$CEt in NCMe.

### 5.2.3 Complexes of Tris(2-pyridylmethyl)amine (TPA)

A drawback to the PNP ligands is that they coordinate to the metal center in a meridinal fashion. It was demonstrated that a potential result of this coordination mode is that the hydrocarbyl ligand and the labile ligand NCMe would be placed *trans* to each other (Figure 5.22). Consequently, if isomerization is not kinetically accessible, olefin insertion and C–H activation could not occur. As a result, we became interested in

developing Fe complexes ligated by tetradentate ligands that would place the remaining coordination sites *cis* (Figure 5.23). Tetraamine ligands have found utility in Fe catalysts for hydrocarbon oxidation reactions.[23, 24] The tris(2-pyridylmethyl)amine ligand (TPA) has been successfully used for hydrocarbon oxidation reactions and, due to its commercial availability, seemed a promising candidate to develop stable Fe pre-catalysts for olefin hydroarylation.

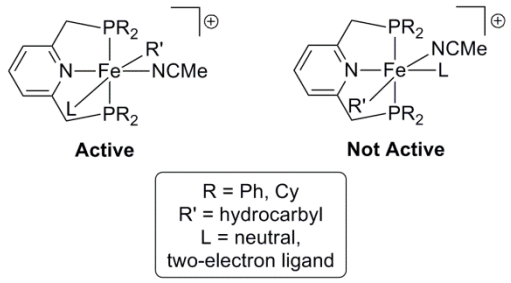


**Figure 5.22.** Comparison of the isomer active for C–H activation and olefin insertion and the isomer that is not active for C–H activation and olefin insertion for (PNP)Fe complexes.

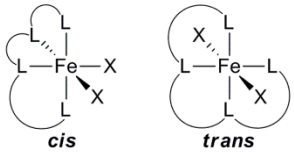


**Figure 5.23.** *Cis* and *trans* isomers possible for tetradentate ligands coordinated to iron.

To gain entry into these complexes, the known complexes (TPA)$FeCl_2$ and (TPA)$Fe(OTf)_2$ were prepared according to Scheme 5.21.[24] Several alkylating reagents and conditions were attempted with no success (Table 5.4). In general, when a Grignard or alkyl lithium reagent was used, the yellow or orange starting complex quickly gave way to a deep purple solution at low temperature (–35 °C or –78 °C) that eventually led to an intractable brown reaction mixture after warming to room temperature. At this

point, we do not know the identity of the unisolable purple product, but other than a desired methyl complex, it could also possibly be an unstable Fe(0) complex since Grignard and alkyl lithium reagents have been reported to reduce Fe(II) complexes to Fe(0) complexes.[25, 26] Other alkylating reagents such as $AlMe_3$ or $Me_4Sn$ did not react even at elevated temperatures. As a result, the (TPA)Fe complexes were not explored further.

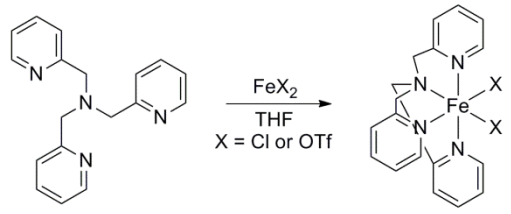


**Scheme 5.21.** Synthesis of (TPA)$FeX_2$ complexes.

**Table 5.4.** Alkylating attempts using (TPA)$FeX_2$ complexes. All reactions performed in THF or THF-$d_8$.

| Entry | X | Reagent (equiv) | Temperature (°C) | Result |
|---|---|---|---|---|
| 1 | OTf | $NaBEt_3H$ (2) | –35 to RT | Decomposition |
| 2 | OTf | $NaBEt_3H$ (2) | RT | Decomposition |
| 3 | OTf | $Me_2(Ph)CH_2MgCl$ (2) | –35 to RT | No reaction |
| 4 | OTf | PhMgBr (2) | –35 to RT | Decomposition |
| 5 | OTf | $TMSCH_2MgCl$ (2) | –35 to RT | Decomposition |
| 6 | OTf | PhMgBr (1) | –35 to RT | Decomposition |
| 7 | OTf | PhLi (2) | –78 to RT | Decomposition |
| 8 | OTf | PhLi (4) | –78 to RT | Decomposition |
| 9 | OTf | $AlMe_3$ (1) | 45 | No reaction – viscous |
| 10 | OTf | $SnMe_4$ | Up to 90 | No reaction |
| 11 | Cl | PhMgBr (2) | RT | Decomposition |
| 12 | Cl | MeLi (2) | –60 to RT | Decomposition |

## 5.3 Conclusions and Outlook

In this chapter, the synthesis of several new Fe complexes outside the Cp*Fe motif were reported. The rationale for pursuing these complexes was based on increasing the stability and avoiding intramolecular reactivity that was prevalent with the Cp*Fe

systems (see Chapters 2-4). Three classes of ligand were investigated, which were functional group appended cyclopentadienyl ligands, PNP ligands, and tetraamine ligands.

The synthesis of viable Fe catalysts with the functional group appended cyclopentadienyl ligands, namely $[Cp(CH_2)_2PPh_2]^-$ and $[Cp(CH_2)_2PMe_2]^-$, was not successful due to the challenges making complexes with labile ligands. Several Fe–methyl complexes were synthesized based off these ligands; however, low yields of the syntheses and the strong coordinating ability of the ancillary ligands limited their utility.

The $^{Ph}$PNP ligand allowed for the synthesis of several new Fe complexes, including the first known example of an Fe–alkyl complex ligated by a PNP ligand. Challenges purifying this complex and its relatively low stability led to the exploration of Fe complexes based on the $^{Cy}$PNP ligand. Preliminary data suggest that the steric profile of the ligand may limit the successful synthesis of desired pre-catalysts. Additionally, we found that the synthetic procedures resulted in multiple products, making the potential to isolate the desired complexes not promising. For both the $^{Ph}$PNP ligand and the $^{Cy}$PNP ligand, additional efforts should be made to cleanly isolate potential pre-catalysts and fully exploring their reactivity (see Chapter 7 for more details).

Due to the meridinal coordination mode of the PNP ligands, and the formation of Fe complexes with the alkyl ligand *trans* to the labile ligand, we began investigating the possibility of using tetraamine ligands. Using the TPA ligand, attempts at alkylating with Grignard reagents or alkyl lithium reagents results in either no reaction or decomposition. Based on preliminary reactions with these complexes, it seems unlikely that (TPA)Fe complexes would make suitable catalysts.

While the synthesis of a promising Fe pre-catalyst based on these ligand motifs was not successful, several important lessons were learned through these studies. A major challenge in developing suitable Fe catalysts is the ability to access a vacant coordination site. The use of $[Cp(CH_2)_2PPh_2]^-$ and $[Cp(CH_2)_2PMe_2]^-$ certainly limited this ability since stable complexes could only be synthesized in which a strongly coordinating ligand was used. Using formally neutral ligands, such as TPA and the PNP ligands, allows for the possibility of accessing a vacant coordination site through halide abstraction, which was demonstrated in the synthesis of [($^{Ph}$PNP)Fe($PMe_3$)(NCMe)Me](Y) (**5.14-Y**). However, tridentate ligands that coordinate in a meridinal fashion may lead to the synthesis of Fe complexes in which the alkyl group is *trans* to the vacant coordination site. This coordination isomer is not suitable for olefin hydroarylation, assuming isomerization is not kinetically accessible. The most promising ligand motif is the *cis*-coordinating tetradentate ligand since a halide could be abstracted from an ($L_4$)Fe(R)(X) ($L_4$ = tetradentate ligand, R = alkyl or aryl ligand, X = halide) complex leading to a vacant coordination site that is *cis* to the alkyl or aryl group. While work with (TPA)Fe complexes does not seem encouraging, other related ligands may give more promising results (see Chapter 7 for more details).

## 5.4 Experimental Section

### 5.4.1 General Methods

Unless otherwise noted, all synthetic procedures were performed under anaerobic conditions in a nitrogen-filled glovebox or by using standard Schlenk techniques. Glovebox purity was maintained by periodic nitrogen purges and was monitored by an oxygen analyzer ($O_2$ < 15 ppm for all reactions). Tetrahydrofuran, diethyl ether and pentane were dried by distillation from sodium/benzophenone. Acetonitrile was distilled

from $P_2O_5$. Hexanes, dichloromethane, and benzene were purified by passage through a column of activated alumina. Deuterated solvents were used as received and stored under a $N_2$ atmosphere over 4 Å molecular sieves. $^1$H NMR spectra were recorded on a Varian 300 MHz, Varian 500 MHz, or a Bruker 600 MHz spectrometer. All $^1$H spectra are referenced against residual proton signals of the deuterated solvents and are reported in ppm. $^{31}$P NMR were recorded on a Varian 300 MHz spectrometer (operating frequency 121 MHz). Ethylene was purchased from GTS-Welco. All other reagents were purchased from commercial sources and used as received. The pro-ligands Li[$CpCH_2Py$],[10] K[$Cp(CH_2)_2PPh_2$],[12] Li[$Cp(CH_2)_2PMe_2$,[12] $^{Ph}$PNP,[18] and $^{Cy}$PNP[18] were synthesized by modifications of the literature procedures. The complexes [(tmeda)$FeCl_2$],[27] ($^{Ph}$PNP)$FeCl_2$ (**5.10**),[19] (TPA)$FeCl_2$,[24] and (TPA)$Fe(OTf)_2$ were made by adaptations of literature procedures.[24] Procedures in which modification from the literature reports were made are outlined below.

K[$Cp(CH_2)_2PPh_2$][12]: Commercially available $KPPh_2$ was used. After reflux, the reaction mixture was reduced to ½ the volume and the product was collected as a white solid.

Li[$Cp(CH_2)_2PMe_2$[12]: $LiPMe_2$ was generated in situ by reaction of $PPhMe_2$ with Li sand.

$^{Ph}$PNP[18]: Commercially available $kPPh_2$ was used. The crude product was purified by stirring as a suspension in a 1:1 mixture of methanol and hexanes and then collecting the solid.

$^{Cy}$PNP[18]: After generating $LiPCy_2$ in situ in THF, the volume of THF was approximately doubled before adding to a THF solution of 2,6-bis(chloromethyl)pyridine.

($^{Ph}$PNP)$FeCl_2$ (**5.10**)[19]: The $^{Ph}$PNP ligand and $FeCl_2$ were stirred overnight in THF to produce a yellow suspension that was subsequently collected.

### 5.4.2 Experimental Procedures

**General Procedure for the Synthesis of [Cp(CH$_2$)$_2$PPh$_2$]Fe(L)Cl (L = P(OCH$_2$)$_3$CEt, PMe$_3$, CN$^t$Bu) (5.1-5.3).** The complex [(tmeda)FeCl$_2$] was dissolved in THF and cooled to –35 °C. To the chilled solution was slowly added a THF solution of K[Cp(CH$_2$)$_2$PPh$_2$] (1 equiv.). After stirring for ~5 min at room temperature, a slight excess of the appropriate ligand L was added, and the resulting mixture was allowed to stir for approximately 1 h. Next, the reaction mixture was concentrated in vacuo. The residue was loaded onto a silica gel plug and washed with benzene or diethyl ether to elute a yellow-green band, which was subsequently discarded. THF was then used to elute the product (purple or green, depending on ligand). After removing the volatiles in vacuo, either hexanes or *n*-pentane was added to the resulting residue. After washing with hexanes or *n*-pentane, the product was collected and dried in vacuo.

**[Cp(CH$_2$)$_2$PPh$_2$]Fe(P(OCH$_2$)$_3$CEt)Cl (5.1):** Dark purple solid (20% yield). $^1$H NMR (300 MHz, CDCl$_3$): δ 8.25 (m, 2H, 2 x PPh$_2$), 7.59 – 7.04 (m, 8H, 8 x PPh$_2$), 5.36 (s, 1H, C$_5$H$_4$), 4.87 (s, 2H, 2 x C$_5$H$_4$), 3.93 (m, 6H, 6 x P(OC*H*$_2$)$_3$CEt ), 3.31 (m, 1H, C$_5$H$_4$), 2.78 (m, 1H, -(C*H*$_2$)$_2$PPh$_2$), 2.51 (m, 1H, -(C*H*$_2$)$_2$PPh$_2$), 1.91 (m, 2H, 2 x -(C*H*$_2$)$_2$PPh$_2$), 1.08 (q, $^3J_{HH}$ = 8 Hz, 2H, 2 x P(OCH$_2$)$_3$CC*H*$_2$CH$_3$), 0.73 (t, $^3J_{HH}$ = 8 Hz, 3H, 3 x P(OCH$_2$)$_3$CCH$_2$C*H*$_3$). $^{31}$P NMR (121 MHz, CD$_3$CN): δ 164.3 (d, $^2J_{PP}$ = 107 Hz, P(OCH$_2$)$_3$CEt), 69.5 (d, $^2J_{PP}$ = 107 Hz, PPh$_2$).

**[Cp(CH$_2$)$_2$PPh$_2$]Fe(PMe$_3$)Cl (5.2):** Dark purple solid (20% yield). $^1$H NMR (300 MHz, acetone-*d*$_6$): δ 8.44 (m, 2H, 2 x PPh$_2$), 7.42 (m, 8H, 8 x PPh$_2$), 4.87 (s, 1H, C$_5$H$_4$), 4.63 (m, 1H, C$_5$H$_4$), 4.42 (s, 1H, C$_5$H$_4$), 3.45 (m, 1H, -(C*H*$_2$)$_2$PPh$_2$), 3.10 (m, 1H, -(C*H*$_2$)$_2$PPh$_2$), 2.36 (s, 1H, C$_5$H$_4$), 1.97 – 1.67 (m, 2H, 2 x -(C*H*$_2$)$_2$PPh$_2$), 1.18 (d, $^3J_{PH}$ = 8

Hz, 9H, $PMe_3$). $^{31}P$ NMR (121 MHz, $C_6D_6$) δ 68.1 (d, $^2J_{PP}$ = 55Hz, -$PPh_2$), 23.2 (d, $^2J_{PP}$ = 55 Hz, $PMe_3$).

**[Cp(CH$_2$)$_2$PPh$_2$]Fe(CN$^t$Bu)Cl (5.3):** Green solid (30% yield). $^1H$ NMR (300 MHz, acetone-$d_6$): δ 8.34 (m, 2H, 2 x $PPh_2$), 7.56 (m, 2H, 2 x $PPh_2$), 7.39 (m, 6H, 6 x $PPh_2$), 5.06 (m, 1H, $C_5H_4$), 4.80 (m, 1H, $C_5H_4$), 4.75 (m, 1H, $C_5H_4$), 3.51 (m, 2H, 2 x -(C$H_2$)$_2$$PPh_2$), 2.77 (m, 2H, 2 x -(C$H_2$)$_2$$PPh_2$), 2.63 (m, 1H, $C_5H_4$), 1.17 (s, 9H, CNC(C$H_3$)$_3$). $^{31}P$ NMR (121 Hz, acetone-$d_6$): 72.1 (s, $PPh_2$).

**General Procedure for the Synthesis of [Cp(CH$_2$)$_2$PPh$_2$]Fe(L)Me (L = P(OCH$_2$)$_3$CEt, PMe$_3$, CN$^t$Bu) (5.4-5.6).** A solution of [Cp(CH$_2$)$_2$PPh$_2$]Fe(L)Cl (L = P(OCH$_2$)$_3$CEt, $PMe_3$, CN$^t$Bu) (**5.1-5.3**) in THF was cooled to –35 °C. At this temperature, MeLi was added (1 equivalent). The solution was allowed to warm to room temperature, turning red within 10 min. After stirring for ~1h, the volatiles were removed in vacuo. The residue was extracted with benzene and filtered through Celite. The resulting filtrate was concentrated in vacuo and washed with minimal *n*-pentane. The resulting solid was dried in vacuo.

**[Cp(CH$_2$)$_2$PPh$_2$]Fe(P(OCH$_2$)$_3$CEt)Me (5.4):** Red solid (67% yield). $^1H$ NMR (300 MHz, $CD_3CN$): δ 7.80 (m, 2H, 2 x $PPh_2$), 7.32 (m, 8H, 8 x $PPh_2$), 4.35 (m, 1H, -(C$H_2$)$_2$$PPh_2$), 4.13 (m, 1H, $C_5H_4$), 4.00 (m, 6H, 6 x P(OC$H_2$)$_3$CEt), 3.82 (m, 1H, $C_5H_4$), 3.74 (m, 1H, $C_5H_4$), 3.32 (m, 1H, -(C$H_2$)$_2$$PPh_2$), 2.82 (m, 1H, -(C$H_2$)$_2$$PPh_2$), 2.34 (m, 1H, -(C$H_2$)$_2$$PPh_2$), 2.21 (m, 1H, -(C$H_2$)$_2$$PPh_2$), 1.59 (m, 1H, $C_5H_4$), 1.12 (t, $^3J_{HH}$ = 8 Hz, 2H, 2 x P(OCH$_2$)$_3$CC$H_2$CH$_3$), 0.73 (t, $^3J_{HH}$ = 8 Hz, 3H, 3 x P(OCH$_2$)$_3$CCH$_2$C$H_3$), –0.87 (vt, 3H, Me). $^{31}P$ NMR (121 Hz, $CD_3CN$): δ 170.8 (d, $^2J_{PP}$ = 91 Hz, P(OCH$_2$)$_3$CEt), 94.7 (d, $^2J_{PP}$ = 91 Hz, $PPh_2$).

**[Cp(CH$_2$)$_2$PPh$_2$]Fe(PMe$_3$)Me (5.5):** Red solid (37% yield). $^1$H NMR (300 MHz, $C_6D_6$): δ 7.65 (m, 2H, 2 x PPh$_2$), 7.42 (m, 2H, 2 x PPh$_2$), 7.12 (m, 6H, 6 x PPh$_2$), 4.07 (br s, 1H, $C_5H_4$), 3.98 (m, 1H, $C_5H_4$), 3.92 (m, 1H, $C_5H_4$), 3.82 (m, 1H, $C_5H_4$), 3.01 (m, 1H, -(C*H*$_2$)$_2$PPh$_2$), 2.62 (m, 1H, -(C*H*$_2$)$_2$PPh$_2$), 1.94 (m, 1H, -(C*H*$_2$)$_2$PPh$_2$), 1.68 (m, 1H, -(C*H*$_2$)$_2$PPh$_2$), 0.90 (d, $^3J_{PH}$ = 7 Hz, 9H, PMe$_3$), –0.25 (dd, $^3J_{PH}$ = 9 Hz, 7 Hz, 3H, Me). $^{31}$P NMR (121 MHz, $C_6D_6$): δ 90.8 (d, $^2J_{PP}$ = 48 Hz, PPh$_2$), 35.5 (d, $^2J_{PP}$ = 48 Hz, PMe$_3$).

**[Cp(CH$_2$)$_2$PPh$_2$]Fe(CN$^t$Bu)Me (5.6):** Isolated as a red oil that was used directly in subsequent reactions. $^1$H NMR (300 MHz, $C_6D_6$): δ 7.83 (m, 2H, 2 x PPh$_2$), 7.39 (m, 2H, 2 x PPh$_2$), 7.10 (m, 6H, 6 x PPh$_2$), 4.68 (m, 1H, $C_5H_4$), 4.40 (br s, 1H, $C_5H_4$), 4.15 (br s, 2H, 2 x $C_5H_4$), 2.87 (m, 1H, -(C*H*$_2$)$_2$PPh$_2$), 2.64 (m, 1H, -(C*H*$_2$)$_2$PPh$_2$), 1.97 (m, 1H, -(C*H*$_2$)$_2$PPh$_2$), 1.67 (m, 1H, -(C*H*$_2$)$_2$PPh$_2$), 1.07 (s, 9H, CNC(C*H*$_3$)$_3$), 0.13 (d, $^3J_{PH}$ = 7 Hz, 3H, Me). $^{31}$P NMR (121 Hz, $C_6D_6$): 97.2 (s, PPh$_2$).

**Synthesis of Crude K[Cp(CH$_2$)$_2$PPh$_2$]Fe(η$^1$-PPh$_2$(CH$_2$)$_2$Cp)Me (5.7).** The complex [(tmeda)FeCl$_2$] (0.024 g, 0.099 mmol) was dissolved in THF (2 mL) and cooled to –35 °C. In a separate flask, K[Cp(CH$_2$)$_2$PPh$_2$] (0.036 g, 0.093 mmol) was dissolved in THF (2 mL) and cooled to –35 °C. The ligand solution was added dropwise to the solution of [(tmeda)FeCl$_2$] while warming to room temperature. After ~5 min, the reaction flask was cooled back down to –35 °C, and MeLi (58 μL, 1.6 M, 0.093 mmol) was added. After the addition of MeLi, the reaction changed from dark purple to red. The reaction was allowed to warm to room temperature and was stirred for ~1 h. After this time, the volatiles were removed in vacuo, and the resulting residue was extracted with diethyl ether and filtered through Celite. The red filtrate was dried in vacuo and washed with *n*-pentane. This residue was reconstituted in $C_6D_6$ and analyzed by NMR

spectroscopy. $^{1}$H NMR (300 MHz, $C_6D_6$): δ 8.64 (d, $J$ = 4 Hz, 2H, 2 x $PPh_2$), 7.74 (t, $^{3}J_{HH}$ = 7 Hz, 2H, 2 x $PPh_2$), 7.58 (m, 2H. 2 x $PPh_2$), 7.46 (m, 2H, 2 x $PPh_2$), 7.10 (m, 8H, 8 x $PPh_2$), 6.93 (m, 2H, 2 x $PPh_2$), 6.77 (dd, $^{3}J_{HH}$ = 8 Hz, 6 Hz, 2H, 2 x $PPh_2$), 4.65 (m, 1H, $C_5H_4$), 4.18 ( br s, 1H, $C_5H_4$), 4.10 (m, 2H, $C_5H_4$), 3.86 (m, 2H, $C_5H_4$), 3.73 (m, 2H, $C_5H_4$), 3.43 (m, 1H, -($CH_2$)$_2$$PPh_2$), 3.13 (m, 1H, -($CH_2$)$_2$$PPh_2$), 2.69 (m, 1H, -($CH_2$)$_2$$PPh_2$), 2.49 – 1.95 (overlapping m, 4H, 4 x -($CH_2$)$_2$$PPh_2$), 1.83 (m, 1H, -($CH_2$)$_2$$PPh_2$), 0.18 (vt, 3H, Me). $^{31}$P NMR (121 MHz, $C_6D_6$): δ 85.45 (d, $^{2}J_{PP}$ = 4 Hz, $PPh_2$), 85.14 (d, $^{2}J_{PP}$ = 4 Hz, $PPh_2$), 70.39 (d, $^{2}J_{PP}$ = 6 Hz, $PPh_2$), 70.08 (d, $^{2}J_{PP}$ = 6 Hz, $PPh_2$). Note: The two sets of resonances in the $^{31}$P NMR appear of equal intensity. Thus, they might be explained by two isomers, although future experiments would be needed to conclusively determine the origin of this phenomenon.

**Synthesis of [Cp(CH$_2$)$_2$PMe$_2$]Fe(P(OCH$_2$)$_3$CEt)Cl (5.8).** The complex [(tmeda)$FeCl_2$] (0.107 g, 0.440 mmol) and P($OCH_2$)$_3$CEt (0.163 g, 0.101 mmol) were dissolved in THF (10 mL) and cooled to –35 °C. To the chilled solution was slowly added a THF (10 mL) solution of K[Cp($CH_2$)$_2$$PPh_2$] (0.100 g, 0.383 mmol) that had been cooled to –35 °C. After stirring overnight at room temperature, the reaction mixture was concentrated in vacuo. The residue was extracted with THF and filtered through a plug of silica gel. Concentration of the filtrate to 2-3 mL and addition of *n*-pentane precipitated an olive-green solid that was collected on a frit and washed with *n*-pentane. The resulting solid was dried in vacuo. (0.086 g, 39% yield). $^{1}$H NMR (300 MHz, acetone-$d_6$): δ 4.93 (m, 1H, $C_5H_4$), 4.64 (m, 1H, $C_5H_4$), 4.44 (br s, 1H, $C_5H_4$), 4.35 (d, $^{3}J_{HH}$ = 5 Hz, 1H, $C_5H_4$), 4.30 (d, $^{3}J_{HP}$ = 5 Hz, 6H, 6 x P(O$CH_2$)$_3$CEt), 3.14 (m, 1H, -($CH_2$)$_2$$PMe_2$), 2.58 (m, 1H, -($CH_2$)$_2$$PMe_2$), 2.36 (m, 1H, -($CH_2$)$_2$$PMe_2$), 1.80 (m, 1H, -($CH_2$)$_2$$PMe_2$), 1.45 (d, $^{2}J_{HP}$

= 11 Hz, 3H, -$(CH_2)_2PMe_2$), 1.43 (dd, $^2J_{HP}$ = 10 Hz, $^4J_{HP}$ = 2 Hz, 3H, -$(CH_2)_2PMe_2$) 1.31 (q, $^3J_{HH}$ = 8 Hz, 2H, 2 x $P(OCH_2)_3CCH_2CH_3$), 0.87 (t, $^3J_{HH}$ = 8 Hz, 3H, 3 x $P(OCH_2)_3CCH_2CH_3$). $^{31}$P NMR (121 Hz, pyridine-$d_5$): 167.9 (d, $^2J_{PP}$ = 118 Hz, $P(OCH_2)_3CEt$), 65.6 (d, $^2J_{PP}$ = 118 Hz, $PMe_2$).

**Synthesis of [Cp(CH$_2$)$_2$PMe$_2$]Fe(P(OCH$_2$)$_3$CEt)Me (5.9).** A THF (3 mL) solution of $[Cp(CH_2)_2PMe_2]Fe(P(OCH_2)_3CEt)Cl$ (**5.8**) (0.025 g, 0.049 mmol) was cooled to –35 °C. To this solution was added MeLi (31 μL, 1.6 M, 0.050 mmol). After stirring at room temperature for 1 h, the red-orange solution was concentrated in vacuo. The resulting residue was extracted with diethyl ether and filtered through Celite. The volatiles were removed in vacuo and the remaining residue was reconstituted in pyridine-$d_5$ and analyzed by NMR spectroscopy. $^1$H NMR (300 MHz, pyridine-$d_5$): δ 4.66 (br s, 1H, $C_5H_4$), 4.24 (br s, 1H, $C_5H_4$), 4.14 (d, $^3J_{HP}$ = 4 Hz, 6H, 6 x $P(OCH_2)_3CEt$), 4.08 (m, 1H, $C_5H_4$), 3.97 (m, 1H, $C_5H_4$), 2.59 (m, 1H, -$(CH_2)_2PMe_2$), 2.49 – 2.11 (m, 2H, 2 x -$(CH_2)_2PMe_2$), 1.89 (m, 1H, -$(CH_2)_2PMe_2$), 1.48 (d, $^2J_{HP}$ = 10 Hz, 3H, -$(CH_2)_2PMe_2$), 1.21 (d, $^2J_{HP}$ = 10 Hz, 3H, -$(CH_2)_2PMe_2$), 0.92 (q, $^3J_{HH}$ = 6 Hz, 2H, 2 x $P(OCH_2)_3CCH_2CH_3$), 0.54 (t, $^3J_{HH}$ = 6 Hz, 3H, 3 x $P(OCH_2)_3CCH_2CH_3$), 0.05 (vt, 3H, Me). $^{31}$P NMR (121 Hz, pyridine-$d_5$): 170.3 (d, $^2J_{PP}$ = 106 Hz, $P(OCH_2)_3CEt$), 71.5 (d, $^2J_{PP}$ = 106 Hz, $PMe_2$).

**Synthesis of [($^{Ph}$PNP)Fe(NCMe)$_3$](PF$_6$)$_2$ (5.11-PF$_6$).** To a mixture of complex **5.10** (0.425 g, 0.705 mmol) in NCMe (5 mL) was added a solution of $NaPF_6$ (0.046 g, 0.27 mmol) in NCMe. The resulting red mixture was allowed to stir overnight. The volatiles were removed in vacuo, and the residue was extracted with $CH_2Cl_2$ and filtered through Celite. The red filtrate was concentrated to ~2 mL and diethyl ether was added. After stirring for several minutes, the red-orange solid was collected, washed with diethyl

ether, and dried in vacuo (0.610 g, 92%). Complex **5.11-BAr'$_4$** was prepared similarly, except $NaBAr'_4$ was used in place of $NaPF_6$ and the complex was isolated by drying down the reaction mixture, extracting with diethyl ether, filtering, and removing all the volatiles in vacuo. $^1$H NMR (300 MHz, $CD_2Cl_2$): δ 8.02 – 7.49 (m, 23H, pyridyl and phenyl), 4.45 (vt, 4H, -C*H*$_2$PPh$_2$), 2.48 (s, 3H, NCMe *trans* to pyridyl), 1.50 (s, 6H, 2 x NCMe apical). $^{31}$P NMR (121 MHz, $CD_2Cl_2$): 59.5 (s, -PPh$_2$).

**Synthesis of *trans*-[($^{Ph}$PNP)Fe(PMe$_3$)(NCMe)$_2$](PF$_6$)$_2$ (5.12-PF$_6$).** To a solution of complex **5.11-PF$_6$** (0.340 g, 0.360 mmol) in $CH_2Cl_2$ (~25 mL) was added $PMe_3$ (38 μL, 0.37 mmol). The solution got slightly darker. After stirring for ~2 h, the reaction solution was concentrated to ~0.5 mL, and diethyl ether was added to precipitate a red solid. The solid was collected, washed with diethyl ether, and dried in vacuo (0.345 g, 98% yield). Complex **5.12-BAr'$_4$** was prepared similarly, except the reaction was worked up by removing all the volatiles in vacuo. $^1$H NMR (300 MHz, $CD_2Cl_2$): δ 8.00 (t, $^3J_{HH}$ = 7 Hz, 1H, pyridyl 4), 7.78 (d, $^3J_{HH}$ = 7 Hz, 2H, pyridyl 3 and 5), 7.60 (m, 20H, phenyls), 4.43 (vt, 4H, -C*H*$_2$PPh$_2$), 1.67 (s, 6H, 2 x NCMe), 1.24 (d, $^2J_{HP}$ = 9 Hz, 9H, $PMe_3$). $^{31}$P NMR ($CD_2Cl_2$): 56.7 (d, $^2J_{PP}$ = 57 Hz, -PPh$_2$), 15.9 (t, $^2J_{PP}$ = 57 Hz, $PMe_3$).

**Synthesis of *cis*-[($^{Ph}$PNP)Fe(P(OCH$_2$)$_3$CEt)(NCMe)$_2$](Y)$_2$ (*cis*-5.13-PF$_6$) and *trans*-[($^{Ph}$PNP)Fe(P(OCH$_2$)$_3$CEt)(NCMe)$_2$](Y)$_2$ (*trans*-5.13-PF$_6$).** To a $CH_2Cl_2$ (3 mL) solution of **5.11-PF$_6$** (0.070 g, 0.074 mmol) was added a $CH_2Cl_2$ (3 mL) solution of $P(OCH_2)_3CEt$ (0.013 g, 0.080 mmol). The reaction solution changed from red to orange. After stirring overnight, the solution was reduced to ~1 mL and diethyl ether was added to precipitate a light orange solid. The solid was collected on a frit, washed with diethyl ether, and dried in vacuo (0.067 g, 85% yield). $^1$H NMR (300 MHz, $CD_2Cl_2$): 7.85 – 7.35

(m, 23H ***cis*-5.13-PF$_6$**, 23H ***trans*-5.13-PF$_6$**, pyridyl and phenyls overlapping), 4.54 (vt, 4H, -C*H*$_2$PPh$_2$ ***cis*-5.13-PF$_6$**), 4.44 (vt, 4H, -C*H*$_2$PPh$_2$ ***trans*-5.13-PF$_6$**), 4.26 (d, $^3J_{HP}$ = 4 Hz, P(OC*H*$_2$)$_3$CEt ***trans*-5.13-PF$_6$**), 3.70 (d, $^3J_{HP}$ = 4 Hz, P(OC*H*$_2$)$_3$CEt ***cis*-5.13-PF$_6$**), 2.53 (s, 3H, NCMe *trans* to pyridyl ***cis*-5.13-PF$_6$**), 1.48 (s, 6H, NCMe ***trans*-5.13-PF$_6$**), 1.25 (s, 3H, NCMe apical ***cis*-5.13-PF$_6$**). 1.25 (overlapping q, 2H, 2 x P(OCH$_2$)$_3$CC*H*$_2$CH$_3$ ***trans*-5.13-PF$_6$**), 0.96 (q, $^3J_{HH}$ = 8 Hz, 2H, 2 x P(OCH$_2$)$_3$CC*H*$_2$CH$_3$ ***cis*-5.13-PF$_6$**), 0.81 (t, $^3J_{HH}$ = 8 Hz, 3H, P(OCH$_2$)$_3$CCH$_2$C*H*$_3$ ***trans*-5.13-PF$_6$**), 0.58 (t, $^3J_{HH}$ = 8 Hz, 3H, P(OCH$_2$)$_3$CCH$_2$C*H*$_3$ ***cis*-5.13-PF$_6$**). $^{31}$P NMR (121 MHz, $CD_2Cl_2$): 162.8 (P(OCH$_2$)$_3$CEt for *cis* and *trans* isomers, overlapping), 62.5 (d, $^2J_{PP}$ = 78 Hz, -PPh$_2$ ***trans*-5.13-PF$_6$**), 51.4 (d, $^2J_{PP}$ = 83 Hz, -PPh$_2$ ***cis*-5.13-PF$_6$**).

**Synthesis of [($^{Ph}$PNP)Fe(PMe$_3$)(NCMe)Me](BAr'$_4$) (5.14-BAr'$_4$).** Complex **5.12-BAr'$_4$** (0.192 g, 0.0795 mmol), AlMe$_3$ (40 μL, 2 M, 0.080 mmol), and THF were combined in a thick-walled pressure tube. The pressure tube was sealed with a Teflon cap and was stirred at 60 °C in an oil bath. After stirring for 17 h, the reaction solution was dried in vacuo. The residue was filtered through a plug of silica gel with 1:1 DCM-hexanes mixture. A red-orange band was collected and dried in vacuo (0.020 g, 16% yield). Complex **5.14-PF$_6$** could be synthesized in a similar fashion. Rather than filtering through silica gel, the reaction mixture was filtered through Celite, dried in vacuo, and reconstituted in a minimal amount $CH_2Cl_2$. The addition of *n*-pentane produced a solid that was collected on a frit and washed with *n*-pentane. $^1$H NMR (300 MHz, $CD_2Cl_2$): δ 7.89 – 7.10 (overlapping, 35H, BAr'$_4$, phenyl, pyridyl), 4.17 (d of vt, $^2J_{HH}$ = 17 Hz, 2H, -C*H*$_2$PPh$_2$), 3.95 (d of vt, $^2J_{HH}$ = 17 Hz, 2H, -C*H*$_2$PPh$_2$), 1.62 (s, 3H, NCMe), 1.02 (d, $^2J_{HP}$

= 8 Hz, 9H, $PMe_3$), –1.10 (vq, 3H, Me). $^{31}P$ NMR (121 MHz, $CD_2Cl_2$): δ 69.68 (d, $^2J_{PP}$ = 50 Hz, -$PPh_2$), 26.59 (t, $^2J_{PP}$ = 50 Hz, $PMe_3$).

**Synthesis of ($^{Cy}$PNP)$FeCl_2$ (5.15).** To a suspension of $FeCl_2$ (0.128 g, 1.01 mmol) in THF (5 mL) was added a THF (10 mL) solution of $^{Cy}$PNP (0.491, 0.982 mmol). The yellow mixture was allowed to stir overnight. After this time, the reaction mixture was dried in vacuo and reconstituted in a minimal amount of THF. A beige solid was filtered off, and the resulting yellow filtrate was concentrated to ~3 mL in vacuo. Hexanes were added to precipitate a yellow solid that was collected by vacuum filtration and dried (0.256 g, 41% yield). Paramagnetic $^1H$ NMR spectrum. See Figure 5.20.

## 5.5 References

(1) Andreatta, J. R.; McKeown, B. A.; Gunnoe, T. B. *J. Organomet. Chem.* **2011**, *696*, 305-315.

(2) Foley, N. A.; Lee, J. P.; Ke, Z. F.; Gunnoe, T. B.; Cundari, T. R. *Acc. Chem. Res.* **2009**, *42*, 585-597.

(3) Goj, L. A.; Gunnoe, T. B. *Curr. Org. Chem.* **2005**, *9*, 671-685.

(4) Kalman, S. E.; Gunnoe, T. B.; Sabat, M. *Organometallics* **2014**, *33*, 5457-5463.

(5) Kalman, S. E.; Petit, A.; Gunnoe, T. B.; Ess, D. H.; Cundari, T. R.; Sabat, M. *Organometallics* **2013**, *32*, 1797-1806.

(6) Lail, M.; Bell, C. M.; Conner, D.; Cundari, T. R.; Gunnoe, T. B.; Petersen, J. L. *Organometallics* **2004**, *23*, 5007-5020.

(7) Oxgaard, J.; Goddard, W. A. *J. Am. Chem. Soc.* **2004**, *126*, 442-443.

(8) Kandepi, V. V. K. M.; Cardoso, J. M. S.; Peris, E.; Royo, B. *Organometallics* **2010**, *29*, 2777-2782.

(9) Wang, T. F.; Juang, J. P.; Wen, Y. S. *J. Organomet. Chem.* **1995**, *503*, 117-128.

(10) Potter, G. D.; Baird, M. C.; Cole, S. P. C. *J. Organomet. Chem.* **2007**, *692*, 3508-3518.

(11) Bradley, S.; Camm, K. D.; Liu, X. M.; McGowan, P. C.; Mumtaz, R.; Oughton, K. A.; Podesta, T. J.; Thornton-Pett, M. *Inorg. Chem.* **2002**, *41*, 715-726.

(12) Graham, D. W.; Llamazares, A.; McDonald, R.; Cowie, M. *Organometallics* **1999**, *18*, 3490-3501.

(13) van der Vlugt, J. I.; Reek, J. N. H. *Angew. Chem. Int. Ed.* **2009**, *48*, 8832-8846.

(14) Langer, R.; Diskin-Posner, Y.; Leitus, G.; Shimon, L. J. W.; Ben-David, Y.; Milstein, D. *Angew. Chem. Int. Ed.* **2011**, *50*, 9948-9952.

(15) Langer, R.; Leitus, G.; Ben-David, Y.; Milstein, D. *Angew. Chem. Int. Ed.* **2011**, *50*, 2120-2124.

(16) Zell, T.; Ben-David, Y.; Milstein, D. *Angew. Chem. Int. Ed.* **2014**, *53*, 4685-4689.

(17) Dahlhoff, W. V.; Nelson, S. M. *J. Chem. Soc. A* **1971**, 2184-2190.

(18) Katayama, H.; Wada, C.; Taniguchi, K.; Ozawa, F. *Organometallics* **2002**, *21*, 3285-3291.

(19) Muller, G.; Klinga, M.; Leskela, M.; Rieger, B. *Z. Anorg. Allg. Chem.* **2002**, *628*, 2839-2846.

(20) Hartwig, J. F., *Organotransition Metal Chemistry: From Bonding to Catalysis*. University Science Books: Sausalito, 2009.

(21) Zhang, J.; Gandelman, M.; Herrman, D.; Leitus, G.; Shimon, L. J. W.; Ben-David, Y.; Milstein, D. *Inorg. Chim. Acta* **2006**, *359*, 1955-1960.

(22) Tolman, C. A. *Chem. Rev.* **1977**, *77*, 313-348.

(23) Chen, K.; Que, L. *Angew. Chem. Int. Ed.* **1999**, *38*, 2227-2229.

(24) Rana, S.; Bag, S.; Patra, T.; Maiti, D. *Adv. Synth. Catal.* **2014**, *356*, 2453-2458.

(25) Bouwkamp, M. W.; Bart, S. C.; Hawrelak, E. J.; Trovitch, R. J.; Lobkovsky, E.; Chirik, P. J. *Chem. Comm.* **2005**, 3406-3408.

(26) Fernandez, I.; Trovitch, R. J.; Lobkovsky, E.; Chirik, P. J. *Organometallics* **2008**, *27*, 109-118.

(27) Davies, S. C.; Hughes, D. L.; Leigh, G. J.; Sanders, J. R.; deSouza, J. S. *J. Chem. Soc. Dalt. Trans.* **1997**, 1981-1988.

# 6 The Partial Oxidation of Light Alkanes Using Periodate and Chloride Salts

## 6.1 Introduction

### 6.1.1 Natural Gas as an Under-Utilized Resource

The previous chapters have been focused on the development of an Fe catalyst for olefin hydroarylation. Another problem that our group has been interested in is the direct, low temperature conversion of natural gas to liquid fuels (i.e., methane to methanol, MTM). Natural gas is an abundant source of energy and a valuable chemical feedstock. The primary component of natural gas (~90% by volume), methane, is used in the production of valuable chemicals, such as methanol, hydrogen, ethane, and ethylene, while the longer chain alkanes in natural gas can be dehydrogenated to olefins.[1-3] It is estimated that the world had 186 trillion cubic meters of natural gas reserves in 2013.[4] However, natural gas is under-utilized as a fuel, with a large quantity of natural gas being flared. For example, over 7.3 billion cubic meters of natural gas were flared in 2013 in the U.S. alone.[5] This means that instead of capturing the natural gas, it is burned.

The reason that natural gas is being flared and not captured and used is that it is expensive to develop the infrastructure needed to transport and store it.[1, 3, 6-10] The current infrastructure has been designed for predominantly liquid fuels. Thus, new infrastructure must be built in order to transport and store natural gas. As an example, the North Slope of Alaska has an abundant reserve of natural gas.[9] Over recent years there has been an effort to construct an 800 mile natural gas pipeline from the Alaskan North Slope to a terminal at Nikiski, Alaska. Along with the pipeline, a treatment plant must be constructed to remove impurities. Additionally, a liquefaction plant, storage, and tanker terminal at Nikiski must be built as well. The estimated cost of this project is $45-65 billion dollars.[9] Therefore, it can be summarized that the major hindrance for taking

advantage of the abundance of natural gas reserves is being able to economically transport and store a gaseous feedstock.

### 6.1.2 Gas-to-Liquid Technologies

As briefly mentioned already, one way that natural gas can be used more readily is to convert it from a gas to a liquid. To liquefy natural gas, it must be cooled to less than –160 °C, which reduces its volume by a factor of more than 600.[10] The liquefaction plants are energy- and capital-intensive, making up 30-45% of the total capital costs of using liquid natural gas. In addition, the ships used to transport liquid natural gas cost nearly $160 million to make, which is more than double the cost of a crude oil tanker. Thus, liquefying natural gas is problematic from an economic standpoint.[10]

Alternatively, it would be desirable to develop a gas-to-liquid process (GTL) that would enable the efficient conversion of natural gas to liquids that can be readily transported and used as a fuel and a chemical feedstock for high value chemicals.[8] One solution is to convert the alkanes (methane, ethane, and propane) in natural gas to alcohols. Since methane makes up the vast majority of natural gas (~90%),[10] much of the chemistry surrounding natural gas has been focused on the conversion of methane to methanol (MTM). Methanol is a desirable target because it can be directly used as fuel for combustion engines or in fuel cell applications.[1, 3, 8] Furthermore, methanol is an important chemical feedstock for producing a variety of valuable chemicals, including olefins, formaldehyde, gasoline, and ethers (Scheme 6.1).[1, 3, 8]

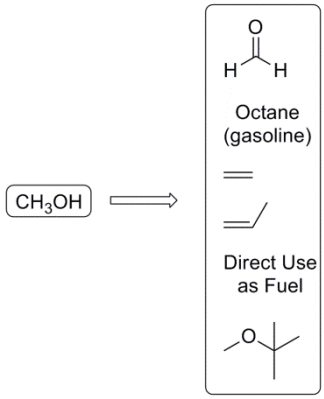


**Scheme 6.1.** Direct use of methanol as a feedstock.

The current industrial method for methane to methanol (MTM) conversion involves Fischer-Tropsch chemistry (Scheme 6.2).[1, 8] The overall process to convert methane to methanol involves two steps. First, methane and water are reformed to a mixture of carbon monoxide and hydrogen, which is known as synthesis gas (syngas). The syngas is then converted to methanol using a heterogeneous catalyst.[1] This method is energy intensive, requiring high temperatures (~900 °C) and pressures.[6] Additionally, to generate syngas, half of the natural gas is burned in the process, making this technology wasteful.[1] As a result, the expense and the high energy input necessary for Fischer-Tropsch synthesis limits the utility of this process for MTM conversion.

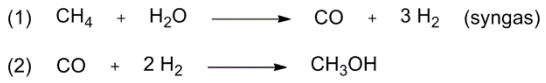


**Scheme 6.2.** Fischer-Tropsch process for the synthesis of methanol via syngas.

With the broad range of utility for methanol coupled with the expansive reserves of natural gas, the chemical community is interested in developing processes to convert light alkanes (R–H) into mono-functionalized products (R–X) selectively at moderate

temperatures (~200 °C) and pressures (~250-1000 psi). For the past several decades, there have been several different strategies for performing this reaction.[6, 7, 11-17]

### 6.1.3 Examples of Alkane Functionalization

Radical-based reactions to convert R–H to R–X have been reported. For instance, undergraduate organic chemistry courses teach that in free radical halogenation a radical (e.g., •Cl) can abstract a hydrogen from an alkane to eventually give RCl (Scheme 6.3).[1, 18] After the initial abstraction, a chain reaction ensues. The problem with radical reactions is that they typically do not stop at the mono-functionalized product. Homolytic bond cleavage is selective for the weaker C–H bond, and the functionalized products typically have weaker bond dissociation energies (BDE), which leads to over-oxidation of the desired product.[18]

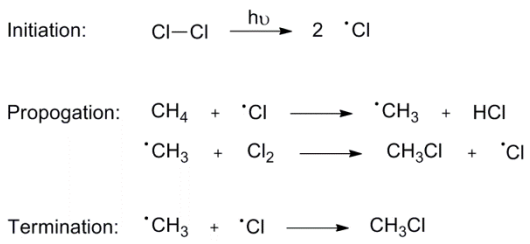


**Scheme 6.3.** Free radical chlorination of methane (one possible termination step shown for simplicity).

Heterogeneous catalysts have been used to convert R–H to R–X. Oxy-chlorination, for example, involves the reaction of methane, HCl, and oxygen over a solid catalyst to give $CH_3Cl$ and $H_2O$ (Scheme 6.4).[19, 20] The industrial methods for oxy-chlorination still result in over oxidation of the methyl chloride product and require temperatures of >350 °C.[19, 20] Thus, the poor selectivity of oxy-chlorination limits its potential to be used as a wide-spread technology for methane conversion to liquid fuels.

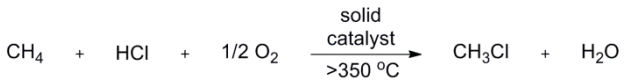


**Scheme 6.4.** Oxy-chlorination of methane to produce methyl chloride.

Another strategy for the conversion of methane to liquid products (e.g., methanol) involves the use of transition metal catalysts. Nature uses metalloenzymes, such as methane monooxygenase (MMO) to oxidize methane to methanol in biological systems.[7, 21] MMO consists of a high valent Fe–oxo core. The precise mechanism for methane oxidation by MMO is still under investigation, but it likely involves H atom abstraction of methane by an Fe–oxo moiety.[7, 21] Several researchers have been pursuing biomimetic approaches to alkane oxidation inspired by metalloenzymes.[21-28] MMO selectively oxidizes methane to methanol, but extending that selectivity to synthetic biomimetic complexes remains a challenge. In addition, examples of methane oxidation by synthetic complexes have not yet been reported. The complexity of biological-related transition metal complexes provides yet another challenge for making this strategy commercially viable.[7] Other than biomimetic metal complexes, metal salts have also been shown to functionalize hydrocarbons by radical-based mechanisms.[29-31]

The seminal work by Shilov demonstrated the promise of transition metal-catalyzed conversion of alkanes to mono-functionalized products (R–X; X = OH, Cl) by non-radical routes.[14, 32] Using a Pt(II) salt as a catalyst in conjunction with a Pt(IV) stoichiometric oxidant in aqueous media allowed for the conversion of alkanes to the corresponding mono-functionalized products (Scheme 6.5). The use of a stoichiometric amount of expensive Pt(IV) as the oxidant limits the economic viability of this system.

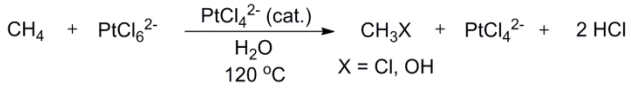


**Scheme 6.5.** Shilov process for the direct conversion of alkanes to functionalized products.

Since Shilov's initial work, transition metal complexes have shown promise for alkane functionalization.[6, 7, 11-13, 33-36] One of the key advancements was reported by Catalytica, Inc.[37, 38] Methane conversion to $MeOSO_3H$ was achieved using (bpym)$PtCl_2$ (bpym = 2,2-bipyrimidine) as a catalyst in oleum, where $SO_3$ serves as the oxidant. Yields of methane functionalization to $MeOSO_3H$ reach 70% yield with >90% selectivity (Scheme 6.6). The bisulfate group protects the $MeOSO_3H$ from over-oxidation. Product inhibition and challenges separating the product from the reaction solution make this method impractical for commercialization. Separation requires distillation, and with the volumetric production of $MeOSO_3H$ being <1 M, this is not viable for scale up.[6, 7] Related examples based on palladium, mercury, thallium, and gold have also been reported, but the use of super acidic reaction media has limited utility.[37-41]

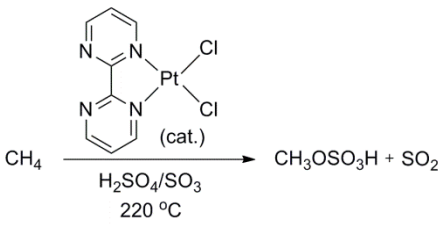


**Scheme 6.6.** Catalytica system for the partial oxidation of methane.

Examples of transition metal mediated alkane oxidation in non-super acidic media have also been reported. Recently, an example of an *N*-heterocyclic carbene ligated Pd complex was demonstrated to functionalize propane in trifluoroacetic acid.[42] In another

approach, Ag complexes are capable of converting alkanes to esters using ethyl diazoacetate,[43, 44] but the use of ethyl diazoacetate makes this process not possible for a large industrial scale. Furthermore, main group metals have been demonstrated to mediate stoichiometric functionalization of hydrocarbons in non-superacids.[45]

More germane to the work presented in this chapter, iodine-containing compounds are able to functionalize methane. For example, it has been reported that bromine with a small amount of iodine can be used to functionalize methane to methyl bromide at 500 °C.[46, 47] The use of iodine is critical for maintaining selectivity for the mono-functionalized product. The selectivity stems from reproportionation reactions of the over-oxidized products.[47] Hypervalent iodine species are competent at functionalizing C–H bonds by non-radical routes; however, they typically take place in either super-acidic media or suffer from low selectivity.[48-54] Additionally, elemental iodine and $KIO_3$ have been shown to functionalize methane in oleum.[55-58] For example, Periana and co-workers showed that iodine in oleum converts methane to $MeOSO_3H$ in 45% yield (based on methane) with over 90% selectivity (Scheme 6.7).[57] The authors proposed an electrophilic substitution mechanism akin to the Shilov system. Bjerrum and co-workers have extended this chemistry to other iodine-containing compounds, such as KI, $KIO_3$, and $KIO_4$.[56] A recent report highlighted the efficacy of a well-defined iodine(III) compound that mediates stoichiometric selective partial oxidation of hydrocarbons, which was demonstrated to proceed by a non-radical mechanism.[59]

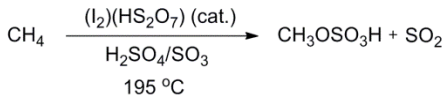


**Scheme 6.7.** Iodine catalyzed methane functionalization to methyl bisulfate.

### 6.1.4 Oxidation of Light Alkanes by Iodate and Chloride and Rationale for Present Study

Our group recently reported the selective mono-oxidation of methane and other light alkanes using iodate salts (e.g, $IO_3^-$) and sub-stoichiometric (i.e., catalytic) amounts of chloride.[60] KCl along with $NH_4IO_3$ efficiently functionalizes methane, ethane, and propane in HTFA (TFA = trifluoroacetate) (Scheme 6.8). In that initial study, we observed a 24% yield of MeTFA relative to methane with greater than 90% selectivity for the mono-functionalized product. The iodate/chloride system gave increased yields of MeTFA with higher pressures. While methane functionalization could be achieved with good activity at 180 °C, it was shown that at 235 °C, a 24% conversion of methane to MeTFA could be achieved in under 20 min. Methane functionalization is also effective in weaker acids, such as acetic acid.[60]

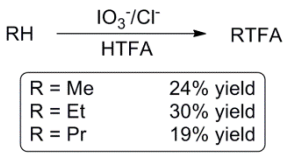


**Scheme 6.8.** Partial oxidation of light hydrocarbons by iodate and chloride.

The iodate/chloride system is also capable of functionalizing other light hydrocarbons.[60] For instance, ~30% yield of EtTFA was obtained in the functionalization of ethane in very high selectivity for the mono-functionalized product (97%). Propane was also functionalized to give 19% yield of products. Here, an approximate 2:2:1 ratio was observed of 2-propyl trifluoroacetate, 1-propyl trifluoroacetate, and 1,2-propanediyl trifluoroacetate. The observation of 1-propyl trifluoroacetate provides evidence of a reaction mechanism that is inconsistent with traditional free radical reactions. It was

demonstrated that both iodate and chloride are necessary for the high alkane conversions.[60]

Based on this initial study, we considered whether iodine in other oxidation states, such as periodate ($IO_4^-$, I(VII)) is viable for this transformation. In this chapter, we disclose the efficient partial oxidation of methane, ethane, and propane using a periodate salt along with catalytic amounts of chloride. We find that the periodate/chloride system operates at low pressures of methane (860 kPa) to give >40% yield of MeX (X = TFA, Cl) within 1 h at 200 °C (Scheme 6.9). The previously reported optimized yield for methane functionalization using iodate/chloride was 24%.[60] The results in this chapter demonstrate that periodate/chloride mixtures can be used to achieve mono-functionalization of light alkanes in high yields, in some cases with increased efficacy compared to iodate/chloride. The results presented in this chapter have been previously published.[61] Dr. George Fortman (UVA) and Nicholas Boaz (Princeton) initially discovered that periodate and chloride could functionalize alkanes, and Dr. Dominik Munz (UVA) performed preliminary reactions that set the foundation for the results presented herein.

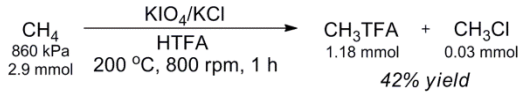


**Scheme 6.9.** Partial oxidation of methane by periodate and chloride using low pressure of methane (rpm = revolutions per minute of stirring).

## 6.2 Results and Discussion

### 6.2.1 Study of Methane Functionalization with Periodate and Chloride

As an initial probe into the reactivity of periodate and chloride, we subjected a mixture of $KIO_4$ (7.7 mmol) and KCl (0.67 mmol) to 3450 kPa of $CH_4$ (10.6 mmol) in

HTFA (HTFA = trifluoroacetic acid) (Scheme 6.10). After stirring at 180 °C for 1 h, analysis of the reaction mixture by $^1$H NMR spectroscopy revealed the formation of 0.86 mmol of MeTFA along with 0.10 mmol of MeCl, which corresponds to ~9% yield of total MeX relative to methane.

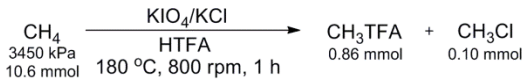


**Scheme 6.10.** Partial oxidation of methane at 180 °C with 3450 kPa of methane.

To optimize yields of MeX, we studied several features of this reaction. To examine the effect of temperature (Figure 6.1), $KIO_4$ (7.7 mmol) and KCl (0.67 mmol) in HTFA were heated over a range of temperatures (150 - 220 °C) for 1 h with 3450 kPa of $CH_4$ (10.6 mmol). Increasing the reaction temperature has a positive effect on the yield of MeX. At 200 °C, the production of MeX reaches 1.55 mmol MeTFA and 0.10 mmol MeCl, and then reaches a plateau. This corresponds to ~16% yield of MeX relative to methane. These data suggest that at temperatures ≥200 °C the reaction is complete within 1 h. In one iteration, the reaction was allowed to proceed for 1.5 h at 200 °C, but no additional MeX was observed. Thus, higher temperatures do not increase yield of MeX after 1 h. Importantly, since the overall reaction is exothermic (e.g., $CH_4$ (g) + ½ $O_2$ (g) → $CH_3OH$ (l), $\Delta H$ = –30 kcal/mol), an industrially viable reaction would ideally be performed between 200 °C and 250 °C to minimize the need to cool the reactor.[12]

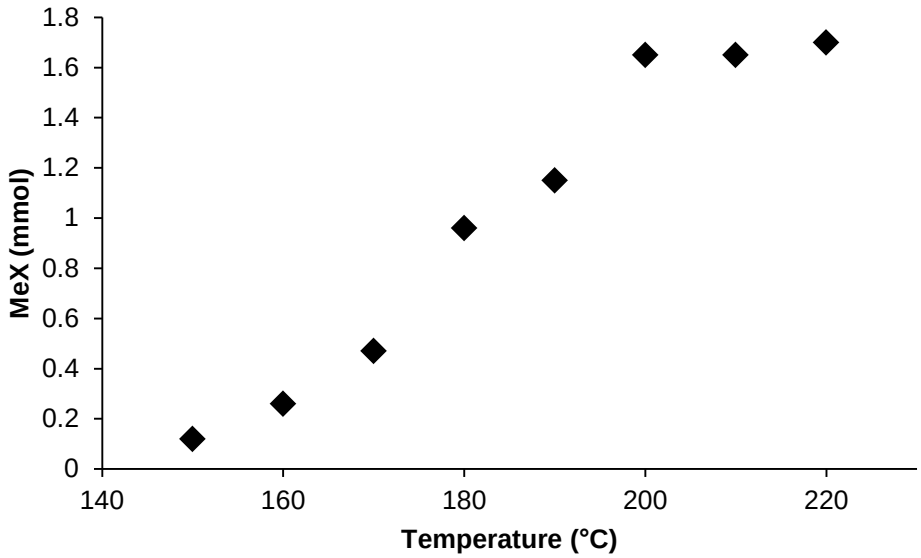


**Figure 6.1.** Dependence of MeX yield on temperature. Conditions: 7.7 mmol $KIO_4$, 0.67 mmol KCl, 8.0 mL HTFA, 3450 kPa $CH_4$, 800 rpm, 1 h.

We next explored the effect of chloride on the yield of MeX (Figure 6.2). In the absence of chloride, we observe a small amount of MeTFA (0.19 mmol) compared to 1.55 mmol of MeTFA observed with the addition of 0.67 mmol of KCl. The yield of MeX increased with increasing concentration of KCl. Adding 0.33 mmol KCl resulted in the production of 0.56 mmol MeX and increasing the KCl loading further to 0.67 mmol resulted in 1.65 mmol MeX. Increasing the concentration of chloride above 0.67 mmol has minimal effect on increasing MeX yields.

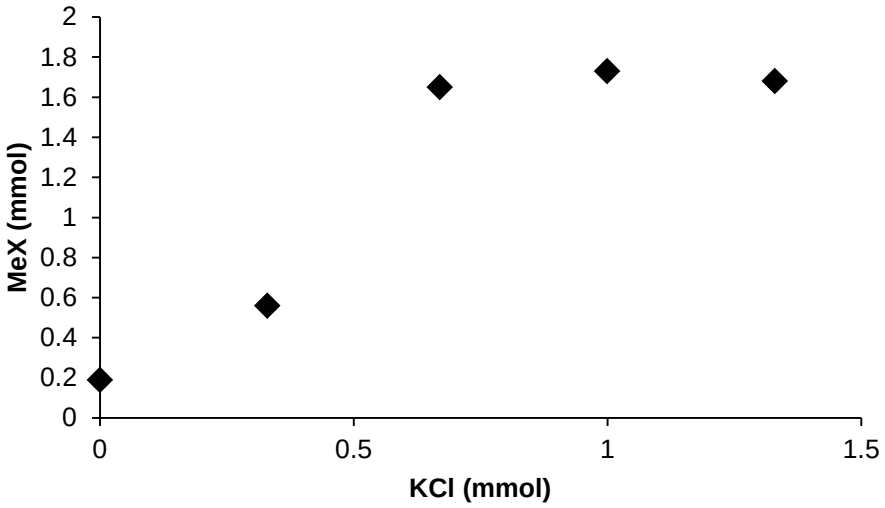


**Figure 6.2.** Dependence of MeX yield on KCl loading. Conditions: 7.7 mmol $KIO_4$; 8.0 mL HTFA; 3450 kPa (10.6 mmol) $CH_4$; 200 °C; 800 rpm, 1 h.

We studied the influence of methane pressure on the yield of MeX (Figure 6.3). Varying the pressure has a negligible effect on the total mmol of MeX produced after 1 h of reaction. We observe a slightly higher MeX production at 3450 KPa $CH_4$, but within the deviation of the experiment there is little difference in amount of MeX produced as $CH_4$ pressure is increased. Thus, percent yields of MeX are optimized at lower $CH_4$ pressures with a yield of 42% MeX with 7.7 mmol $KIO_4$ and 0.67 mmol KCl at 200 °C with 860 kPa $CH_4$ (2.9 mmol) after 1 h.

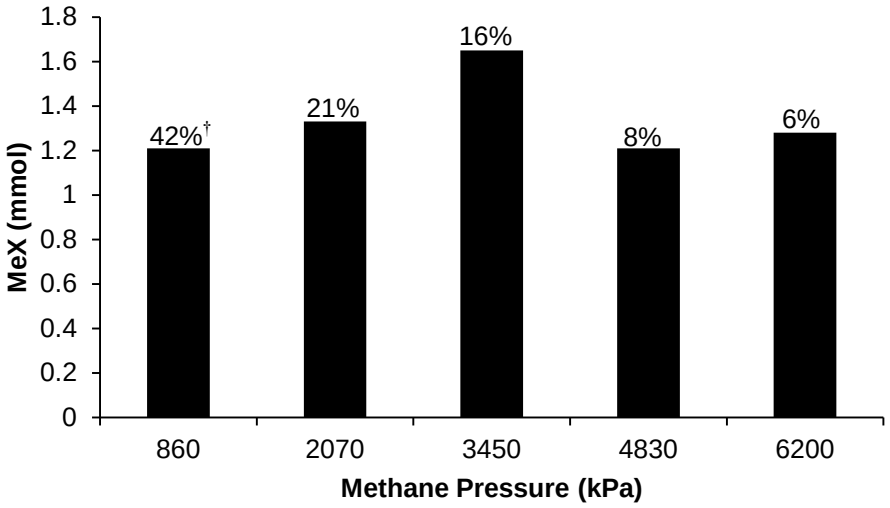


**Figure 6.3.** Dependence of of MeX yield on methane pressure. Conditions: 7.7 mmol $KIO_4$; 0.67 mmol KCl; 8.0 mL HTFA; 200 °C; 800 rpm; 1 h. †Yields based on starting $CH_4$ loading shown above each bar (860 kPa = 2.9 mmol $CH_4$, 2070 kPa = 6.3 mmol $CH_4$, 3450 kPa = 10.6 mmol $CH_4$, 4830 kPa = 15.6 mmol $CH_4$).

We also studied the effect of periodate loading. Since the chloride:periodate ratio must be at least ~1:10 to obtain optimal yields (see Figure 6.2), the amount of chloride was scaled with added periodate. Using 3450 kPa $CH_4$, we increased the loading of $KIO_4$ by ~55%. At lower concentrations of $KIO_4$ there is a linear correlation with MeX production (Figure 6.4). However, at higher $KIO_4$ concentrations there is no additional benefit.

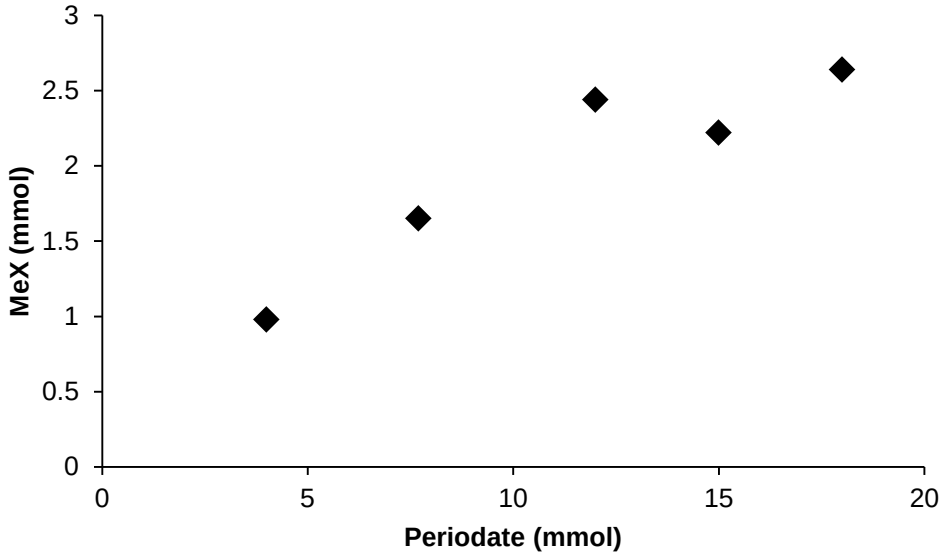


**Figure 6.4.** Dependence of MeX yield on $KIO_4$ loading. Conditions: 0.47 mmol KCl (4.0 mmol $KIO_4$), 0.67 mmol KCl (7.7 mmol $KIO_4$), 1.4 mmol KCl (12 mmol $KIO_4$), 1.8 mmol KCl (15 mmol $KIO_4$), 2.1 mmol (18 mmol $KIO_4$); 8.0 mmol HTFA; 3450 kPa (10.6 mmol) $CH_4$; 200 °C; 800 rpm, 1 h.

Because the standard conditions (7.7 mmol $KIO_4$ and 0.67 mmol KCl) at 2070 kPa and 860 kPa of $CH_4$ gave higher yields relative to $CH_4$, we investigated the effect of higher periodate loading at these pressures. Increasing the periodate loading at 2070 kPa of $CH_4$ has minimal effect on overall yields, especially when compared to the effect at 3450 kPa of $CH_4$ (see above). Heating an HTFA mixture of 12 mmol $KIO_4$ and 1.4 mmol KCl with 2070 kPa of $CH_4$ gave 1.48 mmol MeX, which corresponds to a yield of ~23%. This is only ~10% increase in yield upon increasing the oxidant loading by ~55%. Similarly, at 860 kPa of $CH_4$ the yield of MeX does not increase with added periodate.

### 6.2.2 Partial Oxidation of Ethane and Propane by Periodate and Chloride

The periodate/chloride system is effective at functionalizing other light alkanes. Using the optimized conditions from methane functionalization (12 mmol $KIO_4$ and 1.4 mmol KCl), we studied the partial oxidation of ethane. Heating a trifluoroacetic acid

mixture of 12 mmol $KIO_4$ and 1.4 mmol KCl with 2070 kPa of ethane (9.0 mmol) at 200 °C for 1 h yielded 1.30 mmol EtTFA and 0.50 mmol of EtCl, which corresponds to a ~20% yield based on ethane (Scheme 6.11). We also observed 0.02 mmol of the bis-TFA-ester of ethylene glycol and trace (<0.02 mmol) 1,2-dichloroethane. Notably, the yield of EtCl is higher than what was observed for the iodate/chloride system (see below).[60]

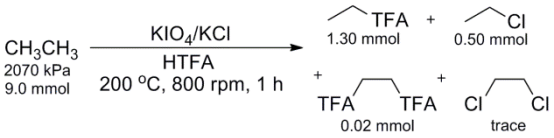


**Scheme 6.11.** Partial oxidation of ethane using periodate and chloride.

Applying the optimized conditions to the partial oxidation of propane (660 kPa, 4.3 mmol) resulted in a deep red reaction mixture from which analysis by $^1$H NMR spectroscopy was challenging due to broad resonances. Decreasing the oxidant loading to 5.2 mmol $KIO_4$ and 0.61 mmol KCl as well as decreasing the reaction time to 30 min allowed for the observation of 0.18 mmol *n*PrTFA, 0.47 mmol *i*PrTFA, 0.19 mmol 1,2-TFA-propane, and 0.10 mmol of *n*PrCl (Scheme 6.12). The total yield of functionalized product (based on initial propane loading) is ~22%.

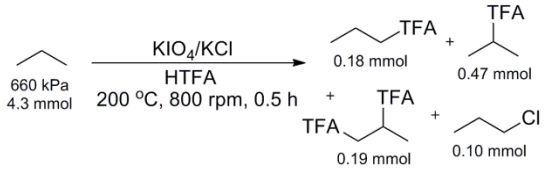


**Scheme 6.12.** Partial oxidation of propane using periodate and chloride.

### 6.2.3 Comparison of the Periodate/Chloride System to the Iodate/Chloride System

It is of interest to compare our previously reported iodate/chloride system with the periodate/chloride system highlighted in this chapter.[60] Because of differences in

experimental design and conditions, we performed some reactions with $NH_4IO_3$ and KCl in order to provide a more accurate comparison with the data presented in this chapter. This comparison is summarized in Table 6.1. Using 7.7 mmol $NH_4IO_3$ and 0.67 mmol KCl at 200 °C with 3450 kPa $CH_4$ (10.6 mmol) produced 2.22 mmol MeTFA and 0.05 mmol MeCl, which corresponds to a 21% yield of MeX (Scheme 6.13). The periodate/chloride system gives 16% yield of MeX under these conditions. However, increasing the amount of periodate/iodate and chloride to 12 mmol and 1.4 mmol, respectively, gave similar yields for both systems (~23%).

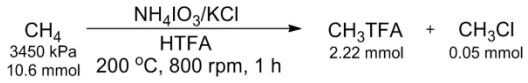


**Scheme 6.13.** Partial oxidation of methane using iodate and chloride under optimized temperature and salt loadings.

With low pressures of $CH_4$ (860 kPa), the periodate/chloride system is considerably more effective than the iodate/chloride system. As mentioned above, reacting 7.7 mmol $KIO_4$ and 0.67 mmol KCl with 860 kPa of $CH_4$ (2.9 mmol) gave 42% yield of MeX after 1 h. Under these conditions, iodate/chloride gave 30% yield MeX. At this point, the source for this difference is not known.

Another difference between the iodate/chloride and periodate/chloride systems is the increased amount of RCl produced for functionalization reactions using periodate. We have previously shown that MeCl is not converted to MeTFA under reaction conditions.[60] The difference in extent of chlorination is most readily observed for the functionalization of ethane. For iodate/chloride, only ~6% of the total functionalized product from ethane is EtCl. In contrast, we observe ~28% EtCl relative to total functionalized product when

using periodate/chloride. One explanation is that there is a higher concentration of chloride present in the reaction with periodate (1.4 mmol vs 0.67 mmol). However, even running the ethane functionalization reaction with 7.7 mmol $KIO_4$ and 0.67 mmol KCl, we still observe ~23% EtCl. The difference in the extent of chlorination between the periodate/chloride and iodate/chloride systems may be attributed to the relative amounts of chlorine and iodine in the reaction solutions (see section 6.3 for details).

Previously, we observed ~1.7:1 ratio of *i*PrTFA to *n*PrTFA for propane functionalization when using $NH_4IO_3$ and KCl. For $KIO_4$/KCl, that ratio is increased to ~2.6:1. Likewise, the ratio of mono- and difunctionalized products for the iodate system was ~1.3:1,[60] while the ratio is ~3.4:1 for the periodate reaction described herein. Thus, the periodate system reported herein is more selective for both the monofunctionalized product and the branched product. However, a potentially relevant comparison is the ratio of the sum of *i*PrTFA and 1,2-difunctionalized product to *n*PrTFA. If the difunctionalized product forms via further reaction of *i*PrTFA, one would expect these ratios to be similar between iodate and periodate, assuming a similar mechanism was operative (Scheme 6.14). Indeed, for both iodine species, the ratio is ~3.6:1 (Table 6.1).[60]

**Table 6.1.** Comparison of the partial oxidation of light hydrocarbons using periodate/chloride or iodate/chloride.

| | **Periodate** | **Iodate** |
|---|---|---|
| Yield at 3450 kPa of $CH_4$ (high loading)[†] | 23% | 23% |
| Yield at 3450 kPa of $CH_4$ (low loading)[‡] | 16% | 21% |
| Yield at 860 kPa of $CH_4$ (low loading)[‡] | 42% | 30% |
| EtTFA:EtCl (low loading)[‡] | 3.3:1 | 16:1[#] |
| *i*PrTFA:*n*PrTFA | 2.6:1 | 1.7:1[#] |
| PrTFA:$PrTFA_2$ | 3.4:1 | 1.3:1[#] |
| [*i*PrTFA+$PrTFA_2$]:*n*PrTFA | 3.7:1 | 3.6:1[#] |

[†]High loading: 12 mmol $IO_x^-$ and 1.4 mmol KCl; [‡]Low loading: 7.7 mmol $IO_x^-$ and 0.67 mmol KCl. [#]Ref. 60.

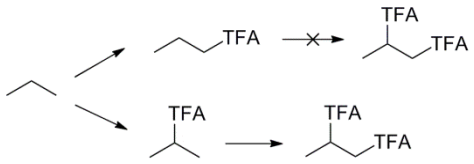


**Scheme 6.14.** Proposed pathway for the formation of 1,2-diTFA-propane.

## 6.3 Summary and Conclusions

In summary, we have demonstrated that the mixture of $KIO_4$ and KCl in HTFA is an efficient system for the mono-functionalization of light alkanes even at low pressures of the alkane. Yields of functionalized products from methane, ethane, and propane reach over 20%, and in the case of methane at 860 kPa, a 42% yield of MeX is observed. Additionally, comparison to our previously reported hydrocarbon functionalization using iodate and chloride salts provides evidence that these two systems operate via a similar pathway.[60] By optimizing the reaction conditions, a greater yield of MeX is observed for the periodate system reported here than for the iodate system at 200 °C. The high activity observed at 200 °C is important for the development of industrially viable systems,

considering the exothermic nature of the reaction and the expense of needing to cool large scale industrial reactions.

Understanding the mechanism of these transformations may allow for the development of more active and efficient catalytic systems for the conversion of natural gas into liquid fuels. Nicholas Boaz (Groves group, Princeton) in collaboration with our research group has proposed a mechanism for the partial oxidation of hydrocarbons using iodate and chloride salts.[62] The proposed mechanism, which is likely also operative in the periodate/chloride system, is shown in Scheme 6.15. Based on UV-vis spectroscopy, the mixture of KCl, $NH_4IO_3$, and HTFA produces $I_2$ and $Cl_2$ under the reaction conditions. Homolytic bond cleavage of $Cl_2$ produces •Cl radical, which abstracts an H atom from $CH_4$ to give HCl and $\bullet CH_3$. Iodine traps $\bullet CH_3$ to give MeI, which upon reaction with HTFA results in MeTFA. Consistent with the observation of $CH_3Cl$, $\bullet CH_3$ can react instead of the chlorine to generate MeCl, which does not convert to MeTFA under the reaction conditions. As mentioned above, the increased amounts of RCl in the periodate/chloride system in comparison to the iodate/chloride system may be a result of a smaller $I_2$:$Cl_2$ ratio in the periodate/chloride system. Thus, the essential elements of the reaction are •Cl, $I_2$, and HX.[62] Efforts into developing more efficient alkane functionalization reactions based on this mechanistic hypothesis are currently underway.

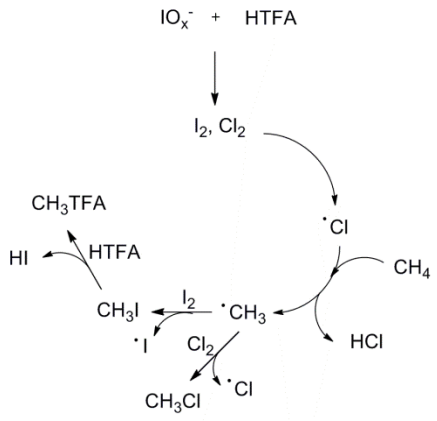


**Scheme 6.15.** Proposed mechanism for the functionalization of alkanes by $IO_x^-$ (x = 3,4) and chloride in HTFA.

## 6.4 Experimental Section

### 6.4.1 General Considerations

All reactions were setup in air. Trifluoroacetic acid, potassium periodate, ammonium iodate, and potassium chloride were purchased from a commercial vendor and used as received. Methane, ethane, and propane were purchased from GTS-Welco. $^1$H NMR spectra were recorded on a Bruker 600 MHz, a Bruker 800 MHz or a Varian 500 MHz spectrometer. NMR spectra were taken in neat HTFA with a capillary of $C_6D_6$ as an internal lock reference. Chemical shifts for $^1$H NMR are reported relative to the internal standards of HOAc (δ 2.04) or dichloromethane (DCM) (δ 5.03). All reactions were performed in house-built high-pressure reactors constructed primarily with stainless steel pieces from Swagelock. The reaction solutions were held in fabricated Teflon liners. The average volume of the reactors with the liner inserted is 16.1 mL. Reactions were stirred using 1.2 cm long rod-shaped stir bars. Reaction temperatures were maintained through inductive heat transfer from tight-fitting custom aluminum blocks. The initial moles of gas reported were determined by weighing the reactor before and after

pressurization. Due to some variations, the mass of gas was averaged from at least 3 separate reactions. The exception to this procedure is when the mass of gas added is too small within the deviation of the balance used (see Section 6.4.4). All amounts of functionalized products are the result of averaging at least 3 independent runs.

### 6.4.2 General Procedures for Functionalization Reactions

**General Procedure for Methane Functionalization with Periodate and Chloride.** A stir bar, $KIO_4$, KCl, and 8.0 mL HTFA were loaded into a tight-fitting Teflon liner. After the reactor was sealed and weighed, it was purged twice with $CH_4$ by pressurizing and slowly venting. The reactor was pressurized a third time with stirring for ~30 sec. After venting the reactor slowly, it was re-pressurized again with the appropriate pressure of $CH_4$ while stirring for 30 sec. The reactor was weighed again to quantify the mass of $CH_4$ added (for 860 kPa, the reactor was brought to a total pressure of ~3450 kPa using Ar at this point), and subsequently placed in a preheated aluminum block at the appropriate temperature. The reactor was stirred (800 rpm) at this temperature for 1 h. After this, it was removed from the heating block and placed in front of a fan for 30 min to cool to room temperature. The reactor was vented and then opened. HOAc was added as a standard and the contents were allowed to stir. An aliquot was removed, centrifuged, placed in an NMR tube containing a capillary filled with $C_6D_6$ and analyzed by $^1$H NMR spectroscopy (Figure 6.5).

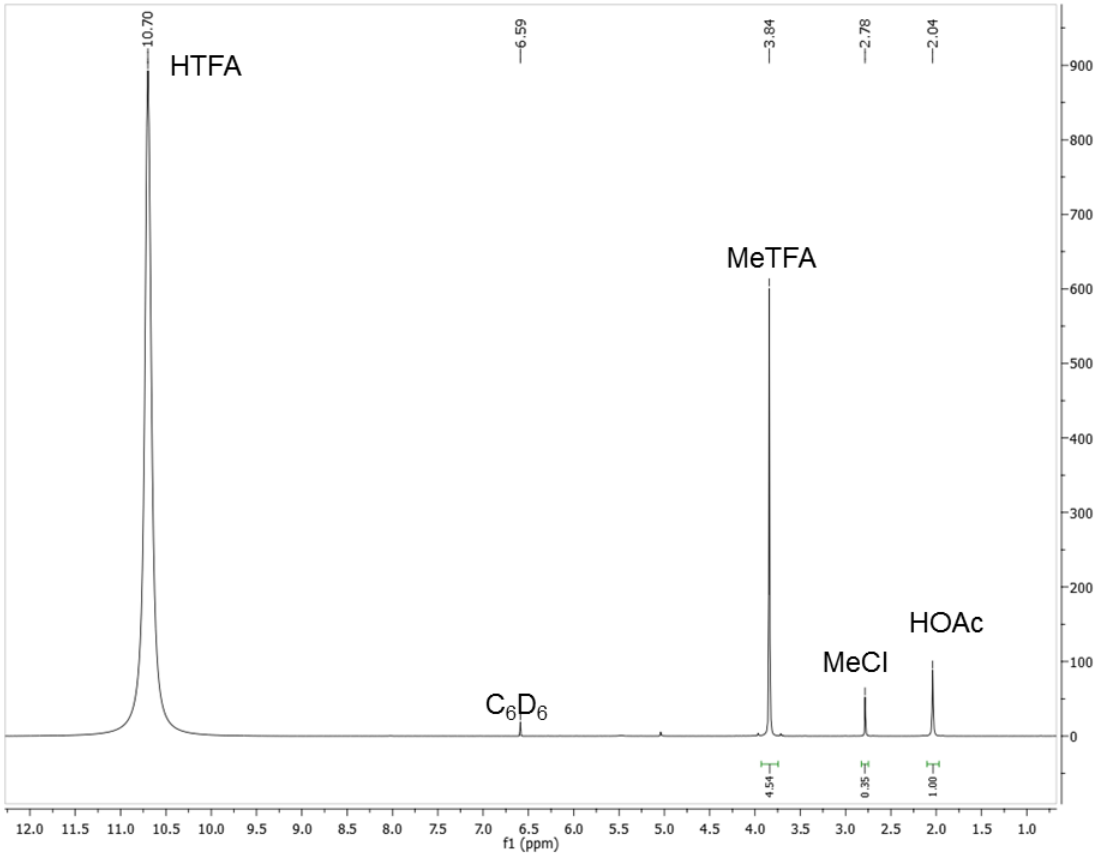


**Figure 6.5.** Sample $^{1}$H NMR spectrum with assignments for methane functionalization by periodate and chloride.

**General Procedure for Ethane Functionalization with Periodate and Chloride.** A stir bar, $KIO_4$, KCl, and 8.0 mL HTFA were loaded into a tight-fitting Teflon liner. After the reactor was sealed and weighed, it was purged twice with $C_2H_6$ by pressurizing and slowly venting. The reactor was pressurized a third time with stirring for ~30 sec. After venting the reactor slowly, it was re-pressurized again with the appropriate pressure of $C_2H_6$ while stirring for 30 sec. The reactor was weighed again to quantify the mass of $C_2H_6$ added, and subsequently placed in a preheated aluminum block at 200°C. The reactor was stirred (800 rpm) at this temperature for 1 h. After this, it was removed from the heating block and placed in front of a fan for 30 min to cool to room

temperature. The reactor was vented and then opened. DCM was added as a standard and the contents were allowed to stir. An aliquot was removed, centrifuged, placed in an NMR tube containing a capillary filled with $C_6D_6$ and analyzed by $^1$H NMR spectroscopy (Figure 6.6).

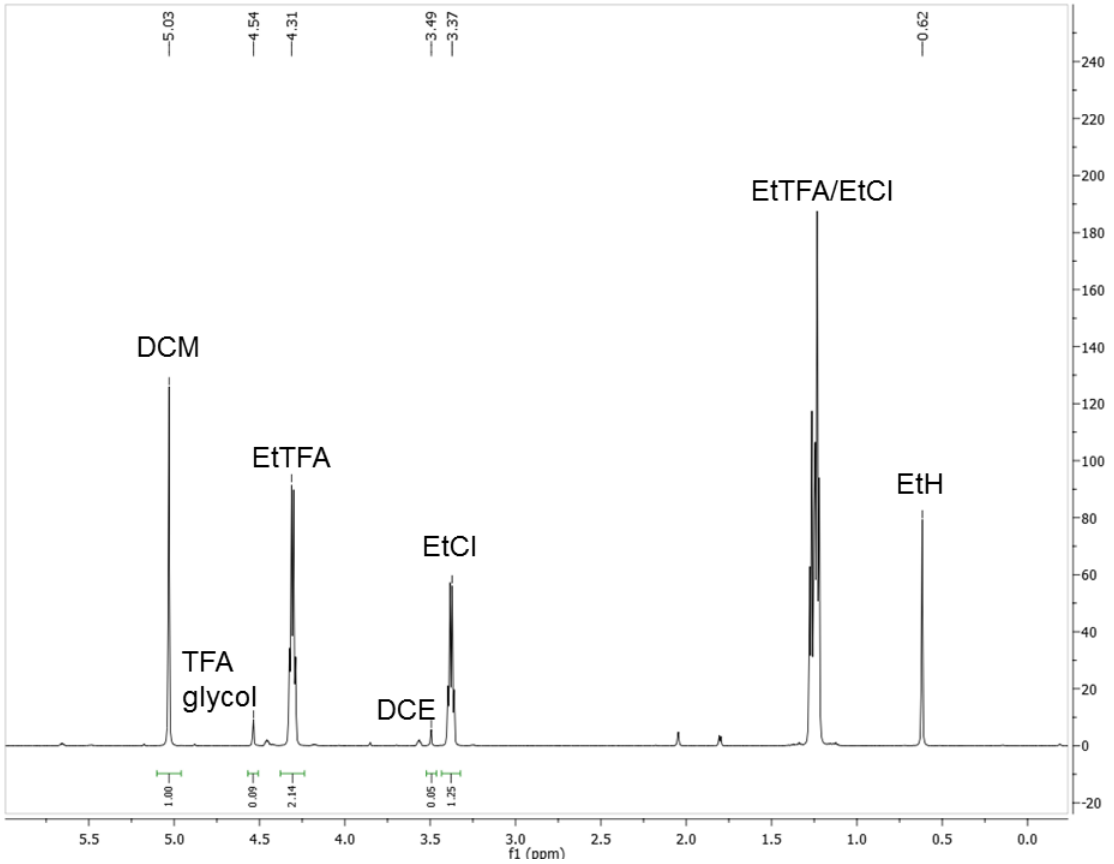


**Figure 6.6.** Sample $^1$H NMR spectrum with assignments for ethane functionalization by periodate and chloride.

**General Procedure for the Functionalization of Propane using Periodate and Chloride.** A stir bar, $KIO_4$ (5.2 mmol), KCl (0.61 mmol), and 8.0 mL HTFA were loaded into a tight-fitting Teflon liner. After the reactor was sealed and weighed, it was purged twice with $C_3H_8$ by pressurizing and slowly venting. The reactor was pressurized a third time with stirring for ~10 sec. After venting the reactor slowly, it was re-pressurized again with 660 kPa of $C_3H_8$ while stirring for 10 sec. The reactor was weighed again to

quantify the mass of $C_3H_8$ added. To the reactor was added Ar to bring the pressure to 2070 kPa. The reactor was subsequently placed in a preheated aluminum block at 200 °C. The reactor was stirred (800 rpm) at this temperature for 0.5 h. After this, it was removed from the heating block and placed in front of a fan for 30 min to cool to room temperature. The reactor was vented and then opened. HOAc was added as a standard and the contents were allowed to stir. An aliquot was removed, centrifuged, placed in an NMR tube containing a capillary filled with $C_6D_6$ and analyzed by $^1$H NMR spectroscopy (Figure 6.7).

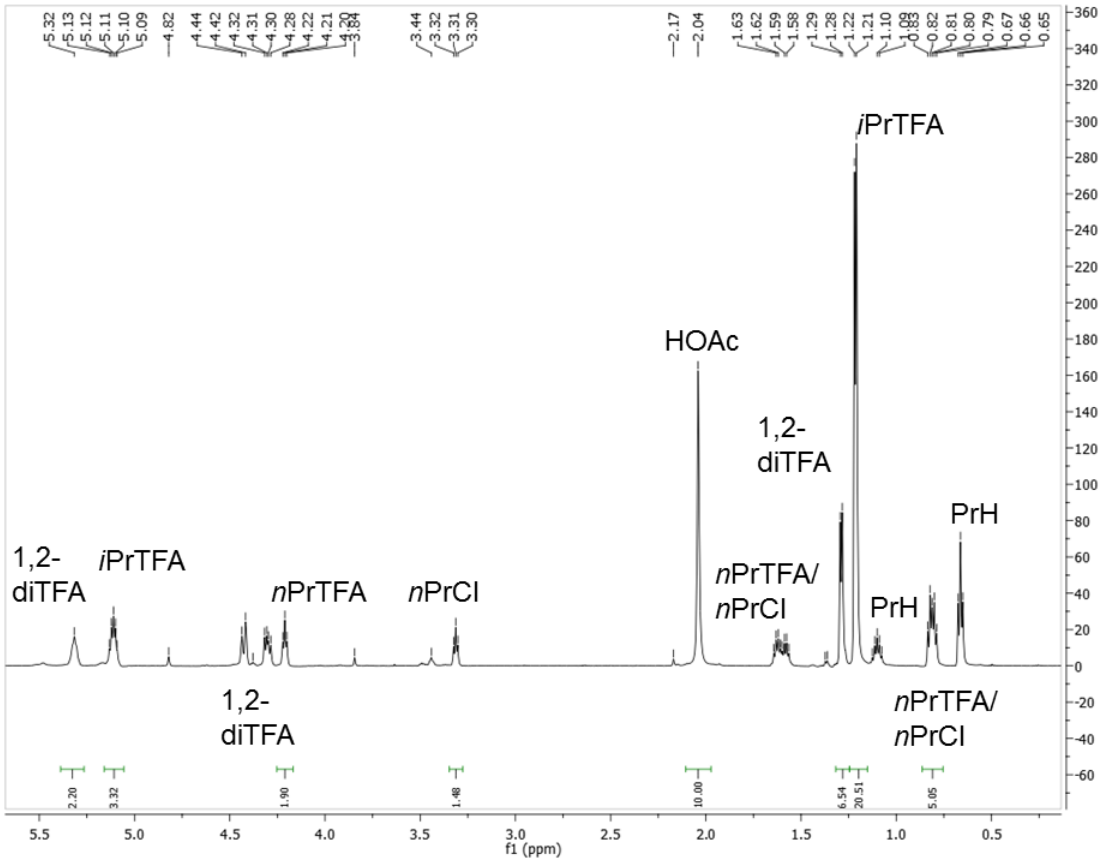


**Figure 6.7.** Sample $^1$H NMR spectrum and assignments for propane functionalization by periodate and chloride.

**General Procedure for Methane Functionalization with Iodate and Chloride.** A stir bar, $NH_4IO_3$, KCl, and 8.0 mL HTFA were loaded into a tight-fitting Teflon liner.

After the reactor was sealed and weighed, it was purged twice with $CH_4$ by pressurizing and slowly venting. The reactor was pressurized a third time with stirring for ~30 sec. After venting the reactor slowly, it was re-pressurized again with 3450 kPa of $CH_4$ while stirring for 30 sec. The reactor was weighed again to quantify the mass of $CH_4$ added, and subsequently placed in a preheated aluminum block at 200 °C. The reactor was stirred (800 rpm) at this temperature for 1 h. After this, it was removed from the heating block and placed in front of a fan for 30 min to cool to room temperature. The reactor was vented and then opened. HOAc was added as a standard and the contents were allowed to stir. An aliquot was removed, centrifuged, placed in an NMR tube containing a capillary filled with $C_6D_6$ and analyzed by $^1H$ NMR spectroscopy (Figure 6.8).

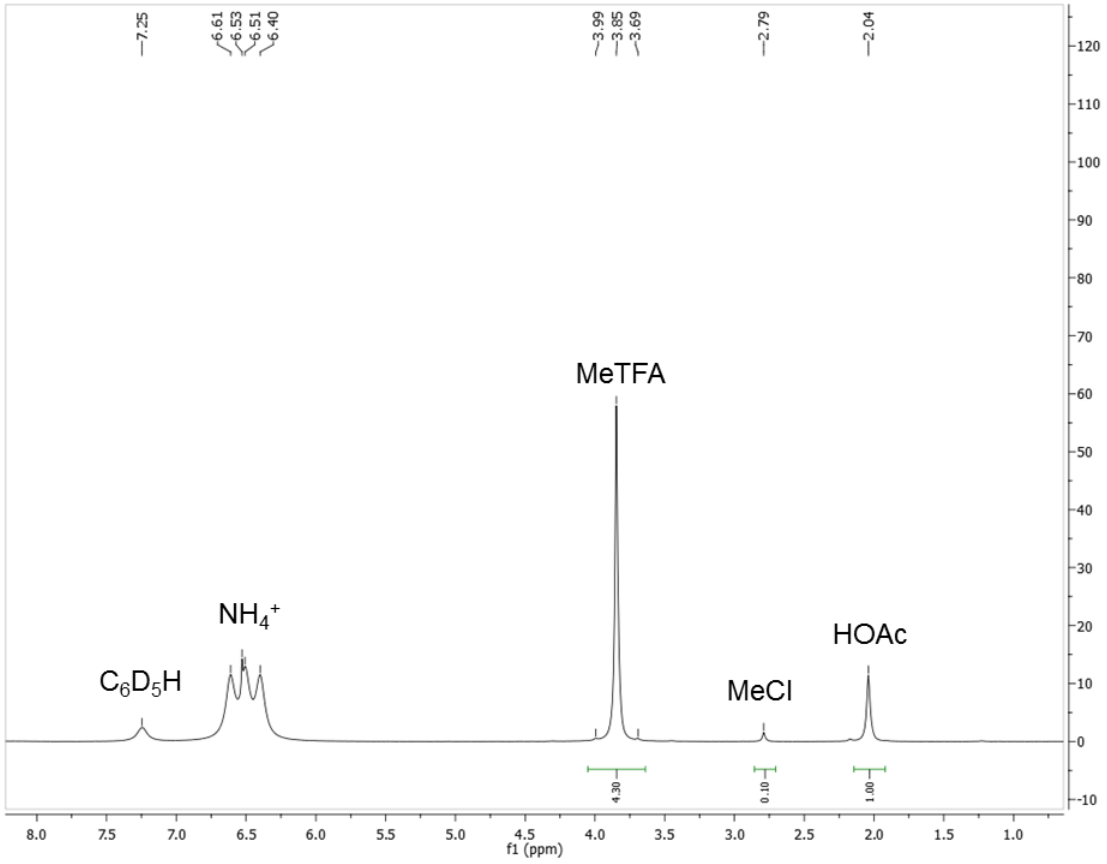


**Figure 6.8.** Sample $^1H$ NMR spectrum with assignments for methane functionalization by iodate and chloride.

### 6.4.3 Appendix of Raw Data

#### 6.4.3.1 Data for Methane Functionalization with Periodate and Chloride

**General Conditions:**
Gas: Methane
HTFA (mL): 8.0
Stirring: 800 rpm
Time: 1 h

| T (°C) | P (kPa) | $KIO_4$ (mmol) | KCl (mmol) | **MeTFA (mmol)** | **MeTFA (dev)** | **MeCl (mmol)** | **MeCl (dev)** | **N** |
|---|---|---|---|---|---|---|---|---|
| 150 | 3450 | 7.7 | .67 | **.063** | **.0053** | **.056** | **.013** | **3** |
| 160 | 3450 | 7.7 | .67 | **.12** | **.02** | **.14** | **.01** | **3** |
| 170 | 3450 | 7.7 | .67 | **.34** | **.11** | **.12** | **.02** | **3** |
| 180 | 3450 | 7.7 | .67 | **.81** | **.11** | **.10** | **.02** | **3** |
| 190 | 3450 | 7.7 | .67 | **1.05** | **.16** | **.10** | **.003** | **3** |
| 200 | 3450 | 7.7 | .67 | **1.55** | **.16** | **.10** | **.02** | **3** |
| 210 | 3450 | 7.7 | .67 | **1.56** | **.20** | **0.09** | **.02** | **3** |
| 220 | 3450 | 7.7 | .67 | **1.62** | **.13** | **.074** | **.005** | **3** |
| 200 | 3450 | 7.7 | 0 | **0.19** | **.06** | **n.d.** | **n.d.** | **3** |
| 200 | 3450 | 7.7 | .33 | **.49** | **.05** | **.07** | **.006** | **3** |
| 200 | 3450 | 7.7 | 1.0 | **1.61** | **.27** | **.12** | **.04** | **3** |
| 200 | 3450 | 7.7 | 1.3 | **1.68** | **.44** | **.16** | **.04** | **4** |
| 200 | 2070 | 7.7 | .67 | **1.24** | **.25** | **.096** | **.020** | **3** |
| 200 | 4830 | 7.7 | .67 | **1.06** | **.20** | **.15** | **.01** | **4** |
| 200 | 6200 | 7.7 | .67 | **1.11** | **.28** | **.17** | **.01** | **3** |
| 200 | 3450 | 12 | 1.4 | **2.25** | **.11** | **.19** | **.02** | **3** |
| 200 | 3450 | 18 | 2.1 | **2.49** | **.04** | **.16** | **.03** | **3** |
| 200 | 2070 | 12 | 1.4 | **1.33** | **.32** | **.15** | **.06** | **3** |
| 200 | 3450 | 4.0 | .47 | **.90** | **.05** | **.074** | **.005** | **3** |
| 200 | 860 | 12 | 1.4 | **1.07** | **.14** | **.039** | **.021** | **3** |
| 200 | 860 | 7.7 | 0.67 | **1.18** | **.01** | **.03** | **0** | **3** |
| 200 | 3450 | 15 | 1.8 | **1.98** | **.54** | **.25** | **.05** | **3** |

#### 6.4.3.2 Data for Ethane Functionalization with Periodate/Chloride

**General Conditions**
Reaction Gas: Ethane
Pressure: 2070 kPa
Temp.: 200 °C
HTFA (mL): 8.0
Stirring: 800 rpm
Time: 1 h

| $KIO_4$ (mmol) | KCl (mmol) | **EtTFA (mmol)** | **EtTFA (dev)** | **EtCl (mmol)** | **EtCl (dev)** | **Glycol (mmol)** | **Glycol (dev)** | **N** |
|---|---|---|---|---|---|---|---|---|
| 7.7 | .67 | **0.95** | **.23** | **.29** | **.03** | **.022** | **.005** | **3** |
| 12 | 1.4 | **1.30** | **.33** | **.50** | **.15** | **.023** | **.004** | **3** |

*Also observed trace (<0.02 mmol) 1,2-dichloroethane

### 6.4.3.3 Data for Propane Functionalization with Periodate/Chloride

**General Conditions**
Reaction Gas: Propane
Pressure: 660 kPa
$KIO_4$(mmol): 5.2
KCl (mmol): 0.61
Temp.: 200 °C
HTFA (mL): 8.0
Stirring: 800 rpm
Time: 0.5 h

| **nPrTFA (mmol)** | **nPrTFA (dev)** | **iPrTFA (mmol)** | **iPrTFA (dev)** | **1,2-diTFA (mmol)** | **1,2-diTFA (dev)** | **nPrCl (mmol)** | **nPrCl (dev)** | **N** |
|---|---|---|---|---|---|---|---|---|
| **0.20** | **.04** | **0.47** | **.10** | **.19** | **.05** | **.10** | **.01** | **3** |

### 6.4.3.4 Data for Methane Functionalization with Iodate and Chloride

**General Conditions**
Reaction Gas: Methane
Temp.: 200 °C
HTFA (mL): 8.0
Stirring: 800 rpm
Time: 1 h

| $NH_4IO_3$ (mmol) | KCl (mmol) | $CH_4$ (kPa) | **MeTFA (mmol)** | **MeTFA (dev)** | **MeCl (mmol)** | **MeCl (dev)** | **N** |
|---|---|---|---|---|---|---|---|
| 7.7 | .67 | 3450 | **2.22** | **.10** | **.054** | **.008** | **3** |
| 12 | 1.4 | 3450 | **2.41** | **.15** | **.063** | **0** | **3** |
| 7.7 | .67 | 862 | **0.80** | **0.03** | **0.02** | **0.003** | **3** |

### 6.4.4 Determination of mmol of methane for 860 kPa

Across the range of pressures used in this study, methane pressure appears to follow Henry's Law and the ideal gas law (Figure 6.9). Due to deviations in the balance for small differences in mass, the following graph (Figure 6.9) was used to calculate the mmol of methane (2.9 mmol) added for reactions with 860 kPa of methane. The trend line was forced through (0,0).

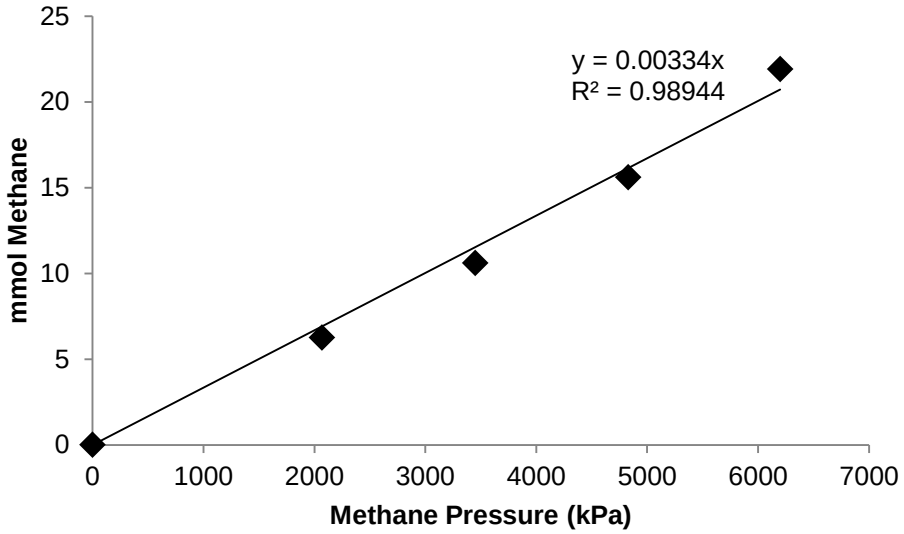


**Figure 6.9.** Plot of mmol $CH_4$ (determined by mass) versus $CH_4$ pressure (kPa).

## 6.5 References

(1) Olah, G.; Molnar, A., *Hydrocarbon Chemistry*. 2nd ed.; Wiley-Interscience: New York, 2003.

(2) Lunsford, J. H. *Catal. Today* **2000**, *63*, 165-174.

(3) Golisz, S. R.; Gunnoe, T. B.; Goddard, W. A.; Groves, J. T.; Periana, R. A. *Catalysis Letters* **2011**, *141*, 213-221.

(4) *BP Statistical Review of World Energy 2014*; BP: London, 2014.

(5) Natural Gas Gross Withdrawals and Production. U.S. Energy Information Administration. http://www.eia.gov/dnav/ng/ng_prod_sum_a_epg0_vgv_mmcf_a.htm (March 30, 2015),

(6) Webb, J. R.; Bolano, T.; Gunnoe, T. B. *ChemSusChem* **2011**, *4*, 37-49.

(7) Labinger, J. A. *J. Mol. Catal. A: Chem.* **2004**, *220*, 27-35.

(8) Olah, G. A.; Goeppert, A.; Prakash, G. K. S., *Beyond Oil and Gas: The Methanol Economy*. 2nd ed.; Wiley-VCH: Weinheim, Germany, 2009.

(9) Alaska LNG Project. Alaska Natural Gas Transportation Projects. http://www.arcticgas.gov/alaska-lng-project (March 30, 2015),

(10) *Liquified Natural Gas: Understanding the Basic Facts*; U.S. Department of Energy: Washington, DC, 2005.

(11) Cavaliere, V. N.; Wicker, B. F.; Mindiola, D. J. *Adv. Organomet. Chem.* **2012**, *60*, 1-47.

(12) Periana, R. A.; Bhalla, G.; Tenn, W. J.; Young, K. J. H.; Liu, X. Y.; Mironov, O.; Jones, C. J.; Ziatdinov, V. R. *J. Mol. Catal. A: Chem.* **2004**, *220*, 7-25.

(13) Stahl, S. S.; Labinger, J. A.; Bercaw, J. E. *Angew. Chem. Int. Ed.* **1998**, *37*, 2181-2192.

(14) Shilov, A. E.; Shul'pin, G. B. *Chem. Rev.* **1997**, *97*, 2879-2932.

(15) Labinger, J. A.; Bercaw, J. E. *Nature* **2002**, *417*, 507-514.

(16) Caballero, A.; Perez, P. J. *Chem. Soc. Rev.* **2013**, *42*, 8809-8820.

(17) Roduner, E.; Kaim, W.; Sarkar, B.; Urlacher, V. B.; Pleiss, J.; Glaser, R.; Einicke, W. D.; Sprenger, G. A.; Beifuss, U.; Klemm, E.; Liebner, C.; Hieronymus, H.; Hsu, S. F.; Plietker, B.; Laschat, S. *ChemCatChem* **2013**, *5*, 82-112.

(18) Wade, L. G., *Organic Chemistry*. 6th ed.; Prentice Hall: Upper Saddle River, NJ, 2005.

(19) Podkolzin, S. G.; Stangland, E. E.; Jones, M. E.; Peringer, E.; Lercher, J. A. *J. Am. Chem. Soc.* **2007**, *129*, 2569-2576.

(20) Joseph, W. J.; Bianchi, A. B. (Dow Chemical). Manufacture of Chlorinated Hydrocarbons. U.S. Patent 2,752,401, June 26, 1956.

(21) Gunay, A.; Theopold, K. H. *Chem. Rev.* **2010**, *110*, 1060-1081.

(22) Nelson, A. P.; DiMagno, S. G. *J. Am. Chem. Soc.* **2000**, *122*, 8569-8570.

(23) Gormisky, P. E.; White, M. C. *J. Am. Chem. Soc.* **2013**, *135*, 14052-14055.

(24) Stoian, S. A.; Xue, G. Q.; Bominaar, E. L.; Que, L.; Munck, E. *J. Am. Chem. Soc.* **2014**, *136*, 1545-1558.

(25) Hintermair, U.; Sheehan, S. W.; Parent, A. R.; Ess, D. H.; Richens, D. T.; Vaccaro, P. H.; Brudvig, G. W.; Crabtree, R. H. *J. Am. Chem. Soc.* **2013**, *135*, 10837-10851.

(26) Liu, W.; Groves, J. T. *J. Am. Chem. Soc.* **2010**, *132*, 12847-12849.

(27) Liu, W.; Groves, J. T. *Angew. Chem. Int. Ed.* **2013**, *52*, 6024-6027.

(28) Liu, W.; Huang, X. Y.; Cheng, M. J.; Nielsen, R. J.; Goddard, W. A.; Groves, J. T. *Science* **2012**, *337*, 1322-1325.

(29) Strassner, T.; Ahrens, S.; Muehlhofer, M.; Munz, D.; Zeller, A. *Eur. J. Inorg. Chem.* **2013**, *2013*, 3659-3663.

(30) Chen, W. S.; Kocal, J. A.; Brandvold, T. A.; Bricker, M. L.; Bare, S. R.; Broach, R. W.; Greenlay, N.; Popp, K.; Walenga, J. T.; Yang, S. S.; Low, J. J. *Catal. Today* **2009**, *140*, 157-161.

(31) Sen, A.; Gretz, E.; Oliver, T. F. *Prepr.-Am. Chem. Soc., Div. Pet. Chem.* **1988**, *33*, 460-462.

(32) Gol'dshleger, N. F.; Es'kova, V. V.; Shilov, A. E.; Shteinman, A. A. *Zh. Fiz. Khim.* **1972**, *46*, 1353-1354.

(33) *Alkane C-H Activation by Single-Site Metal Catalysis*. Springer: Dordrect, Netherlands, 2012; Vol. 38.

(34) Goldberg, K. I.; Goldman, A. S., *Activation and Functionalization of C-H Bonds*. American Chemical Society: Washington, DC, 2004; Vol. 885.

(35) Gunnoe, T. B. Physical Inorganic Chemistry: Reactions, Processes, and Applications. In *Physical Inorganic Chemistry: Reactions, Processes, and Applications,* Bakac, A., Ed. John Wiley & Sons: Hoboken, NJ, 2010; Vol. 2, pp 495-549.

(36) Crabtree, R. H. *J. Chem. Soc. Dalt. Trans.* **2001**, 2437-2450.

(37) Periana, R. A.; Taube, D. J.; Gamble, S.; Taube, H.; Satoh, T.; Fujii, H. *Science* **1998**, *280*, 560-564.

(38) Periana, R. A.; Taube, D. J.; Taube, H.; Evitt, E. R. Catalytic Process for Converting Lower Alkanes to Esters, Alcohols, and to Hydrocarbons. U.S. Patent 5,306,855A, April 26, 1994.

(39) Chepaikin, E. G. *Rus. Chem. Rev.* **2011**, *80*, 363-396.

(40) Jones, C. J.; Taube, D.; Ziatdinov, V. R.; Periana, R. A.; Nielsen, R. J.; Oxgaard, J.; Goddard, W. A. *Angew. Chem. Int. Ed.* **2004**, *43*, 4626-4629.

(41) Kao, L. C.; Hutson, A. C.; Sen, A. *J. Am. Chem. Soc.* **1991**, *113*, 700-701.

(42) Munz, D.; Strassner, T. *Angew. Chem. Int. Ed.* **2014**, *53*, 2485-2488.

(43) Flores, J. A.; Komine, N.; Pal, K.; Pinter, B.; Pink, M.; Chen, C. H.; Caulton, K. G.; Mindiola, D. J. *ACS Catal.* **2012**, *2*, 2066-2078.

(44) Caballero, A.; Despagnet-Ayoub, E.; Diaz-Requejo, M. M.; Diaz-Rodriguez, A.; Gonzalez-Nunez, M. E.; Mello, R.; Munoz, B. K.; Ojo, W. S.; Asensio, G.; Etienne, M.; Perez, P. J. *Science* **2011**, *332*, 835-838.

(45) Hashiguchi, B. G.; Konnick, M. M.; Bischof, S. M.; Gustafson, S. J.; Devarajan, D.; Gunsalus, N.; Ess, D. H.; Periana, R. A. *Science* **2014**, *343*, 1232-1237.

(46) Lorkovic, I. M.; Sun, S. L.; Gadewar, S.; Breed, A.; Macala, G. S.; Sardar, A.; Cross, S. E.; Sherman, J. H.; Stucky, G. D.; Ford, P. C. *J. Phys. Chem. A* **2006**, *110*, 8695-8700.

(47) Ding, K. L.; Metiu, H.; Stucky, G. D. *ACS Catal.* **2013**, *3*, 474-477.

(48) Zhdankin, V. V.; Stang, P. J. *Chem. Rev.* **2008**, *108*, 5299-5358.

(49) Richardson, R. D.; Wirth, T. *Angew. Chem. Int. Ed.* **2006**, *45*, 4402-4404.

(50) Wirth, T. *Angew. Chem. Int. Ed.* **2005**, *44*, 3656-3665.

(51) Dohi, T.; Kita, Y. *ChemCatChem* **2014**, *6*, 76-78.

(52) Moteki, S. A.; Usui, A.; Zhang, T. X.; Alvarado, C. R. S.; Maruoka, K. *Angew. Chem. Int. Ed.* **2013**, *52*, 8657-8660.

(53) Ding, K. L.; Zhang, A. H.; Stucky, G. D. *ACS Catal.* **2012**, *2*, 1049-1056.

(54) Buddrus, J.; Plettenberg, H. *Angew. Chem. Int. Ed.* **1976**, *15*, 436-436.

(55) Michalkiewicz, B.; Jarosinska, M.; Lukasiewicz, I. *Chem. Eng. J.* **2009**, *154*, 156-161.

(56) Gang, X.; Zhu, Y. M.; Birch, H.; Hjuler, H. A.; Bjerrum, N. J. *Appl. Catal., A* **2004**, *261*, 91-98.

(57) Periana, R. A.; Mirinov, O.; Taube, D. J.; Gamble, S. *Chem. Comm.* **2002**, 2376-2377.

(58) Bjerrum, N. J.; Xiao, G.; Hjuler, H. A. Process and Catalyst System for the Oxidation of Gaseous Hydrocarbons into Alcohols. World Patent 9924383A1, May 20, 1999.

(59) Konnick, M. M.; Hashiguchi, B. G.; Devaraja, D.; Boaz, N. C.; Gunnoe, T. B.; Groves, J. T.; Gunsalus, N.; Ess, D. H.; Periana, R. A. *Angew. Chem. Int. Ed.* **2014**, *53*, 10490-10494.

(60) Fortman, G. C.; Boaz, N. C.; Munz, D.; Konnick, M. M.; Periana, R. A.; Groves, J. T.; Gunnoe, T. B. *J. Am. Chem. Soc.* **2014**, *136*, 8393-8401.

(61) Kalman, S. E.; Munz, D.; Fortman, G. C.; Boaz, N. C.; Groves, J. T.; Gunnoe, T. B. *Dalton Trans.* **2015**, *44*, 5294-5298.

(62) Boaz, N. C.; Fortman, G. C.; Kalman, S. E.; Gunnoe, T. B.; Groves, J. T., *Unpublished Work.*

# 7 Summary and Future Outlook

The Gunnoe group has previously demonstrated that TpRu(CO)(NCMe)Ph is an effective catalyst for olefin hydroarylation.[1-5] By studying the impact of the ancillary ligand (L) in TpRu(L)(NCMe)Ph (Tp = hydridotris(pyrazolyl)borate, L = CO, $PMe_3$, P(*N*-pyrrolyl)$_3$, $P(OCH_2)_3CEt$, $P(O)(OCH_2)_2CMe$) complexes, insight into the importance of the electronics and steric profiles of the Ru complex for catalytic activity was obtained.[2, 5] While the more electron-rich TpRu(L)(NCMe)Ph complexes are more active for aromatic C–H activation, it was demonstrated that they are poor catalysts due to olefin C–H activation, which is a result of slow olefin insertion. This led to the hypothesis that more electron poor Ru(II) catalysts might lead to higher catalytic activity. This prediction was confirmed with the synthesis and evaluation of the cationic $[(HC(pz^5)_3)Ru(P(OCH_2)_3CEt)(NCMe)Ph][BAr'_4]$ ($HC(pz^5)_3$ = tris(5-methyl-pyrazolyl)-methane, Ar' = 3,5-bis(trifluoromethyl)phenyl), which gave 565 TO of ethylbenzene at 90 °C (Scheme 7.1).[6]

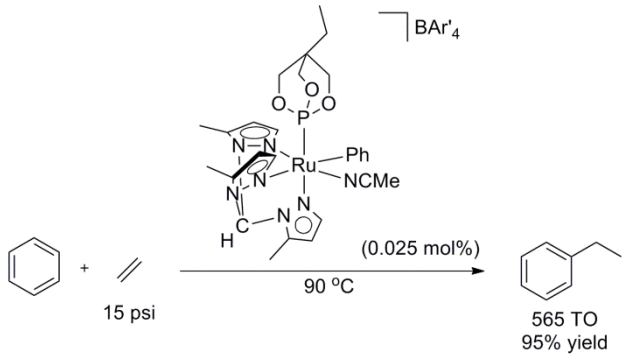


**Scheme 7.1.** Ethylene hydrophenylation catalyzed by $[(HC(pz^5)_3)Ru(P(OCH_2)_3CEt)(NCMe)Ph][BAr'_4]$.

While these results are promising, Ru as well as the other noble transition metals (e.g., Ir and Pt) that have been used in olefin hydroarylation catalysts are

expensive and toxic.[1] The desire to replace these platinum group metals with Earth abundant, first row transition metals for catalytic transformations has been well documented in the literature.[7-11] Thus, we have been interested in extending the catalytic activity observed in the Ru(II) catalysts described above, to ruthenium's Earth abundant, first row counterpart, iron. Developing olefin hydroarylation catalysts based on Fe is challenging because aromatic C–H activation by Fe complexes is rare and Fe has the propensity to favor odd electron reactivity, which could lead to undesired selectivity.[12-17]

## 7.1 Reactivity of Cp*Fe(CO)(NCMe)Ph

### 7.1.1 Summary

In Chapter 2, we demonstrated that Cp*Fe(CO)(NCMe)Ph is highly competent at activating strong aromatic C–H bonds under mild conditions (Scheme 7.2).[18] For instance, the C–H bond of benzene was shown to be broken at just 50 °C. Extending the C–H activation reactivity to heteroaromatic substrates showed that Cp*Fe(CO)(NCMe)Ph regioselectively activates the C–H bond at the 2-position of furan at temperatures even below 0 °C. Through combined experimental and computational studies, we showed that the cleavage of the aromatic C–H bonds proceed through direct interaction between the C–H bond and the iron center, making the complex Cp*Fe(CO)(NCMe)Ph a rare example of Fe-mediated aromatic C–H activation by non-radical routes.[18]

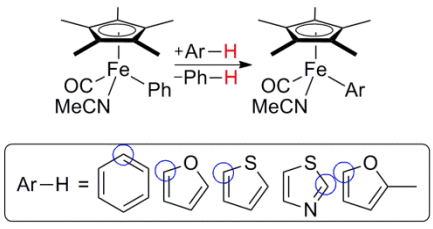


**Scheme 7.2.** Aromatic C–H activation by Cp*Fe(CO)(NCMe)Ph.

Having discovered an example of aromatic C–H activation by an Fe complex, we studied the reactivity of Cp*Fe(CO)(NCMe)Ph toward unsaturated substrates (i.e., olefins and alkynes) in Chapter 3 (Scheme 7.3). It was discovered that under catalytic conditions for ethylene hydrophenylation, Cp*Fe(CO)(NCMe)Ph is a poor catalyst, giving ~1 TO of styrene and ~0.6 TO of ethylbenzene. We hypothesize that competitive β-hydride elimination from the Cp*Fe(CO)($CH_2CH_2Ph$) intermediate results in a catalytically incompetent Fe–hydride species. Attempts to perform catalytic ethylene hydroarylation using furan or thiophene mediated by Cp*Fe(CO)(NCMe)Ar (Ar = 2-furyl, 2-thienyl) were unsuccessful, which we attribute to prohibitively slow ethylene insertion.

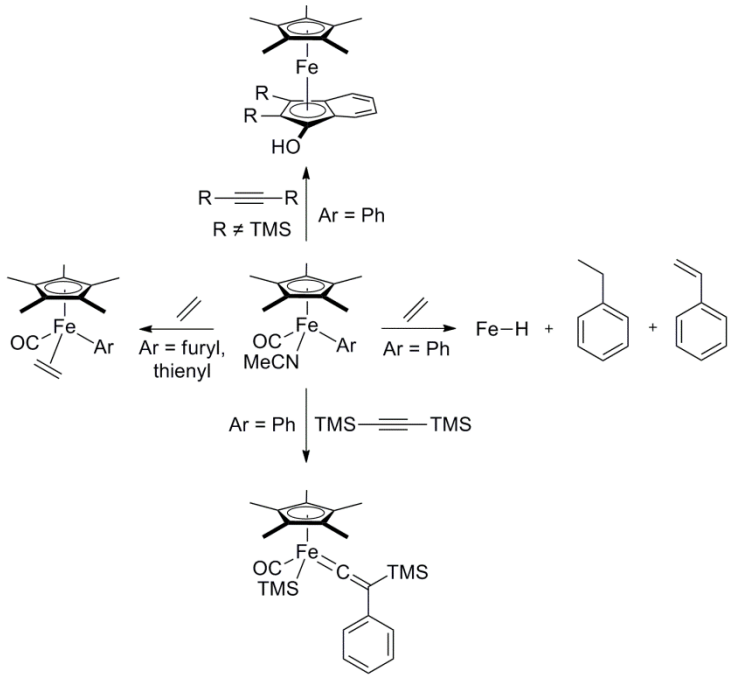


**Scheme 7.3.** Summary of attempted hydroarylation reactions of ethylene and internal alkynes using Cp*Fe(CO)(NCMe)Ph.

Furthermore, Cp*Fe(CO)(NCMe)Ph was applied to catalytic hydrophenylation of internal alkynes. We discovered that, rather than producing vinyl arene product, the

reaction of Cp*Fe(CO)(NCMe)Ph produced novel hydroxyindenyl and vinylidene ligands.[19] Thus, the thermodynamic stability of the resulting hydroxyindenyl Fe sandwich complex or vinylidene complex may responsible for the lack of catalytic activity in alkyne hydrophenylation. Nonetheless, the reactions of Cp*Fe(CO)(NCMe)Ph with internal alkynes to give hydroxyindenyl and vinylidene ligands represents unique reactivity. Importantly, this also highlights a potential challenge for Fe-based catalysts, in which the high stability of sandwich complexes could provide competitive intramolecular reaction pathways that would render the Fe complex catalytically inactive.

### 7.1.2 Future Outlook

From the results summarized in the preceding section, it is clear that Cp*Fe(CO)(NCMe)Ph is not likely to serve as a catalyst for olefin hydroarylation. For ethylene hydrophenylation, the main issue with the Cp*Fe(CO)(NCMe)Ph complex is irreversible β-hydride elimination from Cp*Fe(CO)($CH_2CH_2Ph$). The irreversibility of β-hydride elimination may be a result of associative displacement of styrene by ethylene in Cp*Fe(CO)($\eta^2$-styrene)H due to a Cp* ring slip.

Since it appears that the reactivity of Cp*Fe(CO)(NCMe)Ph with olefins and alkynes is what is causing poor catalytic performance, it would be worthwhile to apply the C–H activation by Cp*Fe(CO)(NCMe)Ph to catalytic C–H activation/C–C bond forming reactions that do not involve olefin or alkyne insertion. Catalytic aromatic C–H functionalization reactions by Fe complexes are rare.[12, 13] As such, the development of an Fe catalyst for C–H bond functionalization involving non-radical routes would be an important achievement. In future work, Cp*Fe(CO)(NCMe)Ph should be evaluated as a catalyst for biaryl coupling reactions (Scheme 7.4). The synthesis of biaryl compounds is an important area of research since this motif is found in many biologically relevant

molecules.[20, 21] In the proposed reaction, an aromatic molecule (e.g., benzene) and an aryl halide (e.g., iodobenzene) are coupled to give biphenyl in the presence of a base and a catalytic amount of Cp*Fe(CO)(NCMe)Ph. The base serves to quench stoichiometric HI produced in the reaction and provide a thermodynamic driving force for the reaction. A survey of the literature reveals that biaryl coupling involving C–H bond activation is dominated by platinum group metals, such as Pd, Rh, and Ru.[20, 21] Examples of Fe catalysts for biaryl formation involve the use of stoichiometric amounts of Grignard reagents or other reducing agents.[20, 21] While biphenyl is not a particularly important molecule, the C–C coupling of benzene and iodobenzene would provide a test reaction to evaluate the catalytic efficacy of Cp*Fe(CO)(NCMe)Ph for this class of reaction. After optimizing reaction conditions using benzene and iodobenzene, the catalytic reaction could be applied to heterocoupling reactions as well as functionalized aromatics that may be more relevant to organic chemists.[20, 21]

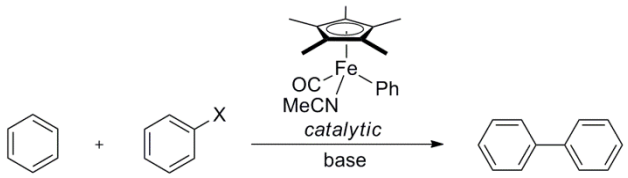


**Scheme 7.4.** Proposed biaryl coupling catalyzed by Cp*Fe(CO)(NCMe)Ph (X = halide).

## 7.2 Reactivity of Cp*Fe[P(OCH$_2$)$_3$CEt]$_2$Ph

### 7.2.1 Summary

In Chapter 4, we attempted to study the impact of replacing CO from Cp*Fe(CO)(NCMe)Ph with the P(OCH$_2$)$_3$CEt, but we were unable to successfully synthesize Cp*Fe[P(OCH$_2$)$_3$CEt](NCMe)Ph. However, we did demonstrate that under photolytic conditions, Cp*Fe[P(OCH$_2$)$_3$CEt]$_2$Ph activates the C–H bonds of furan, 2-

methylfuran, and thiophene (Scheme 7.5). At this point, the substrate scope for aromatic C–H activation is limited, which we believe is, at least in part, due to strong coordinating ability of the $P(OCH_2)_3CEt$ ligand even under photolytic conditions. Ethylene hydroarylation using furan was unsuccessful, leading to decomposition of the starting complex. The attempted hydroarylation of 2-butyne using furan did not produce any 2-but-2-en-2-ylfuran. Instead, we isolated $Cp^*Fe[\eta^5\text{-}C_5Me_4(CH{=}CHCHO)]$, which likely forms from a reaction involving double insertion of 2-butyne followed by furyl C–O bond cleavage (Scheme 7.5). To the best of our knowledge, C–O bond cleavage of furan is unprecedented with Fe. Like Cp*Fe(CO)(NCMe)Ph, the reaction of $Cp^*Fe[P(OCH_2)_3CEt]_2$(2-furyl) with alkynes is dominated by an intramolecular reaction the results in the formation of a very stable ferrocene derivative.

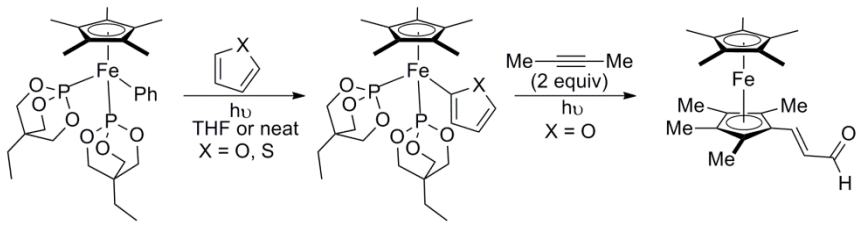


**Scheme 7.5.** Summary of the reactivity of $Cp^*Fe[P(OCH_2)_3CEt]_2Ph$.

### 7.2.2 Future Outlook

The C–H activation chemistry demonstrated with $Cp^*Fe[P(OCH_2)_3CEt]_2Ph$ highlights the efficacy of Cp*Fe complexes for aromatic C–H activation.[13, 14, 18] At this point, it appears that aromatic C–H activation by $Cp^*Fe[P(OCH_2)_3CEt]_2Ph$ is limited to furans and thiophenes. For thiophene, the reaction is slow and inconsistent, which may prohibit further study with this substrate. However, the C–H activation of furan is more facile and could provide opportunities for additional research. For instance,

$Cp^*Fe[P(OCH_2)_3CEt]_2$(2-furyl) could serve as a catalyst for biaryl coupling in analogy with the proposed research with Cp*Fe(CO)(NCMe)Ph. Thus, the photolytic reaction of furan and a furyl halide in the presence of a base and a catalytic amount of $Cp^*Fe[P(OCH_2)_3CEt]_2$(2-furyl) should be evaluated. While the CO ligand in Cp*Fe(CO)(NCMe)Ph could complicate the reaction, this would not be a concern for $Cp^*Fe[P(OCH_2)_3CEt]_2$(2-furyl).

Additionally, the discovery of furyl C–O bond cleavage from the photolytic reaction of $Cp^*Fe[P(OCH_2)_3CEt]_2$(2-furyl) with 2 equivalents of 2-butyne will certainly be an area of future work. The cleavage of a C–O bond in furan by an Fe complex is unprecedented, and the ring opening of furans is relevant for the conversion of biomass into liquid fuels.[22, 23] We will perform reactions that can give insight into the mechanism of this transformation. First, we will attempt to observe intermediates from the reaction of $Cp^*Fe[P(OCH_2)_3CEt]_2$(2-furyl) and 2-butyne. Possible intermediates are shown in Scheme 7.6. This might be achieved by photolyzing the reaction of $Cp^*Fe[P(OCH_2)_3CEt]_2$(2-furyl) and excess 2-butyne for a short period of time (<30 min) or using 1 equivalent of 2-butyne. Furthermore, the reaction of $Cp^*Fe[P(OCH_2)_3CEt]_2$[2-(5-methylfuryl)] and excess 2-butyne may also give valuable insight into the reaction mechanism (Scheme 7.7). If the mechanism involves coordination of the oxygen in the furyl ligand to Fe or a second C–H activation at the α position of the furyl ligand, the methyl group could serve to block that position and result in no furyl ring opening (Scheme 7.7).

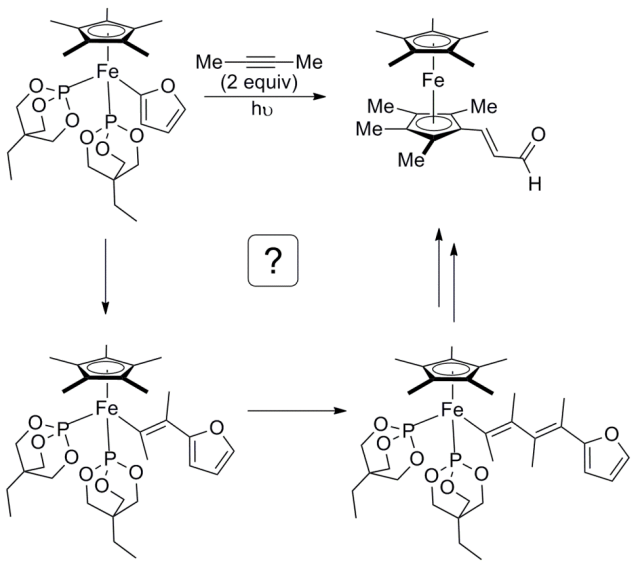


**Scheme 7.6.** Possible intermediates in the conversion of Cp*Fe[$P(OCH_2)_3CEt]_2$(2-furyl) and excess 2-butyne to Cp*Fe[$\eta^5$-($C_5Me_4$(CH=CHCHO))].

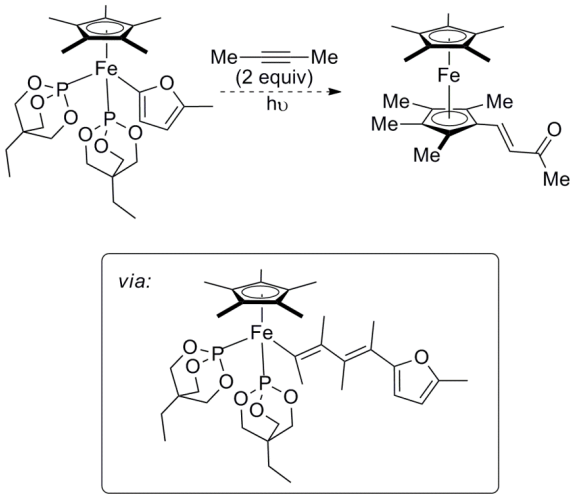


**Scheme 7.7.** Possible reaction of Cp*Fe[$P(OCH_2)_3CEt]_2$[2-(5-methylfuryl)] and excess 2-butyne.

## 7.3 Synthesis and Reactivity of (PNP)Fe Complexes

### 7.3.1 Summary

We have explored the synthesis of complexes of the type [($^R$PNP)Fe(L)(NCMe)Me][Y] (R = phenyl, cyclohexyl; L = $PMe_3$, $P(OCH_2)_3CEt$; Y =

$BAr'_4$, $PF_6$) in Chapter 5. We demonstrated the synthesis and isolation of [($^{Ph}$PNP)Fe($PMe_3$)(NCMe)Me][Y]. For this complex, the methyl ligand and NCMe ligand are *trans* to each other. If there is no isomerization under catalytic conditions, this isomer would not be active for C–H activation or olefin insertion since the coordinated C–H bond or the olefin must be *cis* to the hydrocarbyl ligand (Figure 7.1). The synthesis of *cis*- and *trans*-[($^{Ph}$PNP)Fe($P(OCH_2)_3CEt$)$(NCMe)_2$][$PF_6$]$_2$ has also been achieved. Preliminary attempts to methylate this complex have produced complex mixtures of products; however $^1$H NMR data suggest the Fe complex has been methylated. We have also reported initial synthetic efforts toward [($^{Cy}$PNP)Fe($P(OCH_2)_3CEt$)(NCMe)Me][Y]. For this study, it has been observed that the $^{Cy}$PNP ligand prevents the coordination of $PMe_3$ to the metal center. At this point, we only have evidence for $P(OCH_2)_3CEt$ coordination.

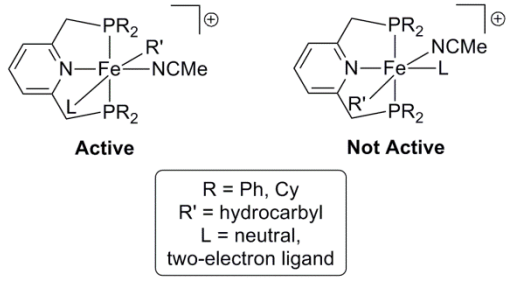


**Figure 7.1.** Possible isomers for [($^R$PNP)Fe(L)(NCMe)Me][Y] complexes. Hydrocarbyl ligand and labile ligand must be *cis***.**

### 7.3.2 Future Outlook

The study of (PNP)Fe complexes is at this point too preliminary to draw any definitive conclusions. Our initial work does seem to suggest that the meridinal coordination mode of the PNP ligands may introduce challenges involving isomers where the hydrocarbyl ligand and the coordinated C–H bond or olefin are *trans* to one another.

However, the synthetic procedures described in Chapter 5 provide a way to access novel Fe–hydrocarbyl complexes based on PNP ligands. Additionally, the chemistry surrounding ($^{Ph}$PNP)Fe complexes is largely unexplored, and we have provided synthetic routes to access a variety of new complexes. For these reasons, more effort should be directed toward cleanly synthesizing and fully characterizing [($^{R}$PNP)Fe(L)(NCMe)Me][Y] complexes.

At this point, only [($^{Ph}$PNP)Fe($PMe_3$)(NCMe)Me][Y] has been isolated. The main challenges with the synthesis and isolation of this complex has been finding a suitable solvent for the reaction of [($^{Ph}$PNP)Fe($PMe_3$)$(NCMe)_2$][Y]$_2$ and $AlMe_3$. When Y = $PF_6$, the starting complex has poor solubility in non-polar solvents. We have been able to use THF, but it appears that $AlMe_3$ may polymerize THF since the reaction solution becomes very viscous. We initially focused efforts on using $PF_6$ as the anion because it was expected to be easier to purify complexes by precipitation or crystallization. Therefore, efforts should be re-focused to work predominantly with complexes containing the BAr'$_4$ anion, as this would have better solubility in non-polar solvents. For example, diethyl ether could be used as the solvent for the reaction of [($^{Ph}$PNP)Fe($PMe_3$)$(NCMe)_2$][BAr'$_4$]$_2$ and $AlMe_3$. Another option could be to use another alkylating reagent, such as MeLi. Early methylation attempts involved using MeLi, and we observed a methyl peak corresponding to [($^{Ph}$PNP)Fe($PMe_3$)(NCMe)Me][Y] in the crude $^1$H NMR spectrum. With some efforts optimizing reaction conditions, the reaction of [($^{Ph}$PNP)Fe($PMe_3$)$(NCMe)_2$][Y]$_2$ and MeLi in THF could be a suitable way to make [($^{Ph}$PNP)Fe($PMe_3$)(NCMe)Me][Y]. Following the successful syntheses of

[($^{R}$PNP)Fe(L)(NCMe)Me][Y] complexes, they should be systematically tested for olefin hydroarylation along with aromatic C–H activation and olefin insertion.

## 7.4 Concluding Remarks and Future Directions

One important conclusion from this work is that Fe-mediated olefin hydroarylation is feasible. This conclusion is primarily based on the observation that Cp*Fe(CO)(NCMe)Ph can perform ethylene insertion and benzene C–H activation in a single step. We have also learned that our initial hypothesis, that we could develop Fe catalysts for olefin hydroarylation that are closely related to our successful TpRu(L)(NCMe)Ph complexes, is only partly true. We have been unable to make TpFe(CO)(NCMe)Ph, but we have demonstrated that the related Cp*Fe(CO)(NCMe)Ph complex is highly active for aromatic C–H activation.

From the work in this Dissertation, it is likely that a successful Fe catalyst for olefin hydroarylation is going to need different ligand motifs or even different oxidation states from what has been successful with the Ru catalysts. One direction that should be explored is the development of potential Fe catalysts based on tetraamine ligands. In Chapter 5, we have reported initial synthetic efforts based on the TPA ligand (TPA = tris(2-pyridylmethyl)amine). Using the TPA ligand, we have been unable to produce stable Fe–hydrocarbyl complexes. In the literature, there is the report of an Fe dimethyl complex based on a tetraamine ligand, dimethyl[*N*,*N*'-(6,6'-dimethylphenyl-2,2'-diyl)bis(2-pyridylmethyl)diamine]iron(II).[24] This complex could be treated with HBAr'$_4$, for example, in a coordinating solvent, such as NCMe, to afford the cationic mono-methyl complex, which can be tested for olefin hydroarylation (Scheme 7.8).

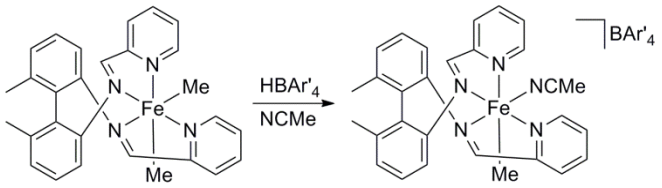


**Scheme 7.8.** Protonation of dimethyl[*N*,*N*'-(6,6'-dimethylphenyl-2,2'-diyl)bis(2-pyridylmethyl)diamine]iron(II).

In addition, it would be worthwhile to pursue Fe(0) catalysts for olefin hydroarylation. It has been proposed that previous examples of olefin or alkyne hydroarylation using first row transition metals have been based on low valent catalysts (i.e., Co(I), Ni(0)).[25-28] For example, recently Hartwig and co-workers reported olefin hydroarylation using a Ni(0)-NHC (NHC = *N*-heterocyclic carbene) catalyst (Scheme 7.9).[26] The catalyst system is more effective with electron deficient arenes and does not work well with benzene, but C–H oxidative addition from Ni(0) to Ni(II) appears to be important for the success of this catalyst system. Examples of Co-catalyzed olefin and alkyne hydroarylation generally involve chelate assisted C–H activation from a low valent NHC or phosphine ligated Co(I) or Co(0) complex, which is generated in situ from $CoBr_2$ and an excess of a reducing agent, such as a Grignard reagent (Scheme 7.10).[27] The mechanism is not well understood, but C–H activation likely proceeds via oxidative addition from Co(I) or Co(0).

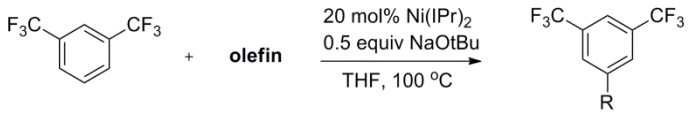


**Scheme 7.9.** Ni catalyzed olefin hydroarylation reported by Hartwig and coworkers (IPr = 1,3-bis(2,6-di(isopropylphenyl)imidazole-2-ylidene).

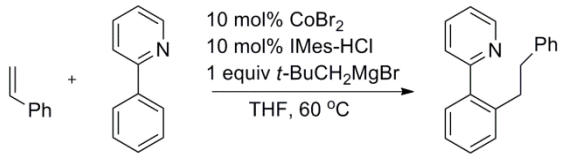


**Scheme 7.10.** Example of Co catalyzed hydroarylation of styrene (IMes-HCl = 1,3-bis(2,4,6-trimethylphenyl)imidazolium chloride).

As discussed in Chapter 1, the seminal examples of Fe-mediated C–H activation occur by C–H oxidative addition from an Fe(0) complex.[12, 15-17] Fe-catalyzed aldimine formation likely proceeds by benzene C–H activation from Fe(0) with insertion of the isonitrile occurring at Fe(II).[12] By analogy, a mechanism for Fe-catalyzed ethylene hydrophenylation can be proposed that involves oxidative addition of a benzene C–H bond to give an Fe(II) intermediate, insertion of ethylene into the Fe–H bond, and reductive elimination of the phenyl and ethyl ligands to give ethylbenzene, which regenerates the catalyst (Scheme 7.11). Recently, Yoshikai and co-workers reported that an Fe-NHC catalyst generated from $Fe(acac)_3$ (acac = acetylacetonate), an NHC salt, and a Grignard reagent mediates the addition of a C–H bond from an indole across vinyl arenes and alkynes (Scheme 7.12).[29] Only preliminary mechanistic data have been obtained, but the authors propose that C–H activation occurs at low valent Fe and alkyne or vinyl arene insertion occurs at Fe(II), similar to the proposed catalytic cycle shown in Scheme 7.11.

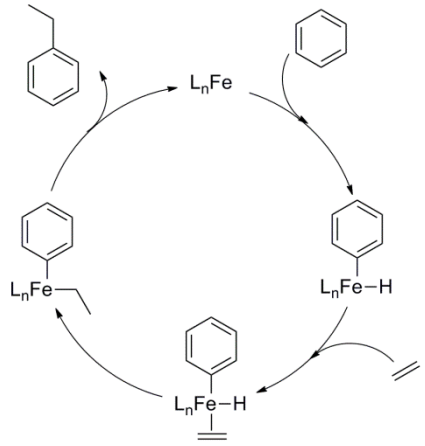


**Scheme 7.11.** Proposed catalytic cycle for ethylene hydrophenylation involving Fe(0) and Fe(II).

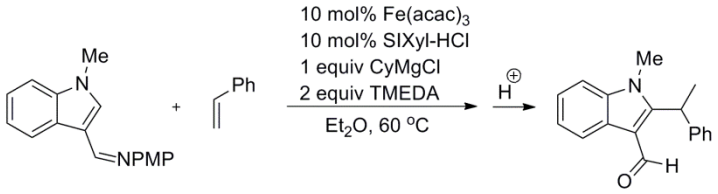


**Scheme 7.12.** Example of imine-directed hydroarylation of styrene using indole with an Fe catalyst (PMP = *p*-methoxyphenyl, SIXyl-HCl = bis(2,6-dimethylphenyl)imidazolinium chloride, TMEDA = *N*,*N*,*N*',*N*'-tetramethylethylenediamine).

Therefore, it would be useful to begin investigating well defined, low valent Fe complexes, most likely ligated with NHC ligands.[30] Based on literature precedent, strongly donating ligands will likely be necessary to promote benzene C–H oxidative addition.[12, 15-17] There are two possible approaches to the synthesis of Fe(0) catalysts. First, one may synthesize potential Fe(0) catalysts directly. One might also consider isolating Fe(II) pre-catalysts that, upon reductive elimination, generate the Fe(0) active catalyst. An example of the second strategy could involve preparing the complex $(IMes)_2Fe(Me)_2$ (IMes = 1,3-bis(2,4,6-trimethylphenyl)imidazaol-2-ylidene) or an Fe complex with a related NHC.[30, 31] It is possible that under thermal conditions, ethane

could reductively eliminate ethane producing an $(IMes)_2Fe(0)$ complex, which may be active for olefin hydroarylation (Scheme 7.13). Fe-NHC pincer complexes have been demonstrated to give isolable Fe(0) complexes.[30, 32-34] The pincer ligands used in the preparation of these complexes are based on the C-N-C motif, where the central donor group is a pyridine (Figure 7.2).[33, 34] Fe(0) complexes based on these ligands have not been shown to mediate C–H activation. It is possible that synthesizing a related complex with a more strongly donating ligand could allow for C–H activation. For example, a P~C~P ligand has been reported on Rh that, when on Fe, may provide the necessary electronic properties for C–H activation (Figure 7.2).[32, 35]

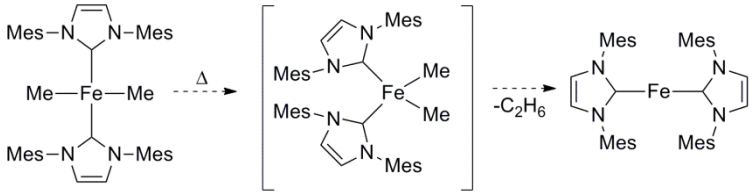


**Scheme 7.13.** Proposed generation of $(IMes)_2Fe(0)$ species by reductive elimination of ethane (Mes = mesityl).

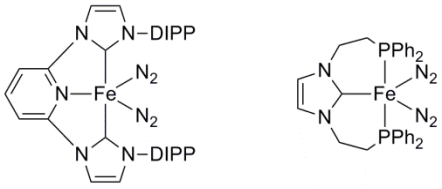


**Figure 7.2.** Comparison of known (CNC)Fe(0) complex and proposed (PCP)Fe(0) complex (DIPP = 1,3-diisopropylphenyl).

Therefore, the development of Fe catalysts for olefin hydroarylation is promising, given that Fe can mediate aromatic C–H activation and olefin insertion in a single reaction. Moving forward, it will be important to explore ligand motifs that are outside

the cyclopentadienyl family as well as investigate low valent Fe complexes as catalysts for olefin hydroarylation. The extension of the reactivity from our group's previously reported Ru(II) catalysts to suitable Fe catalysts is not trivial, but the work presented in this Dissertation provides hope that using the right ligand set, an Fe catalyst for olefin hydroarylation can be discovered.

## 7.5 References

(1) Andreatta, J. R.; McKeown, B. A.; Gunnoe, T. B. *J. Organomet. Chem.* **2011**, *696*, 305-315.

(2) Foley, N. A.; Lee, J. P.; Ke, Z. F.; Gunnoe, T. B.; Cundari, T. R. *Acc. Chem. Res.* **2009**, *42*, 585-597.

(3) Lail, M.; Arrowood, B. N.; Gunnoe, T. B. *J. Am. Chem. Soc.* **2003**, *125*, 7506-7507.

(4) Lail, M.; Bell, C. M.; Conner, D.; Cundari, T. R.; Gunnoe, T. B.; Petersen, J. L. *Organometallics* **2004**, *23*, 5007-5020.

(5) Joslin, E. E.; McMullin, C. L.; Gunnoe, T. B.; Cundari, T. R.; Sabat, M.; Myers, W. H. *Organometallics* **2012**, *31*, 6851-6860.

(6) Burgess, S. A.; Joslin, E. E.; Gunnoe, T. B.; Cundari, T. R.; Sabat, M.; Myers, W. H. *Chem. Sci.* **2014**, *5*, 4355-4366.

(7) Bullock, R. M., *Catalysis without Precious Metals*. Wiley-VCH Verlag & Co.: Weinheim, Germany, 2010.

(8) Enthaler, S.; Junge, K.; Beller, M. *Angew. Chem. Int. Ed.* **2008**, *47*, 3317-3321.

(9) Jia, F.; Li, Z. *Org. Chem. Front.* **2014**, *1*, 194-214.

(10) Sun, C. L.; Li, B. J.; Shi, Z. J. *Chem. Rev.* **2011**, *111*, 1293-1314.

(11) Bauer, I.; Knoelker, H.-J. *Chem. Rev.* **2015**, ASAP, DOI:10.1021/cr500425u.

(12) Jones, W. D.; Foster, G. P.; Putinas, J. M. *J. Am. Chem. Soc.* **1987**, *109*, 5047-5048.

(13) Hatanaka, T.; Ohki, Y.; Tatsumi, K. *Chem. Asian J.* **2010**, *5*, 1657-1666.

(14) Ohki, Y.; Hatanaka, T.; Tatsumi, K. *J. Am. Chem. Soc.* **2008**, *130*, 17174-17186.

(15) Ittel, S. D.; Tolman, C. A.; English, A. D.; Jesson, J. P. *J. Am. Chem. Soc.* **1978**, *100*, 7577-7585.

(16) Baker, M. V.; Field, L. D. *J. Am. Chem. Soc.* **1986**, *108*, 7433-7434.

(17) Baker, M. V.; Field, L. D. *J. Am. Chem. Soc.* **1986**, *108*, 7436-7438.

(18) Kalman, S. E.; Petit, A.; Gunnoe, T. B.; Ess, D. H.; Cundari, T. R.; Sabat, M. *Organometallics* **2013**, *32*, 1797-1806.

(19) Kalman, S. E.; Gunnoe, T. B.; Sabat, M. *Organometallics* **2014**, *33*, 5457-5463.

(20) Hussain, I.; Singh, T. *Adv. Synth. Catal.* **2014**, *356*, 1661-1696.

(21) McGlacken, G. P.; Bateman, L. M. *Chem. Soc. Rev.* **2009**, *38*, 2447-2464.

(22) Sutton, A. D.; Waldie, F. D.; Wu, R. L.; Schlaf, M.; Silks, L. A.; Gordon, J. C. *Nature Chem.* **2013**, *5*, 428-432.

(23) Chatterjee, M.; Matsushima, K.; Ikushima, Y.; Sato, M.; Yokoyama, T.; Kawanami, H.; Suzuki, T. *Green Chem.* **2010**, *12*, 779-782.

(24) Vedder, C.; Schaper, F.; Brintzinger, H. H.; Kettunen, M.; Babik, S.; Fink, G. *Eur. J. Inorg. Chem.* **2005**, 1071-1080.

(25) Nakao, Y.; Kashihara, N.; Kanyiva, K. S.; Hiyama, T. *Angew. Chem. Int. Ed.* **2010**, *49*, 4451-4454.

(26) Bair, J. S.; Schramm, Y.; Sergeev, A. G.; Clot, E.; Eisenstein, O.; Hartwig, J. F. *J. Am. Chem. Soc.* **2014**, *136*, 13098-13101.

(27) Gao, K.; Yoshikai, N. *Acc. Chem. Res.* **2014**, *47*, 1208-1219.

(28) Nakao, Y.; Kashihara, N.; Kanyiva, K. S.; Hiyama, T. *J. Am. Chem. Soc.* **2008**, *130*, 16170-16171.

(29) Wong, M. Y.; Yamakawa, T.; Yoshikai, N. *Org. Lett.* **2015**, *17*, 442-445.

(30) Riener, K.; Haslinger, S.; Raba, A.; Hogerl, M. P.; Cokoja, M.; Herrmann, W. A.; Kuhn, F. E. *Chem. Rev.* **2014**, *114*, 5215-5272.

(31) Hashimoto, T.; Urban, S.; Hoshino, R.; Ohki, Y.; Tatsumi, K.; Glorius, F. *Organometallics* **2012**, *31*, 4474-4479.

(32) Pugh, D.; Danopoulos, A. A. *Coord. Chem. Rev.* **2007**, *251*, 610-641.

(33) Danopoulos, A. A.; Pugh, D.; Smith, H.; Sassmannshausen, J. *Chem. Eur. J.* **2009**, *15*, 5491-5502.

(34) Danopoulos, A. A.; Wright, J. A.; Motherwell, W. B. *Chem. Comm.* **2005**, 784-786.

(35) Zeng, J. Y.; Hsieh, M. H.; Lee, H. M. *J. Organomet. Chem.* **2005**, *690*, 5662-5671.